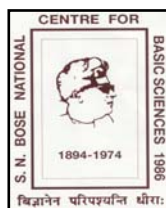


**MEDIUM EFFECTS ON CHEMICAL REACTION IN  
ELECTROLYTE SOLUTIONS, BINARY MIXTURES AND  
CONFINED ENVIRONMENTS: A SPECTROSCOPIC STUDY**

Thesis Submitted for the Degree of  
**Doctor of Philosophy (Science)**

of  
Jadavpur University

By  
Tuhin Pradhan



Department of Chemical, Biological and Macromolecular Sciences  
S. N. Bose National Centre for Basic Sciences  
Block-JD, Sector – III, Salt Lake City  
Kolkata -700098, India  
February 2009

## CERTIFICATE FROM THE SUPERVISORS

This is to certify that the Thesis entitled “*Medium Effects on Chemical Reactions in Electrolyte Solutions, Binary Mixtures and Confined Environments : A Spectroscopic Study*” submitted by Sri **Tuhin Pradhan**, who got his name registered on 9<sup>th</sup> July, 2004 for the award of **Ph. D. (Science ) degree** of **Jadavpur University**, is absolutely based upon his own work under the supervision of **Dr. Ranjit Biswas** and **Dr. Jaydeb Chakrabarti** at the S. N. Bose National Centre for Basic Sciences, Kolkata, India and that neither this thesis nor any part of it has been submitted for either any degree/diploma or any other academic award anywhere before.

Dr. Jaydeb Chakrabarti  
Research Co-supervisor

Dr. Ranjit Biswas  
Research Supervisor

*Dedicated to*

*My father Sri Chinmoy Pradhan  
And  
Mother Smt. Debi Rani Pradhan*

## Acknowledgement

I would like to express my deep sense of gratitude to my research supervisor Dr. Ranjit Biswas for his good guidance, patience and enthusiasm. My research and the subsequent fulfillment of my dream to earn a Ph.D degree would not have been possible without his help and encouragement. I also thank him for his extreme care about my non-academic life.

Thanks are also extended to my research co-supervisor Dr. Jaydeb Chakrabarti for the fruitful discussions in the several group meetings to enhance my understanding. I also acknowledge Prof. A. K. Raychaudhuri for providing good experimental facilities in our Institute. I thank the Head, Department of Chemical, Biological and macromolecular Sciences for his kind support. I am grateful to Dr. S. K. Pal for several discussions. I am thankful to Prof. Sital Chattopadhyay, Kalyani University and Prof. Amitavo Sarkar, IACS for their help in synthesizing molecules that I have used in many of my investigations. I am indebted to Prof. A. P. Chattopadhyay, Kalyani University for his invaluable guidance on many academic activities. I thank Prof. Sanjoy Bandyopadhyay for his valuable advice. It is a pleasure to thank Professor M. Maroncelli for his kind support and assistance. I thank Prof. B. M. Deb for his encouragement and advices that helped building my character.

Special thanks are offered to our group members who contributed in many ways to my research: Dr. Nashiour Rohman, Piue Ghoshal, Arup Ratan Das, Sucheta Sengupta, Hemant Kumar Kashyap, Harun Al Rasid Gazi, Manoj Raula, Biswajit Guchhait and Snehasis Das Chakraborti. It was my pleasure to work in a nice and beautiful group where everybody is most co-operative and helpful.

I thank all faculty members, students and office members of our Centre for creating good research environment and for their eager co-operation and help. I specially thank Mr. Sukanta Mukherjee and Mr. Sunish Deb for their enormous help.

I am grateful to all my friends: Dipankar , Pramod, Sudarshan, Kartick, Soumendu, Kunal, Anjan, Roby, Badiur, Santosh, Arindam, Moshiur, Mitali, Anindadi, Dipankarda, Rajibda, Sitenduda, Sudeshna, Manoj, Ajay, Swarup, Rupa, Sankar, Bipul, Rwitick, Sourav, Navin, Mrinal , Avishek and Ratanda for their friendship and help.

I would like to thank Prof. Ashim Roy and Prof. Rabin Banerjee for their encouragement. I am grateful to my college teachers Mr. Chityaranjan Das, Dr. Debasish Banerjee, Mr. Timir Sinha, Mrs. Sujata Gosh, Dr. Ranjan Gosh and school teachers Mr. Indubhusan Maiti and Mr. Sanjay Bandapadyay for their constant encouragement. I also thank to my childhood friends Prabhat, Palash and Suvrankur for their encouragement. I acknowledge to my friend Tuhina for providing mental support and encouragement. I also thank my college friends Biswajit, Bilash, Tuhin and Paramita for their encouragement.

I wish to take this opportunity to thank Dr. Parijat Das (Madam) for her kind love and encouragement to the group members.

I am grateful to University Grants Commission (UGC), India for providing me a research fellowship.

I would like to thank my sister (Tapasi) and brother (Tarun ) for their love and constant support from childhood. I thank my aunt (Madhabi) and brother-in-law (Surajitda) for their help and encouragement.

Finally I take this opportunity to dedicate this Thesis to my parents whose love and affection always enlightened my way toward completeness and freedom.

At the end, I convey my heartiest love to little Rwitaban for his cuteness.

## Abstract

In this Thesis we have studied medium effects on excited state intramolecular charge transfer reaction (ICT) in electrolyte solutions, binary mixtures and confined environments using fluorescence steady state and time resolved spectroscopy. Solvent dynamical modes as well as structural effects that couple with the reactive mode have been explored by following the reaction rate and equilibrium constants. Various complex environments are chosen in such that solution dynamical time scale ranges between a few picoseconds to a several hundreds of picoseconds or even in nanoseconds. Reactant molecules have been synthesized by following methods described in the relevant literature.

The first chapter of the Thesis provides an introduction of the present work with a brief review of the relevant literature. In chapter 2 and 3, experimental results of electrolyte effects on ICT reaction rate in solutions of low to high electrolyte concentrations have been presented in detail. The validity of Zwan-Hynes theory that connects the average solvation time with the reaction rate has also been tested for ICT reactions in solutions containing electrolyte in large concentration. Chapter 4 contains the experimental results of temperature dependence on ICT reactions in electrolyte solutions. Solvent isotope effects on ICT reaction are discussed in chapter 5. Effects of microscopic heterogeneity in binary solution structure on ICT reaction have been detailed in chapter 6. The effects of reduced polarity, slowed down dynamics and confinement on ICT reaction have been investigated in aqueous reverse micelle and results are presented in chapter 7. Chapter 8 describes the experimental results of catalytic activity of horseradish peroxidase (HRP) enzyme in catanionic reverse micelles. A few research problems have been discussed in chapter 9, which could be studied in future. Supporting information is included in the form of 'Appendix' wherever necessary.

## List of Publications

- (1) '*Electrolyte Concentration and Ion-Size Dependence of Excited State Intramolecular Charge Transfer Reaction in (Alkylamino)benzonitriles : Steady State Spectroscopic Studies*' by **Tuhin Pradhan** and Ranjit Biswas, *J. Phys. Chem. A*, **2007**, *111*, 11514.
- (2) '*Electrolyte Concentration and Ion-Size Dependence of Excited State Intramolecular Charge Transfer Reaction in (Alkylamino)benzonitriles : Time Resolved Fluorescence Emission Studies*' by **Tuhin Pradhan** and Ranjit Biswas, *J. Phys. Chem. A*, **2007**, *111*, 11524.
- (3) '*Excited State Intramolecular Charge Transfer Reaction in Binary Mixtures of Water and Tertiary Butanol (TBA): Alcohol Mole Fraction Dependence*' by **Tuhin Pradhan**, Piue Ghoshal and Ranjit Biswas, *J. Phys. Chem. A*, **2008**, *112*, 915.
- (4) '*Structural Transition in Alcohol-Water Binary Mixtures: A Spectroscopic Study*' by **Tuhin Pradhan**, Piue Ghoshal and Ranjit Biswas, *J. Chem. Sci*, **2008**, *120*, 275.
- (5) '*Intramolecular Charge Transfer Reaction, Polarity and Dielectric Relaxation in AOT/Water/Heptane Reverse Micelles: Pool Size Dependence*' by Ranjit Biswas, Nashiour Rohman, **Tuhin Pradhan** and Richard Buchner *J. Phys. Chem. B*, **2008**, *112*, 9379.
- (6) '*Spectroscopic Studies of Catanionic Reverse Microemulsion: Correlation with the Superactivity of Horseradish Peroxidase Enzyme in a Restricted Environment*' by by Ranjit Biswas , Arup R. Das, **Tuhin Pradhan**, Didier Touraud, Werner Kunz and Sekh Mahiuddin, *J. Phys. Chem. B*, **2008**, *112*, 6620.

- (7) 'Excited State Intramolecular Charge Transfer Reaction in 4-(1-azetidiny)benzonitrile: Solvent Isotope Effects ' by **Tuhin Pradhan**, Piu Ghoshal and Ranjit Biswas, *J. Chem. Sci*, **2009**, *121*, 95
- (8) 'Intramolecular Charge Transfer Reaction in Solutions of Low to High Electrolyte Concentrations: Interplay between Friction and Solvation ' by **Tuhin Pradhan** and Ranjit Biswas, *J. Sol. Chem.* **2009** (*in press*).
- (9) 'Excited State Intramolecular Charge Transfer Reaction in Non-aqueous Electrolyte Solutions: Temperature Dependence' by **Tuhin Pradhan**, Harun Al Rasid Gazi and Ranjit Biswas, *J. Chem. Phys*, (*Submitted*).
- (10)\* 'Limiting Ionic Conductivity and Solvation Dynamics in Formamide' by Hemant K. Kashyap, **Tuhin Pradhan** and Ranjit Biswas, *J. Chem. Phys.* **2006**, *125*, 174506

*\*Not included in this Thesis*

# Contents

<b>Chapter1: Introduction</b> .....	13
References.....	24
<b>Chapter 2: Excited State Intramolecular Charge Transfer</b>	
<b>Reaction in Electrolyte Solutions</b> .....	<b>30</b>
2. 1. Introduction .....	30
2.2. Experimental Details .....	33
2.3. Results & Discussion .....	36
2.3.1. Spectral Properties .....	38
2.3.2. Quantum Yields and Transition Moments .....	48
2.3.3. Average Reaction Rates: Electrolyte Concentration Dependence.....	55
2.3.4. Average Reaction Rates: Cation Size Dependence.....	62
2.3.5. Zwan-Hynes Theory: Comparison with Experiments.....	63
2.4. Conclusion.....	68
References and Notes.....	71
<b>Chapter 3: Intramolecular Charge transfer Reaction in Solutions of     Low to High Electrolyte Concentrations: Interplay between     Friction and Solvation.....</b>	<b>75</b>
3.1. Introduction.....	75
3.2. Experimental Details.....	77
3.3. Results & Discussion.....	77
3.3.1. Steady State Spectroscopic Studies.....	77
3.3.2. Time Resolved Fluorescence Studies.....	84
3.4. Conclusion.....	90
References and Notes.....	92
<b>Chapter 4: Excited state intramolecular Charge Transfer     Reaction in Non-aqueous Electrolyte Solutions:     Temperature Dependence.....</b>	<b>93</b>



7.1. Introduction.....	157
7.2. Experimental.....	160
7.3. Results & Discussion.....	162
7.3.1. Estimation of the Average $\varepsilon_0$ of the Confined Pool in Aqueous Reverse Micelles.....	162
7.3.2. TICT Reactions in AOT/water/heptane Reverse Micelles: Steady State Fluorescence Study.....	165
7.3.3. Time Resolved Studies of TICT Reaction in Reverse Micelles: Pool Size Dependence .....	173
7.4. Conclusion.....	178
References and Notes.....	181
<b>Chapter 8: Spectroscopic Studies of Catanionic Reverse Microemulsion: Correlation with the Superactivity of Horseradish Peroxidase Enzyme in a Restricted Environment .....185</b>	
8.1. Introduction.....	185
8.2. Experimental Details.....	187
8.2.1. Materials.....	187
8.2.2. Preparation of Microemulsion.....	188
8.2.3. Spectroscopic Experiments.....	189
8.2.4. DLS Experiment.....	191
8.3. Results & Discussion.....	192
8.3.1. Distribution of C153 in Microemulsion.....	192
8.3.2. Solubilization of n-Hexanol and Enzyme Activity.....	195
8.3.3. Polarity of the Confined Fluid and its Dynamics.....	196
8.3.4. Influence of Surfactant and Buffer on the Droplet Size and Dynamics.....	199
8.3.5. Solute Dynamics: Time Resolved Fluorescence Anisotropy Study.....	202
8.4. Conclusion.....	206
References and Notes.....	208
<b>Chapter 9: Concluding Remarks and Future Problems.....213</b>	

9.1. Anion Dependence on Excited State Intramolecular Charge Transfer Reaction.....	213
9.2. Non-monotonic Electrolyte Concentration Dependence of Reaction Rate by ZH theory.....	214
9.3. Exploring Non-Arrhenius Temperature Dependence of the TICT reaction Rate.....	214
9.4. Interplay between Hydrophobic and H-bonding Interactions in TBA-Water Binary Mixtures.....	215
9.5. Excited State Intramolecular charge Transfer Reaction in Non-aqueous Reverse Micelles: Electrolyte Concentration Dependence .....	215
9.6. Probing Medium Dynamics by Charge Transfer Reaction in Catanionic Reverse Micelle .....	216
9.7. Charge Transfer Reaction in DTN in Electrolyte Solutions.....	216
9.8. Effects of Mixed Electrolytes on Excited State Intramolecular Charge Transfer Reaction.....	217
References .....	219
Appendices.....	221

# Chapter 1

## Introduction

Chemical reactions occurring in solutions are often considerably affected by the surrounding environment<sup>1-23</sup>. For a reaction where an activation barrier separates the reactant from the product, the medium effects mainly include the modification of the activation barrier and the rearrangement of the surrounding environment when the reactant crosses the barrier in order to form the product. As a result, a significant amount of effort has been devoted to understand the medium effects on a variety of chemical reactions, ranging from reactions that involve sizeable barriers to those with no barrier at all. While several studies have investigated the solvent effects on reactions that occur within a molecule (such as cis-trans isomerization and intramolecular charge transfer reactions), reactions requiring at least two separate molecules have also been looked at. The use of time resolved fluorescence spectroscopic techniques and the subsequent development of theoretical frameworks connecting the reaction rate to the medium friction have generated much of the present day understanding in this area of research.

In this Thesis we have studied the photo-induced intramolecular charge transfer (ICT) reaction in electrolyte solutions of solvents of differing polarity and associating character, in binary polar solvent mixtures, isotopically labeled solvents, and in confined environments created by reverse micelles of varying droplet sizes. These differing and complex environments are chosen in order to explore the solution dynamic effects on ICT reaction since the solvation time scales in these media have been found to be often in the range of a few hundreds of picoseconds to more than a nanosecond<sup>24-30</sup>. The connection between the solvation and reaction time scales have been explored elegantly by Hynes and coworkers<sup>31-32</sup> and this could

be briefly described as follows. Because the reaction time scale is determined by the inverse of the frequency ( $\omega_b$ ) with which the reactant crosses the barrier, the barrier crossing time scale lies in the range of a few picoseconds even for a broad barrier reaction. The much slower time scale of the environment reorganization then leads to the reaction to occur in a non-equilibrium situation where the reactant at each point during the barrier crossing is in 'improperly' solvated state. This produces extra solvent resistance to the reactive mode and is known as 'dynamic medium effects'. The change in static dielectric constant ( $\epsilon_0$ ) can also affect a reaction profoundly via the modification of the activation barrier. For example, increase (decrease) in static dielectric constant reduces (increases) the activation barrier which leads to the increase (decrease) in rate constant. This can be regarded as 'static medium effects'. The change in average solution polarity ( $\epsilon_0$ ) can be very easily induced by either dissolving electrolyte in a polar solvent or by adding another solvent component (as done in binary mixtures). In addition, confinement of polar solvent in organized assemblies reduces the dielectric constant appreciably<sup>33</sup>. Therefore, medium static and dynamic effects are expected to substantially affect an ICT reaction occurring in these complex media.

Since dissociation of a given electrolyte in a particular solvent depends on its concentration<sup>34-36</sup>, the effects of electrolyte on a reaction is expected to be more complex than what would be from the simple consideration of increase in the average solution dielectric constant. Conductivity studies reveal the presence of various types of ion-pairs in appreciable concentrations in electrolyte solutions containing moderate to large electrolyte concentration. These ion-pairs can act as effective dipoles which contribute significantly to the solvation energy of a dissolved polar solute molecule. In addition, the faster rotation (relative to translation) of these dipoles shifts the solvation energy relaxation time scales towards the relatively faster wing of the solution dynamics. However, in very dilute solutions where electrolyte dissociation is almost complete, the slow translational motion of the ions dominates the solvation time scale. Now if a reaction involves rotation of a dipolar moiety, the reactive mode is likely to experience an extra friction in dilute solutions (due to

stronger ion-dipole interaction) than in concentrated ones where the dipole-dipole interaction dominates. In such a situation, a competition between the frictional resistance induced by the ions and facilitation of the reaction by faster solution dynamics is expected to give rise to non-monotonic electrolyte concentration dependence of reaction time scale. The effects of electrolyte on ICT reaction rate in solutions of low to high electrolyte concentrations have been studied in detail in this Thesis and the relevant experimental results are presented in chapters 2 and 3. The validity of Zwan-Hynes theory<sup>31-32</sup> that connects the average solvation time with the reaction rate has also been tested for ICT reactions in solutions containing electrolyte in large concentrations (chapter 2).

Because solvent relaxation times and dielectric constant depend upon temperature, change in solution temperature can also modify ICT reaction rate via both static and dynamic medium effects. Since the temperature dependence of dielectric constant is much weaker than that of solvent viscosity, temperature induced solvent static effects via the barrier modulation is expected to be small. In such a situation, one can estimate the activation barrier by carrying out a temperature dependent study. However, there could be a temperature range for a given solvent where the change in temperature alters the dielectric constant appreciably. This means that the activation barrier itself depends on temperature at these solution conditions where the Arrhenius rate law becomes insufficient for describing the temperature dependence of the reaction rate. This also provides an opportunity to explore the validity of the Arrhenius rate law for the ICT reaction with the kind of molecules considered here at several electrolyte concentrations, ranging from very dilute solutions to highly concentrated ones in solvents of different polarities and associative characters. The activation energies for the ICT molecules determined from the temperature dependent study have been found to be in good agreement with the estimates from the quantum mechanical calculations<sup>37</sup>. In addition, the temperature dependence in dilute electrolyte solutions of moderately polar solvent (such as ethyl acetate) is found to be different from that in large concentrations. These results have been described in detail in chapter 4 of the present Thesis.

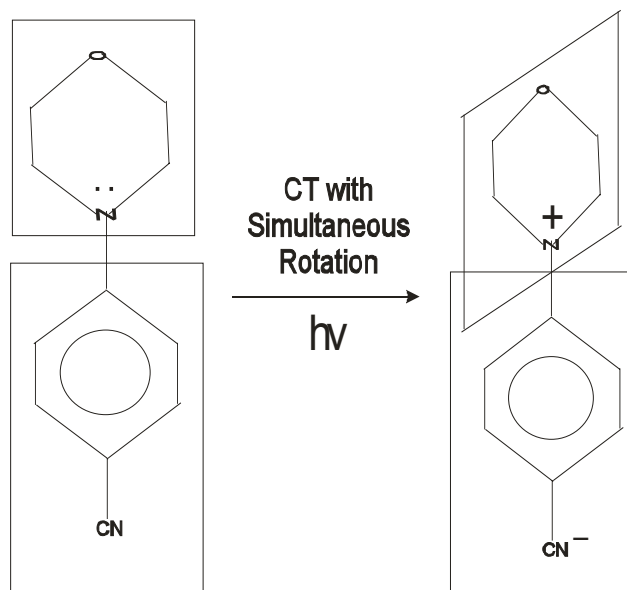
Recent experimental and theoretical studies have revealed that dipolar solvation dynamics for a photo-induced solute probe in isotopically labeled solvents is ~20% slower than those in unlabeled counterparts<sup>38-39</sup>. It is known that solvent isotope substitution leads not only to a small increase in static dielectric constant but slows down the relaxation times also. One therefore expects a competition between the solvent static and dynamic effects on an ICT reaction carried out in isotope-substituted solvents. Such a study have been carried out and reported in chapter 5 of the present Thesis. Note here that a couple of earlier studies report solute isotope effects on fluorescence life time, quantum yield and intersystem crossing yield. However, these studies have not investigated the solvent control of the reaction rate of ICT molecules in isotope-substituted solvents.

Microscopic heterogeneity in solution structure is another aspect that plays an important role in determining the rate of a reaction in solvent mixtures<sup>40</sup>. If the interaction among solvent molecules of same and different species leads to formation of domains with different relaxation time and polarity, reaction occurring in such media would likely to be affected by both the temporal and spatial heterogeneity<sup>41-43</sup>. Several experimental and simulation studies have indicated the presence of microscopic heterogeneity in aqueous mixtures of tertiary butyl alcohol (TBA) where strengthening of hydrogen bonding (H-bonding) has been found to dictate the solution structure at low alcohol concentrations<sup>44-58</sup>. The effects of TBA induced solution structure on ICT reaction have been explored and the experimental results are presented in chapter 6. The effects of solution structure on rotational dynamics have also been investigated by using a fluorescent non-reactive dye molecule which suggests that TBA induced structural transition can indeed be followed by monitoring the fluorescence dynamics of both reactive and non-reactive fluorescent molecules in these mixtures. This is also discussed in chapter 6 of the present Thesis. Last several years have witnessed intense efforts to understand the structure and dynamics of water molecules that are confined in aqueous micro-emulsion droplets of sub-nanometer to several nanometer dimensions<sup>24-26, 59-69</sup>. The motivation for

these studies stems largely from the desire to correlate the function of biologically active moieties with the structure and dynamics of water molecules that are present near to those active surfaces. A new term - 'biological water'<sup>70</sup> - has been coined to distinguish the water molecules near to the bioactive surfaces from those in the bulk and are believed to be responsible for normal functioning of the bioactive moiety or surface. Moreover, experimental and simulation studies have indicated that relaxation dynamics of and in biological water are much slower than those in the bulk<sup>71</sup>. Similar slowing down of dynamics in polar solvent pools confined in reverse micelles has also been repeatedly observed by several authors. Therefore, the sluggish dynamics coupled with the dramatic reduction in average dielectric constant is expected to significantly slow down the progress of a reaction that has an appreciable barrier to surmount. Recently, we have studied photo-induced intramolecular charge transfer reaction in aqueous reverse micelles and a dramatic slow down in the reaction time scale has been observed. The relevant results are presented in chapter 7. Subsequently, the effects of slowed down dynamics in confined media have been investigated on the catalytic activity of an enzyme in confinement. Experimental results seem to suggest that the activity of the enzyme studied is correlated with the slow dynamics of the medium. These results are discussed in chapter 8.

Since investigation of medium effects on photo-induced ICT reaction constitutes a major part of this Thesis, we briefly describe here the salient features of ICT reaction, the kinetic framework and the reactant molecules that have been used to study the complex environment effects. Excited state (photo-induced) intramolecular charge transfer reactions in substituted aminobenzonitrile derivatives have been an area of intense research for quite some time now.<sup>37, 72-75</sup> These molecules, upon photo-excitation, show an anomalously red-shifted fluorescence that occurs in addition to the normal fluorescence in polar solvents. The emergence of this red shifted fluorescence has been a matter of considerable debate and discussion.<sup>37, 74-84</sup> Even though several models have been proposed to understand the nature of the anomalously red shifted fluorescence, none of them could explain satisfactorily all

aspects of the excited state intramolecular charge transfer reaction. However, all these models attribute the anomalous fluorescence to an electronic state of charge transfer (CT) character. The state that emits normal fluorescence is assumed to possess charge distribution similar to that of the ground state and is termed as locally excited (LE) state. Upon photo-excitation, a substantial amount of charge is transferred from the amino group to the benzonitrile ring with some intramolecular rearrangement. Several mechanisms are in vogue to rationalize the intramolecular rearrangement although many experimental, theoretical and semi-empirical calculation studies support the twisted intramolecular charge transfer mechanism (TICT) <sup>78-86</sup>. In this mechanism, charge transfer occurs simultaneously with a twisting of the alkyl group from a conformation roughly coplanar with the benzonitrile ring to a perpendicular arrangement. This is shown in SCHEME 1.

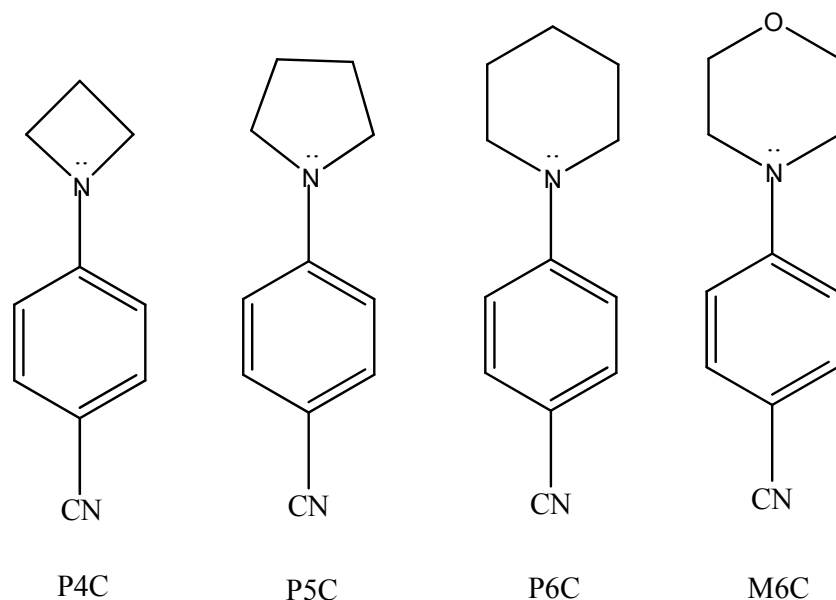


SCHEME 1

However, this model is also not universally accepted since there have been many experimental evidences <sup>76-77</sup> which are difficult to explain by using TICT mechanism.

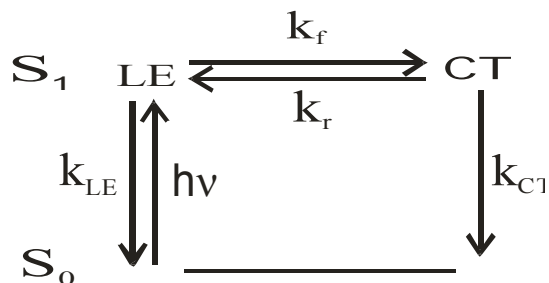
Recently, Maroncelli and coworkers <sup>37</sup> have studied the excited state charge transfer reactions of 4-(1-azetidiny) benzonitrile (P4C), 4-(1-pyrrolidinyl)benzonitrile (P5C)

and 4-(1-piperidiny)benzonitrile (P6C) in several solvents of varying polarity. The chemical structures of these molecules and another closely related molecule, 4-(1-morpholenyl)benzonitrile (M6C) are shown in SCHEME 2. Maroncelli and coworkers<sup>37</sup> have explained their results by assuming the validity of twisted intramolecular charge transfer



**SCHEME 2**

(TICT) mechanism and found that the rate of reaction in these molecules is substantially modified by the dynamical modes of the solvent in which the reaction is studied. SCHEME 3 represents photo-excitation of a TICT molecule and the subsequent formation of charge transferred (CT) state where  $k_f$  and  $k_r$  are respectively the forward and backward rate



SCHEME 3

constants.  $k_{LE}$  and  $k_{CT}$  represent the net (radiative *plus* non-radiative) rate constants for LE and CT states, respectively. Near to room temperature in polar solvents the interconversion between LE and CT states, which is the charge transfer reaction, is more rapid than the times associated with the population decay (inverse of  $k_{LE}$  and  $k_{CT}$ ) to the ground state ( $S_0$ ). Note that these rate constants are time independent quantities. As seen earlier and also later in this Thesis that Inter-conversion between LE and CT states is the charge transfer reaction. The rate of this inter-conversion depends *crucially* on two factors: intramolecular twisting and solvation<sup>37</sup>. Naturally therefore, modification of one of these factors affects the rate at which the reaction progresses. These molecules possess higher dipole moments in CT<sup>37</sup> states and hence formation of CT population is favored in polar solvents. We would like to mention here that we have synthesized the ICT molecules shown in SCHEME 2 in our laboratory following literature method.

Representative emission spectra of one of the ICT molecules in moderately polar (ethyl acetate) and non-polar (perfluorohexane) solvents are shown in Fig. 1.1. The presence of two distinct peaks in the emission spectrum in ethyl acetate and the absence of it in perfluorohexane clearly demonstrate that non-polar solvent does not support the formation of the CT state in this molecule. When one considers the kinetic framework shown in SCHEME 3 in order to explore the time evolution of LE and CT intensities, the following expressions are obtained<sup>37, 87</sup> (see Appendix 1 for the full derivation)

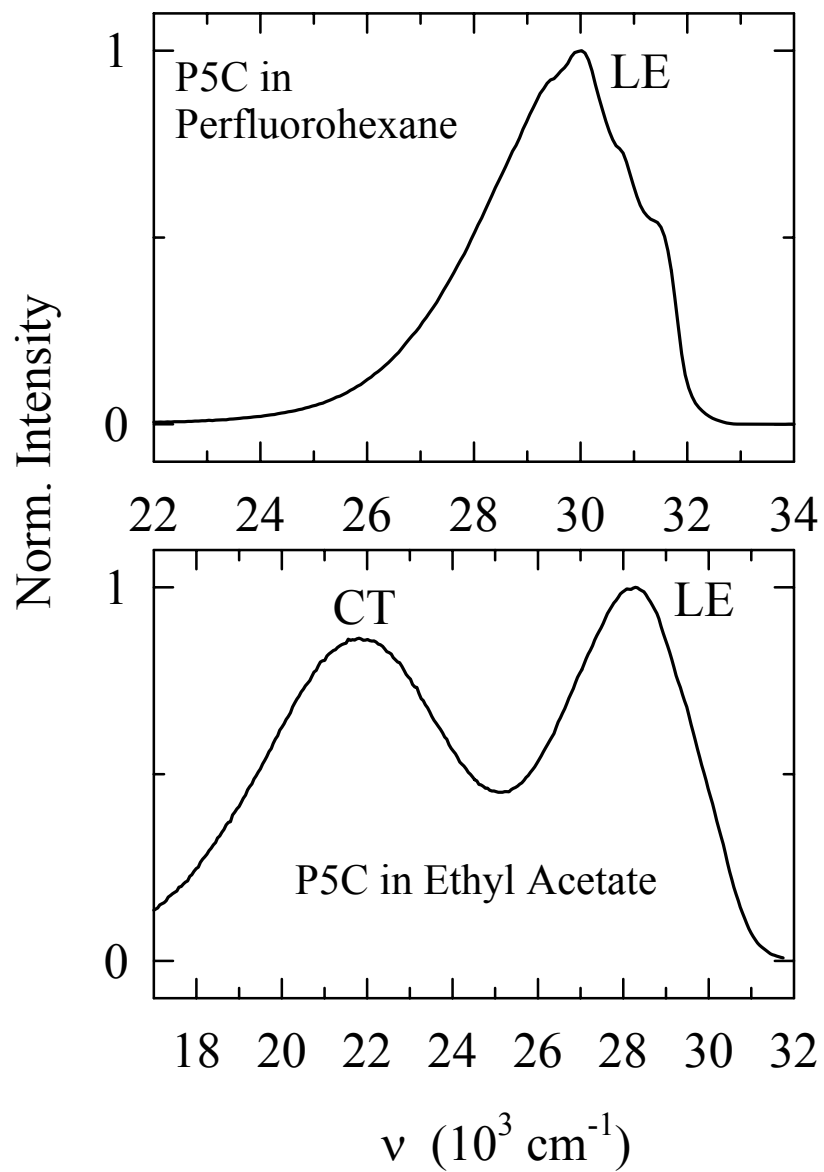


**Fig. 1.1:** Representative emission spectra of P5C in non-polar (perfluorohexane) and moderately polar (ethyl acetate) solvents.

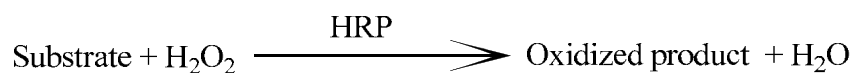
$$I_{LE}(t) \propto k_{LE}^{rad} \frac{[LE(t)]}{[LE(0)]} = k_{LE}^{rad} \frac{1}{\lambda_1 - \lambda_2} \left\{ (Y - \lambda_2)e^{-\lambda_2 t} + (\lambda_1 - Y)e^{-\lambda_1 t} \right\} \quad (1.1)$$

$$\text{and } I_{CT}(t) \propto k_{CT}^{rad} \frac{[CT(t)]}{[LE(0)]} = k_{CT}^{rad} \frac{k_f}{\lambda_1 - \lambda_2} \left\{ e^{-\lambda_2 t} - e^{-\lambda_1 t} \right\}, \quad (1.2)$$

where  $k_{LE}^{rad}$  and  $k_{CT}^{rad}$  denote respectively the rate constants associated with the LE and CT population decays to the ground state. Eqs. 1.1 and 1.2 indicate that in polar environments the time evolution of the LE intensity should be characterized by a fast and a slow decay components with very different time constants whereas that of CT intensity should describe a fast rise followed by a slow decay. The time constant associated with the fast component of either the LE or CT intensity decay can then be considered as the time constant associated with the LE  $\rightarrow$  CT conversion reaction. The relatively longer time constant then describes the time scale associated with the population decay from the S<sub>1</sub> to the S<sub>0</sub> state. This should be the scenario irrespective of the monitoring wavelength across either the LE or CT bands. However, in non-polar solvents where the charge transfer reaction is not supported, one expects a single exponential decay across the fluorescence emission spectrum of the ICT molecule.

It has been observed earlier that the two state reversible interconversion reaction scheme depicted in SCHEME 3 and considered above can successfully describe the time dependence of the LE and CT emission intensities of these ICT molecules in neat polar solvents. Interestingly, the complex environments that have been studied in the present Thesis gives rise to the bi-exponential decay of the time dependent LE intensities of these molecules. In addition, the decay profiles at various temperatures can also be described adequately by bi-exponential functions of time. These observations lend further support to the general validity of the reaction scheme discussed above.

Next we describe the effects of confinement on the enzymatic activity of horseradish peroxidase in aqueous micro emulsion droplets. It is known that every enzyme has a characteristic three-dimensional structure which is prerequisite for its activity and is maintained by hydrogen bonding and hydrophobic interaction with environments. Horseradish peroxidase (HRP) is a glycoprotein containing 18% carbohydrate with heme (iron protoporphyrin) as prosthetic group<sup>88-89</sup>. It is stable and active over a broad pH and temperature range which makes it utility for different purposes in various media<sup>90-92</sup>. Enzymes, in general, show high selectivity on the nature of the catalyzed substrate and on the mode of interaction with the substrate itself. HRP can oxidize small aromatic molecules which can approach the porphyrin ring. These include phenols, biphenols, anilines, benzidines and related heteroaromatic compounds. HRP oxidizes substrates in presence of hydrogen peroxide (H<sub>2</sub>O<sub>2</sub>) with the production of oxidized product and H<sub>2</sub>O as byproducts<sup>93</sup>.



The kinetics of substrate oxidation catalyzed by horseradish peroxidase enzyme i.e., the enzymatic activity can be monitored spectrophotometrically by using UV-VIS spectrophotometer. Note here that the catalytic activity of the enzyme (HRP) in reverse micelles at various droplet sizes has not been studied in this Thesis. Rather, a correlation between the solvent dynamical time scales and the activity has been attempted by studying polar solvation and fluorescence depolarization dynamics in these microemulsion droplets. As already mentioned, results presented in chapter 8 appear to suggest that the activity of HRP in confined environment is correlated with the slow dynamics of the medium.

Since concluding remarks will be presented separately in each of the chapters (chapters 2-8), a separate chapter is not provided for the overall conclusion. However, we take this opportunity to discuss several future problems which should be studied for better understanding of the effects discussed in the Thesis (chapter 9).

## References:

1. Fleming, G. R. ; Wolynes, P.G. *Phys. Today* **1990**, 43, 36
2. Voth, G.A.; Hochstrasser, R.M. *J. Phys. Chem.* **1996**, 100, 13034 and references therein.
3. Mukamel, S.; Yan, Y.J. *Acc. Chem. Res.* **1989**, 22, 301 and references therein
4. Kramers, H.A. *Physica* **1940**, 7, 284
5. Grote, R.F.; Hynes, G.T. *J. Chem. Phys.* **1980**, 73, 2715
6. Hangii, P.; Talkner, P.; Berkovec, M. *Rev. Mod. Phys.* **1990**, 62, 250
7. Makinen, M.W.; Schichman, S.A.; Gill, S.C. ; Gray, H.B. *Science* **1983**, 222, 929
8. Closs, G.L.; Miller, J.R. *Science* **1988**, 240, 440
9. Mclendon, G. *Acc. Chem. Res.* **1988**, 21, 160
10. Kosower, E.M.; Huppert, D. *Annu. Rev. Phys. Chem.* **1986**, 37, 127
11. Marcus, R. A.; Sutin, N.; *Biochem. Biophys. Acta* 1985, 811, 275 ; Sumi, H.; Marcus, R.A. *J. Chem. Phys.* **1986**, 84, 4894
12. Barbara, P.F.; Jarzeba, W. *Adv. Photochem.* **1990**, 15, 1
13. (a) Fleming, G.R. *Chemical Applications of Ultrafast Spectroscopy* (Oxford University Press, 1986) (b) *Femtosecond Reaction Dynamics*; edited by Wiersma, D.A. (North Holland, Amsterdam, 1994); *Femtochemistry : Ultrafast Dynamics of the Chemical Bond*; edited by Zewail, A.H. (World Scientific, Singapore, 1994).
14. Hynes, J.T.; *Annu. Rev. Phys. Chem.* **1985**, 36, 573; Simon, J.D. *Acc. Chem. Res.* **1988**, 21, 128; Rossky, P.J.; Simon, J.D. *Nature* 1994, 370, 263

15. (a) Bagchi, B. *Annu. Rev. Phys. Chem.* **1989**, *40*, 115 (b) Bagchi, B.; Chandra, A. *Adv. Chem. Phys.* **1991**, *80*, 1
16. Roy, S.; Bagchi, B. *J. Chem. Phys.* **1995**, *102*, 7937; Roy, S. ; Bagchi, B. *J. Chem. Phys.* **1995**, *102*, 6719
17. Bagchi, B.; Gayathri, N. *Adv. Chem. Phys.* **1999**, *107*, 1, Special Issue “*Electron Transfer Reactions - From Isolated Molecules to Bio-molecules*” edited by Jortner, J.; Bixon, M.; Gayathri, N.; Bagchi, B. *J. Phys. Chem.* **1996**, *100*, 3056; *ibid. J. Chem. Phys.* **1996**, *93*, 1652
18. Mukamel, S.; *Adv. Chem. Phys.* **1988**, *70*, 165 (Part 1); Mukamel, S.; Loring, R.F. *J. Opt. Soc. Am.* **1986**, *B3*, 595; Yan, Y. J. ; Mukamel, S. *J. Chem. Phys.* **1987**, *87*, 5840; Sparpaglione, M.; Mukamel, S. *J. Chem. Phys.* **1988**, *88*, 3263; *ibid. J. Chem. Phys.* **1988**, *88*, 4300; Yan, Y.J. ; Sparpaglione, M.; Mukamel, S. *J. Phys. Chem.* **1988**, *92*, 4842
19. Hochstrasser, R.M.; *Pure Appl. Chem.* **1980**, *52*, 2683; Hochstrasser, R.M.; Wiesman, R.B. *In Radiationless Transitions*; edited by Lin, S.H. (Academic Press, New York, 1982 )
20. Waldeck, D.H. *Chem. Rev.* **1991**, *91*, 415 and references therein
21. *Activated Barrier Crossing*, edited by Fleming, G.R.; Hangii, P. (World Scientific, Singapore, **1993**)
22. Heitele, H. *Angew. Chem. Int. Ed. Engl.* **1993**, *32*, 359
23. Weaver, M.J. *Chem. Rev.* **1992**, *92*, 463; Weaver, M.J.; McMannis III, G.E. *Acc. Chem. Res.* **1990**, *23*, 294
24. Levinger, N. E. *Science*, **2002**, *298*, 1722.
25. Bhattacharyya, K. *Acc. Chem. Res.* **2003**, *36*, 95 and references therein.
26. Ghosh, S.; Mandal, U.; Adhikari, A.; Dey, S.; Bhattacharyya, K. *Int. Rev. Phys. Chem.* **2007**, *26*, 421.
27. Chapman, C.F.; Maroncelli, M. *J. Phys. Chem.* **1991**, *95*, 9095

28. Huppert, D.; Ittah, V.; Kosower, M. *Chem. Phys. Lett.* **1989**, *159*, 267
29. Bart, E.; Huppert, D. *Chem. Phys. Lett.* **1992**, *195*, 37
30. Itah, V.; Huppert, D. *Chem. Phys. Lett.* **1990**, *173*, 496
31. Van der Zwan, G. , Hynes, J. T. *Chem. Phys.* **1991**, *152*, 169.
32. Hynes, J. T., Simon, J. D. (editor): *Charge -Transfer Reactions and Solvation Dynamics in Ultrafast Dynamics of Chemical Systems*, Kluwer, Dodrecht, (1994); p.345.
33. Biswas, R., Rohman, N., Pradhan, T., Buchner, R. *J. Phys. Chem. B.* **2008**, *112*, 9379.
34. Barthel, J.; Deser, R. *J. Solution Chem.* **1994**, *23*, 1133.
35. Barthel, J.; Kleebauer, M.; Buchner, R. *J. Solution Chem.* **1995**, *24*, 1.
36. Barthel, J.; Wachter, R.; Gores, H. J. *In Modern Aspects of Electrochemistry*; Conway, B. E.; Bockris, J. O'M., Eds. Plenum, New York, 1979, Vol. 13, p.1.
37. Dahl, K.; Biswas, R.; Ito, N.; Maroncelli, M. *J. Phys. Chem. B*, **2005**, *109*, 1563.
38. Nandi, N.; Roy, S.; Bagchi, B., *J. Chem. Phys.* **1995**, *102*, 1390.
39. Zolotov, B.; Gan, A.; Fainberg, B.D.; Huppert, D., *J. Luminesce*, **1997**, *72-74*, 842.
40. Jin, H.; Li, X; Maroncelli, M. *J. Phys. Chem. B* **2007**. *111*, 13473
41. Mandal, P.K.; Sarkar, M.; Samanta, A. *J. Phys. Chem. A* **2004**. *108*, 9048
42. Adhikari, A.; Sahu, K.; Dey, S.; Ghosh, S.; Mandal, U.; Bhattacharya, K. *J. Phys. Chem. B*, **2007**, *111*, 12809
43. Jin, H.; Baker, G.A.; Arzhantsev, S.; Dong, J.; Maroncelli, M. *J. Phys. Chem. B* **2007**, *111*, 7291
44. Dixit, S.; Crain, J.; Poon, W. C. K.; Finney, J. L.; Soper, A. K. *Nature* **2002**, *416*, 829.
45. Soper, A. K.; Finney, J. L. *Phys. Rev. Lett.* **1993**, *71*, 4346.
46. Iwasaki, K.; Fujiyama, T. *J. Phys. Chem.* **1979**, *83*, 463; **1977**, *81*, 1908.
47. Euliss, G. W.; Sorensen, C. M.; *J. Chem. Phys.* **1984**, *80*, 4767.

48. Nishikawa, K.; Kodera, Y.; Iijima, T. *J. Phys. Chem.* **1987**, *91*, 3694.
49. Nishikawa, K.; Iijima, T. *J. Phys. Chem.* **1993**, *97*, 10824.
50. Koga, Y. *Chem. Phys. Lett.* **1984**, *111*, 176.
51. Murthy, S. S. N.; *J. Phys. Chem. A* **1999**, *103*, 7927.
52. Sato, T.; Buchner, R. *J. Chem. Phys.* **2003**, *119*, 10789.
53. Yoshida, K.; Yamaguchi, T. *Z. Naturforsch. A* **2001**, *56*, 529.
54. Wojtkow, D.; Czarnecki, M. *J. Phys. Chem. A* **2005**, *109*, 8218.
55. Kusalik, P. G.; Lyubartsev, A. P.; Bergman, D. L.; Laaksonen, A. *J. Phys. Chem. B* **2000**, *104*, 9533.
56. Nakanishi, K.; Ikari, K.; Okazaki, S.; Touhara, H. *J. Chem. Phys.* **1984**, *80*, 1656.
57. Yoshida, K.; Yamaguchi, T.; Kovalenko, A.; Hirata, F. *J. Phys. Chem. B* **2002**, *106*, 5042.
58. Omelyan, I.; Kovalenko, A.; Hirata, F. *J. Theo. Comput. Chem.* **2003**, *2*, 193.
59. Balasubramanian, S.; Bagchi, B. *J. Phys. Chem. B* **2001**, *105*, 12529.
60. Das, S.; Datta, A.; Bhattacharyya, K. *J. Phys. Chem. A* **1999**, *101*, 3299.
61. Sarkar, N.; Das, K.; Datta, A.; Das, S.; Bhattacharyya, K. *J. Phys. Chem.* **1996**, *100*, 10523.
62. Datta, A.; Mandal, D.; Pal, S. K.; Bhattacharyya, K. *J. Phys. Chem. B* **1997**, *101*, 10221.
63. Riter, R. E.; Willard, D. M.; Levinger, N. E. *J. Phys. Chem. B* **1998**, *102*, 2705.
64. Moilanen, D. E.; Levinger, N. E.; Spry, D. B.; Fayer, M. D. *J. Amer. Chem. Soc.* **2007** *129*, 14311.
65. Tan, H-S. ; Piletic, I. R.; Fayer, M. D. *J. Chem. Phys.* **2005**, *122*, 174501.
66. Piletic, I. R.; Tan, H-S.; Fayer, M. D. *J. Phys. Chem. B* **2005**, *109*, 21273.
67. Faeder, J.; Ladanyi, B. M. *J. Phys. Chem. B* **2001**, *105*, 11148.
68. Faeder, J.; Ladanyi, B. M. *J. Phys. Chem. B* **2000**, *104*, 1033.
69. Bhattacharyya, K. ; Bagchi, B. *J. Phys. Chem. A* **2000**, *104*, 10603.
70. Nandi, N.; Bagchi, B. *J. Phys. Chem. B* **1997**, *101*, 10954
71. Pal, S. K.; Peon, J.; Bagchi, B.; Zewail, A. H. *J. Phys. Chem. B.* **2002**, *106*,

12376.

72. Grabowski, Z. R.; Rotkiewicz, K.; Rettig, W. *Chem. Rev.* **2003**, *103*, 3899.
73. Lippert, E.; Rettig, W.; Bonacic-Koutecky, V.; Heisel, F.; Mische, J. A. *Adv. Chem. Phys.* **1987**, *68*, 1.
74. Zachariasse, K. A.; Druzhinin, S. I.; Bosch, W.; Machinek, R. *J. Am. Chem. Soc.* **2004**, *126*, 1705.
75. Techert, S.; Zachariasse, K. A., *J. Am. Chem. Soc.* **2004**, *126*, 5593.
76. Zachariasse, K. A. *Chem. Phys. Lett.* **2000**, *320*, 8.
77. Zgierski, M. Z.; Lim, E. C. *Chem. Phys. Lett.* **2004**, *393*, 143.
78. Rettig, W. *J. Luminesc.* **1980**, *26*, 21; *J. Phys. Chem.* **1982**, *86*, 1970
79. Rettig, W.; Gleiter, R.; *J. Phys. Chem.* **1985**, *89*, 4674.
80. Rettig, W.; Wermuth, G. *J. Photochem.* **1985**, *28*, 351; Al-Hassan, K. A.; Rettig, W. *Chem. Phys. Lett.* **1986**, *126*, 273; LaFemina, J. P.; Duke, C. B.; Rettig, W. *Chem. Phys.* **1990**, *87*, 2151; Braun, D.; Rettig, W. *Chem. Phys.* **1994**, *180*, 231; *Chem. Phys. Lett.* **1997**, *268*, 110.
81. Rettig, W. *Ber. Bunsen-Ges. Phys. Chem.* **1991**, *95*, 259.
82. Yatsushashi, T.; Trushin, S. A.; Fuss, W.; Rettig, W.; Schmid, W. E.; Zilberg, S. *Chem. Phys.* **2004**, *296*, 1.
83. Zachariasse, K. A.; Grobys, M.; von der Haar, T.; Hebecker, A.; Il'ichev, Y. V.; Jiang, Y.-B.; Morawski, O.; Kuhnle, W.; *J. Photochem. Photobiol. A* **1996**, *102*, 59.
84. Rettig, W.; Zeitz, B. *Chem. Phys. Lett.* **2000**, *317*, 187.
85. Maroncelli, M. *private communication*.
86. Parusel, A. B. *J. Chem. Phys. Lett.* **2001**, *340*, 531.
87. Laws, W. R.; Brand, L. J. *Phys. Chem.* 1979, *83*, 795
88. Veitch, N. C. *Phytochemistry* **2004**, *65*, 249.
89. Berglund, G. I.; Carlsson, G. H.; Smith, A. T.; Szołke, H.; Henriksen, A.; Hajdu, J. *Nature* **2002**, *417*, 463.
90. Laszlo, J. A.; Compton, D. L. *J. Mol. Catal. B* **2002**, *18*, 109.
91. Smith, K.; Silvermail, N. J.; Rodger, K. R.; Elgren, T. E.; Castro, M.; Parker, R. M. *J. Am. Chem. Soc.* **2002**, *124*, 4247.

92. Klibanov, A. M. *Nature* **2001**, *409*, 241

93. Dunford, H. B. *CBC* **1998**, *3*, 195

## Chapter 2

### Excited State Intramolecular Charge Transfer Reaction in Electrolyte Solutions

#### 2.1. Introduction

As already discussed in chapter 1, addition of electrolyte in a polar solvent changes the solution polarity and hence affect reaction rate via modulating the activation barrier. However, electrolyte solutions at moderate to high concentrations in strongly polar solvents and even at low concentrations in weakly polar solvents contain free ions, ion-pairs (solvent shared and solvent separated), triple ions and neutral triple ions in varying proportions<sup>1-31</sup>. For example, dielectric and infrared spectroscopic studies of perchlorates salts of alkali and alkaline earth metal ions in acetonitrile at room temperature<sup>4</sup> suggest that contact ion-pair concentration increases from ~10 % to about 50% for LiClO<sub>4</sub> and to about 30% for NaClO<sub>4</sub> for increasing the electrolyte concentration from 0.1 M to 0.9 M. On the other hand, solvent separated ion-pair concentration decreases from ~10% with electrolyte concentration to almost negligible proportion at higher concentrations<sup>4</sup>. For Mg (ClO<sub>4</sub>)<sub>2</sub> and Ca (ClO<sub>4</sub>)<sub>2</sub>, however, the estimated concentration of contact ion-pair is large (~30-50 %,.) even at 0.1M and varies non-monotonically with electrolyte concentration. Moreover, appreciable amount of triple and neutral triple ions are present in solutions of these bivalent metal perchlorates in acetonitrile<sup>4</sup>. Conductivity studies of LiClO<sub>4</sub> solutions in ethyl acetate<sup>1, 6, 23-28</sup> suggest that ion-pair concentration is appreciable even at electrolyte concentration as low as 0.01 M. In addition, the formation of triple ions is found to make a significant contribution to the overall conductivity, suggesting strong ion-solvent interactions leading to structure enhanced ion association<sup>24, 32</sup> and formation of composite species such as triple ions, cyclic ion-pair dimer and apolar aggregates. The ion-pairs are characterized by large dipole moments<sup>1, 4-5</sup> which take part in modifying the interaction of a polarity probe with the environment and its dynamics. Moreover, the presence of other composite species significantly affect the

structure and hence dynamics of the medium through Coulomb and non-Coulomb interactions<sup>32</sup>. Therefore, reactions occurring in these media would be affected in a more complicated manner than expected from the enhanced polarity of the medium alone.

Further inputs to the understanding of electrolyte solutions originate from the studies on solvation dynamics in electrolyte solutions<sup>1-3, 33</sup>. Dynamics of electrolyte solutions is expected to be very different from that of pure polar solvents since the ion-atmosphere relaxation and time dependent ion-solute interaction dominate the ionic solution dynamics at low electrolyte concentrations<sup>1-3, 33</sup>. At higher concentration, the solution dynamics is even more complex due to the presence of triple ion, ion pairs (solvent shared and solvent separated) and other non-polar ion-solvent composite species<sup>1-6</sup>. Several authors have already studied the dynamics of electrolyte solutions in solvents of varying polarity and found that electrolyte solution dynamics is characteristically different from that of the pure solvent<sup>1-3, 33</sup>. The reaction rate is affected in a more complex manner than the dynamical solvent modes because of the following reasons. The experimentally observed dynamics in electrolyte solutions is at least 1000 times slower than the microscopic time scale for barrier crossing which is in the order of 1 ps even for a fairly broad-barrier reaction.<sup>34-35</sup> This means that the ion-atmosphere remains out of equilibrium during barrier crossing. If we now assume that the TICT mechanism is valid for these molecules, this non-equilibrium ion-atmosphere would exert more electrodynamic friction<sup>34</sup> on the twisting mode. Consequently, the TICT reaction rate will be substantially modified. Since the dynamics becomes faster with the increase in electrolyte concentration, the coupling between the reactive mode and the environment dynamics becomes further modified. This modification also contributes to the electrolyte concentration dependence of the LE→CT conversion rate. As correctly pointed out in Ref.34, experimental studies are required to determine the effects of such concentration dependent non-equilibrium solvation. The present study is an attempt towards this direction.

In this chapter we report steady state and time resolved spectroscopic results on the excited state intramolecular charge transfer reactions of 4-(1-azetidyl)benzonitrile

(P4C), 4-(1-pyrrolidiny)benzonitrile (P5C) and 4-(1-piperidiny)benzonitrile (P6C) in electrolyte solutions of several alkali and alkaline earth metal perchlorates at different concentrations. We use the TICT model to analyze our data as done earlier<sup>36</sup>. Note here that the above three compounds were first studied by Rettig and co-workers<sup>37-41</sup>. Zachariasse and his group<sup>42</sup> investigated the excited state charge transfer reaction in the above group of compounds containing three to eight-membered rings and represented them as  $P_nC$  series ( $n$  being the number of atoms constituting the ring). In addition to these experimental studies, semi-empirical<sup>43-44</sup>, density functional<sup>45</sup> and ab-initio calculations<sup>44</sup> have also been carried out with these molecules. However, studies of electrolyte effects on TICT reactions have not been performed before and such a study is reported here for the first time to the best of our knowledge. In addition, we have performed similar steady state spectroscopic studies with a non-reactive probe, namely, coumarin 153 (C153) in these electrolyte solutions in order to compare the electrolyte effects on a non-reactive excited state. Note here that similar studies with C153 in acetonitrile and ethyl acetate in presence of 1.0 M  $\text{LiClO}_4$  or  $\text{NaClO}_4$  have already been carried out<sup>1, 33</sup>. Our studies with C153 in these solvents at higher electrolyte concentrations indicates a natural extension of the low concentration data already reported in the literature<sup>1-3, 33</sup> and hence are complimentary to these earlier data.

The choice of ethyl acetate as low polarity solvent comes from its ability to dissolve a large amount of  $\text{LiClO}_4$  which provides an opportunity to study the effects of electrolyte on TICT reaction for a wide range of electrolyte concentrations. The cation size dependence of the average reaction rate in ethyl acetate has also been investigated. It has been found that the theory developed by Zwan and Hynes (ZH) for studying isomerization reactions in electrolyte solutions<sup>34</sup> can be applied to understand the observed electrolyte concentration dependence of reaction rate in these TICT molecules. We have used the kinetic framework as discussed in Ref.36 to analyze our time resolved emission data reported in this chapter. This means that the reaction is assumed to be in the rapid equilibration limit and a biexponential decay of intensity with time is expected. We would like to mention here that the rapid

equilibration limit may not be realized in electrolyte solutions since the solution dynamics is considerably slower. However, a biexponential function with two different time constants is found to be sufficient to fit the time dependent intensity decay for all combinations with P4C and P5C. For P6C, however, a tri-exponential function is required to properly fit the intensity decays. The average reaction time constant falls off exponentially with electrolyte concentration and decreases linearly as  $z/r_{\text{ion}}$  ( $z$  being the valence on the ion) increases. At all electrolyte concentrations ( $\geq 0.10$  moles-litre<sup>-1</sup>) in ethyl acetate, the observed average reaction rate for these TICT molecules is found to be in good agreement with the prediction from the theory by Zwan and Hynes<sup>34</sup> in the broad barrier overdamped limit with barrier frequency,  $\omega_b \approx 2 \times 10^{12} \text{ s}^{-1}$ . The other parameters necessary for calculating the average rates from the ZH theory<sup>34</sup> are obtained from the relevant experiments.

The organization of the rest of the chapter is as follows. Experimental details are given in the next section. Section 2.3 contains experimental results from our steady state and time resolved spectroscopic studies. Supporting information is given in Appendix 2. The article then ends with concluding remarks in section 2.4.

## 2.2. Experimental Details

4-(1-azetidiny) benzonitrile (P4C), 4-(pyrrolidiny) benzonitrile (P5C) and 4-(1-piperidiny) benzonitrile (P6C) were synthesized by following the protocol given in Ref.37. P4C and P6C were re-crystallized from cyclohexane (Merck, Germany) and P5C from kerosene-free petroleum ether (re-crystallized thrice). Purity of these compounds were checked by thin layer chromatography and monitoring the excitation wavelength dependence of fluorescence emission. Coumarin 153 was purchased from Exciton and used as received.

Ethyl acetate and acetonitrile were used as received (spectrophotometric grade) from Aldrich. Tetrabutylammonium perchlorate (<sup>t</sup>Bu<sub>4</sub>NClO<sub>4</sub>), lithium perchlorate (LiClO<sub>4</sub>), sodium perchlorate (NaClO<sub>4</sub>), magnesium perchlorate (Mg (ClO<sub>4</sub>)<sub>2</sub>),

calcium perchlorate ( $\text{Ca}(\text{ClO}_4)_2$ ), strontium perchlorate ( $\text{Sr}(\text{ClO}_4)_2$ ) were obtained from either Aldrich or Fluka (anhydrous and/or highest available grade) and vacuum dried before use. Solutions were prepared by dissolving a measured amount of electrolyte in 10 ml volumetric flask and stirring the solution for half-an-hour. Caution was exercised to ensure the complete dissolution of the added electrolyte. An aliquot of this stock solution was then transferred into a quartz cuvette of optical path length 1 cm. Subsequently, a small grain of solute (P4C / P5C / P6C) was dissolved and stirred the solution for about 10 minutes and absorption spectrum recorded (Model UV-2450, SHIMADZU). The emission spectra were recorded (SPEX Fluoromax-3, Jobin-Yvon, Horiba) after adjusting the absorbance of the solution to 0.1 or less with excitation wavelength fixed at 305 nm. This wavelength was chosen to minimize the loss of the fluorescence spectrum at both blue and red ends. Solvent blanks were subtracted from the emission spectra prior to analysis and converted to frequency representation after properly weighting the intensity with  $\lambda^2$ . A few samples were bubbled with dry argon gas to investigate the effects of dissolved oxygen on the absorption and emission spectra. These initial runs showed very little or no effects on the overall appearance of the spectra and hence most of the samples were not deoxygenated. This was also the observation in one of the earlier studies with these TICT molecules<sup>36</sup>.

We then deconvoluted each emission spectrum into two fragments by using emission spectrum of the corresponding TICT molecule in perfluorohexane as reference<sup>36</sup>. This deconvolution provided area under each fragment (measure of population under a particular band) which was then used to calculate the equilibrium constants and change in reaction free energies for the LE to CT conversion. Emission peak frequencies were calculated as follows. Shifts of the emission spectra from the peak of the reference emission spectrum were calculated and added to the *average* peak frequency of the reference emission spectrum. The *average* of the reference emission peak was calculated by averaging the numbers obtained by fitting the upper half of the reference emission spectrum with an inverted parabola, first moment and the arithmetic mean of the frequencies at half intensities on both blue and red ends of the emission spectrum<sup>46-47</sup>. Absorption peak frequencies were obtained by calculating

the first moments of the absorption spectra. Conductivity measurements of electrolyte solutions were performed using a multimeter (Sension<sup>TM</sup> 378, Hach) fitted with a conductivity cell of cell constant 0.45 ( $\pm 10\%$ ). The electrode was dipped in the sample until equilibrium was reached and reading becomes stable. After proper calibration, selected samples were checked three times and no significant differences were observed. Life time data for measuring radiative and non-radiative rates for the TICT molecules and C153 in electrolyte solutions were obtained from time-correlated single photon counting (Lifespec, Edinburgh Instruments) apparatus with excitation wavelengths at 299 nm and 293 nm for TICT molecules, and 409 nm for C153. Time resolved emission studies have been performed using time correlated single photon counting (TCSPC) instrument based on a ps Ti:sapphire laser with excitation light at wavelength ( $\lambda$ ) at 293 nm (third harmonic). The detail of this instrumentation is discussed elsewhere<sup>48</sup> and hence only brief information will be given here. The emission fluorescence has been collected at magic angle at both LE and CT peak positions (of steady state spectrum) with an emission band pass of 8 nm. The effective resolution (full width at half maximum) of the instrument response function (IRF) is approximately 50 ps. Subsequently, collected decays have been de-convoluted from the IRF and fitted to multi-exponential function using an iterative reconvolution algorithm. Such fitting enables one to capture decay kinetics with time constant as fast as  $\sim 10$  ps with reasonable accuracy<sup>36</sup>, the rate data for P5C and P6C at higher electrolyte concentration might be trusted with some confidence. For a few cases, emission decays have been collected at two or three different emission wavelengths around the LE and CT peaks and average data have been shown for them. Note that in such cases the data associated with different wavelengths are found to vary *insignificantly* and hence regarded as fluctuation. Therefore, these small variations do not seem to indicate any different relaxation process or different species involved.

Since the average solvation time is required for rate calculation from ZH theory, we have also measured average solvation time of a polarity probe in electrolyte solutions of ethyl acetate. Time resolved emission spectra at each electrolyte concentration

have been constructed from a series of 18 – 22 emission decays at equally spaced wavelengths across the steady state emission spectrum of coumarin 153 (C153)<sup>46</sup> collected via time correlated single photon counting (TCSPC) method by using a diode laser based system (Lifespec-ps, Edinburgh, UK). A diode laser is used to provide 409 nm light as excitation. The effective resolution (fwhm) of the instrument response function is ~75 ps. Note that this resolution might miss the relatively faster component of the solvent response in ethyl acetate in presence of electrolyte but is expected to capture the long time dynamics well. Same instrumental set up has been used to collect emission decays of P4C at LE & CT peaks with 299 nm light as excitation. The effective resolution (fwhm) of the instrument response function with 299 nm excitation source is ~475 ps. All the measurements reported here were performed at  $T = 298.15 \pm 0.1$  K, unless otherwise mentioned.

### **2.3. Results & Discussion**

Let us first begin with the conductivity of  $\text{LiClO}_4$  solutions in ethyl acetate that have been measured up to 2.5 M. The results are shown in Fig. 2.1. Conductivity data for the same solutions up to 1.0 M reported by Huppert et al<sup>1</sup> are also shown in the same figure for comparison. As usual, the conductivity of the solution decreases with the addition of electrolyte at low  $\text{LiClO}_4$  concentration and then increases. The increase in conductivity after initial drop is well-known and has been explained in terms of triple ion formation<sup>7-8</sup>.

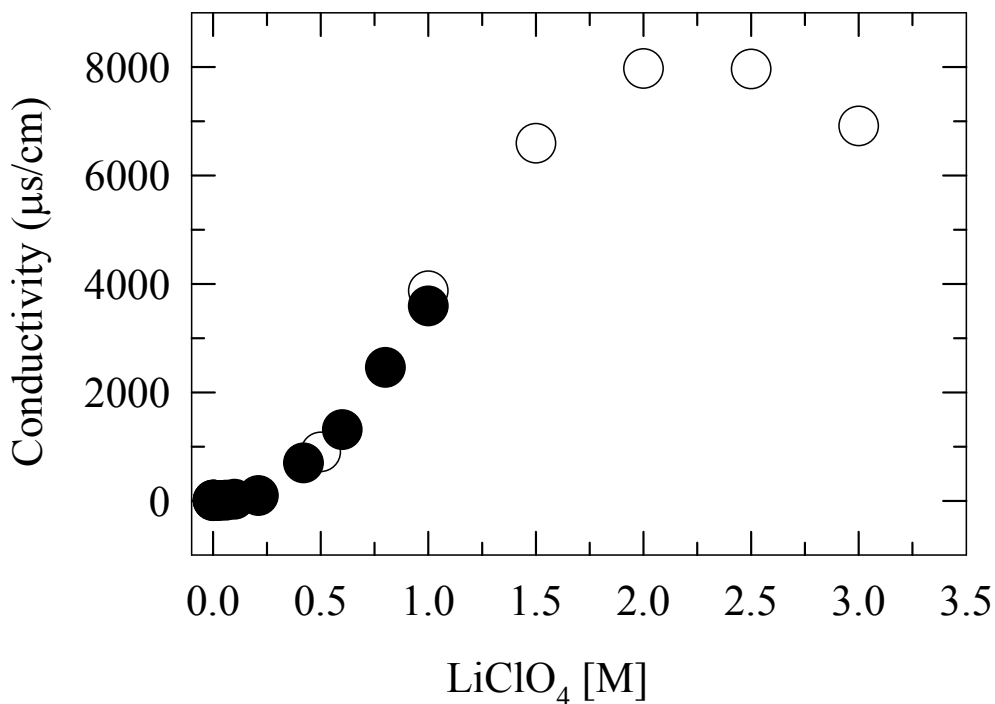


**Fig.2.1:** Conductivity of LiClO<sub>4</sub> solutions in ethyl acetate. Open circles represent the conductivity data recorded by us. Filled circles represent the data reported by Huppert and coworkers (Ref. 1).

Fuoss-Krauss analysis of experimental conductivity of LiClO<sub>4</sub> in ethyl acetate up to 1.0 M by Huppert and coworkers<sup>1</sup> indicates that the concentrations of ion pair and triple ion increase with electrolyte concentration. Moreover, concentrations of both ion pair and triple ion become at least an order of magnitude larger than that of free ion at ~0.02 M. The present data clearly indicate that the concentration of triple ion continues to increase even up to 2.0 M and then decreases probably due to the formation of dipolar or apolar species at concentrations higher than 2.0 M. Fourier transformed infra-red and dielectric spectroscopic studies, as done with electrolyte solutions in acetonitrile<sup>4</sup> and other solvents<sup>49</sup>, would have been very useful to estimate the concentration of various ionic, polar and apolar species in the medium. However, even without those studies, it is obvious that ion-pair and triple ions are

present in these solutions at large proportions and their effects on TICT reactions will be significant.

### 2.3.1. Spectral Properties

Representative absorption and emission spectra of P4C in several concentrations of LiClO<sub>4</sub> in ethyl acetate and acetonitrile are shown in Fig.2.2. Similar absorption and emission spectra for P5C and P6C are provided in Appendix 2 (figures A1 and A2). It is interesting to note that the solubility of LiClO<sub>4</sub> in ethyl acetate is more than that in acetonitrile though the static dielectric constant ( $\epsilon_0$ ) of the former is 6 times less than that of the latter<sup>50</sup>. Formation of cluster between the electrolyte and the solvent is believed to be the reason for such a large solubility of LiClO<sub>4</sub> in ethyl acetate<sup>51</sup>. As a result, we could extend the LiClO<sub>4</sub> concentration up to 2.5 M in ethyl acetate whereas we could go only up to 1.0 M in acetonitrile. As expected, the presence of electrolyte does not alter the shape of the absorption spectrum of P4C other than inducing a total red shift  $\Delta\nu_{abs}^{ea} = [\nu_{abs}^{ea}(0M) - \nu_{abs}^{ea}(2.5M)] \approx 600\text{cm}^{-1}$  in ethyl acetate and  $\Delta\nu_{abs}^{acn} = [\nu_{abs}^{acn}(0M) - \nu_{abs}^{acn}(1M)] \approx 300\text{cm}^{-1}$  in acetonitrile. Interestingly, at 1.0 M LiClO<sub>4</sub> the absorption peak shift (relative to that in pure solvent) is  $\sim 300\text{cm}^{-1}$  in both ethyl acetate and acetonitrile. For P5C and P6C,  $\Delta\nu_{abs}^{ea}$  is approximately twice as large as that in P4C whereas  $\Delta\nu_{abs}^{acn} \approx 400\text{cm}^{-1}$  (see figures A1 and A2, Appendix 2). Also, the absorption peak shifts for P5C and P6C are  $\sim 500\text{cm}^{-1}$  and  $\sim 400\text{cm}^{-1}$  at 1 M LiClO<sub>4</sub> in ethyl acetate and acetonitrile, respectively. This difference in behavior for P4C from the other two solutes can be understood if we consider the net absorption transition moments of the composite ( $S_0 \rightarrow L_a + S_0 \rightarrow L_b$ ) absorption bands given in Table 2.3. The concentration averaged net absorption transition moment ( $\langle M_{abs} \rangle$ ) for P4C in ethyl acetate is  $\sim 3.9\text{D}$  while those for P5C and P6C are  $\sim 5\text{D}$  and  $4.9\text{D}$ , respectively.

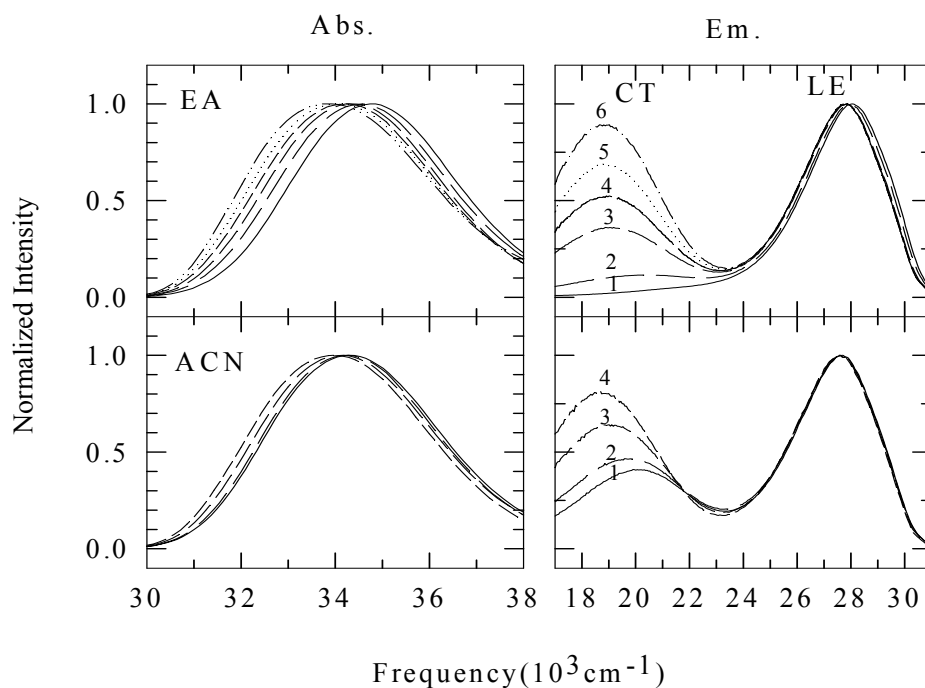


**Fig. 2.2:** Absorption and emission spectra of 4-(1-azetidiny) benzonitrile (P4C) in several concentrations of  $\text{LiClO}_4$  in ethyl acetate (upper panel) and acetonitrile (lower panel). For ethyl acetate solutions, spectra shown here are for the following  $\text{LiClO}_4$  concentrations (M): 0.0 (1), 0.5 (2), 1.0 (3), 1.5 (4), 2.0 (5), 2.5 (6). For acetonitrile solutions, spectra shown here correspond to the following concentrations (M): 0.0 (1), 0.1 (2), 0.5 (3), 1.0 (4).

If we now consider that the major contribution to  $\langle M_{abs} \rangle$  comes from the more polar  $S_0 \rightarrow L_a$  transition<sup>36</sup>, it becomes clear why the absorption peak shift in P4C is smaller than those in P5C and P6C. The electrolyte ( $\text{LiClO}_4$ ) concentration dependence of the absorption, CT and LE emission peak frequencies ( $\nu_{abs}, \nu_{CT}, \nu_{LE}$ ) and absorption line-width ( $\Gamma_{abs}$ ) of P4C, P5C and P6C in ethyl acetate and

acetonitrile is shown in Fig. 2.3. The inhomogeneous CT and LE line-widths are also shown in the same figure.

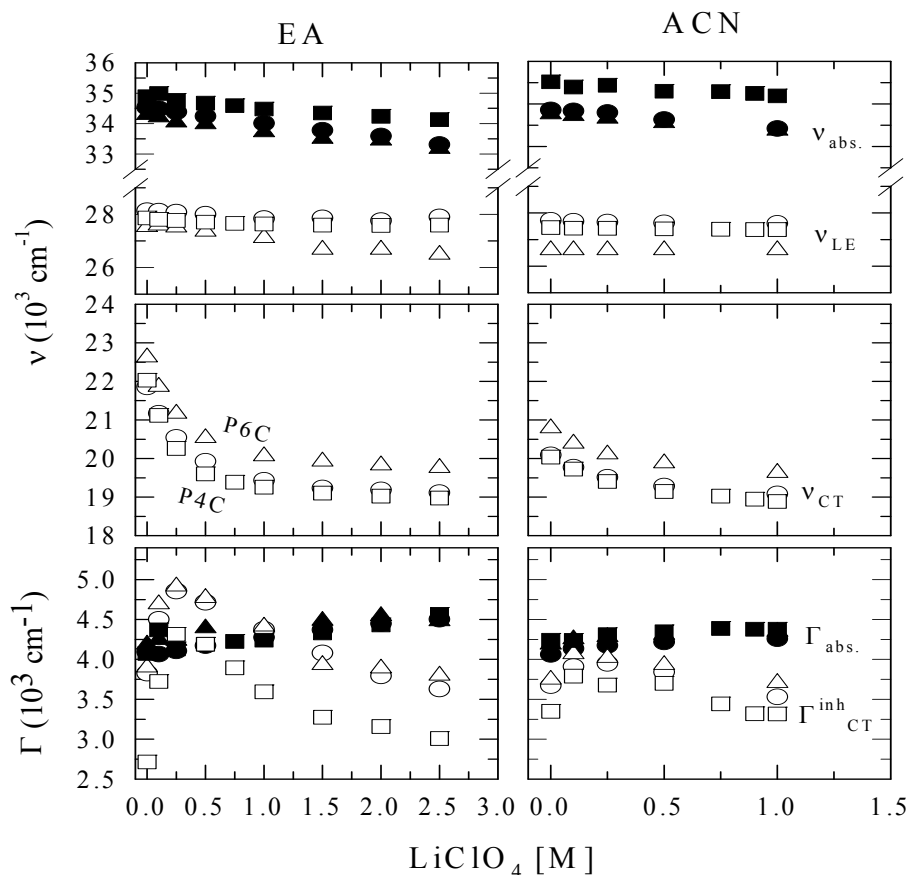


**Fig. 2.3:** Electrolyte ( $\text{LiClO}_4$ ) concentration dependence of absorption ( $\nu_{abs}$ ) and emission ( $\nu_{LE}$ ) peak frequencies and line widths (full width at half maxima,  $\Gamma$ ) of the absorption spectra and CT bands of 4-(1-azetidiny)benzonitrile (P4C), P5C and P6C in ethyl acetate (left panel, marked with ‘EA’) and acetonitrile (right panel, marked with ‘ACN’). The squares represent the solute P4C, while the circles and triangles are P5C and P6C respectively. Filled symbols represent absorption peak frequencies ( $\nu_{abs}$ ) and line widths ( $\Gamma_{abs}$ ). LE and CT peak frequencies ( $\nu_{LE}$  and  $\nu_{CT}$ ) and the inhomogeneous line width ( $\Gamma_{CT}^{inh}$ ) for CT band are represented by open symbols. These quantities have been obtained after deconvoluting the experimental emission spectra by broadening and shifting a reference spectrum with a Gaussian (representing inhomogeneous solvent broadening). For further details, see text and Ref. 36. The estimated uncertainty in frequencies and widths is  $\pm 300 \text{ cm}^{-1}$  (except when the LE is too small).

It is clear from Fig.2.3 that the electrolyte induced shift in the CT emission band is very large due to its more polar nature while the LE band shows either very little or no shift upon addition of electrolyte in these solvents. Also, the peak frequency of the CT emission band of these TICT molecules decreases exponentially with the increase in LiClO<sub>4</sub> concentration<sup>52</sup>. For P4C, increase in concentration of LiClO<sub>4</sub> from 0.0 M to 2.5 M in ethyl acetate enhances the CT/LE area ratio by a factor of ~27 (relative to that in pure ethyl acetate) and shifts the CT emission peak towards lower energy by about 3000 cm<sup>-1</sup>. In acetonitrile, the enhancement factor is function ~2 and the CT peak shift is ~1100 cm<sup>-1</sup> for increasing the LiClO<sub>4</sub> concentration from 0.0 M to 1.0 M. Note that the amount of CT is very small in pure ethyl acetate and at low LiClO<sub>4</sub> concentrations and hence the error associated with the CT peak determination in such cases is  $\pm 500$  cm<sup>-1</sup>. This large error is reduced to  $\pm 150$  cm<sup>-1</sup> as the CT population grows with further addition of electrolyte. In cases where the population (LE or CT) is found to be less than 10%, the peak shift (relative to the reference) and the inhomogeneous width have been fixed. This removes any inconsistency in the peak-shift determination and band area calculation. It is interesting to note that in presence of 1.0 M LiClO<sub>4</sub> the CT emission peak shift of these TICT molecules is in the range of 2500 cm<sup>-1</sup> in ethyl acetate while that in acetonitrile is ~1000 cm<sup>-1</sup>. Also, for these molecules at 1.0 M LiClO<sub>4</sub> solutions the area ratio (CT/LE) relative to that in pure solvent is several times larger in ethyl acetate than in acetonitrile. All these observations seem to indicate that for these TICT molecules in general and for P5C and P6C in particular that the effects of electrolyte on the LE  $\rightarrow$  CT conversion are stronger in ethyl acetate than in acetonitrile. This may be due to the fact that acetonitrile, being more polar (static dielectric constant,  $\epsilon_0$  being 35.94 for acetonitrile as compared to 6.02 for ethyl acetate)<sup>50</sup>, could probably supply almost all of the energy for P5C and P6C required for the conversion and subsequent solvent stabilization of CT state. Naturally therefore, the formation of CT population predominates for P5C and P6C in pure acetonitrile and there is not much left to be driven by the enhanced interaction between the solute (P5C or P6C) and various species present in electrolyte solutions (see figures A1 and A2, Appendix 2). It may also be linked to the solvent polarity

dependence of activation barrier<sup>4</sup> associated with the LE → CT conversion (static solvent effects).

An important feature to be noted in Fig. 2.3 is the variation of width in both absorption and CT emission bands with electrolyte concentration in these solvents. Due to the interaction with the environment, the absorption spectra of these molecules in electrolyte solutions are shifted to lower frequency and broadened with broadening ranged between 200-400  $\text{cm}^{-1}$  in ethyl acetate and acetonitrile. This broadening is due to the microscopic heterogeneity in the environment surrounding a solute in the solution. The CT emission band shows narrowing with the increase in electrolyte concentration with a maximum narrowing  $\sim 1000 \text{ cm}^{-1}$ . If we now recall that  $\epsilon_0$  of electrolyte solution increases with electrolyte concentration<sup>53</sup>, these peak-shifts and variation in spectral widths could be termed as similar to what have been observed earlier with C153 in neat polar solvents<sup>46</sup> and in electrolyte solutions (discussed later). However, the narrowing of CT emission band in these TICT molecules is 3 - 4 times more than what has been observed with C153 in neat solvents, suggesting a more complex interaction between the excited state of a TICT molecule and the environment surrounding it. One therefore needs further study to understand the reasons for such a large electrolyte-induced narrowing of emission width in these molecules.

Before going further into the discussion about the steady state results with these TICT molecules, we would like to digress here briefly to relate the concentration dependent peak shifts and spectral widths observed for the above molecules to those obtained for C153 in  $\text{LiClO}_4$  solutions of ethyl acetate and acetonitrile. Data summarized in Table A1 in the Appendix 2 indicate that the total absorption peak shift of C153 between 0.0 M to 2.5 M  $\text{LiClO}_4$  in ethyl acetate is  $\sim 1500 \text{ cm}^{-1}$  which is similar in magnitude to what has been found for P5C and P6C molecules in this concentration range in ethyl acetate. In acetonitrile, the absorption peak shift (between 0.0 M and 1.0 M) of C153 is similar to what has been found ( $\sim 400 \text{ cm}^{-1}$ ) for the TICT molecules studied here. The corresponding emission peak shift in

electrolyte solutions of ethyl acetate is  $\sim 2000 \text{ cm}^{-1}$  which is approximately two-third of the CT emission peak shift found for the TICT molecules considered here. In acetonitrile, however, the emission peak shift in C153 is similar to what has been found for TICT molecules upon increasing the  $\text{LiClO}_4$  concentration from 0.0 M to 1.0 M. These spectral shifts are associated with spectral broadening (for absorption) and narrowing (for emission). We will see later that quantum yield and other relevant quantities of C153 also exhibit similar concentration dependence as those found for P4C, P5C and P6C molecules. Therefore, these data indicate that the effects of electrolyte on these two types of molecules (non-reactive and reactive) are qualitatively similar and hence, study of electrolyte effects using one (type) of these molecules as probe would be able to explain the general behavior of the other in electrolyte solutions.

The ion size dependence of  $\nu_{CT}$  for P4C, P5C and P6C in ethyl acetate and acetonitrile containing 0.5(M) perchlorate of different metal cations is shown in Fig. 2.4. Other relevant quantities obtained from the steady state studies in ethyl acetate are summarized in Table 2.2. Corresponding data for acetonitrile are provided in the Appendix 2 (Table A2). Two important features are to be noted in this figure. First, except for  $\text{Mg}^{+2}$ , the CT emission frequencies of these molecules in perchlorate solutions of ethyl acetate and acetonitrile show a linear dependence on  $z/r_{ion}$ . Second, the CT emission frequency shifts by  $\sim 900 \text{ cm}^{-1}$  and  $\sim 750 \text{ cm}^{-1}$  respectively in ethyl acetate and acetonitrile (see Table A2, Appendix 2) as one moves from  $\text{Na}^+$  to  $\text{Ca}^{+2}$ . This indicates that the solute-ion interaction becomes stronger as  $z/r_{ion}$  becomes larger<sup>33</sup>. The absorption frequencies (see Table 2.2 and Table A2) of these solutes in ethyl acetate and acetonitrile also exhibit linear  $z/r_{ion}$  dependence for all ions examined here.

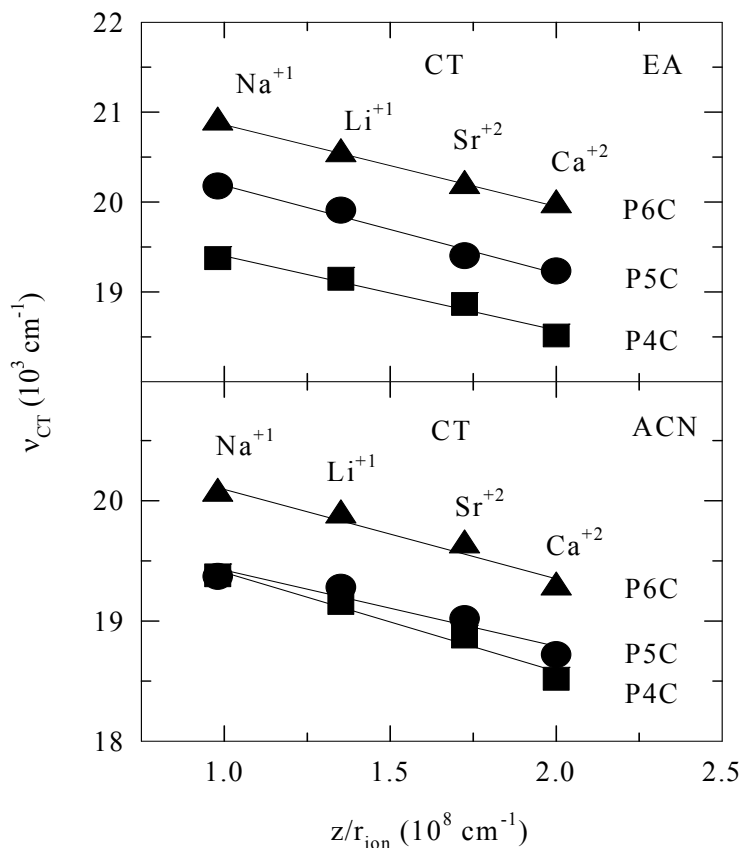


**Fig. 2.4.:** Ion size dependence of emission peak frequencies of P4C, P5C and P6C in 0.5(M) perchlorate solution of ethyl acetate. In this figure, squares represent P4C while P5C and P6C are represented by circles and triangles respectively. Perchlorate salts of the following cations have been used:  $\text{Na}^+$ ,  $\text{Li}^+$ ,  $\text{Sr}^{+2}$ ,  $\text{Ca}^{+2}$  and  $\text{Mg}^{+2}$ . Note that  $\text{Mg}^{+2}$  has not been shown in the figure. In presence of  $\text{Mg}^{+2}$  ions in ethyl acetate, the values of  $\nu_{\text{CT}}$  (in  $10^3 \text{ cm}^{-1}$ ) for P4C, P5C and P6C respectively are 19.33, 19.90 and 20.61. In acetonitrile, the corresponding values are 19.33, 19.32 and 20.01

Similar behavior is also found earlier in the context of solvation studies in electrolyte solutions using several non-reactive probes<sup>33</sup>. It has been argued<sup>1-3,33</sup> that emission shift saturates with  $z/r_{ion}$  because the environment dynamics slows down considerably as  $z/r_{ion}$  increases and the equilibrium solvation cannot be attained during the probe's lifetime. Therefore, in presence of  $\text{Mg}^{+2}$  the CT emission is

occurring from an improperly equilibrated excited state and hence the observed peak frequency is larger than what would have been for a properly equilibrated one.

Fig. 2.5 shows the CT/ LE area ratio ( $\alpha_{CT}/\alpha_{LE}$ ) for P4C, P5C and P6C in ethyl acetate and acetonitrile as a function of LiClO<sub>4</sub> concentration. The area under each band ( $\alpha_x$ ,  $x = CT$  or  $LE$ ) has been calculated as discussed earlier and in Ref. 36. Note here that the CT/LE ratio increases as the electrolyte concentration is increased indicating the formation of CT state is strongly favored upon addition of electrolyte. For the three molecules, formation of CT states is more favored in pure acetonitrile than in ethyl acetate due to the larger static dielectric constant of acetonitrile. However, the electrolyte concentration dependence is stronger in ethyl acetate than in acetonitrile. As the area ratio is connected to the equilibrium constant ( $K_{eq}$ ), the change in reaction free energy ( $\Delta G_r$ ) for the LE  $\rightarrow$  CT conversion is calculated from the following relation<sup>36</sup>

$$\Delta G_r = -RT \ln K_{eq} = -RT \ln \left[ \alpha_{CT} \nu_{LE}^3 / \alpha_{LE} \nu_{CT}^3 \right], \quad (2.1)$$

and shown in Fig. 2.6. As expected,  $\Delta G_r$  in acetonitrile is larger due to its larger dielectric constant. As expected,  $\Delta G_r$  is following the trend of  $\alpha_{CT}/\alpha_{LE}$  depicted in the previous figure (Figure 2.5) and the possible reasons discussed. Note that the concentration dependent  $-\Delta G_r$  for P4C in ethyl acetate varies from negative to positive values indicating that an unfavorable LE  $\rightarrow$  CT conversion reaction in pure ethyl acetate becomes highly favorable upon addition of electrolyte. In fact, the equilibrium constant for the LE  $\rightarrow$  CT conversion reaction in P4C is  $\sim 50$  times larger in presence of 2.5 M LiClO<sub>4</sub> than that in pure ethyl acetate. For P5C and P6C in ethyl acetate at 2.5 M LiClO<sub>4</sub>,  $-\Delta G_r$  is enhanced by a factor of  $\sim 4$  and  $\sim 2.5$ , respectively. This means that the equilibrium constant is increased by an order of magnitude for P5C and doubled for P6C in ethyl acetate at 2.5 M LiClO<sub>4</sub> with respect to the values in the absence of electrolyte.

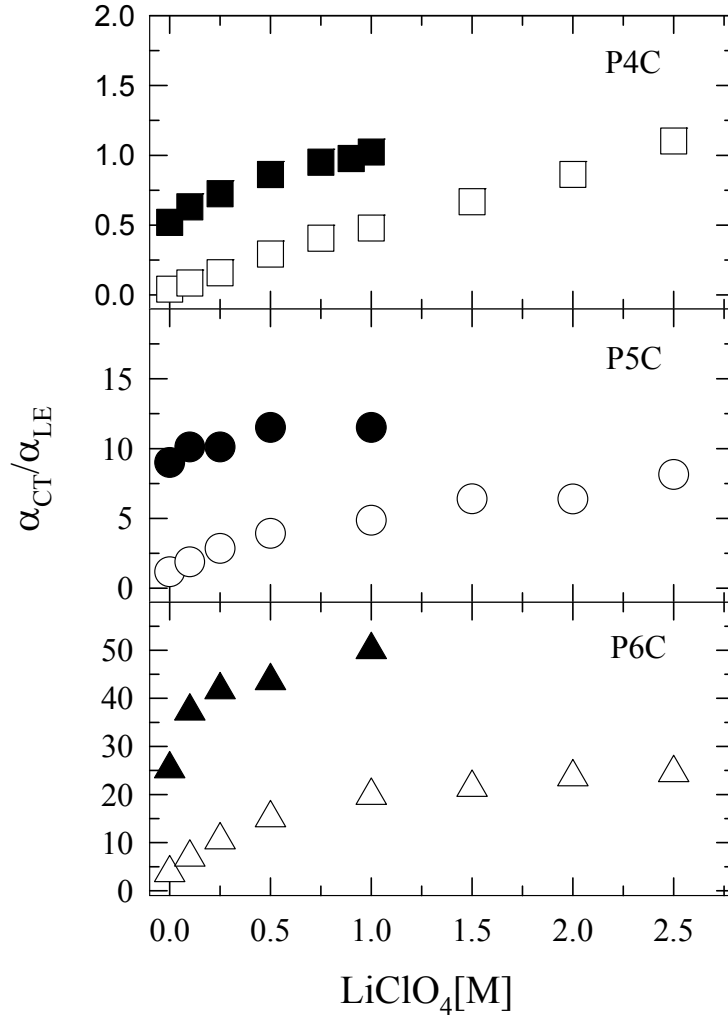


**Fig. 2.5.:** Electrolyte concentration dependence of formation of CT population in ethyl acetate (open symbols) and acetonitrile (filled symbols). The ratio ( $\alpha_{CT}/\alpha_{LE}$ ) between areas under the CT and LE bands (obtained after deconvolution as discussed in the text and in Ref.36) are shown as a function of  $LiClO_4$  concentration. Squares represent the ratio for P4C in the upper panel, circles for P5C in the middle panel and triangles for P6C in the lower panel. The uncertainty for CT band area is typically within  $\pm 10\%$ .

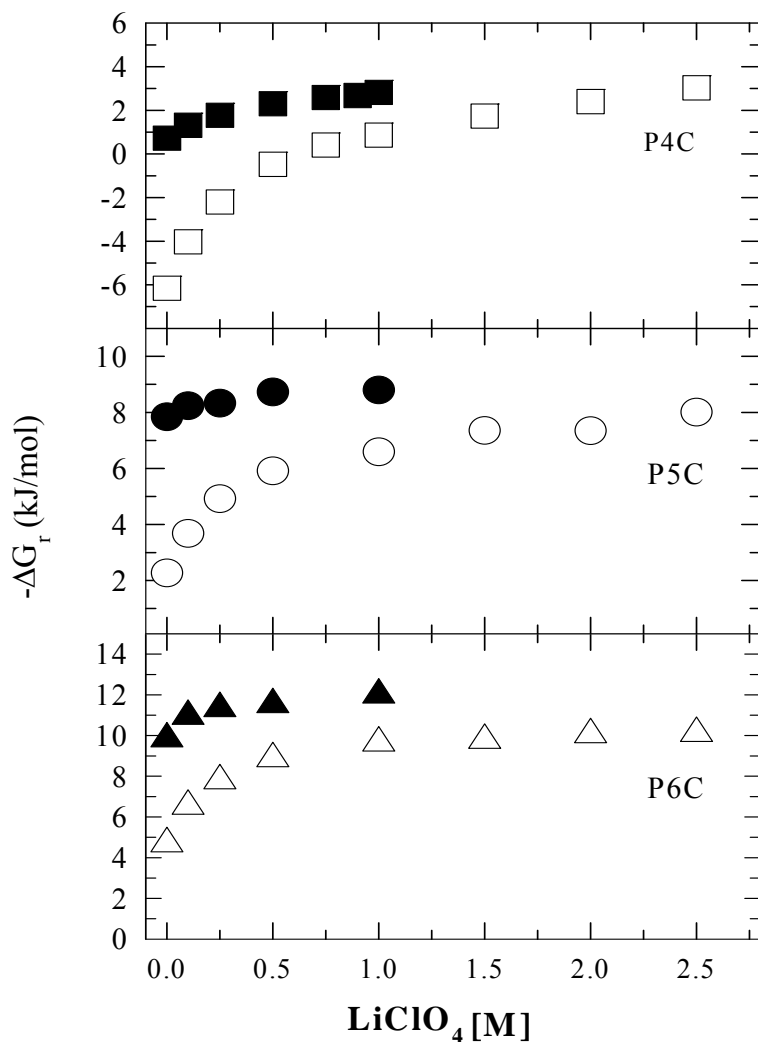


**Fig. 2.6.:** Electrolyte concentration dependence of the change in reaction free energy ( $-\Delta G_r$ ) for LE  $\rightarrow$  CT conversion for P4C, P5C and P6C in ethyl acetate (open symbols) and acetonitrile (filled symbols).  $\Delta G_r$  is obtained from the area ratio (shown in Fig.2.5) by using Eq. 2.1. Squares (open and filled) denote  $-\Delta G_r$  for P4C in the upper panel. Circles (open and filled) denote  $-\Delta G_r$  for P5C in the middle panel. The results for P6C are shown by open and filled triangles in the lower panel.

For P4C in acetonitrile with 1.0 M LiClO<sub>4</sub>,  $-\Delta G_r$  is  $\sim 4$  times larger than that in the absence of electrolyte while it is limited within  $\sim 10$ -20% for P5C and P6C. Therefore, the electrolyte concentration dependence of LE  $\rightarrow$  CT conversion

reaction is stronger in P4C than that in P5C and P6C. The large activation barrier ( $\Delta E_{act}$ ) in P4C is probably the reason for such a strong electrolyte concentration dependence. The ion size dependence<sup>54</sup> of  $-\Delta G_r$  for these molecules in ethyl acetate and acetonitrile containing 0.5(M) perchlorate salts of different cations has also been studied. It has been found that  $-\Delta G_r$  shows a very weak dependence on  $z/r_{ion}$  (see figure A3 in the Appendix 2).

### 2.3.2 Quantum Yields and Transition Moments

We have measured quantum yield, radiative and non-radiative rates, and transition moments for P4C, P5C and P6C in various concentrations of LiClO<sub>4</sub> in ethyl acetate and acetonitrile. The following well-known relation has been used to determine the quantum yield<sup>36</sup>

$$\Phi_S = \Phi_R \left( \frac{n_S^2}{n_R^2} \right) \left( \frac{I_S}{I_R} \right) \left( \frac{1 - 10^{-0.5A_R}}{1 - 10^{-0.5A_S}} \right) \quad (2.2)$$

Quinine sulphate dihydrate in 0.05M H<sub>2</sub>SO<sub>4</sub> has been used as reference ( $\Phi_R = 0.508$ )<sup>55</sup>. In Eq. 2.2,  $n_x$  represents refractive index of the reference solution (R) and sample (S),  $I$  the integrated emission intensity and  $A$  the absorbance. Refractive indices of the electrolyte solutions have been measured ( $296.15 \pm 1K$ ) and reported in Table 2.1. Values of net quantum yields for both P5C and P6C in cyclohexane have been reproduced within  $\pm 10\%$  uncertainty<sup>56</sup> about the value reported in the literature. Fig. 2.7 depicts the electrolyte (LiClO<sub>4</sub>) concentration dependence of net quantum yield in ethyl acetate. Quantum yields of individual parts (LE and CT) for these molecules in various concentrations of LiClO<sub>4</sub> in ethyl acetate have also been determined and provided in figure A4 of the Appendix 2. It is clear from these figures that the presence of electrolyte decreases the quantum yield appreciably. For example, the net quantum yield for these TICT molecules at 2.5 M LiClO<sub>4</sub> in ethyl acetate is reduced by a factor of  $\sim 7$  from the value obtained in pure ethyl acetate.

**Table 2.1: LiClO<sub>4</sub> Concentration Dependence of radiative and non-radiative rates of TICT molecules in ethyl acetates <sup>(a)</sup>**

Conc. (M)	P4C			P5C		P6C	
	n (ref. index)	$k_{LE}^{rad}$	$k_{LE}^{nr}$	$k_{LE}^{rad}$	$k_{LE}^{nr}$	$k_{LE}^{rad}$	$k_{LE}^{nr}$
0.0	1.368	3.60	4.00	4.53	25.86	1.93	22.69
0.1	1.369	2.82	5.49	3.57	40.29	1.47	39.69
0.25	1.371	3.44	7.81	3.66	75.95	1.23	58.10
0.5	1.374	3.27	11.74	3.54	124.65	1.06	92.49
1.0	1.382	2.88	18.23	3.06	160.98	1.26	150.4
1.5	1.387	2.76	23.99	3.79	285.34	1.16	172.30
2.0	1.392	2.26	27.86	3.14	269.96	1.15	185.07
2.5	1.395	2.05	32.91	2.59	302.77	1.13	195.96

(a)  $k_{LE}^{rad}$  (in the unit of  $10^7 \text{ cm}^{-1}$ ) and  $k_{LE}^{nr}$  (in the unit of  $10^8 \text{ cm}^{-1}$ ) denote respectively the radiative and nonradiative rates associated with LE band.

The net quantum yield of these molecules in acetonitrile at 1.0 M LiClO<sub>4</sub> is almost half of that in the pure solvent (see figure A5, Appendix 2). Note that the concentration dependence of the net quantum yield for these molecules could also be fitted to a biexponential function of electrolyte concentration<sup>57</sup>. Values for radiative ( $k_{rad}$ ) and non-radiative ( $k_{nr}$ ) rates, and average life times ( $\langle \tau_{avg} \rangle$ ) have been determined by using our experimental data in the relations given in literature<sup>36</sup>. For individual parts, however, we use the following relations<sup>36</sup>:

$$k_{LE}^{rad} = \phi_{LE} / \langle \tau_{LE} \rangle \quad (2.3)$$

where the average LE lifetime has been calculated from the amplitudes ( $a_i$ ) and time constants ( $\tau_i$ ) obtained by fitting the relevant LE emission decays as follows<sup>36</sup>:

$$\langle \tau_{LE} \rangle = \sum_i a_i \tau_i / \sum_i a_i. \quad (2.4)$$

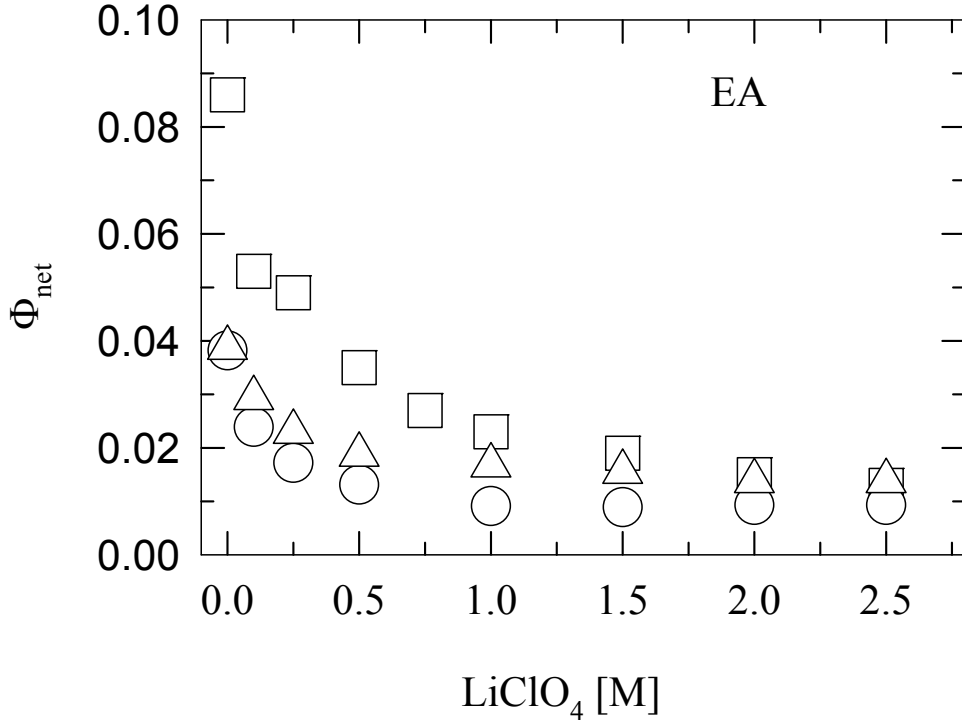


**Fig. 2.7.:** Electrolyte (LiClO<sub>4</sub>) concentration dependence of quantum yield ( $\Phi$ ) for P4C, P5C and P6C in ethyl acetate. Open squares show the quantum yield for P4C, open circles show that for P5C and the quantum yield of P6C has been shown by open triangles. Estimated errors for these calculations are within  $\pm 10\%$  about the average for most of the cases.

The non-radiative rate for LE ( $k_{LE}^{nr}$ ) is then calculated by using the relation<sup>36</sup>,

$$k_{LE}^{nr} = (1 - \phi_{LE}) / \langle \tau_{LE} \rangle. \quad (2.5)$$

For CT, the radiative rate is obtained as follows<sup>36</sup>:

$$k_{CT}^{rad} = \phi_{CT} k_{dec} (1 + K_{eq}^{-1}) \quad (2.6)$$

where the average excited state population decay constant ( $k_{dec}$ ) is determined from the net rate constants  $k_{LE}$  and  $k_{CT}$  using  $k_{dec} = (k_{LE} + k_{CT})/2$ , and assuming rapid

equilibrium between LE and CT states<sup>36</sup>. These quantities have been calculated for P4C, P5C and P6C in electrolyte solutions and are summarized in Table 2.1. The decay parameters necessary for the calculations of  $\langle\tau_{LE}\rangle$  and  $k_{CT}$  are discussed in the time resolved part of this chapter. The error bar associated with the calculation of these radiative and non-radiative rates is typically  $\pm 15\%$  about the values reported here. Data in Table 2.1 indicate that radiative and non-radiative rates show a weak to moderate electrolyte concentration dependence. The ion size ( $z/r_{ion}$ ) dependence of quantum yield is shown in Fig.2.8. It is evident from this figure that quantum yield of these TICT molecules behave as a function of  $z/r_{ion}$  in a manner similar to what have been observed for CT emission peak frequency (see Fig. 2.4). The corresponding values for radiative and non-radiative rates are listed in Table 2.2 which shows no particular dependence on ion size. Transition dipole moment of the radiative transitions,  $M_x$ , has been determined from the radiative rate data by using the following relation<sup>36, 58</sup>

$$M_x/D = 1785.7 \left( \frac{k_x^{\text{rad}} / \text{s}^{-1}}{n_s^3 (\tilde{\nu}_x^3 / \text{cm}^{-3})} \right)^{1/2}, \quad (2.7)$$

where  $\overline{\nu_x^3} = \int F_x(\nu) d\nu / \int F_x(\nu) \nu^{-3} d\nu$  with  $F_x(\nu)$  denoting the fluorescence spectrum of species  $x = \text{LE}$  or  $\text{CT}$ . The results are summarized in Table 2.3. Transition moments for CT of P4C, P5C and P6C determined here in ethyl acetate are consistent with the reported values for these molecules in methyl acetate ( $\epsilon_0$  for methyl acetate and ethyl acetate are 6.68 and 6.02, respectively).

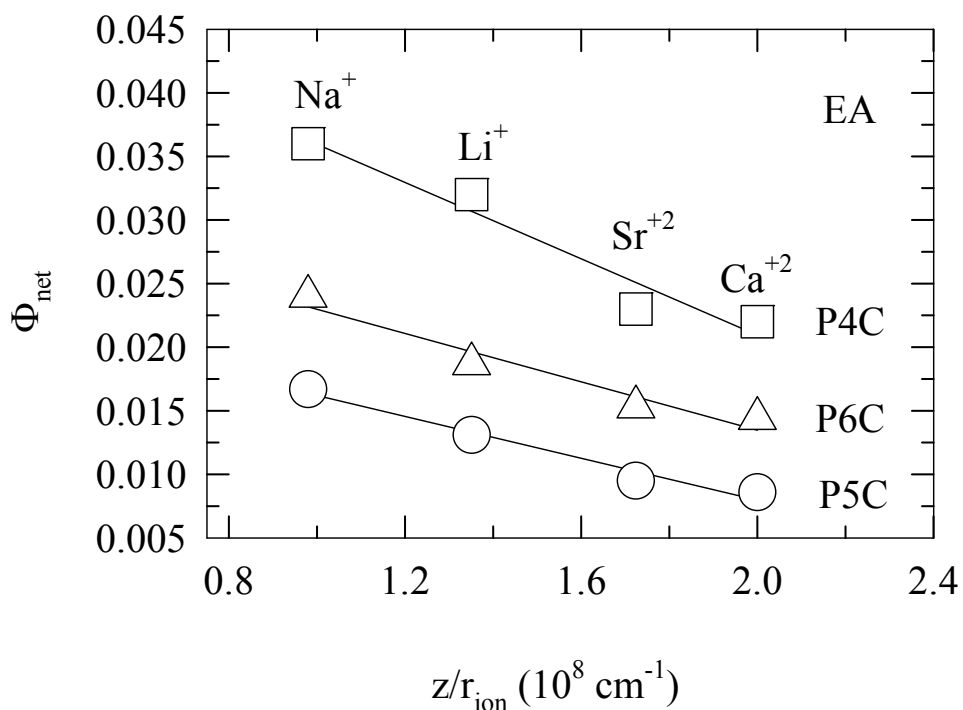


**Fig. 2.8:** Ion size dependence of quantum yield of P4C, P5C and P6C in 0.5(M) perchlorate solution of ethyl acetate. In this figure, squares represent P4C while circles and triangles represent P5C and P6C, respectively. Perchlorate salts of the following cations have been used: Na<sup>+</sup>, Li<sup>+</sup>, Sr<sup>+2</sup>, Ca<sup>+2</sup> and Mg<sup>+2</sup>. Note that Mg<sup>+2</sup> has not been shown in the figure. In presence of Mg<sup>+2</sup> ion in ethyl acetate, the values of ( $\Phi$ ) for P4C, P5C and P6C respectively are 0.026, 0.011 and 0.018.

The error bar is typically  $\pm 15\%$  but larger when emission spectrum is overwhelmingly dominated by either LE or CT bands. It is interesting to note in Table 2.3 that CT transition moment is very *weakly* dependent on (or even *insensitive* to) the LiClO<sub>4</sub> concentration. Similar results have also been found with these molecules in neat (pure) solvents where polarity had either very weak or no effects on the transition dipole moments<sup>36</sup>. Data on transition moments for these molecules given in Table 2.3 suggest that the electrolyte concentration-averaged LE

transition moment follows the order P4C > P5C > P6C. Also, the CT transition moments for P6C in various concentrations of LiClO<sub>4</sub> in ethyl acetate are slightly larger than for P5C in similar conditions. Similar results have also been observed earlier in neat solvents<sup>36</sup>. Note in Table 2.3 that the CT transition moments for P4C at low electrolyte concentrations are not reported because these values are associated with large errors as the CT band areas are very small at these electrolyte concentrations. The cation size dependence of these transition moments is investigated and the results are summarized in Table 2.2. These data indicate that the transition moments are insensitive to  $z/r_{ion}$ .

**Table 2 2: Ion Size Dependence of spectral properties and transition moments of TICT molecules in 0.5(M) perchlorate solutions in ethyl acetate**

**P4C**

Ion	$z/r_{ion}$	$\nu_{abs}$ (a)	$\Gamma_{abs}$	$\Gamma_{CT}^{inh}$	$\frac{\alpha_{CT}}{\alpha_{LE}}$	$k_{LE}^{rad}$	$k_{LE}^{nr}$	$M_{LE}$	$M_{abs}$
Na <sup>+</sup>	0.980	34.60	4.08	3.8	0.29	2.97	10.32	1.4	4.3
Li <sup>+</sup>	1.351	34.67	4.19	4.19	0.29	3.27	11.74	1.4	3.9
Sr <sup>+2</sup>	1.724	34.47	4.59	3.33	0.76	1.78	25.73	1.1	4.1
Ca <sup>+2</sup>	2.000	34.56	4.47	3.80	0.57	3.32	23.37	1.4	4.5
Mg <sup>+2</sup>	2.780	34.26	4.62	3.58	0.27	2.03	9.72	1.1	4.6

**P5C**

Ion	$\nu_{abs}$	$\Gamma_{abs}$	$\Gamma_{CT}^{inh}$	$\frac{\alpha_{CT}}{\alpha_{LE}}$	$k_{LE}^{rad}$	$k_{LE}^{nr}$	$M_{LE}$	$M_{abs}$
Na <sup>+</sup>	34.53	4.20	4.29	4.03	3.46	158.38	0.89	4.93
Li <sup>+</sup>	34.35	4.17	4.73	3.93	3.54	124.65	0.90	5.11
Sr <sup>+2</sup>	34.24	4.42	4.19	6.06	3.13	232.25	0.86	4.97
Ca <sup>+2</sup>	33.99	4.42	4.64	4.84	3.77	256.03	0.93	5.03
Mg <sup>+2</sup>	34.07	4.65	4.57	4.09	4.00	232.25	0.95	5.04

## P6C

Ion	$\nu_{\text{abs}}$	$\Gamma_{\text{abs}}$	$\Gamma_{CT}^{inh}$	$\frac{\alpha_{CT}}{\alpha_{LE}}$	$k_{LE}^{rad}$	$k_{LE}^{nr}$	$M_{LE}$	$M_{\text{abs}}$
Na <sup>+</sup>	34.29	4.41	4.35	12.51	1.09	61.241	0.52	4.80
Li <sup>+</sup>	34.16	4.39	4.77	15.10	0.07	92.490	0.51	4.97
Sr <sup>+2</sup>	33.98	4.59	3.54	19.90	0.69	94.271	0.43	5.14
Ca <sup>+2</sup>	33.80	4.91	4.10	13.60	0.90	93.368	0.49	5.16
Mg <sup>+2</sup>	34.09	4.63	4.68	15.61	0.85	78.655	0.45	4.95

(a) Peak frequencies ( $\nu$ ) and band widths ( $\Gamma$ , fwhm) are in the units of  $10^3 \text{ cm}^{-1}$ .  $\frac{\alpha_{CT}}{\alpha_{LE}}$

denotes area ratio between the CT and LE emission bands.  $k^{rad}$  and  $k^{nr}$  are in the units of  $10^7 \text{ s}^{-1}$  and  $10^8 \text{ s}^{-1}$  respectively).  $r_{ion}$  is in the units of  $10^{-8} \text{ cm}$ .

We have further calculated the net absorption transition moments of the composite absorption band ( $S_0 \rightarrow L_a + S_0 \rightarrow L_b$ ) by using the following relation<sup>58-59</sup>

$$M_{\text{abs}}/D = 9.584 \times 10^{-2} \left[ \frac{1}{n_{\text{abs}}} \int (\epsilon(\nu)/M^{-1} \text{cm}^{-1}) \frac{d\nu}{\nu} \right]^{1/2} \quad (2.8)$$

where  $\epsilon(\nu)$  is the molar decadic extinction coefficient. The results for P4C, P5C and P6C in LiClO<sub>4</sub> solutions of ethyl acetate are summarized in Table 2.3. Again, these absorption transition moments do not show any dependence on electrolyte concentration. Note that the average net absorption transition moment obtained here is very close to the average value obtained for both these molecules in neat (pure) solvents. The net absorption transition moments of these molecules have also been determined in ethyl acetate and acetonitrile solutions containing perchlorate salts of different cations. The results are shown in Table 2.2 with a maximum error bar  $\pm 15\%$ . Again, there are no effects of  $z/r_{ion}$  on net absorption transition moment.

**Table 2.3: LiClO<sub>4</sub> concentration dependence of transition moments of TICT molecules in ethyl acetates<sup>a</sup>**

Conc. (M)	P4C			P5C			P6C		
	M <sub>LE</sub>	M <sub>CT</sub>	M <sub>abs</sub>	M <sub>LE</sub>	M <sub>CT</sub>	M <sub>abs</sub>	M <sub>LE</sub>	M <sub>CT</sub>	M <sub>abs</sub>
0.0	1.5	-	3.8	1.03	0.65	4.95	0.69	0.77	4.79
0.1	1.3	-	4.3	0.91	0.71	4.96	0.60	0.83	4.89
0.25	1.5	-	3.8	0.94	0.73	4.97	0.55	0.76	4.72
0.5	1.4	0.92	3.9	0.90	0.76	5.11	0.51	0.72	4.97
1.0	1.3	0.92	4.0	0.84	0.66	5.08	0.56	0.72	4.95
1.5	1.3	0.94	3.7	0.92	0.66	4.81	0.55	0.67	5.08
2.0	1.2	0.90	4.0	0.83	0.58	5.23	0.54	0.66	5.00
2.5	1.1	0.89	3.9	0.75	0.54	5.09	0.54	0.58	5.06

(a) M<sub>LE</sub>, M<sub>CT</sub> and M<sub>abs</sub> are in Debye unit. Since the amounts of CT for P4C in ethyl acetate in presence of 0.0, 0.1 and 0.25 M LiClO<sub>4</sub> concentrations are very small, the error associated with the calculation of M<sub>CT</sub> at these concentrations are very large. Hence, these values are not cited here.

We have also measured quantum yield, radiative, non-radiative rates and transition moments for C153 in various concentrations of LiClO<sub>4</sub> in ethyl acetate and acetonitrile. These data are summarized in figure A5 and Table A1 of the Appendix 2. It is clear from these data that at the highest LiClO<sub>4</sub> concentrations studied in these solvents the quantum yield of C153 decreases by ~40% from those in the absence of electrolyte. This is in contrast with what have been observed for TICT molecules where the reduction in quantum yields are by *at least* a factor of 4 and 2 at LiClO<sub>4</sub> concentrations 2.5 M in ethyl acetate and 1.0 M in acetonitrile, respectively. The ion size dependent quantum yield of C153 (see Table A3 of the Appendix 2), however, is found to be linear with  $z/\Gamma_{ion}$  which is also the observation (except for Mg<sup>+2</sup>) with the TICT molecules studied here.

### 2.3.3. Average Reaction Rates: Electrolyte Concentration Dependence

Time resolved emission decay measurements have been performed with P4C, P5C and P6C molecules in ethyl acetate containing LiClO<sub>4</sub> in concentrations ranging from 0.1 M to 2.5 M. We have used 0.5 M solutions of perchlorate salts containing

$\text{Li}^+$ ,  $\text{Mg}^{+2}$ ,  $\text{Ca}^{+2}$ ,  $\text{Na}^+$ ,  $\text{Sr}^{+2}$  and  $(\text{tBu})_4\text{N}^+$  in ethyl acetate in order to investigate the cation size dependence of the average reaction rate in these TICT molecules. This choice of cations provides an order of magnitude spread over crystallographic ionic radius ( $\sim 0.7\text{\AA}$  for  $\text{Li}^+$  to  $\sim 5\text{\AA}$  for  $(\text{tBu})_4\text{N}^+$ )<sup>33</sup>. As already discussed, a time dependent biexponential function has been found to fit emission decays containing P4C and P5C in all electrolyte concentrations in ethyl acetate. For P6C, however, a tri-exponential function is required for properly fitting the collected decays. An example of such a fit is shown in Fig.2.9 for P4C in 0.1 M  $\text{LiClO}_4$  solution of ethyl acetate and the fit parameters listed. This shows that a biexponential function is sufficient to describe the observed emission decay as the residual does not contain any non-random pattern<sup>56</sup> and the ‘goodness of fit parameter’ ( $\chi^2$ ) is close to 1.

The biexponential fit parameters for the electrolyte concentration dependent LE emission decays obtained for P4C and P5C in  $\text{LiClO}_4$  solutions of ethyl acetate are summarized in Table 2.4. Note that all the decays can be fitted to biexponential functions even in the presence of electrolyte at all concentrations and therefore the decay kinetics for P5C in electrolyte solutions conform to the classical two state reversible reaction mechanism as described by Maroncelli and coworkers in Ref.36. We would like to mention here that the collected emission decays at wavelengths near to CT emission peaks could also be fitted to biexponential functions with the same or similar time constants as found for the corresponding LE decays. For example, for P5C in presence of 0.1 M  $\text{LiClO}_4$  in ethyl acetate, fitting of CT emission decay with no constraints produces time constants 46 ps (rise time) and 2149 ps with  $\chi^2 = 1.33$ . This time constant (rise time) is thus very similar to the fast time constant (decay time, 62 ps) of the LE decay indicating that these time constants are essentially associated with the average reaction rate<sup>36</sup>. When the rise time is fixed

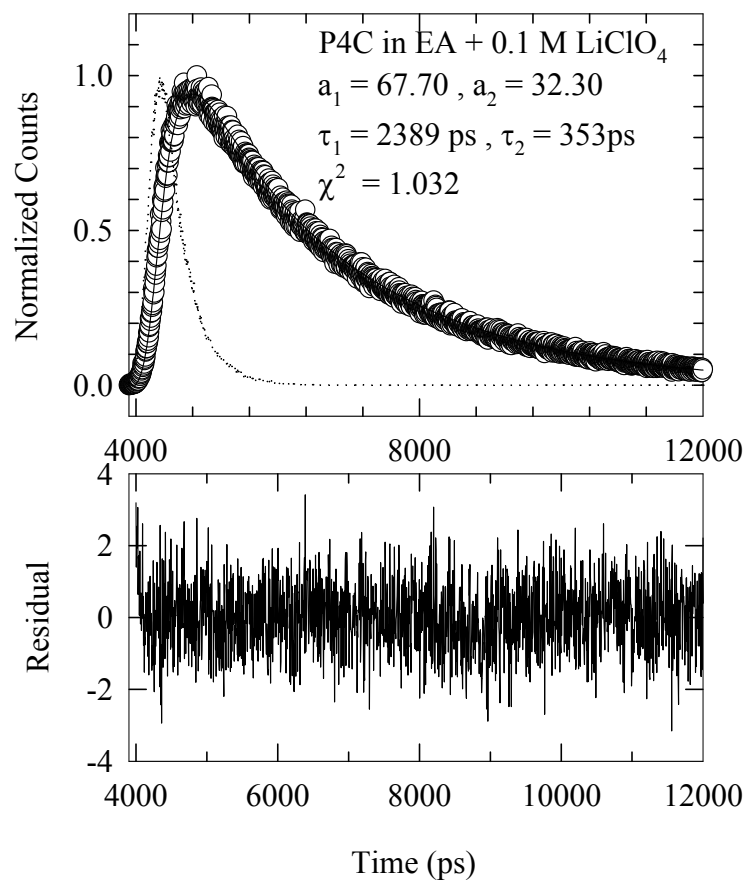


**Fig. 2.9.:** Representative LE emission decay of P4C in ethyl acetate in presence of 0.1(M) LiClO<sub>4</sub>. The data are represented by the circles, while the fit through the data are by the solid line. The instrument response function (IRF) is shown by the dashed line. The fit (biexponential) results are also provided in the *upper panel*. The LE peak count is ~4000. Residuals are shown in the *lower panel* ( $\pm 5$  full scale).

**Table 2.4: Electrolyte Conc. Dependence: Fit Parameters for the LE Emission Decays in LiClO<sub>4</sub> Solutions of Ethyl Acetate**

P4C

Conc. (M)	$\tau_1$ (ps)	$\tau_2$ (ps)	$a_1$	$a_2$	$\chi^2$
0.0	2916	274	76.4	23.6	1.054
0.1	2389	353	67.70	32.31	1.032
0.25	1796	333	61.11	38.89	1.056
0.5	1209	326	57.02	42.98	1.022
0.75	940	320	51.12	48.88	1.137
1.0	842	308	43.46	56.54	1.09
1.5	714	277	30.84	69.16	1.092
2.0	660	263	23.33	76.67	1.056
2.5	655	238	15.43	84.57	1.033

P5C

Conc. (M)	$\tau_1$ (ps)	$\tau_2$ (ps)	$a_1$	$a_2$	$\chi^2$
0.0	2867	54	11.7	88.3	1.34
0.10	1912	66	9.9	90.9	0.99
0.25	1315	52	6.8	93.2	1.05
0.5	1076	48	3.7	96.3	1.09
1.0	1241	47	1.3	98.7	1.03
1.5	1090	33	0.7	99.3	1.04
2.0	1251	33	0.5	99.5	0.91
2.5	1506	31	0.4	99.6	1.01

P6C

Conc. (M)	$\tau_1$ (ps)	$\tau_2$ (ps)	$\tau_3$ (ps)	$a_1$	$a_2$	$a_3$	$\chi^2$
0.0	2918	453	15	19.3	4.8	75.9	1.14
0.1	2068	562	15	10.5	3.7	85.8	1.06
0.25	1920	567	15	6.3	4.9	87.8	1.03
0.5	1930	632	15	2.7	6.8	90.5	0.91
1.0	2050	502	15	1.6	3.9	93.5	1.05
1.5	2194	464	15	1.2	3.7	95.1	1.05
2.0	2329	480	15	1.1	3.0	95.9	1.16
2.5	2827	535	15	0.8	2.4	96.8	1.19

to the fast decay time constant observed for the corresponding LE emission decay (62 ps), the same fit produces 2142 ps as the long time constant with  $\chi^2 = 1.36$ . Addition of a third exponential did not produce a better fit. It is therefore interesting to note that addition of electrolyte has not induced any deviation from the behavior (biexponential) observed earlier for P4C and P5C in pure ethyl acetate<sup>36</sup>. As discussed earlier, the LE emission decays of P6C in LiClO<sub>4</sub> solutions in ethyl acetate require tri-exponential functions to adequately fit the time dependent decays. The fit results are also summarized in Table 2.4. Note that the smallest time constant (15 ps) in these decays have been fixed to get reasonable fit. The CT emission decays are still described by a sum of two exponentials. However, the time constants do not match with the LE time constants. This is similar to what has been described in Ref.1 as ‘type III’ systems while studying TICT reactions with P6C in neat solvents. These reactions have been explained in terms of time dependent reaction rate involved in LE → CT conversion. Therefore, the decay kinetics of P6C in electrolyte solutions is similar to what have already been found in neat solvents<sup>36</sup>.

The average reaction time has been calculated from the collected LE emission decay using the following relation<sup>36</sup>:

$$\tau_{rxn}^{avg} = \frac{\sum_{i=1}^{n-1} a_i \tau_i}{\sum_{i=1}^{n-1} a_i}, \quad (2.9)$$

where  $a_i$  and  $\tau_i$  are the fractional amplitudes and time constants observed in  $n$ -exponential fit. The electrolyte (LiClO<sub>4</sub>) concentration dependent average reaction time ( $\tau_{rxn}^{avg}$ ) for P4C, P5C and P6C molecules in ethyl acetate are shown in the upper panel of Fig. 2.10. The ratio between the average reaction time constants in presence and absence of LiClO<sub>4</sub> in ethyl acetate ( $\tau_{ratio} = \tau_{rxn}^{avg}(M)/\tau_{rxn}^{avg}(M=0)$ ) as a function of electrolyte concentration are shown in the lower panel of this figure (Fig. 2.10). Note that the average reaction time is larger at lower electrolyte concentrations than

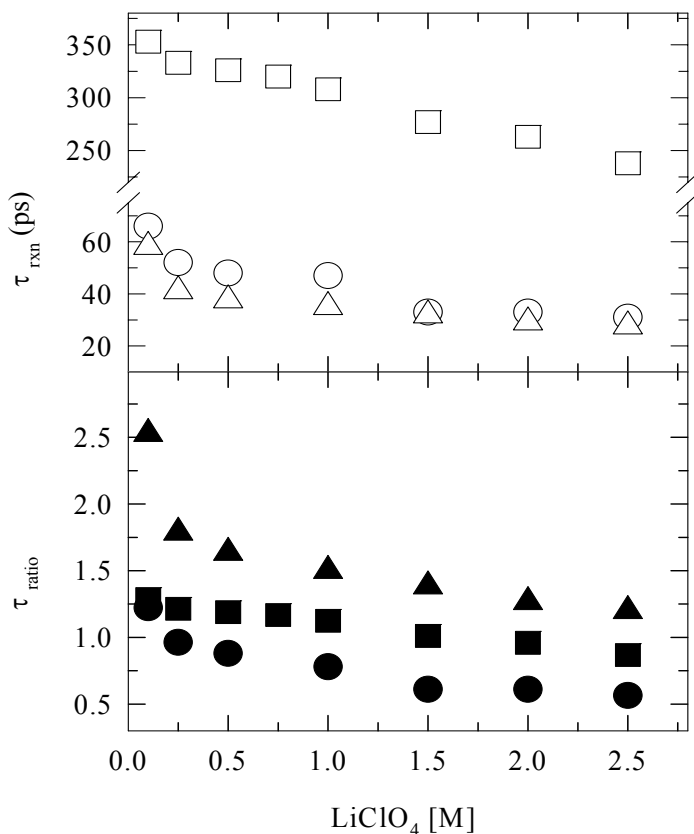


**Fig.2.10:** Electrolyte ( $\text{LiClO}_4$ ) concentration dependence of average reaction time ( $\tau_{rxn}^{avg}$ ) in ethyl acetate. *Upper panel:*  $\tau_{rxn}^{avg}$  for P4C is represented by squares, for P5C by circles and for P6C by triangles. Note that  $\tau_{rxn}^{avg}$  has been calculated from the relevant fit parameters by using Eq. 2.9 of the text. *Lower panel:* The ratio between average reaction times obtained in presence and absence of electrolyte ( $\tau_{ratio} = \tau_{rxn}^{avg}(M)/\tau_{rxn}^{avg}(M=0)$ ) is shown as a function of electrolyte concentration in ethyl acetate. The value of  $\tau_{rxn}^{avg}(M=0)$  for P6C is taken from Ref.36. representations by the filled symbols are the same as those by their open counter-parts in the upper panel.

in pure ethyl acetate. Further addition of electrolyte in ethyl acetate decreases the average reaction time<sup>60</sup>. At 2.5 M  $\text{LiClO}_4$  in ethyl acetate, the average reaction time reduces by almost a factor of 2 for P4C and P5C from those at 0.1 M. This indicates that the reaction proceeds at an average rate approximately *twice* as fast in ethyl

acetate containing 2.5 M LiClO<sub>4</sub> as that at 0.1 M. The enhancement of reaction rate at higher electrolyte concentration in solution may originate from the concentration induced enhancement of solvation rate<sup>1-3, 33</sup>. The reaction is slowed down at low electrolyte concentrations because the friction experienced by the twisting mode due to ion-dipole interaction is larger than the solvation stabilization of the product (CT state in this case). At larger electrolyte concentrations, ion-pair dominates which is dipolar in nature and therefore solvation processes become faster. Moreover, formation of ion-pair reduces the friction (mainly the dielectric part of it) as dipole-dipole interaction is weaker than ion-dipole interaction and therefore the reaction proceeds at a faster rate.

However, for P6C (lower panel of Fig.2.10), the ratio between the reaction time constants determined in the presence and absence of LiClO<sub>4</sub>, remains always above 1. This indicates that the reaction rate in P6C is slowed down by LiClO<sub>4</sub> at all concentrations in ethyl acetate. At the lowest electrolyte concentration, the reaction in P6C is slowed down by a factor of ~2.5 whereas that in P4C and P5C is only by 1.2. The following reasons may be responsible for the observed differences. Effects of electrolyte on reaction in P6C may be more pronounced due to higher dipole moment that couples strongly with the various ionic and dipolar species present in the electrolyte solution. The barrier height in P6C may also be altered differently by the presence of ions and ion-pairs. Since the average reaction rate for P6C in pure ethyl acetate is 2.5 times faster than P5C, we may also have missed a considerable part of the initial fast decay due to the limited time resolution available to us. This will induce some error by putting extra weight artificially on the slower component of the tri-exponential fit function and hence on the average reaction time. However, the reaction in P6C becomes *doubly* fast at 2.5 M LiClO<sub>4</sub> than at 0.1 M in ethyl acetate which has also been observed for P4C and P5C.

### 2.3.4 Average Reaction Rates: Cation Size Dependence

The cation size dependent data obtained after fitting the LE emission decays for P4C, P5C and P6C in presence of 0.5 M perchlorate salts in ethyl acetate are summarized in Table 2.5. The effects of cation size on emission decays are quite evident from this table.

**Table 2.5: Ion Size Dependence: Fit Parameters for the LE Emission Decays in 0.5(M) Perchlorate Solutions of Eethyl Acetate**

#### P4C

Salt	Conc. (M)	$\tau_1$ (ps)	$\tau_2$ (ps)	$a_1$	$a_2$	$\chi^2$
(tBu) <sub>4</sub> NClO <sub>4</sub>	0.5	2619	452	25.34	74.66	1.053
NaClO <sub>4</sub>	0.5	2033	473	28.42	71.58	1.197
LiClO <sub>4</sub>	0.5	1209	326	57.02	42.98	1.022
Sr (ClO <sub>4</sub> ) <sub>2</sub>	0.5	903	308	13.06	86.94	1.089
Ca (ClO <sub>4</sub> ) <sub>2</sub>	0.5	765	296	26.78	73.22	1.073
Mg (ClO <sub>4</sub> ) <sub>2</sub>	0.5	1894	429	39.49	60.51	1.120

#### P5C

Salt	Conc. (M)	$\tau_1$ (ps)	$\tau_2$ (ps)	$a_1$	$a_2$	$\chi^2$
(tBu) <sub>4</sub> NClO <sub>4</sub>	0.5	2494	50	2.9	97.1	1.297
NaClO <sub>4</sub>	0.5	1686	47	2.6	93.4	1.055
LiClO <sub>4</sub>	0.5	1076	42	3.7	96.3	1.09
Sr (ClO <sub>4</sub> ) <sub>2</sub>	0.5	1042	37	0.8	99.2	1.093
Ca (ClO <sub>4</sub> ) <sub>2</sub>	0.5	912	36	0.8	99.2	0.963
Mg (ClO <sub>4</sub> ) <sub>2</sub>	0.5	1136	39	2.7	97.3	0.969

#### P6C

Salt	Conc. (M)	$\tau_1$ (ps)	$\tau_2$ (ps)	$\tau_3$ (ps)	$a_1$	$a_2$	$a_3$	$\chi^2$
(tBu) <sub>4</sub> NClO <sub>4</sub>	0.5	3803	368	15	5.2	14.7	80.1	1.072
NaClO <sub>4</sub>	0.5	2391	490	15	3.9	11.7	84.4	1.197
LiClO <sub>4</sub>	0.5	1912	615	13	2.6	6.6	90.6	0.898
Sr (ClO <sub>4</sub> ) <sub>2</sub>	0.5	1926	327	15	2.2	8.9	88.9	1.104
Ca (ClO <sub>4</sub> ) <sub>2</sub>	0.5	1675	325	15	1.6	9.1	89.3	1.012
Mg (ClO <sub>4</sub> ) <sub>2</sub>	0.5	2867	642	15	1.9	9.3	88.8	1.327

As mentioned earlier, a sum of two exponentials is required to fit the emission decays of P4C and P5C for all the ions studied here while a third exponential is required to adequately fit the P6C decays. The average reaction times ( $\tau_{rxn}^{avg}$ ), obtained from these fits by using Eq. 2.9, are shown in Fig.2.11 that describes the effects of ion size on TICT reactions in these molecules. For the three molecules, the average reaction time,  $\tau_{rxn}^{avg}$ , decreases in a similar manner as  $z/r_{ion}$  increases. For P4C and P6C, however, the effects of ion-size on  $\tau_{rxn}^{avg}$  are stronger than that for P5C. It is interesting to note that the average reaction rate becomes larger for ions possessing higher values of  $z/r_{ion}$ . This is counter-intuitive in the sense that larger  $z/r_{ion}$  is expected to exert stronger dielectric friction on twisting and therefore the rate should be smaller (conversely,  $\tau_{rxn}^{avg}$  larger). Solvation dynamics studies in 1.0 M perchlorate solutions containing different cations in acetonitrile have shown that the average solvation time increases as  $z/r_{ion}$  increases<sup>33</sup>. This is explained in terms of larger binding strength between the probe and ions possessing higher  $z/r_{ion}$  values. For TICT reactions, the stronger binding is likely to stabilize more the CT state. This may be one of the reasons for the observed enhancement of the average reaction rate ( $1/\tau_{rxn}^{avg}$ ) with  $z/r_{ion}$ .

### 2.3.5 Zwan-Hynes Theory: Comparison with Experiments

Here we discuss the essential part of the theory proposed by Zwan and Hynes (ZH)<sup>34</sup> in order to compare our experimental results with the prediction of this theory. In ZH theory, isomerization reaction in a dipolar molecule dissolved in electrolyte solution of dipolar solvent has been studied after connecting the electrical friction on reactive mode with the solvation dynamics in electrolyte solutions. Their model assumes ion-atmosphere around a dipolar solute and the solvent as a structureless continuum. Subsequently, this is solved for dilute solutions of electrolytes containing ions of low valence in solvents of moderate to large dielectric constants.

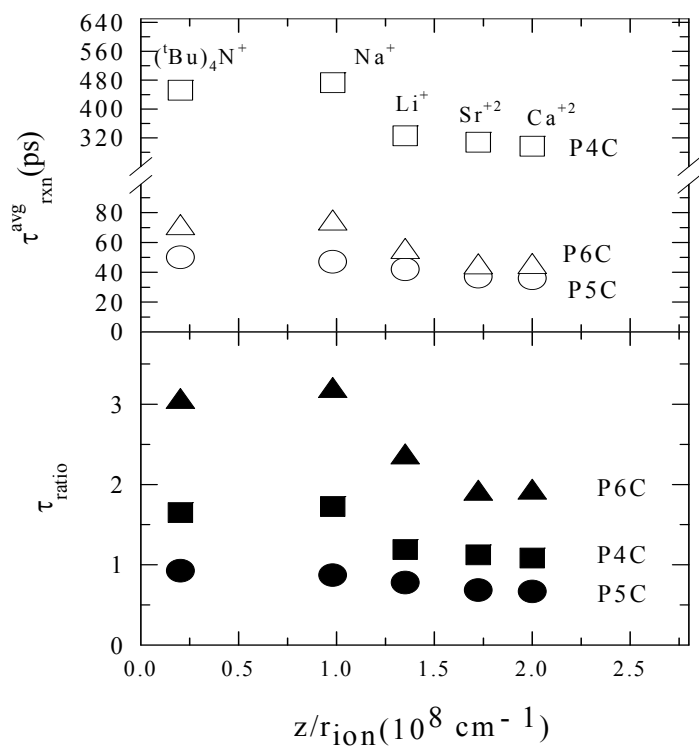


**Fig.2.11:** Ion size dependence of average reaction time ( $\tau_{rxn}^{avg}$ ) for P4C (squares), P5C (circles) and P6C (triangles) in ethyl acetate solutions of 0.5(M) perchlorate salts. *Upper panel* shows the variation of  $\tau_{rxn}^{avg}$  as a function of ionic potential in 0.5(M) perchlorate salt solutions in ethyl acetate containing  $(^t\text{Bu})_4^+$ ,  $\text{Na}^+$ ,  $\text{Li}^+$ ,  $\text{Sr}^{+2}$ , and  $\text{Ca}^{+2}$ . Eq.2.9 is used to obtain  $\tau_{rxn}^{avg}$  from the relevant fit parameters. Data for  $(^t\text{Bu})_4^+$  is obtained by using tetrahydrofuran solution due to solubility restriction in ethyl acetate. Note that  $\tau_{rxn}^{avg}$  in presence of  $\text{Mg}^{+2}$  is not included as it shows large deviation.  $\tau_{rxn}^{avg}$  (in ps) for P4C, P5C and P6C in presence of  $\text{Mg}^{+2}$  are 429, 39 and 74, respectively.

We have used the expressions derived for studying the broad barrier and over-damped reactions in order to explore the applicability of ZH theory<sup>34</sup> in our systems. This is done with the assumption that the twisting in TICT processes will experience the friction in the same manner as the rotating moiety during isomerization reaction in electrolyte solutions. In addition, since these molecules possess low activation

barrier ( $3 - 4 k_B T$ )<sup>36</sup>, the reaction involving these molecules are assumed to be broad-barrier and over-damped. The ZH theory provides the following expression for transmission coefficient<sup>34</sup>,  $\kappa_r$  ( $= k/k_{TST}$ ) for *broad barrier* reactions with barrier frequency,  $\omega_b$

$$\kappa_r = \left[ \kappa_r + \frac{\zeta_0}{I_m \omega_b} + \frac{1}{\omega_b} \int_0^\infty dt e^{-\omega_b \kappa_r t} \delta\zeta_I(t) \right]^{-1}, \quad (2.10a)$$

where  $\zeta_0$  and  $\delta\zeta_I$  are, respectively, the solvent (collisional and dielectric) and ion atmosphere contributions to the total friction experienced by the reactive mode.  $I_m$  denotes the moment of inertia and is calculated from the reduced mass of the rotating moiety.

Reactions involving broad barriers are likely to be overdamped and the ZH theory obtains the following expression for calculating the transmission coefficient in this limit<sup>34</sup>

$$\kappa_r = \left[ \frac{\zeta_0}{I\omega_b} + \frac{1}{I\omega_b} \int_0^\infty dt e^{-\omega_b \kappa_r t} \delta\zeta_I(t) \right]^{-1}, \quad (2.10b)$$

$$\text{with } \delta\zeta_I(t) = \delta\zeta_I(t=0) \exp(-t/\tau_s). \quad (2.11)$$

The ion-atmosphere friction at  $t=0$ ,  $\delta\zeta_I(t=0)$ , can then be calculated from the static dielectric constant ( $\epsilon_0$ ) of the solvent, dipole moment of the solute ( $\mu$ ) and its cavity radius ( $a$ ) by using the relation<sup>34</sup>

$$\delta\zeta_I(t=0) = \frac{\mu^2}{a^3} \left[ \frac{2(\epsilon_0 - 1)}{2\epsilon_0 + 1} + \frac{3\epsilon_0 y}{(2\epsilon_0 + 1)(2\epsilon_0 + 1 + \epsilon_0 y)} \right], \quad (2.12)$$

where  $y$  is related to the inverse Debye screening length ( $\kappa$ ) as follows<sup>34</sup>

$$y = (1 + \kappa a)^{-1} (\kappa a)^2, \quad \kappa^2 = \frac{4\pi N_A e^2}{1000 \epsilon_0 k_B T} \sum_i z_i^2 c_i. \quad (2.13)$$

Here  $N_A$  is the Avogadro number,  $k_B$  is Boltzmann's constant,  $e$  the electronic charge, and  $c_i$  and  $z_i$  are concentration (M) and valence of the  $i$ -th ionic species. The average solvation time,  $\tau_s$  is connected to the spectral response function,  $S(t)$  by the

relation<sup>46</sup>:  $\tau_s = \int_0^{\infty} dt S(t)$ . In our calculation,  $\tau_s$  for ethyl acetate in presence of various concentrations of LiClO<sub>4</sub>, has been obtained from the experimentally determined spectral response function,  $S(t)$  by following the time dependent fluorescence Stokes shift of a polarity probe dissolved in solution<sup>61</sup>.  $\zeta_0 = 6\eta_0(4\pi R^3/3)$ , with  $\eta_0$  and  $R$  being the solvent viscosity and radius of the rotating moiety, respectively. Once these quantities are determined and  $\omega_b$  fixed,  $\kappa_r$  can be obtained by solving Eqs.2.10 (a) and 2.10(b) self-consistently. Finally, the rate ( $k$ ) is calculated by using the relation<sup>34</sup>

$$k = \kappa_r \frac{k_B T}{h} \exp(-\Delta G^*/k_B T) = \kappa_r \nu_R \exp\left(-\Delta G^*/k_B T\right), \quad (2.14)$$

where the activation barrier ( $\Delta G^*$ ) is obtained from the change in reaction free energy  $\Delta G_r$  (which, in turn, is determined from Eq.2.1) by using the correlation<sup>36</sup>,  $\Delta G^* \approx \alpha \Delta G_r$ , with  $\alpha$  values reported in Ref. 36.

We now use Eqs. 2.10(a) and 2.10(b) in order to compute the electrolyte concentration dependent transmission coefficients ( $\kappa_r$ ) in broad barrier and broad barrier overdamped limits for reactions in P4C, P5C and P6C. Subsequently, the rate ( $k$ ) is obtained by using Eq.2.14. The computed results ( $1/k$ ) are shown in Fig.2.12 where the upper panel represents the results for P4C, middle panel for P5C and the lower panel for P6C. The theoretical results are computed with  $\omega_b \sim 2 \times 10^{12} \text{ s}^{-1}$ . No other fitting parameters have been used for calculating the rate from the ZH theory<sup>34</sup>. We also show the experimental results ( $\tau_{rxn}^{avg}$ ) in the same figure for comparison. The agreement between the theory and experiment is surprisingly good for these TICT molecules. The deviation in larger electrolyte concentration may have originated from the partial neglect of the ion-pair effects on reaction rate. The observed agreement between the experimentally determined electrolyte concentration dependent average reaction time and the predictions from the ZH theory is rather interesting and warrants the following comments. First, the ZH theory has been developed to study isomerization dynamics in electrolyte solutions which involve

only the rotation of the polar moiety through the solution. Simultaneous charge transfer with rotation has not been dealt with in the ZH theory. However, if the intramolecular charge transfer becomes very fast compared to the rotational time scale, then the situation becomes similar as envisaged in the ZH theory. Second, the inputs required to calculate the average reaction time have been obtained from the relevant experiments and hence contain effects of ion, triple ion,

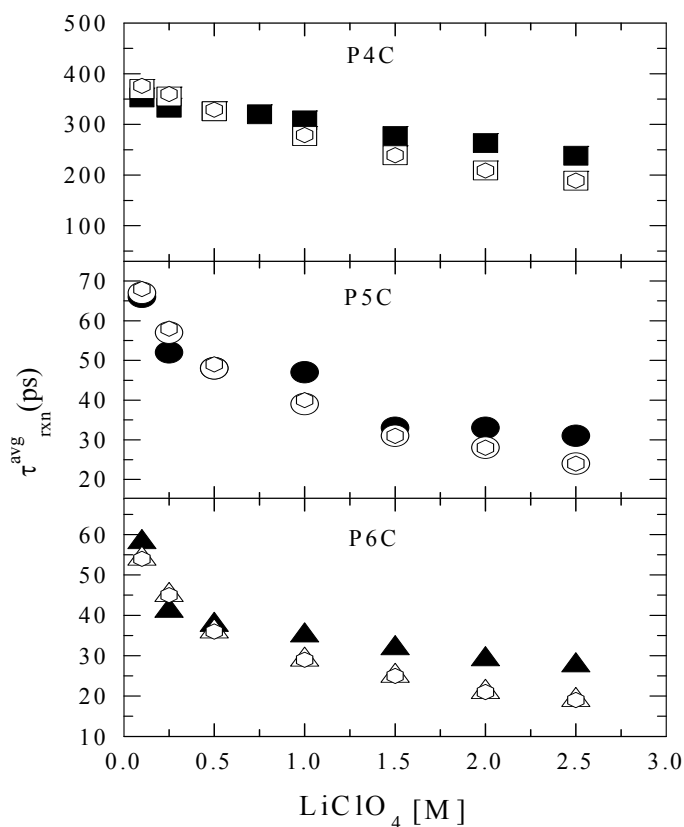


**Fig. 2.12.:** Comparison between experimentally obtained average reaction times ( $\tau_{rxn}^{avg}$ ) at different electrolyte concentrations and those predicted by the theory of van der Zwan and J. T. Hynes for P4C (*upper panel*, squares), P5C (*middle panel*, circles) and P6C (*lower panel*, triangles). While the experimental data are shown by the filled symbols, the predictions are denoted by the open symbols. The hexagons denote the calculation of the rate in the broad-barrier limit given by Eq. 2.10(a) in the text. The ZH predictions in the broad-barrier over-damped limit are calculated by using Eq. 2.10(b) and are shown by squares (P4C, upper panel), open circles (P5C, middle panel) and open triangles (P6C, lower panel). For the three molecules, calculations are done by using a single value of  $\omega_b = 2 \times 10^{12} \text{ s}^{-1}$ .

ion-pair and other species implicitly. This may be another reason for the calculated reaction time constants tallying so well with the experimental data obtained for (LiClO<sub>4</sub> + ethyl acetate) solution where ion-pairs and higher order aggregates are expected to dominate.

## 2.4. Conclusion

Let us first summarize the main results of this work. Steady state fluorescence studies with P4C, P5C and P6C in ethyl acetate and acetonitrile indicate that the addition of electrolyte continuously shifts the absorption and emission spectra towards lower energy and does *not* alter the shape of the bands. The shifts in the absorption and emission spectra are associated with spectral broadening (for absorption) and narrowing (for emission). These observations are consistent with earlier studies with C153 in neat polar solvents and also in electrolyte solutions. Addition of electrolyte decreases the quantum yield of these TICT molecules appreciably while the reduction for C153 is only ~40% from that in the absence of electrolyte. The enhancement of CT/LE area ratio upon addition of electrolyte is much larger in ethyl acetate than in acetonitrile. Since the area ratio is related to the change in reaction free energy ( $-\Delta G_r$ ) via equilibrium constant,  $-\Delta G_r$  for P4C in ethyl acetate is found to vary between negative and positive values indicating that the unfavorable LE  $\rightarrow$  CT conversion reaction in pure ethyl acetate becomes highly favorable at large electrolyte concentration. This is much less in acetonitrile, being ~20% for both P5C and P6C molecules. Also, the electrolyte effects are more pronounced in P4C than those found for P5C and P6C. For example, upon increasing the LiClO<sub>4</sub> concentration from 0.0 M to 2.5 M the equilibrium constant for the LE  $\rightarrow$  CT conversion reaction is enhanced by a factor of ~50 for P4C, ~10 for P5C and ~2 for P6C compared to those in pure ethyl acetate. In acetonitrile, however, the modification of the equilibrium constant in presence of electrolyte is confined within 2 - 4 times only. The ion-size dependent study indicates that,  $-\Delta G_r$  depends very weakly on  $z/r_{\text{ion}}$ . Linear correlations with  $z/r_{\text{ion}}$  are observed for the CT emission frequency ( $\nu_{\text{CT}}$ ) and quantum yield of these TICT molecules. Quantum yield and

emission peak frequency of a non-reactive probe such as C153 in electrolyte solutions are also found to be linear with  $z/r_{ion}$ . In all these cases, however, values obtained in presence of  $Mg^{+2}$  deviate from the observed linearity. This may be due to a considerable slowing down of environmental dynamics in presence of ions with large values of  $z/r_{ion}$  that inhibits the photo-excited probe to attain the complete equilibrium during its fluorescence lifetime<sup>33</sup>. Since the degree of dissociation is different for different electrolytes in the same solvent and also different for the same electrolyte in different solvents, the apparent ion-size dependence may derive contributions from different species present in electrolyte solutions<sup>4, 49</sup>. Therefore, further investigation is required to quantify the effects of ion size in electrolyte solutions.

Time resolved fluorescence emission studies in ethyl acetate containing  $LiClO_4$  reveal a moderate to strong electrolyte concentration dependence of average reaction rate for  $LE \rightarrow CT$  conversion in P4C, P5C and P6C. The average reaction time (average rate) is found to decrease (increase) for all these molecules as the concentration of  $LiClO_4$  is increased. The average reaction times for P4C and P5C are found to be even smaller in solution of higher electrolyte concentration than that in pure ethyl acetate which may be attributed to the interplay between the electrolyte-solute interaction and the effects due to the increased dielectric constant<sup>1-3, 33</sup>. The average reaction time for P6C does not fall below that in pure solvent at higher electrolyte concentration, even though it decreases with electrolyte concentration. It could very well be that the average reaction time for P6C also becomes smaller at high electrolyte concentration than in pure ethyl acetate. Since the reaction rate in P6C in pure ethyl acetate is much faster than that in P5C, a good portion of the initial fast decay of P6C at higher electrolyte concentration might have been missed due to the limited time resolution ( $\sim 50$  ps) available to us. As a result, the average reaction time obtained at higher  $LiClO_4$  concentration involves larger uncertainty as it derives contributions incorrectly from the relatively slower decay components. Time resolved studies also reveal that the average reaction time decreases linearly with  $z/r_{ion}$  provided the data for  $Mg^{+2}$  are not included in the correlation. It is to be

mentioned here that similar linear correlation has been found in the steady state studies of these TICT molecules and also in the studies of dynamics in electrolyte solution<sup>33</sup> using several non-reactive solvation probes<sup>33</sup>. As indicated in these studies<sup>33</sup> the deviation of  $Mg^{+2}$  and other ions with larger value of  $z/r_{ion}$  from the observed linearity arises because the time dependent rearrangement of the environment surrounding the photo-excited probe (reactive or non-reactive) is considerably slowed down in presence of such ions and hence the ion-solvent composite dynamics is not complete within the average excited state life time of the probe

We have also calculated the electrolyte concentration dependent average reaction time in ethyl acetate for the three molecules by using a theory proposed by Zwan and Hynes using  $\omega_b \sim 2 \times 10^{12} \text{ s}^{-1}$  in the broad barrier and broad-barrier over-damped limits<sup>34</sup>. All other parameters in our calculation have been obtained from the relevant experiments. For all the molecules studied here, the calculated average reaction times are found to be in semi-quantitative agreement with experiments at all electrolyte concentrations. Note here that a better time resolution than employed here may slightly alter the values of the electrolyte concentration dependent average solvation time used here for the calculation. This means that a different value of  $\omega_b$  may be required. However, a reasonable value of  $\omega_b$  can capture the electrolyte concentration dependence of average reaction rate for these TICT molecules in ethyl acetate where ion pairing and higher order aggregation phenomena dominate. It has been shown in the works of Zwan and Hynes<sup>34</sup> that a semi-quantitative description of isomerization reaction in electrolyte solutions of weakly polar solvent (such as ethyl acetate) can be obtained provided the time dependent dielectric friction is supplied from relevant experiments. Even though this extension involves approximation, the use of experimental data takes care of the effects of ion-pairing and other complex species which is probably responsible for the observed agreement between theory and experiments.

## References and Notes

1. Huppert, D.; Ittah, V.; Kosower, M. *Chem. Phys. Lett.* **1989**, *159*, 267.
2. Bart, E.; Huppert, D. *Chem. Phys. Lett.* **1992**, *195*, 37.
3. Ittah, V.; Huppert, D. *Chem. Phys. Lett.* **1990**, *173*, 496.
4. Eberspacher, P.; Wismeth, E.; Buchner, R.; Barthel, J. *J. Mol. Liq.* **2006**, *129*, 3.
5. Barthel, J.; Hetzenauer, H.; Buchner, R. *Ber. Bunsenges. Phys. Chem.* **1992**, *96*, 1424.
6. Kalugin O. N.; Panchenko, V. G.; V'yunnik, I. N.; *Russian J. Phys. Chem.* **2005**, *79*, 629.
7. Fuoss, R. M.; Kraus, C. A. *J. Am. Chem. Soc.* **1933**, *55*, 2387.
8. Fuoss, R. M.; Kraus, C. A. *J. Am. Chem. Soc.* **1933**, *55*, 1019.
9. Marcus, Y.; Hefter, G. *Chem. Rev.* **2004**, *104*, 3405.
10. Richardi, J.; Fries, P. H.; Krienke, H. *J. Chem. Phys.* **1998**, *108*, 4079.
11. Spanberg, D.; Hermansson, K. *Chem. Phys.* **2004**, *300*, 165.
12. Mollner A. K.; Brooksby, P. A.; Loring, J. S.; Bako, I.; Palinkas, G.; Fawcett, W. R. *J. Phys. Chem. A.* **2004**, *108*, 3344.
13. Fawcett, W. R.; Liu, G. *J. Phys. Chem.* **1992**, *96*, 4231.
14. Barthel, J.; Deser, R. *J. Solution Chem.* **1994**, *23*, 1133.
15. Loring, J. S.; Fawcett, W. R.; *J. Phys. Chem. A.* **1999**, *103*, 3608.
16. Cha, J. N. Cheong, B. S. Cho, H. G. *J. Phys. Chem. A.* **2001**, *105*, 1789.
17. Rudolph, W. W.; Irmer, G.; Hefter, G. T. *Phys. Chem. Chem. Phys.* **2003**, *5*, 5253.
18. Barthel, J.; Kleebauer, M.; Buchner, R. *J. Solution Chem.* **1995**, *24*, 1.
19. Buchner, R.; Chen, T.; Hefter, G. *J. Phys. Chem. B.* **2004**, *108*, 2365.
20. Chen, T.; Hefter, G.; Buchner, R. *J. Solution Chem.* **2005**, *34*, 1045.
21. Barthel, J.; Wachter, R.; Gores, H. J. *In Modern Aspects of Electrochemistry*; Conway, B. E.; Bockris, J. O'M., Eds. Plenum, New York, 1979, Vol. 13, p.1.
22. Buchner, R.; Hefter, G. T.; May, P. M. *J. Phys. Chem. A.* **1999**, *103*, 1.
23. Salomon, M.; Uchiyama, M. C. *J. Solution Chem.* **1987**, *16*, 21.

24. Salomon, M.; Slane S.; Plichta, E.; Uchiyama, M. C. *J. Solution Chem.* **1989**, *18*, 977.
25. Delsignore, M.; Farber, H.; Petrucci, S. *J. Phys. Chem.* **1985**, *89*, 4968.
26. Delsignore, M.; Farber, H.; Petrucci, S. *J. Phys. Chem.* **1986**, *90*, 66.
27. Salomon, M.; Uchiyama, M.; Xu, M.; Petrucci, S. *J. Phys. Chem.* **1989**, *93*, 4374.
28. Petrucci, S.; Eyring, M. *J. Phys. Chem.* **1991**, *95*, 1731.
29. Cachet, H.; Cyrot, A.; Fakir, M.; Lestrade, J. C. *J. Phys. Chem.* **1979**, *83*, 2419.
30. Chen, Z.; Hojo, M. *J. Phys. Chem. A.* **1997**, *101*, 10896.
31. Henderson, W. A.; Brooks, N. R.; Brennessel, W. W.; Young Jr. V. J. *J. Phys. Chem. A.* **2004**, *108*, 225.
32. Diamond, R. M. *J. Phys. Chem.* **1963**, *67*, 2513.
33. Chapman, C. F.; Maroncelli, M. *J. Phys. Chem.* **1991**, *95*, 9095.
34. Zwan, van der G.; Hynes, J. T. *Chem. Phys.* **1991**, *152*, 169.
35. Hynes, J. T. *Charge -Transfer Reactions and Solvation Dynamics In Ultrafast Dynamics of Chemical Systems*; Simon, J. D., Ed.; Kluwer: Dodrecht, 1994; p.345.
36. Dahl, K.; Biswas, R.; Ito, N.; Maroncelli, M. *J. Phys. Chem. B*, **2005**, *109*, 1563.
37. Rettig, W. *J. Luminesc.* **1980**, *26*, 21; *J. Phys. Chem.* **1982**, *86*, 1970
38. Rettig, W.; Gleiter, R.; *J. Phys. Chem.* **1985**, *89*, 4674.
39. Rettig, W.; Wermuth, G. *J. Photochem.* **1985**, *28*, 351; Al-Hassan, K. A.; Rettig, W. *Chem. Phys. Lett.* **1986**, *126*, 273; LaFemina, J. P.; Duke, C. B.; Rettig, W. *Chem. Phys.* **1990**, *87*, 2151; Braun, D.; Rettig, W. *Chem. Phys.* **1994**, *180*, 231; *Chem. Phys. Lett.* **1997**, *268*, 110.
40. Rettig, W. *Ber. Bunsen-Ges. Phys. Chem.* **1991**, *95*, 259.
41. Yatsushashi, T.; Trushin, S. A.; Fuss, W.; Rettig, W.; Schmid, W. E.; Zilberg, S. *Chem. Phys.* **2004**, *296*, 1.

42. Zachariasse, K. A.; Grobys, M.; von der Haar, T.; Hebecker, A.; Il'ichev, Y. V.; Jiang, Y.-B.; Morawski, O.; Kuhnle, W.; *J. Photochem. Photobiol. A* **1996**, *102*, 59.
43. Rettig, W.; Zeitz, B. *Chem. Phys. Lett.* **2000**, *317*, 187.
44. Maroncelli, M. *private communication*.
45. Parusel, A. B. *J. Chem. Phys. Lett.* **2001**, *340*, 531.
46. Horng, M. L.; Gardecki, J. A.; Papazyan, A.; Maroncelli, M. *J. Phys. Chem. B* **1995**, *99*, 17311.
47. Lewis, J. E.; Biswas, R.; Robinson, A. G.; Maroncelli, M. *J. Phys. Chem. B* **2001**, *105*, 3306.
48. Natarajan, P.; Raja, C. *Eur. Polym. J.* **2005**, *41*, 2496.
49. Wachter, W.; Fernandez, S.; Buchner, R.; Hefter, G.; *J. Phys. Chem. B*, **2007**, ASAP article, *published on web, June 30, 2007*.
50. Riddick, J. A.; Bunger, W. B.; Sakano, T. K. *Organic Solvents*; Wiley: New York, 1986.
51. Pocker, Y.; Ciula, J. C. *J. Am. Chem. Soc.* **1989**, *111*, 4728.
52. The electrolyte concentration dependence of  $\nu_{CT}$  (in  $10^3 \text{ cm}^{-1}$ ) for these TICT molecules can be fitted to a bi-exponential function of the following form:  $\nu_{CT}(c) = a_1 \exp[-b_1 * c] + a_2 \exp[-b_2 * c]$  with  $c$  as the electrolyte concentration (moles/litre). In  $\text{LiClO}_4$  solutions of ethyl acetate the respective values of the fitting parameters for P4C, P5C and P6C are:  $a_1 = 2.67, 2.41, 2.46$ ;  $a_2 = 19.37, 19.43, 20.15$ ;  $b_1 = 4.17, 2.98, 3.41$  and  $b_2 = 0.009, 0.007, 0.008$ . For acetonitrile containing  $\text{LiClO}_4$ , the parameters are:  $a_1 = 0.76, 0.71, 0.68$ ;  $a_2 = 19.28, 19.39, 20.11$ ;  $b_1 = 4.74, 5.09, 7.00$ ;  $b_2 = 0.02, 0.016, 0.024$ , with  $r^2 \cong 1$  for all cases.
53. Huppert, D.; Ittah, V.; Kosower, M. *Chem. Phys. Lett.* **1989**, *159*, 211.
54. Shannon, R. D.; Prewitt, C. T., *Acta Crystallogr.* **1970**, *B26*, 1076
55. Velapoldi, R.; Mielenz, K. *A Fluorescence Standard Reference Material: Quinine Sulfate Dihydrate*; National Bureau of Standards: Washington, DC, 1980; Vol. Special Publications 260 – 64.

56. Bevington, P. R. *Data Reduction and Error Analysis for the Physical Sciences*; McGraw-Hill: New York, 1969.
57. Electrolyte concentration dependent net quantum yield of these TICT molecules in ethyl acetate can also be fitted nicely to a biexponential function of the following form:  $\Phi(c) = A_1 \exp[-B_1 * c] + A_2 \exp[-B_2 * c]$  with the following fitting parameters for P4C, P5C and P6C (sequentially):  $A_1 = 0.035, 0.026, 0.02$ ;  $A_2 = 0.051, 0.012, 0.019$ ;  $B_1 = 17.37, 6.54, 6.03$  and  $B_2 = 0.677, 0.118, 0.142$ . For acetonitrile containing  $\text{LiClO}_4$ , the fitting parameters are:  $A_1 = 0.005, 0.004, \text{ and } 0.008$ ;  $A_2 = 0.025, 0.019, \text{ and } 0.011$ ;  $B_1 = 15.75, 14.47, \text{ and } 11.92$  and  $B_2 = 0.618, 0.455, 0.348$ , with  $r^2 \cong 1$  for all cases.
58. Lewis, J. E.; Maroncelli, M. *Chem. Phys. Lett.* **1998**, 282, 197.
59. Briks, J.B. *Photophysics of Aromatic Molecules*; Wiley: London, 1970
60. The electrolyte ( $\text{LiClO}_4$ ) concentration dependent average reaction time can be fitted to the following biexponential function  $\tau_{rxn}^{avg}(c) = \tau_1 \exp[-ac] + \tau_2 \exp[-bc]$  with the following parameters (in proper units) for P4C, P5C and P6C (sequentially):  $\tau_1 = 153, 376, 80$ ;  $\tau_2 = 201, 55, 41$ ;  $a = 0.16, 34.48, 14.88$ ;  $b = 0.16, 0.26, 0.16$  with  $r^2 \sim 1.0$  for all cases. It is interesting to note that similar bi-exponential fitting has also been obtained for several steady state properties.
61. The average solvation time ( $\tau_s$ , in ps) determined experimentally by using C153 as solvation probe in  $\text{LiClO}_4$  solutions of ethyl acetate is found to obey the following relation with electrolyte concentration ( $c$ , moles/litre) within the range (0.1 – 2.5 M) studied here:  $\tau_s(c) = A \exp[-Bc]$ , where  $A = 919$ ,  $B = 0.28$ , and  $r^2 = 0.99$ .

## Chapter 3

# Intramolecular Charge Transfer Reaction in Solutions of Low to High Electrolyte Concentrations: Interplay between Friction and Solvation

### 3.1. Introduction

In this chapter we present results of our spectroscopic studies on the photo-excited intramolecular charge transfer reaction in 4-(1-azetidiny)benzotrile (P4C) in LiClO<sub>4</sub> solutions of ethyl acetate, ethanol and acetonitrile with the electrolyte (LiClO<sub>4</sub>) concentrations ranging from very dilute to the highest concentrations accessible (limited by the solubility) in these media. While the three solvents considered here represent solvents from three different categories (non-associating weakly polar, associating and non-associating strongly polar), the reaction rate being the slowest<sup>1-4</sup> in P4C among the molecules in the PnC series suits best to the broad time resolution available to us. As before, the formation of the locally excited (LE) state upon photo-excitation of P4C and its subsequent conversion to the charge-transferred (CT) state is explained in terms of the well-known twisted intramolecular charge transfer (TICT) mechanism<sup>1-7</sup>. We use the Eq. 1.1 & 1.2 derived in Chapter 1 in order to analyze the time dependence of the LE or CT intensity as well as to determine the rate of the LE → CT conversion reaction in P4C. We would like to mention here that data (both from steady state and time resolved studies) obtained for solutions with very low electrolyte concentrations (<0.10 moles-litre<sup>-1</sup>) in ethyl acetate and data in ethanol for the entire electrolyte concentration range as well as the time resolved data for electrolyte solutions in acetonitrile are presented here for the first time. In order to show the continuous variation of the reaction yield and rate in the full range of the electrolyte concentration (from very low to very high) in these solvents, results<sup>1,7</sup> at high LiClO<sub>4</sub> concentration in ethyl acetate and acetonitrile

(steady state only) which have been presented already in chapter 2 are also shown here.

The main results of the chapter are as follows. The total red-shift in the absorption spectrum of P4C for increasing the concentration of LiClO<sub>4</sub> upto 1.0 M in ethyl acetate, ethanol and acetonitrile is in the range of 300 – 400 cm<sup>-1</sup>, which increases to ~1000 cm<sup>-1</sup> and 700 cm<sup>-1</sup>, respectively, in ethyl acetate and ethanol upon increasing the concentration to 3.0 M. Further increase of LiClO<sub>4</sub> concentration upto 5.0 M in ethanol produces an additional red-shift of about 50 cm<sup>-1</sup> only. Even though the electrolyte-induced red-shift in the LE band is very small (~100 cm<sup>-1</sup>) in all these solvents, the total shift in the CT band is quite large, approximately 3000 cm<sup>-1</sup> in ethyl acetate and ~1100 cm<sup>-1</sup> in ethanol and acetonitrile for the full concentration range studied. As observed earlier (chapter 2) in electrolyte solutions of ethyl acetate and acetonitrile<sup>1, 7</sup>, the total emission quantum yield of P4C in ethanol also decreases exponentially<sup>8</sup> with electrolyte concentration. In all these solvents, the formation of the CT population increases with the increase in electrolyte concentration, the rate of increase being the steepest for ethyl acetate. A bi-exponential function of time has been found to fit adequately the time resolved LE or CT fluorescence emission intensity at all concentrations in these solvents. Most interestingly, the reaction time for the LE → CT conversion in P4C has been found to increase with electrolyte concentration in the low electrolyte concentration range (≤ 0.10 moles-litre<sup>-1</sup>) which, upon further increase of concentration, decreases, giving rise to a non-monotonic electrolyte concentration dependence of the reaction rate. The non-monotonic nature is found to be the strongest for ethyl acetate and weakest for ethanol, even though the electrolyte-induced increase in reaction rate at higher concentration is the highest in ethanol.

The organization of the rest of the chapter is as follows. Experimental details are given in the next section. Section 3.3 contains experimental results from our steady state and time resolved studies. Supporting information is given wherever necessary in Appendix 2. The article then ends with concluding remarks in section 3.4.

### 3.2. Experimental Details

Synthesis of P4C and sample preparation has been discussed in chapter 2. Ethyl acetate and acetonitrile were used as received (spectrophotometric grade) from Aldrich. Ethanol (spectrophotometric grade) was purchased from SRL, India. Lithium perchlorate ( $\text{LiClO}_4$ ) was obtained from Aldrich (anhydrous and highest available grade) and vacuum dried before use. Steady state and time resolved measurement techniques and the corresponding data analysis procedures have also been described in that chapter. Here also at all concentrations of  $\text{LiClO}_4$  in these solvents, each of the LE emission decays was found to fit with one short time constant and one long time constant, whereas each of the CT emission decays (collected wherever possible) could be fit with one rise-time (similar to short time constant of LE decay) and one long time constant. Therefore, the short time constant associated with the LE decay was considered as the reaction time. In non-polar pure solvents, such as in heptane or hexane, the LE decay of P4C was found to decay single-exponentially with one time constant in the range of a couple of nanosecond<sup>1,7</sup>. For a few cases, emission decays were collected at two or three different emission wavelengths around the LE and CT peaks and the analyzed data were found to vary within a small uncertainty. All the experiments were performed at room temperature,  $295 \pm 0.5$  K.

### 3.3. Results & Discussion

#### 3.3.1 Steady State Spectroscopic Studies

Representative absorption and emission spectra of P4C in  $\text{LiClO}_4$  solutions of ethanol at five different concentrations are presented in Fig.3.1 in order to show the effects of electrolyte on absorption and emission spectra of this intramolecular charge transfer molecule. Fig.3.1 shows that relative to the absorption spectrum (upper panel) in pure ethanol, electrolyte concentration as high as 1.0 M does not induce much shift in the spectrum ( $\sim 350$   $\text{cm}^{-1}$ ), except broadening the envelop by another  $\sim 250$   $\text{cm}^{-1}$ . Upon increasing the concentration to 5.0 M, the absorption spectrum broadens further by  $\sim 500$   $\text{cm}^{-1}$  with a concomitant red-shift by  $\sim 750$   $\text{cm}^{-1}$ .

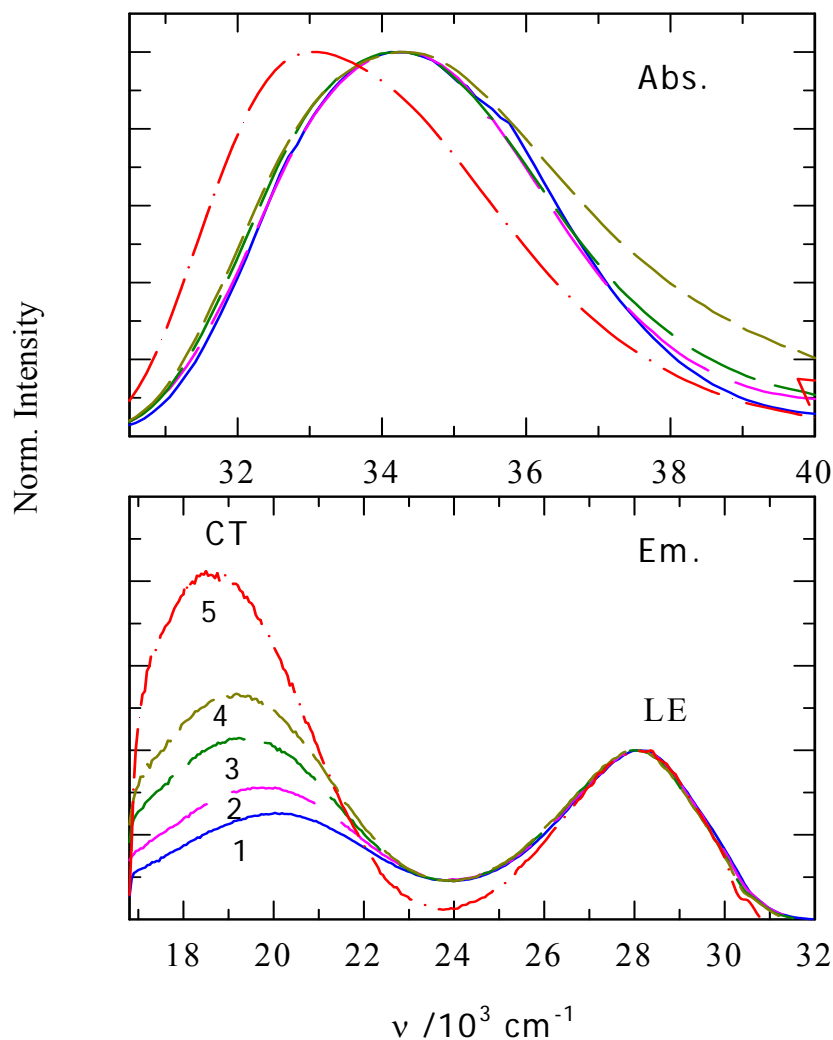


**Fig.3.1:** Representative absorption (upper panel) and emission (lower panel) spectra of 4-(1-azetidiny)benzotrile (P4C) in several concentrations of LiClO<sub>4</sub> in ethanol. Spectra shown in color here are for the following LiClO<sub>4</sub> concentrations (M): 0.0 (1), 0.1 (2), 0.5 (3), 1.0 (4) and 5.0 (5). The color code remains the same for both the absorption and emission spectra.

Relative to the observed moderate effects on absorption spectrum, the electrolyte-induced change in emission spectrum is more pronounced. The emission spectra of P4C in pure ethanol and ethanolic solutions of LiClO<sub>4</sub> shown in the lower panel clearly suggest that the CT population increases as the electrolyte concentration is increased in the solution. In fact, the CT population increases by almost a factor of 4

at 5.0 M solution from that in pure ethanol along with a red-shift in the CT band by about  $1150\text{ cm}^{-1}$ . These changes are discussed in more detail below.

The electrolyte concentration dependence of spectral peaks (absorption and CT emission) and band-widths of P4C in solutions of ethyl acetate, ethanol and acetonitrile are shown respectively in Figs.3.2 and 3.3. As already discussed, the absorption spectra in all these solvents at 1.0 M  $\text{LiClO}_4$  solutions show a red-shift by  $\sim 400\text{ cm}^{-1}$  from those in pure solvents, which is further shifted by  $\sim 300 - 500\text{ cm}^{-1}$  upon increasing the concentration to 3.0 M in ethyl acetate and ethanol. The electrolyte concentration dependence of the LE band is negligible and is summarized in Table A4 in Appendix 2. The shift in the CT band is, however, much larger and in presence of 3.0 M  $\text{LiClO}_4$  the red-shift is approximately 3.5 times more in ethyl acetate than that in ethanol even-though the dielectric constant ( $\epsilon_0$ ) of the former is  $\sim 4$  times lower than the latter. Note that the increase of electrolyte concentration to 0.5 M produces  $\sim 70\text{-}80\%$  of the total observed shift in all these solvents which indicate the presence of direct ion-solute interaction in dilute electrolyte solutions. Further increase in concentration does contribute to the stabilization energy (red-shift) but by relatively a small amount and originates mostly from the increase in average dielectric constant of the solution because of the presence of ion-pairs at appreciable concentration at high electrolyte concentrations. The large concentrations of ion-pairs (solvent-separated and solvent-shared) are also probably responsible for making the solution dynamics faster at the high concentration regime because the fast rotational motion of these ion-pairs enhances the rate of the orientational polarization relaxation<sup>9</sup> of the medium. The electrolyte ( $\text{LiClO}_4$ ) concentration dependence of the width of the absorption spectrum and that of the inhomogeneous width of the CT emission band, shown in figure 3.3, warrants the following comments. As it is seen here and also was observed earlier<sup>2</sup> that in both ethyl acetate and acetonitrile the CT width show non-monotonic electrolyte concentration dependence.

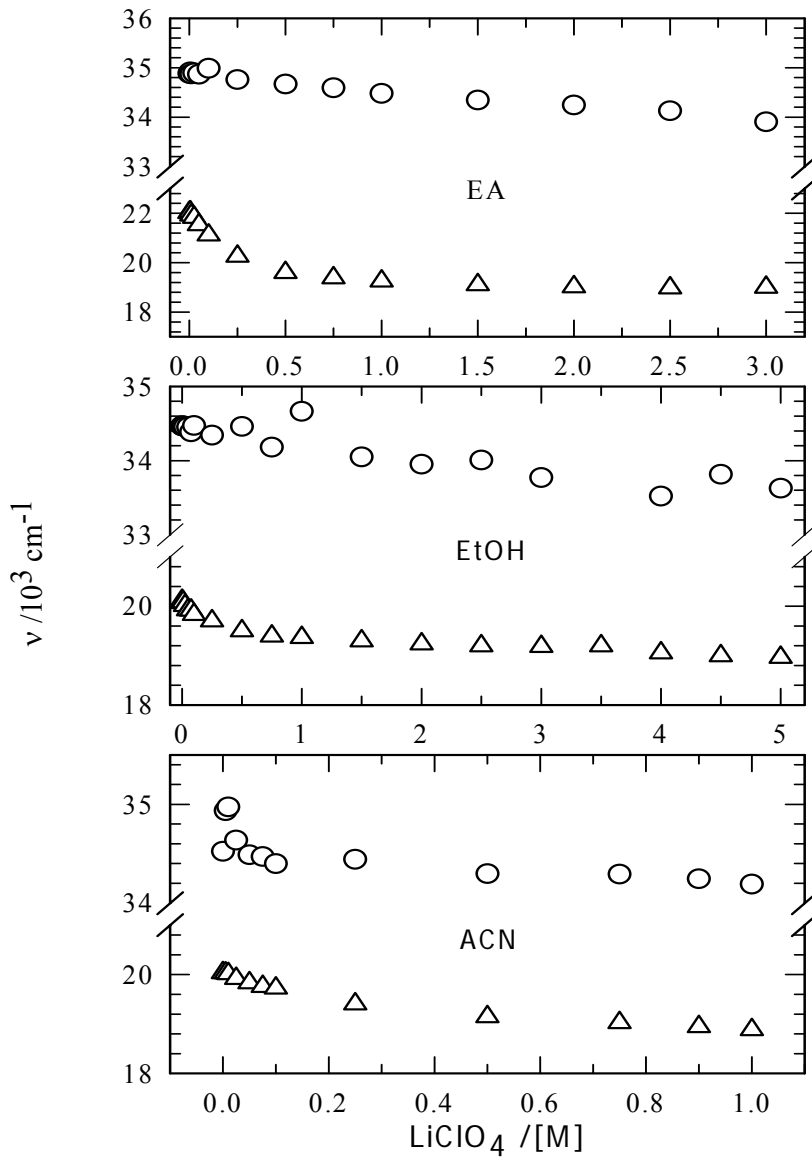


**Fig.3.2.** Electrolyte ( $\text{LiClO}_4$ ) concentration dependencies of absorption (circles) and emission (triangles) peak frequencies 4-(1-azetidiny)benzonitrile (P4C) in solutions of ethyl acetate (upper panel, 'EA'), ethanol (middle panel, 'EtOH') and acetonitrile (lower panel, 'ACN'). For discussions, see text.

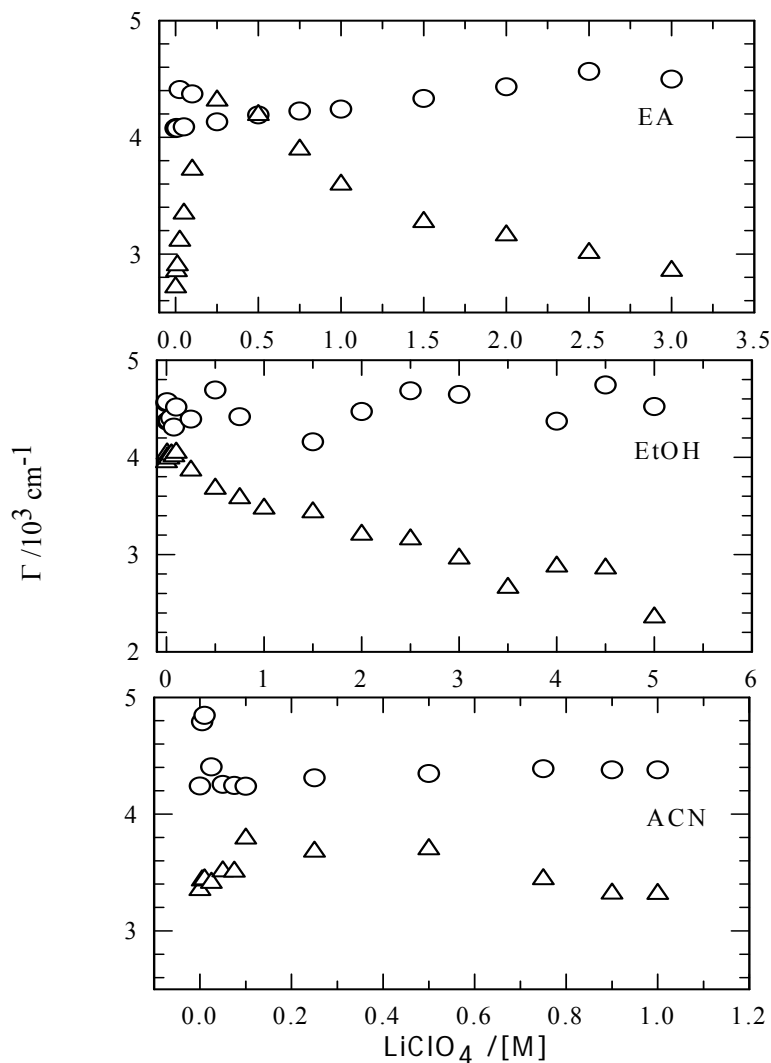


**Fig.3.3:** Electrolyte ( $\text{LiClO}_4$ ) concentration dependence of line widths (full width at half maxima,  $\Gamma$ ) of the absorption spectra and CT bands of 4-(1-azetidynyl) benzonitrile (P4C) in solutions of ethyl acetate (upper panel, ‘EA’), ethanol (middle panel, ‘EtOH’) and acetonitrile (lower panel, ‘ACN’). Absorption and CT width are denoted by circles and triangles, respectively. Note that the CT band-width shown here is the ‘inhomogeneous’ width required to fit the CT emission band while dissecting the entire emission spectrum into two fragments.

Relative to the inhomogeneous CT width in neat ethyl acetate and acetonitrile, the CT band broadens by more than  $1500\text{ cm}^{-1}$  and  $500\text{ cm}^{-1}$  in  $0.25\text{ M LiClO}_4$  solutions in ethyl acetate and acetonitrile, respectively. Recently, such dependence for the CT width has also been found for another closely related ICT molecule in AOT/heptane/water reverse micelles where the static dielectric constant of confined

water pool has been estimated to be similar to those of moderately polar organic solvents<sup>7</sup>. As the spectral width depends both on solute-environment interactions and solution heterogeneity, the presence of ion-solute direct interaction contributes to the width. Secondly, formation of various ion-solvent complexes in electrolyte solutions gives rise to microscopic heterogeneity in the medium that can also modify the spectral width. Upon further addition of electrolyte, concentrations of ion-pairs increase which make the environment less heterogeneous. This, in turn, reduces the spectral width at moderate and high electrolyte concentrations. However, the non-monotonic electrolyte concentration dependence of the CT band-width is not found for LiClO<sub>4</sub> solutions in ethanol, even though the CT width at higher electrolyte concentrations (>0.50 M) remain very similar for P4C in all these solvents. Whether the different concentration dependence of CT width in ethanol is because of its associative nature or not cannot be ascertained from this study as that would require further investigation with several other alcohols. While the LE width does not change with electrolyte concentration (Table A4, Appendix 2), the absorption band-width varies by a small amount (<500 cm<sup>-1</sup>) in electrolyte solutions of these solvents. Figure 3.4 shows the variations of CT/LE area ratio ( $\alpha_{CT}/\alpha_{LE}$ ), equilibrium constant ( $K_{eq}$ ) for the LE  $\rightarrow$  CT conversion reaction in P4C and change in reaction free energy ( $-\Delta G_r$ ) associated with the conversion in ethyl acetate, acetonitrile and ethanol as a function of LiClO<sub>4</sub> concentration. Note that the CT/LE area ratio (upper panel) increases with electrolyte concentration and the rate of increase is the steepest for ethyl acetate. For example, the area ratio increases by a factor of 36 in ethyl acetate upon increasing the electrolyte concentration from 0.0 M to 3.0 M. On the other hand, the area ratio increases by a factor of 2.5 and 2 for increasing the electrolyte concentration from 0.0 M to 5.0 M in ethanol and to 1.0 M in acetonitrile. These changes in area ratio then lead to the increase in equilibrium constant by a factor of  $\sim 57$  in ethyl acetate,  $\sim 3$  in ethanol and  $\sim 2$  in acetonitrile.

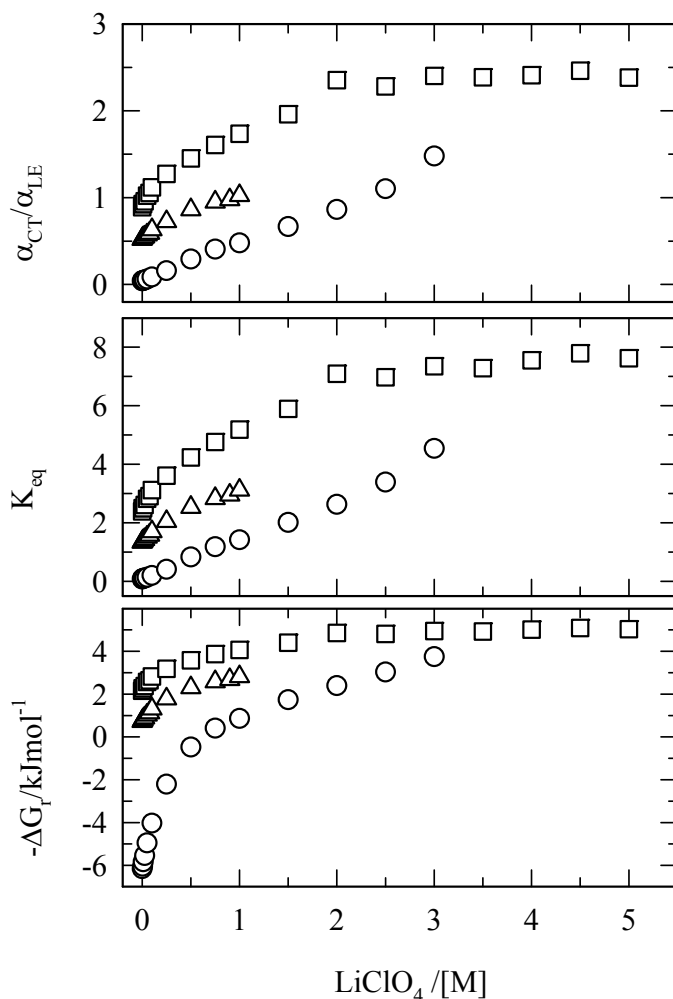


**Fig. 3.4:** Electrolyte concentration dependencies of ratio of population under the CT and LE emission bands ( $\alpha_{CT}/\alpha_{LE}$ , upper panel), equilibrium constant ( $K_{eq}$ , middle panel) and change in reaction free energy ( $-\Delta G_r$ , lower panel) associated with the LE  $\rightarrow$  CT conversion reaction in solutions of ethyl acetate, ethanol and acetonitrile. While the data in ethyl acetate are shown by circles, those in ethanol and acetonitrile are represented respectively by squares and triangles.

This means that the formation of the CT state is most strongly favored upon addition of electrolyte in the lowest polarity solvent (ethyl acetate) among these three solvents considered here. This is further reflected in the electrolyte concentration dependence of reaction free energy (lower panel, Fig. 3.4) where  $-\Delta G_r$  increases by a factor of  $\sim 2.5$  and  $\sim 4.0$  for acetonitrile and ethanol when compared between the data in neat

solvents and those at the highest LiClO<sub>4</sub> concentrations considered in these solvents. For ethyl acetate, however,  $-\Delta G_{\text{r}}$  increases sharply upto 0.5 M and finally changes its sign (from negative to positive) around this concentration, indicating an unfavorable reaction is becoming highly favorable upon addition of electrolyte. Note  $-\Delta G_{\text{r}}$  for the conversion reaction in ethyl acetate at 1.0 M LiClO<sub>4</sub> becomes comparable to that in neat acetonitrile even though the solution dielectric constant is estimated to be half of that of neat acetonitrile<sup>10</sup>. This further stresses the role of direct interaction between the reactant and various species present in solutions of low polarity solvents that control the intramolecular charge transfer reaction in such media. Interestingly,  $-\Delta G_{\text{r}}$  in ethanol remains larger than acetonitrile at all LiClO<sub>4</sub> concentrations which is somewhat counter-intuitive since ethanol is less polar ( $\epsilon_0 \approx 24.5$ ) than acetonitrile ( $\epsilon_0 \approx 36$ )<sup>11</sup>.

### 3.3.2. Time Resolved Fluorescence Studies

Here we present the electrolyte concentration dependence of reaction rate (inverse of reaction time) for the LE  $\rightarrow$  CT conversion reaction of P4C as well as that of average LE decay time and decay amplitudes in three solvents – ethyl acetate, ethanol and acetonitrile. As already mentioned, the reaction rates in ethyl acetate at higher electrolyte concentrations have already been presented in chapter 2 and the results at low concentrations in this solvent are new and never presented before. In addition, results obtained from time dependent studies in electrolyte solutions of ethanol and acetonitrile are discussed here for the first time.

Fig.3.5 shows the time resolved decay of LE intensity for P4C in neat ethanol ('1') and in ethanolic solution of 2.5 M LiClO<sub>4</sub> ('2') along with the bi-exponential fits where the fit parameters are also tabulated. Note here that even though the amplitude of the long time component is very small, mono-exponential function of time has been found to be insufficient to describe the intensity decay.

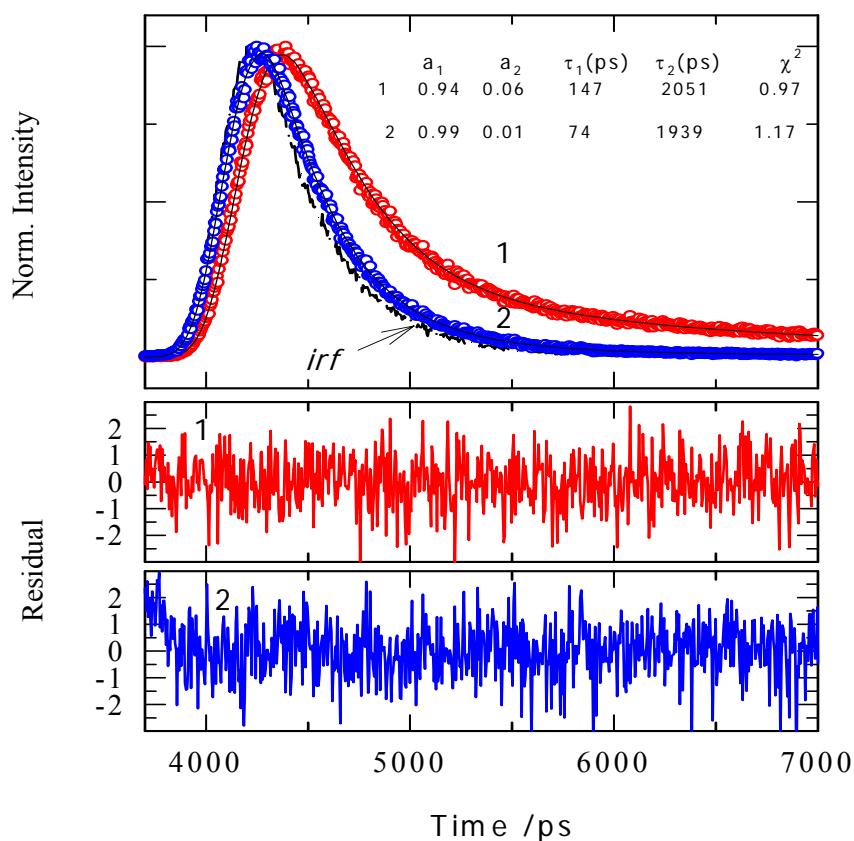


**Fig. 3.5:** Representative LE emission decays of P4C in pure ethanol (‘1’) and in presence of 2.5(M) LiClO<sub>4</sub> (‘2’). While the data are represented by the circles, bi-exponential fits through the data are represented by the solid lines. The instrument response function (IRF) is also shown (dashed line). Results obtained from fits are also provided in the upper panel. Residuals are shown in the *lower panel*.

The values for the ‘goodness of fit’ parameter ( $\chi^2$ ) and the time dependence of the residuals (shown in the two lower panels) suggest that bi-exponential function can indeed adequately fit these decays. Similar fits have also been obtained for other concentrations in ethanol as well as in ethyl acetate and acetonitrile at all electrolyte concentrations. It is evident from this figure that electrolyte affects the reaction rate significantly and in fact the reaction rate becomes *double* in ethanolic solution of 2.5

M LiClO<sub>4</sub> than that in neat ethanol. We would like to mention that the collected emission decays at wavelength near CT emission peaks could also be fitted to bi-exponential functions with same or similar time constants as found for the corresponding LE decays. For example, in presence of 0.10 M LiClO<sub>4</sub> in ethanol, fitting of CT emission decay with no constraints produces time constants 128 ps (rise time) and 2024 ps with  $\chi^2 = 1.04$ . This time constant (rise time) is very similar to the fast time constants (decay time, 138 ps) of the LE decay, indicating that these time constants are essentially associated with the reaction rate<sup>1-4</sup>. Addition of a third exponential did not produce a better fit which has also been observed in several of our earlier studies<sup>3-7</sup>. However, missing of a faster component due to the limited time resolution employed in our experiments may also lead to the observed bi-exponential decay of the time dependent emission intensity. The short time constants obtained from the bi-exponential fits to the LE emission decays are therefore considered as reaction times for P4C in solutions of these solvents at various electrolyte concentrations. Fig.3.6. shows the electrolyte (LiClO<sub>4</sub>) concentration dependence of reaction time ( $\tau_{\text{rxn}}$ ) for P4C in ethyl acetate, ethanol and acetonitrile. The low concentration data for ethanol and acetonitrile are shown separately in the *insets*. Interestingly, in all these solvents,  $\tau_{\text{rxn}}$  increases upon addition of electrolyte in the low concentration regime (<0.05 M) and then decreases systematically upon further addition of electrolyte. Relative to the reaction time in neat solvent,  $\tau_{\text{rxn}}$  in the low concentration regime increases by a maximum of ~30% in ethyl acetate and only by ~5% in ethanol and acetonitrile (see Fig. A6, Appendix 2). This electrolyte-induced increase of  $\tau_{\text{rxn}}$  can be explained as follows: (i) electrolyte solution dynamics being very slow at low concentration, the reactive mode (rotating moiety) experiences excess dynamic friction<sup>12-13</sup> and (ii) slow stabilization of the charge-transferred state due to slow solution dynamics.

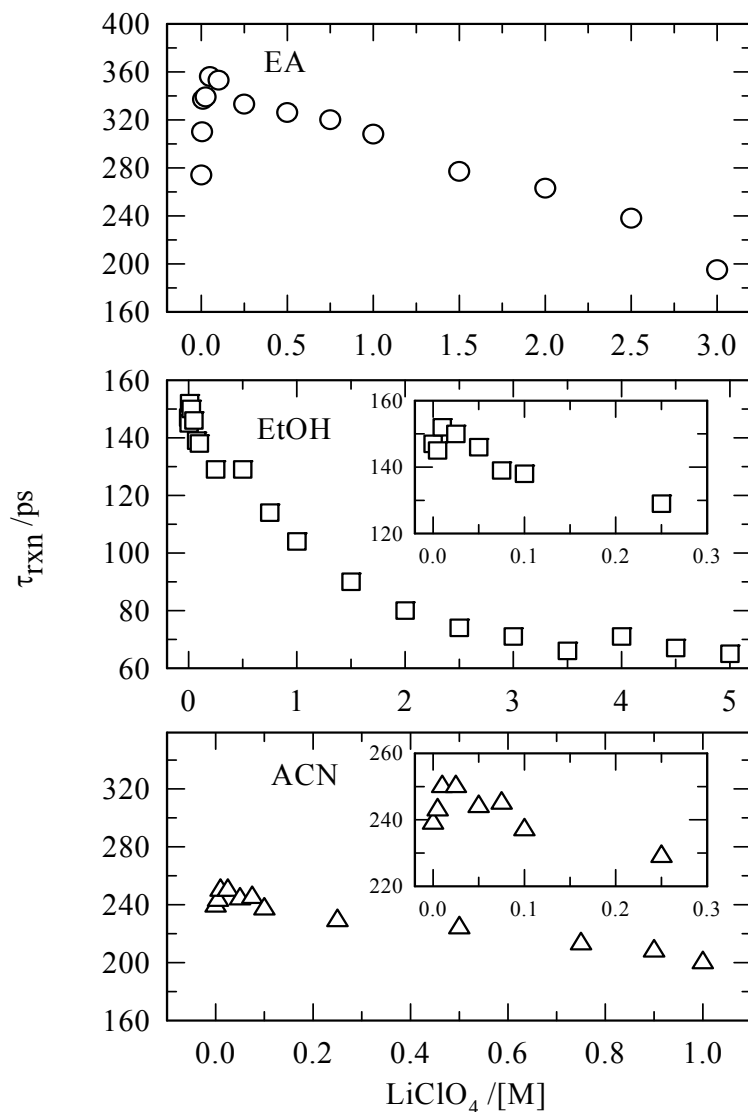


**Fig.3.6:** Electrolyte ( $\text{LiClO}_4$ ) concentration dependence of reaction time ( $\tau_{rxn}$ ) for the  $\text{LE} \rightarrow \text{CT}$  conversion reaction of P4C in solutions of ethyl acetate (upper panel), ethanol (middle panel) and acetonitrile (lower panel). Note that the low concentration data in electrolyte solutions of ethanol and acetonitrile are presented separately in the *insets* in order to show the non-monotonic electrolyte concentration dependence of the reaction rate.

In this concentration range the increase in solution dielectric constant is not significant and hence the barrier height remains largely unchanged<sup>14-15</sup>. However, at higher electrolyte concentrations, the average solution dielectric constant increases considerably which reduces the barrier height. This leads to an increase in reaction rate (static solvent effects). Moreover, the electrolyte solution dynamics being faster

at higher concentrations, the dynamic friction experienced by the reactive mode is relatively less in this limit, leading to an enhancement of the reaction rate (dynamic solvent effects)<sup>12-13</sup>. The combined effects of lowering of the barrier height due to increase in solution dielectric constant and faster environmental reorganization then lead to the LE  $\rightarrow$  CT conversion reaction of P4C to proceed at a rate  $\sim$ 30% higher at 3.0 M in ethyl acetate,  $\sim$ 60% higher at 5.0 M in ethanol and  $\sim$ 15% higher at 1.0 M in acetonitrile solutions than those in neat solvents (Fig. A6, Appendix 2). Therefore, the different modification of reaction rate by electrolyte at low and high concentration limits is probably arising out of a novel interplay between environmental friction and reorganization (solvation) effects.

Just as the short time constant (considered as  $\tau_{\text{rxn}}$ ) is affected by the electrolyte concentration, the long time constant ( $\tau_{\text{long}}$ ) associated with the LE decay also shows significant LiClO<sub>4</sub> concentration dependence. In fact,  $\tau_{\text{long}}$  decreases by a factor of  $\sim$ 5 at 3.0 M in ethyl acetate and by a factor of  $\sim$ 2.5 at 1.0 M in acetonitrile from the neat solvent values (Fig. A7, Appendix 2). However, the electrolyte effects on  $\tau_{\text{long}}$  in ethanol is very small, being only  $\sim$ 15% less at 5.0 M LiClO<sub>4</sub> than that in pure ethanol. The concentration dependence of the respective amplitudes ( $a_{\text{short}}$  and  $a_{\text{long}}$ ) of the LE decay in ethyl acetate, ethanol and acetonitrile are shown in Fig.3.7. As expected, the amplitude that associates with the reaction time ( $a_{\text{short}}$ ) increases with LiClO<sub>4</sub> concentration with simultaneous decrease of  $a_{\text{long}}$  in all the three solvents. Note that the electrolyte-induced variation of  $a_{\text{short}}$  and  $a_{\text{long}}$  are weak in the two relatively more polar solvents (ethanol and acetonitrile) as the driving force (changes in the reaction free energy) is predominantly supplied by the solvent polarities themselves. For ethyl acetate, the variations of these amplitudes are more dramatic, with a cross-over at 0.75 M LiClO<sub>4</sub>, a concentration at which  $-\Delta G_{\text{r}}$  also shows a change in sign (lower panel, Fig.3.4). Also, both the components change by a factor of  $\sim$ 4 at 3.0 M from that in the neat ethyl acetate. As the changes in reaction free energy is related to the ratio of these

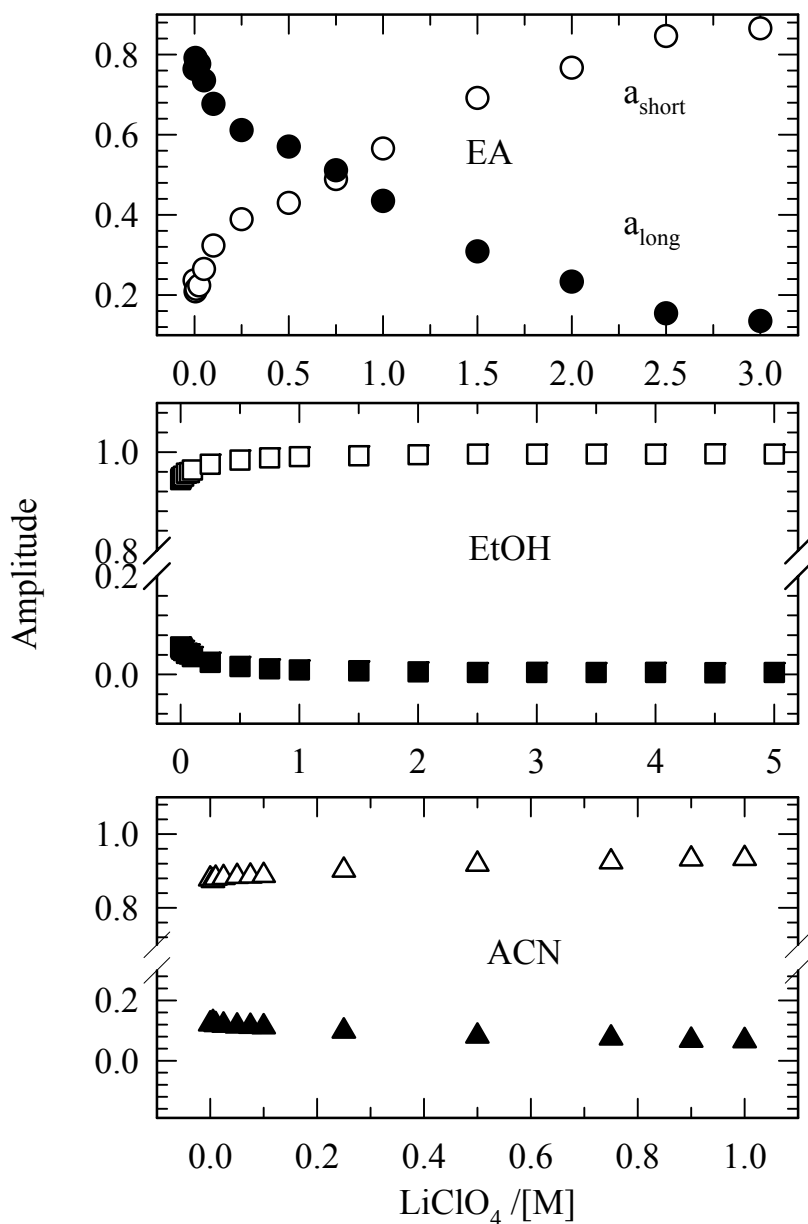


**Fig.3.7:** Electrolyte ( $\text{LiClO}_4$ ) concentration dependence of amplitudes ( $a_{short}$  and  $a_{long}$ ) associated with the  $\text{LE} \rightarrow \text{CT}$  conversion reaction of P4C in electrolyte solutions in ethyl acetate ('EA'), ethanol ('EtOH') and acetonitrile ('ACN'). Note that  $a_{short}$  is denoted by open symbols, whereas  $a_{long}$  is represented by the solid ones.

amplitudes ( $-\Delta G_{r\infty} \ln[a_{short}/a_{long}]$ ), the variation of these components is also consistent with the steady state results presented in Fig. 3.4.

### 3.4. Conclusion

The study of electrolyte concentration dependence of the ICT reaction in P4C in solvents of different polarity and nature (hydroxylic and non-hydroxylic) has revealed several interesting aspects. For example, electrolyte effects seem to be the strongest in ethyl acetate which is the least polar among the three solvents considered here. The reason behind such a strong effect could be the direct ion-reactant interactions in low polar solvents due to ineffective screening of the ions in low polar solvents. Since the driving force for the LE  $\rightarrow$  CT conversion reaction of P4C in ethanol and acetonitrile derives much of the contribution from the solvent polarity itself, equilibrium constant and other related properties grow at a rate with electrolyte concentration in these solvents much slower than in ethyl acetate. Note that even though ethanol is less polar ( $\epsilon_0 \sim 24.5$ ) than acetonitrile ( $\epsilon_0 \sim 36$ ), the area ratio along with reaction equilibrium constant and the change in reaction free energy are larger in former than the latter. Similar difference has also been observed while comparing the results obtained from time resolved studies in these two solvents. Whether this is due to the associative nature of ethanol or due to specific reactant-solvent interactions is not known to us at present and therefore needs further investigation with several other associative and hydroxylic solvents.

The concentration dependence of the time resolved data are even more dramatic where reaction rate is found to be slowed down in all the three solvents upon addition of electrolyte in the limit of very low LiClO<sub>4</sub> concentration. The slowing down has been found to be as large as  $\sim 30\%$  in ethyl acetate solution and  $\sim 5\%$  in other two solvents. However, at the highest electrolyte concentrations investigated in these solvents, the increase in reaction rate (relative to that in the neat solvent) is the maximum in ethanol ( $\sim 60\%$ ) compared to those in ethyl acetate ( $\sim 30\%$ ) and acetonitrile ( $\sim 15\%$ ) solutions. The average solvation times in ethanol, ethyl acetate and acetonitrile are 16 ps, 0.85 ps and 0.26 ps, respectively<sup>11</sup>. The electrolyte concentration induced decrease and increase of reaction rates in these media can therefore be interpreted as arising out of a novel interplay between friction and

solvation (environment reorganization) experienced by the reactant while undergoing the conversion reaction.

## References and Notes

1. Dahl, K., Biswas, R., Ito, N., Maroncelli, M. *J. Phys. Chem. B*, **2005**, *109*, 1563.
2. Pradhan, T., Ghoshal, P., Biswas, R. *J. Phys. Chem. A* **2008**, *112*, 915
3. Pradhan, T., Biswas, R. *J. Phys. Chem. A* **2007**, *111*, 11514
4. Pradhan, T., Biswas, R. *J. Phys. Chem. A* **2007**, *111*, 11524.
5. Grabowski, Z. R., Rotkiewicz, K., Rettig, W. *Chem. Rev.* **2003**, *103*, 3899.
6. Lippert, E., Rettig, W., Bonacic-Koutecky, V., Heisel, F., Mische, J. A. *Adv. Chem. Phys.* **1987**, *68*, 1.
7. Biswas, R., Rohman, N., Pradhan, T., Buchner, R. *J. Phys. Chem. B* **2008**, *112*, 9379.
8. The electrolyte concentration (M, moles/litre) dependence of net quantum yield ( $\Phi$ ) of P4C in ethanol can be fitted to the following bi-exponential function of concentration:  $\Phi(M) = a \exp[-bM] + c[dM]$ , where  $a = 0.007$ ,  $b$  (litre/moles) = 5.619,  $c = 0.014$ ,  $d$  (litre/moles) = 0.229 with  $R = 0.99$ .
9. Bagchi, B., Biswas, R. *Adv. Chem. Phys.* **1999**, *109*, 207.
10. Huppert, D., Ittah, V., Kosower, M. *Chem. Phys. Lett.* **1989**, *159*, 267.
11. Horng, M. L., Gardecki, J. A., Papazyan, A., Maroncelli, M. *J. Phys. Chem.* **1995**, *99*, 17311.
12. Van der Zwan, G., Hynes, J. T. *Chem. Phys.* **1991**, *152*, 169.
13. Hynes, J. T., Simon, J. D. (editor): Charge -Transfer Reactions and Solvation Dynamics In Ultrafast Dynamics of Chemical Systems, Kluwer, Dodrecht, (1994); p.345.
14. Hicks, J., Vandersall, M., Babarogic, Z., Eisenthal, K. B. *Chem. Phys. Lett.*, **1985**, *116*, 18.
15. Hicks, J., Vandersall, M.T., Sitzmann, E. V., Eisenthal, K. B. *Chem. Phys. Lett.*, 1987, *135*, 413.

## Chapter 4

### Excited State Intramolecular Charge Transfer Reaction in Non-aqueous Electrolyte Solutions: Temperature Dependence

#### 4. I. Introduction

In this chapter, we study the temperature dependence of photo-induced ICT reaction of 4-(1-azetidiny)benzotrile (P4C) in ethyl acetate, acetonitrile and ethanol in presence of LiClO<sub>4</sub> at several concentrations with a motivation to investigate the following: (i) whether the temperature dependence of ICT reaction rate is qualitatively similar in the electrolyte solutions of three different type of solvents (mildly polar, polar aprotic and protic) considered here, (ii) whether both the dilute and concentrated solutions exhibit the similar temperature dependence and (iii) whether the temperature dependent rate can be described in terms of Arrhenius type of law. This becomes more pertinent for solutions with high electrolyte concentrations since large amount of electrolyte is expected to cause deviations of simple laws that are valid for dilute solutions. In addition, the temperature dependent study also provides an avenue to estimate the barrier height and its electrolyte concentration dependence. Note here that several authors have already carried out temperature dependent studies with P4C and its higher analogues in several pure solvents.<sup>1-4</sup> However, temperature dependence of the ICT reaction in electrolyte solutions of solvents with varying polarity and association character has not been investigated yet. We use P4C to conduct such a study because the reaction is relatively slower in this molecule which suits the time resolution (discussed later) available to us. As done earlier in this Thesis, the twisted intramolecular charge transfer (TICT) model<sup>5-13</sup> has been used to explain the decay kinetics of 4-(1-azetidiny)benzotrile (P4C) even though alternative models<sup>4,14-16</sup> are also available to describe the kinetics of photo-excited intramolecular charge transfer reaction. The organization of the rest of the chapter is as follows. Experimental details are given in

the next section. Section 4.3 contains experimental results from our steady state and time resolved studies. Supporting information is given wherever necessary in Appendix 2. The article then ends with concluding remarks in section 4.4.

## **4.2. Experimental**

Synthesis of 4-(1-azetidiny) benzonitrile (P4C), sample preparation, steady state and time resolved measurements have been given in chapter 2 and chapter 3. The deconvolution of the steady state emission spectra for area calculations and other spectral properties are already elaborated in chapter 2 and chapter 3. Experiments were performed in the temperature range 267.15 K - 343.15 K by using a temperature controller (Julabo). The boiling temperatures of ethyl acetate, acetonitrile and ethanol are respectively  $\sim 350$  K,  $\sim 352$  K and  $\sim 355$  K. We restricted our experimental temperature far below to the boiling temperature of the sample to prevent evaporation of the solvents. Note that the solubility of  $\text{LiClO}_4$  in ethyl acetate is unusually large and could extend  $\text{LiClO}_4$  concentration much beyond 3.0 M (mol/L is hereafter abbreviated as M) in ethyl acetate whereas we can go only up to 1.0 M in acetonitrile at room temperature. At lower temperature, however, solubility of  $\text{LiClO}_4$  decreases and hence the maximum  $\text{LiClO}_4$  concentrations studied are 1.0 M for ethyl acetate, 0.5 M for acetonitrile and 3.0 M for ethanol at the lowest temperature ( $\sim 267$  K) investigated. Electrolyte concentrations higher than considered here were not attempted as lowering of temperature might lead to the precipitation of the dissolved electrolyte.

The time resolved LE and CT emission decays in electrolyte solutions were collected by using the time correlated single photon counting (TCSPC) which has been discussed in chapters 2 and 3 of this Thesis. The analysis method and interpretation of time scales of the time resolved decay components also remain the same as discussed in those chapters.

### 4.3. Results & Discussion

#### 4.3.1. Steady State Spectral Properties

Representative absorption and emission spectra of P4C in ethyl acetate and acetonitrile in presence of 0.5 M LiClO<sub>4</sub> and ethanolic solution of 0.1 M LiClO<sub>4</sub> at three different temperatures are shown in Fig.4.1 It is evident from Fig.4.1 that increase in temperature does not affect the shape but can shift the peak frequencies of the spectra (absorption or emission) and modify the areas under the LE and CT emission bands due to the change in polarity. This is more clearly shown in Fig.4.2 where the temperature dependence of the absorption, LE and CT emission peak frequencies of P4C in ethyl acetate and acetonitrile are presented. Note in Fig.4.2 that the temperature-induced shift in the CT emission frequency is relatively large due to its more polar nature whereas the shift in the LE band is very small. Moreover, the CT emission band decreases almost linearly with the decrease in temperature for all LiClO<sub>4</sub> concentrations in these three solvents. The increase in average dielectric constant of the electrolyte solution upon lowering the temperature<sup>17-18</sup> and direct ion-probe (P4C here) interaction<sup>19</sup> might be responsible for the observed red-shift of the CT peak frequency at lower temperature. Note that for increasing the solution temperature from 274 K to 343 K at low LiClO<sub>4</sub> concentrations ( $\leq 0.10$  M) in ethyl acetate and acetonitrile, the CT peak shift (1000 - 1500 cm<sup>-1</sup>) is almost *twice* than that at higher concentrations. This indicates that direct ion-solute interactions<sup>19</sup> are facilitated in dilute electrolyte solutions as the degree of electrolyte dissociation is greater at low electrolyte concentrations. This also explains the temperature dependent peak shift data in ethanol at various electrolyte concentrations (Table A5 in Appendix 2). The LE shift, as expected, is much smaller for the same temperature range at all electrolyte concentrations in these solvents. Except for pure ethyl acetate and at 0.01 M LiClO<sub>4</sub> in the same solvent where the CT bandwidth is kept fixed due to small CT band area, spectral (absorption, LE and CT emission) bands of P4C in these solvents at all electrolyte

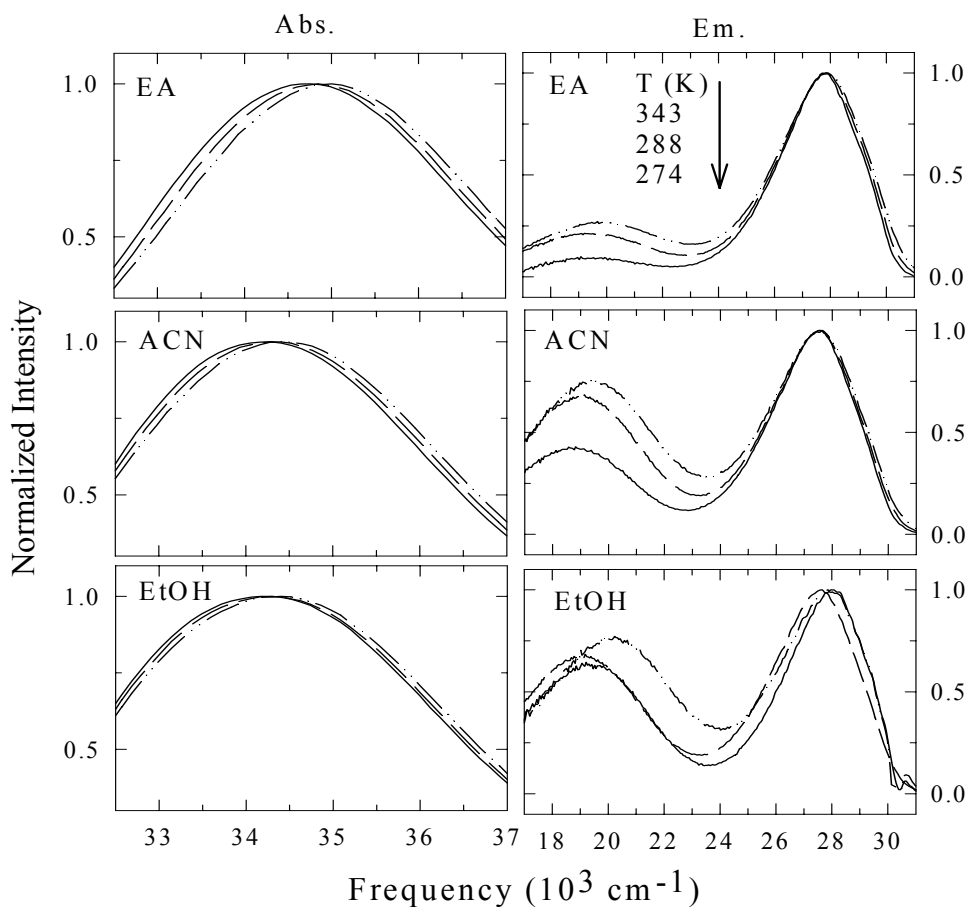


**Fig.4.1:** Representative temperature dependent absorption (left panel, ‘Abs.’) and emission spectra (right panel, ‘Em.’) of 4-(1-azetidiny)benzonitrile (P4C) at 0.50 M LiClO<sub>4</sub> concentration in ethyl acetate (‘EA’) and acetonitrile (‘ACN’), and at 0.10 M in ethanol (‘EtOH’). The spectra at 274 K are represented by the solid lines, at 288 K by the dashed lines and at 343 K by the dashed-dot-dot lines.

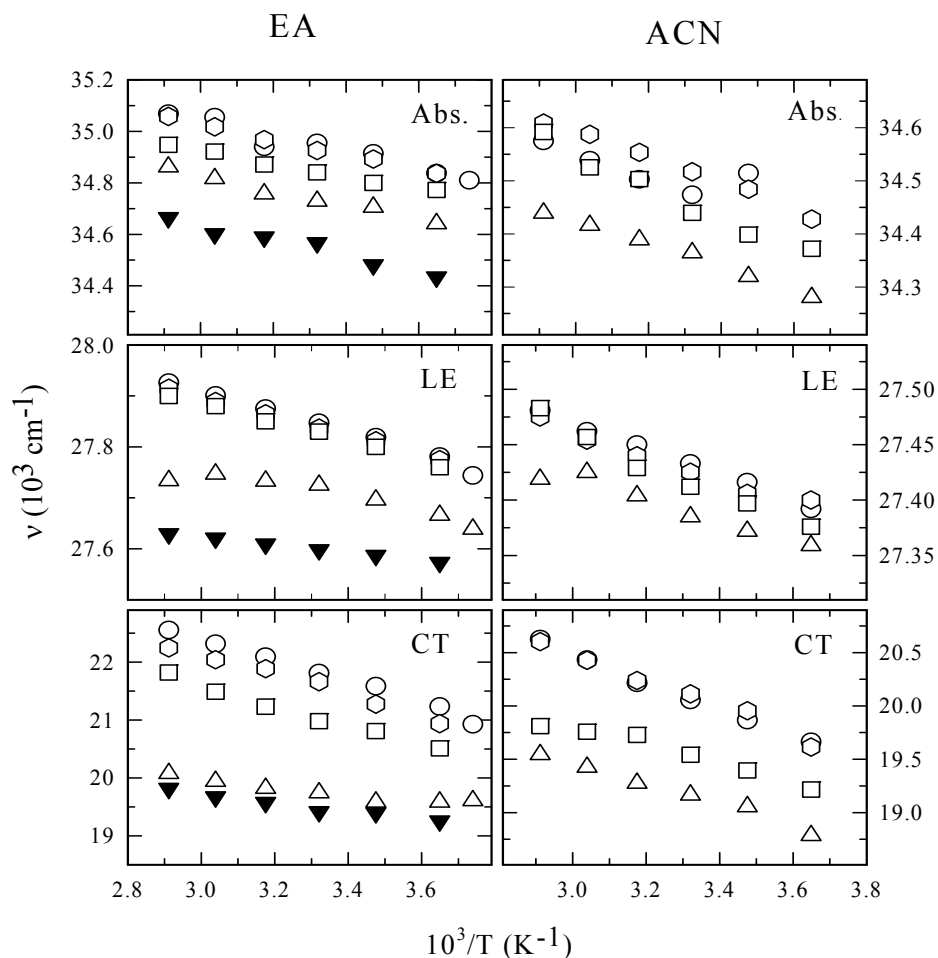


**Fig.4.2:** Temperature dependence of absorption and emission (LE and CT) peak frequencies of P4C at several concentrations of LiClO<sub>4</sub> in ethyl acetate (left panel, ‘EA’) and acetonitrile (right panel, ‘ACN’). The circles, hexagons, squares, triangles and filled inverted triangles represent respectively the LiClO<sub>4</sub> concentrations (M) of 0.0, 0.01, 0.1, 0.5, 1.0M in ethyl acetate and acetonitrile.

concentrations show narrowing with lowering of temperature (see Fig. A8, Appendix 2). This is counterintuitive since lowering of temperature is expected to induce microscopic heterogeneity in the solution structure, which should broaden the spectral bandwidth.<sup>20</sup> However, the distribution of the ground and excited state energies at lower temperature could be very narrow (due to limited thermal

fluctuations) which may contribute to the observed narrowing of the bandwidth upon lowering the temperature.

The temperature dependence of the CT/LE area ratio for P4C at several LiClO<sub>4</sub> concentrations in ethyl acetate, acetonitrile and ethanol are shown in Fig.4.3. The most interesting aspect of this figure is that the temperature dependence of the area ratio at higher electrolyte concentrations is roughly opposite to that at lower electrolyte concentrations in these solvents. For example, in ethyl acetate at LiClO<sub>4</sub> concentrations 0.50 M and 1.0 M, an increase in temperature from 274 K to 343K enhances the CT/LE area ratio by a factor of ~3, whereas at low concentrations ( $\leq 0.10$  M), the same rise in temperature induces a small decrease in area ratio. The increase in area ratio with the rise in temperature at higher electrolyte concentrations is probably due to more rapid decrease in solution viscosity than the lowering of average solution dielectric constant. Similar temperature dependence of area ratio has also been found for electrolyte solutions in acetonitrile and ethanol. In fact, in acetonitrile and ethanol at lower electrolyte concentrations (including the pure solvent), the area ratio appears to show non-monotonic temperature dependence. In pure solvents and in presence of electrolyte at low concentrations, the effects due to temperature induced decrease in average dielectric constant seems to be stronger than those due to the decrease in viscosity. As a result, the CT/LE area ratio decreases at higher temperatures but the viscosity effects win at lower temperatures which decreases the area ratio. A competition between the temperature induced modulation of the average polarity of the electrolyte solution and its viscosity can give rise to such non-monotonic temperature dependence in CT/LE area ratio. Temperature dependent dielectric relaxation and viscosity measurements at various LiClO<sub>4</sub> concentrations in these solvents are therefore necessary for a more quantitative explanation of these data. The temperature dependent change in reaction free energy ( $-\Delta G_r$ ) at several LiClO<sub>4</sub> concentrations in these solvents are shown in Fig.4.4. The calculation procedure of this quantity from the area ratio ( $\alpha_{CT}/\alpha_{LE}$ ) is already discussed in previous chapters. As expected,  $-\Delta G_r$ , being larger in solvents

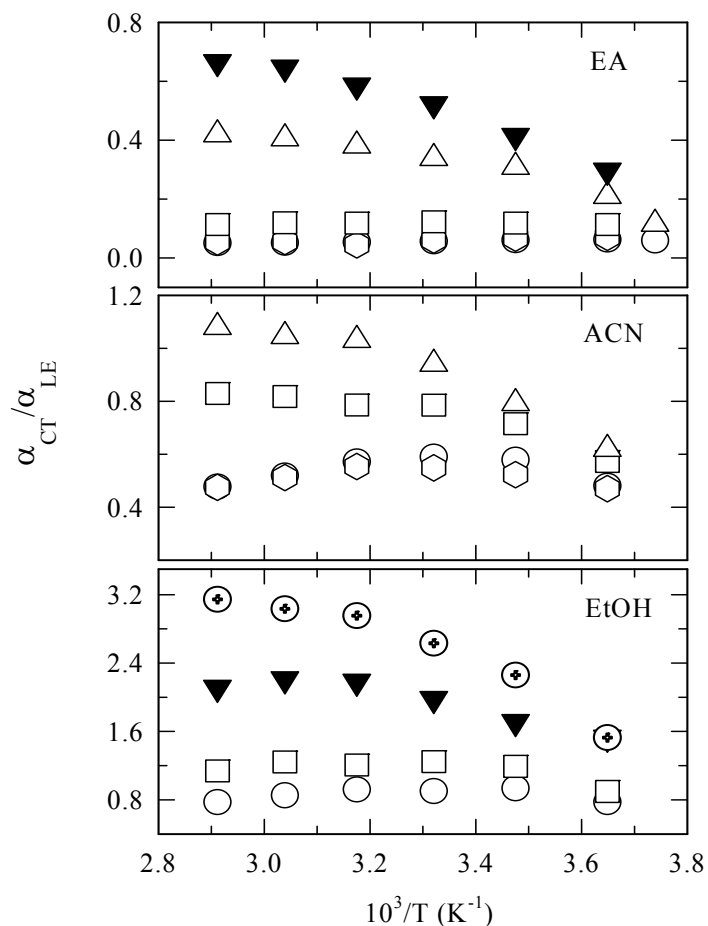


**Fig.4.3:** Temperature dependence of the ratio between the areas under the CT and LE emission bands of P4C at several  $\text{LiClO}_4$  concentrations in ethyl acetate ('EA'), acetonitrile ('ACN') and ethanol ('EtOH'). The area ratio,  $\alpha_{CT}/\alpha_{LE}$  at different  $\text{LiClO}_4$  concentrations (M) in ethyl acetate, acetonitrile and ethanol are represented as follows: 0.0 by circles, 0.01 by hexagons, 0.10 by squares, 0.5 by triangles and 1.0 by filled inverted triangles. The circles with crosshair in ethanol represent the data at 3.0 M. The maximum uncertainty for the above area determination is  $\pm 15\%$ .

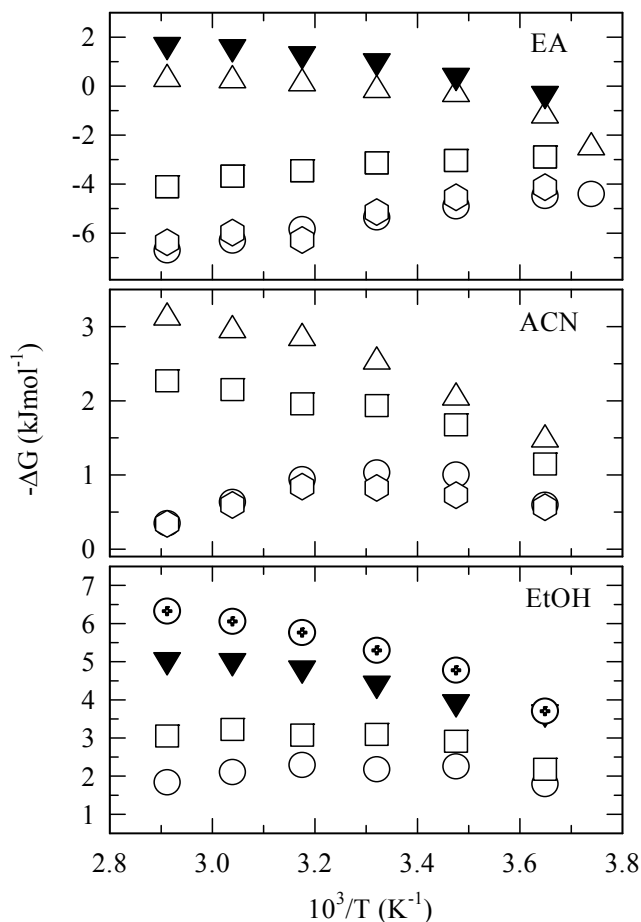


**Fig. 4.4** Temperature dependence of the change in reaction free energy ( $-\Delta G_r$ ) associated with the LE  $\rightarrow$  CT conversion reaction of P4C in ethyl acetate ('EA'), acetonitrile ('ACN') and ethanol ('EtOH').  $-\Delta G_r$  is obtained from the area ratio by using Eq.2.1(chapter 2). Circles, hexagons, squares, triangles and filled inverted triangles indicate data respectively at 0.0, 0.01, 0.10, 0.50 1.0 M  $\text{LiClO}_4$  solutions in ethyl acetate, acetonitrile and ethanol. The circles with crosshair in ethanol represent the data at 3.0 M. Note the ratio between the equilibrium constants for the LE  $\rightarrow$  CT conversion reaction in P4C at 343 K and 274 K ( $K_{\text{eq}}^{343}/K_{\text{eq}}^{274}$ ) in ethyl acetate (at 0.5 M  $\text{LiClO}_4$ ) is  $\sim 4$ , in acetonitrile (at 0.5 M)  $\sim 2$  and in ethanol (3.0 M)  $\sim 1.5$ .

with higher dielectric constant, follows the temperature dependence of  $\alpha_{\text{CT}}/\alpha_{\text{LE}}$  depicted in Fig. 4.3. Note that  $\Delta G_r$  remains always negative for acetonitrile and ethanol, indicating that the conversion reaction is strongly favored at all concentrations of  $\text{LiClO}_4$  in these two highly polar solvents for the whole

temperature range. However, in ethyl acetate at higher electrolyte concentrations,  $\Delta G_r$  varies from negative to positive upon lowering the temperature, indicating a favorable LE  $\rightarrow$  CT conversion at higher temperature becomes unfavorable upon decreasing the temperature. Note in Fig.4.4 that the slope of the temperature dependence of  $-\Delta G_r$  in pure solvents and at lower electrolyte concentrations is opposite to that at higher concentrations. The probable reason for such a difference is already discussed while presenting the area ratio in Fig.4.3. At these low electrolyte concentrations (and pure solvents), the maximum change in  $K_{eq}$  is found to vary within 25 – 50 % of the value at the lowest temperature. Therefore, temperature dependence of the LE  $\rightarrow$  CT reaction in P4C is stronger at higher electrolyte concentrations than in the electrolyte solutions at low concentrations or in pure solvents. This is one of the main results of the present chapter.

#### **4.3.2. Time Resolved Studies: Temperature Dependence of the Reaction Rate**

For the whole temperature range (267 K to 343 K ) at all  $\text{LiClO}_4$  concentrations in these solvents, time resolved emission decays of P4C have been found to be adequately described by bi-exponential functions of time. Representative decays at three different temperatures in 0.5 M  $\text{LiClO}_4$  solutions in ethyl acetate and acetonitrile, and in ethanol containing 0.1 M  $\text{LiClO}_4$  are shown in Fig.4.5 along with the bi-exponential fits and instrument response function. The fit parameters are also tabulated in the corresponding panels. The *goodness of fit* parameter ( $\chi^2$ ) associated with these fits ( $1.05 \pm 0.04$ ) and the residuals shown in the same figure indicate that the kinetics is indeed bi-exponential and hence, conform to the classical two state reversible reaction mechanism as observed earlier with P4C in different reaction environments.<sup>6,8,10-11</sup> A few CT emission decays<sup>21</sup> have also been found to fit adequately with bi-exponential functions, producing rise time constants similar to the fast time constants found in LE emission decays. Therefore, the short time constant is ascribed to the reaction time whereas the long time constant is assumed to be the average life time of the states involved.<sup>6</sup>

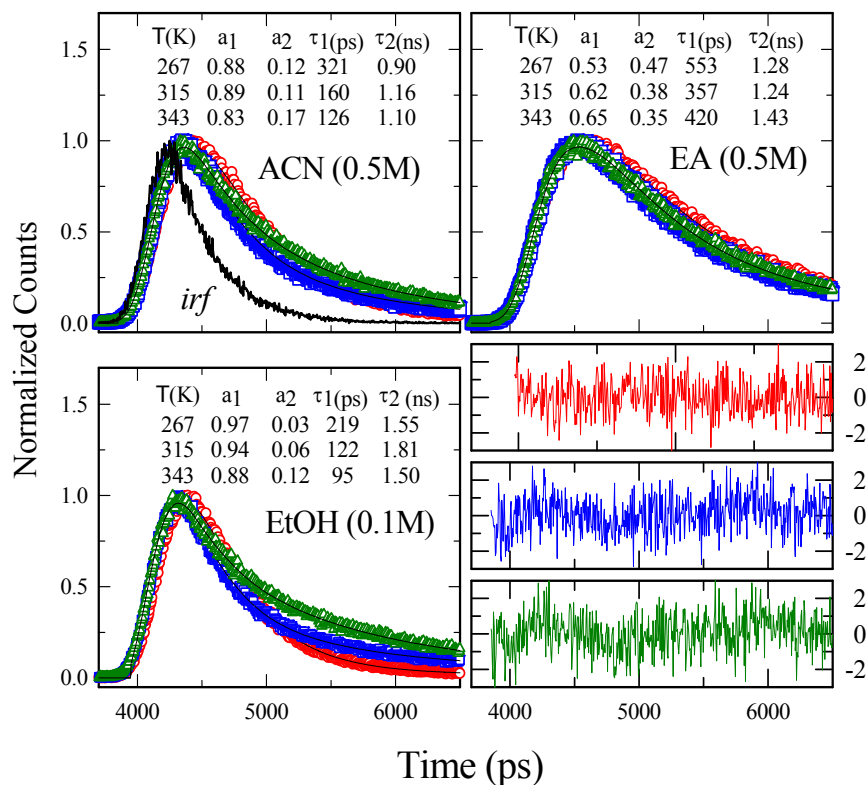


**Fig. 4.5:** Representative LE emission decays of P4C at 0.50 M LiClO<sub>4</sub> in ethyl acetate (‘EA’) and acetonitrile (‘ACN’), and at 0.10 M LiClO<sub>4</sub> in ethanol (‘EtOH’) at three different temperatures. The data at 267 K are represented by circles (red), at 315 K by squares (blue) and at 343 K by triangles (dark green). The biexponential fits through the data are shown by the solid lines. The instrument response function (‘*irf*’) is also shown in one of the panels. The fit (biexponential) results are also provided in the inset of each *panel*. The LE peak count is ~5000. Residuals are shown in the *lower of the right panel* ( $\pm 2$  full scale).

The temperature dependent reaction time ( $\tau_{\text{rxn}}$ ) for P4C molecule in these three solvents at several LiClO<sub>4</sub> concentrations are shown in Fig.4.6. Note that irrespective of electrolyte concentration in acetonitrile and ethanol, the reaction rate ( $k_{\text{rxn}} = \tau_{\text{rxn}}^{-1}$ ) decreases almost *linearly* upon lowering the temperature from 343 K to

267 K where the ratio between the rates ( $k_{\text{ratio}} = k_{\text{rxn}}^{343\text{K}} / k_{\text{rxn}}^{267}$ ) at the two extreme temperatures is approximately 3. Similar linear temperature dependence is also observed for reaction occurring in pure ethyl acetate and in presence of 0.01 M electrolyte where  $k_{\text{ratio}}$  is found to be  $\sim 5$ . This decrease in reaction rate is due to the increase in solution viscosity upon lowering the temperature. Interestingly, at higher electrolyte concentrations ( $> 0.01$  M) in ethyl acetate, the reaction time shows non-linear temperature dependence with the reaction rate peaking at  $\sim 303$  K. Above  $\sim 303$  K in ethyl acetate with  $\text{LiClO}_4$  concentrations higher than 0.01 M, the retardation due to the decrease in solution polarity and greater dissociation of electrolyte probably dominates over the rate acceleration caused by the decrease in solution viscosity with the rise in temperature. Therefore, these results demonstrate not only that the effects of temperature on ICT reaction rate are different for solvents with differing polarity ( $\epsilon_0$  of ethyl acetate, acetonitrile and ethanol are respectively, 6.02, 35.94 and 24.55) but the temperature dependence in solutions of moderately polar solvents with large electrolyte concentration is also *qualitatively* different from that at low concentrations and pure solvent. The above observation leads to a more detailed investigation of the electrolyte concentration dependence of the ICT reaction rate in these solutions at different temperature. Figures A9 – A11 (Appendix 2) depict the  $\text{LiClO}_4$  concentration dependence of the reaction rate measured at seven different temperatures in ethyl acetate, acetonitrile and ethanol. The following features are to be noted from the data (limited though) presented in these figures.

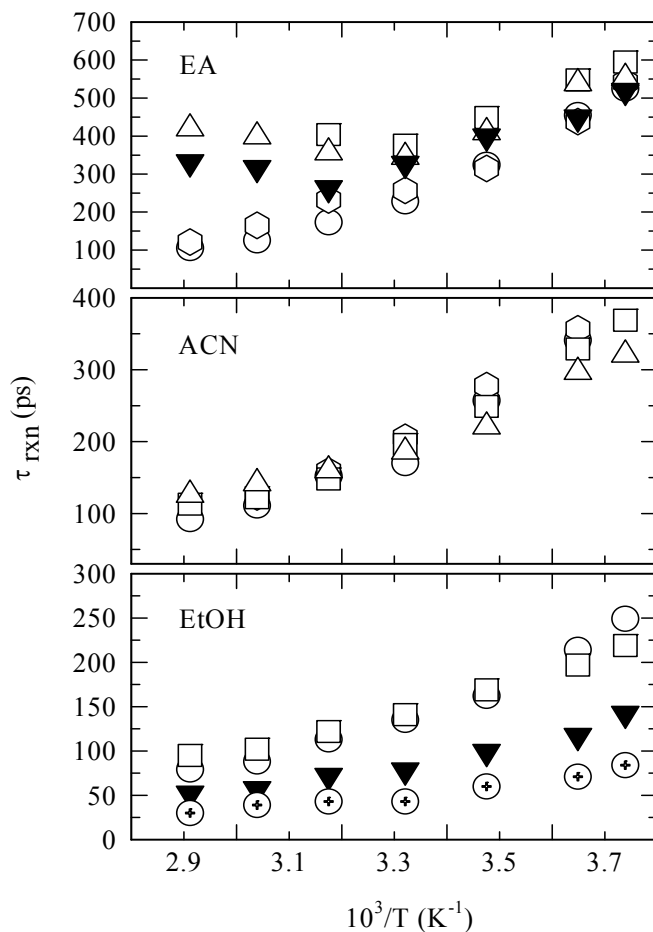


**Fig. 4.6.** Temperature dependence of the reaction time ( $\tau_{rxn}$ ) in  $\text{LiClO}_4$  solutions. Circles represent  $\tau_{rxn}$  at 0.0 M (pure solvent), hexagons at 0.01 M, squares at 0.10 M, triangles at 0.50 M and filled inverted triangles at 1.0 M  $\text{LiClO}_4$  in ethyl acetate ('EA', acetonitrile ('ACN') and ethanol. The circles with crosshair in ethanol represent the data at 3.0 M  $\text{LiClO}_4$ .

At all temperatures in ethyl acetate the reaction rate decreases initially with electrolyte concentration (upto  $\sim 0.2$  M) and then increases, whereas in ethanol the rate increases linearly with electrolyte concentration. In acetonitrile at temperatures below 300 K, the rate increases linearly with concentration. However, at temperatures beyond 300 K, the rate decreases with electrolyte concentration. Note that the electrolyte concentration induced increase in reaction rate for P4C and

related molecules in ethyl acetate have already been explained<sup>10-11</sup> in chapter 2 by using the Zwan-Hynes theory.<sup>22</sup> In that study,<sup>10-11</sup> however, the effects of electrolyte at very low concentration were not investigated and the present study shows that in dilute ethyl acetate solutions and in acetonitrile at higher temperatures the reaction rate decreases with electrolyte concentration. Note that an earlier study of ICT reaction using a donor-bridge-acceptor system in tetrahydrofuran (THF) reported electrolyte-induced dramatic rate reductions in dilute electrolyte solution.<sup>23</sup> The enhanced dissociation of electrolyte in the limit of very low concentration can increase the frictional resistance to the rotating moiety via ion-dipole electrostatic interaction, leading to a decrease of the reaction rate in this regime. At higher electrolyte concentrations, formation of ion-pairs leads to a decrease in rotational friction but enhances the solvent reorganization energy, which, in turn, increases the ICT reaction rate. The enhanced degree of dissociation of LiClO<sub>4</sub> in acetonitrile at temperatures above 300 K may be responsible for the observed concentration-induced decrease in reaction rate in this temperature regime. However, this is purely an assumption which needs experimental verification.

Next we investigate whether the ICT reaction of P4C in electrolyte solutions belong to Marcus inverted region<sup>24-32</sup> and the increase in solvation energy ( $\lambda_s$ ) upon addition of electrolyte induces a crossover to the normal region. In Fig.A12 (Appendix 2) the dependence of the reaction rate on the change in reaction free energy ( $-\Delta G_T$ ), calculated by using Eq. 2.1 (chapter 2) at five different LiClO<sub>4</sub> concentrations, is shown. It is interesting to note that while in solutions of acetonitrile and ethanol the reaction traces the normal region (rate increases as  $-\Delta G_T$  increases), this is so in ethyl acetate only at the highest two electrolyte concentrations (0.5 M and 1.0 M). The reaction, however, falls in the Marcus inverted region in pure ethyl acetate and in presence of electrolyte at very low concentrations (rate decreases as  $-\Delta G_T$  increases). Therefore, this study clearly demonstrates that step-wise increase of solvation energy via successive addition of electrolyte in a moderately polar solvent can induce the ICT reaction of P4C to crossover from the Marcus inverted region to the normal region. This could very

well be the case for other members of the (PnC) series which requires further investigation. Subsequently, the electrolyte concentration dependent activation energy ( $\Delta G^\ddagger$ ) has been obtained from the reaction time constants ( $\tau_{rxn}$ ) by using the well known Arrhenius rate equation<sup>33</sup>

$$\ln k_r = \ln A - \left( \frac{\Delta G^\ddagger}{RT} \right), \quad (4.1)$$

where  $k_r$  ( $=\tau_{rxn}^{-1}$ ) denotes the rate constant and A is a constant associated with the rate expression. The variation of rate constant with inverse temperature ( $1/T$ ) is shown in Fig.4.7. The linear fits (correlation coefficient  $\sim 1.0$ ) through the data points are also shown in the same figure (solid line). Note that reaction rates at higher temperatures (above  $\sim 300$  K) in ethyl acetate containing larger  $\text{LiClO}_4$  concentrations seem to deviate from the Arrhenius type temperature dependence. The decrease of reaction rate with the rise in temperature beyond  $\sim 300$  K at higher electrolyte concentrations is probably due to the domination of the decrease in average solution polarity over the lowering of solution viscosity at these temperatures. This means that the activation energy does not remain constant in these electrolyte solutions at temperatures beyond  $\sim 300$  K. It is possible that in low polarity solvents such as ethyl acetate, the dissociation of electrolyte into ions is facilitated with the rise in temperature which markedly reduces the concentrations of ion pairs (solvent shared and solvent separated). As the concentrations of ion pairs decrease in solution at higher temperatures, the average polarity of the medium also decreases. This decrease in polarity may then lead to the increase in barrier height which, in turn, slows down the reaction.<sup>7</sup> Additionally, if the concentration of free ion increases, the reaction slows down further due to stronger ion-solute interactions. The above explanation is, however, purely speculative in the absence of any conductometric and dielectric relaxation studies of ethyl acetate containing high

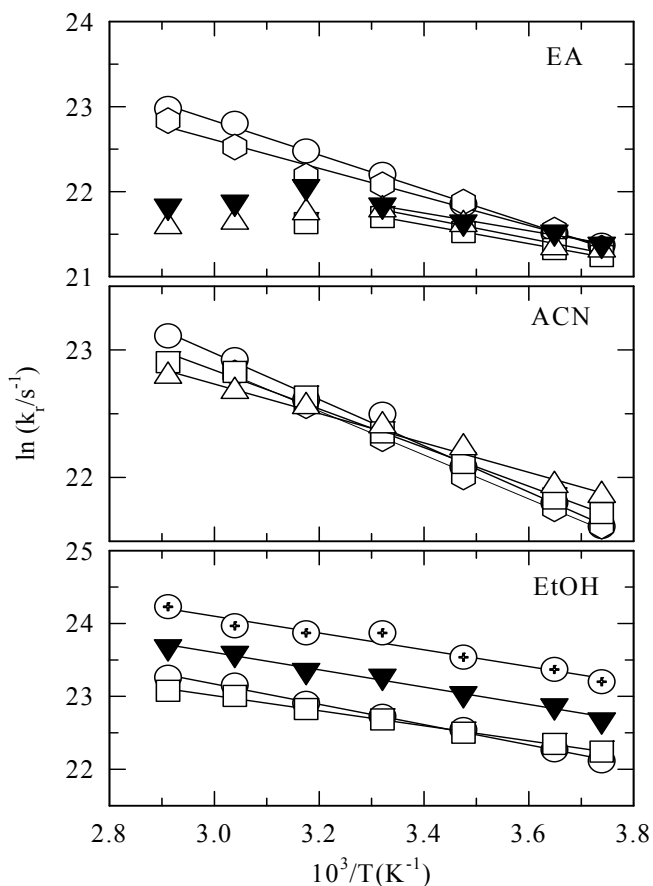


**Fig.4.7:** Arrhenius plot of  $\text{LiClO}_4$  concentration dependent reaction rate ( $k_r = 1/\tau_{rxn}$ ) in ethyl acetate, acetonitrile and ethanol. The linear fits through the data points are shown the solid lines. The data representations remain the same as in Fig.4.6. The activation energies ( $\Delta G^\ddagger$ ) obtained from the slopes of these fits are summarized in Table 4.1 of the text.

$\text{LiClO}_4$  concentrations at various temperatures which should be carried out to understand the observed non-Arrhenius temperature dependence of the TICT reaction rate at these solution conditions. Activation energies at different  $\text{LiClO}_4$  concentrations in ethyl acetate (except high concentration data at higher temperatures), acetonitrile and ethanol obtained from the slopes of the  $\ln k_r$  versus  $1/T$  plots (shown in Fig. 4.7) are summarized in Table 4.1. It is interesting to note in Table 4.1 that the activation energies obtained for these pure solvents are close to the

activation energy for the LE → CT conversion reaction of P4C calculated earlier by Maroncelli and coworkers<sup>6</sup> in the limit of zero solvent friction where the TICT reaction is predicted to be largely governed by the solvent variation of the sizeable barrier height to the reaction. The activation energies tabulated here (Table 4.1) are therefore identified with the electrolyte concentration

**Table 4.1:** Electrolyte (LiClO<sub>4</sub>) concentration dependence of activation energy ( $\beta\Delta G^\ddagger$ ) for the LE → CT conversion reaction of P4C in ethyl acetate, acetonitrile and ethanol

Ethyl Acetate <sup>a</sup>		Acetonitrile		Ethanol	
Conc.(M)	$\beta\Delta G^\ddagger$	Conc.(M)	$\beta\Delta G^\ddagger$	Conc.(M)	$\beta\Delta G^\ddagger$
0.0	6.75	0.0	6.08	0.0	4.68
0.01	5.97	0.01	5.77	0.1	3.48
0.1	3.72	0.1	5.09	1.0	3.99
0.5	4.04	0.5	3.87	3.0	3.86
1.0	3.49				

a) Data at temperatures higher than ~303 K have not been considered for determining the  $\beta\Delta G^\ddagger$  for P4C in ethyl acetate at 0.50 M and 1.0 M LiClO<sub>4</sub>.  $\beta = (k_B T)^{-1}$ .

dependent activation energies for the LE → CT conversion reaction of P4C in ethyl acetate, acetonitrile and ethanol containing LiClO<sub>4</sub> at different concentrations. The activation energy found in pure ethanol is about  $1.5k_B T$  less than the average of those in pure ethyl acetate and acetonitrile. Whether this difference in activation energy between the polar protic and polar aprotic solvents is due to the H-bonding cannot be ascertained from the present study as answer to this question requires further studies with several other associating solvents. The barrier height, however, decreases with LiClO<sub>4</sub> concentration in all these solvents, the decrease being the maximum in ethyl acetate and the minimum in ethanol. The fact that the barrier height in ethyl acetate at 1.0 M LiClO<sub>4</sub> decreases by almost a factor of 2 from that in the absence of any electrolyte is probably correlated with the increase in solution dielectric constant of the pure solvent by a factor of 3 upon addition of 1.0 M LiClO<sub>4</sub> in ethyl acetate. Since the increase in average solution dielectric constant is a much

weaker function of electrolyte concentrations in acetonitrile and alcohols,<sup>34-38</sup> the relatively less softening of the barrier height in acetonitrile and ethanol further indicates barrier height modulation by the average polarity of the reaction medium.

#### 4.4. Conclusion

Temperature dependent studies of photo-induced twisted intramolecular charge transfer reaction of 4-(1-azetidiny)benzonitrile (P4C) at several LiClO<sub>4</sub> concentrations in ethyl acetate, acetonitrile and ethanol have been performed. Steady state spectral properties such as absorption and emission peak frequencies have been found to decrease with decreasing temperature at all electrolyte concentrations as well as in pure solvents, indicating increase in average solution polarity with the lowering of solution temperature. Except in the pure solvents and at very low electrolyte concentrations, the absorption and emission peak shifts with temperature is directly correlated with the ratio between the areas under the CT and LE bands ( $\alpha_{CT}/\alpha_{LE}$ ), stressing the dominance of the solution viscosity in regulating the formation of the CT state via twisting upon photo-excitation and the role of solution polarity for the subsequent stabilization of the CT state. A subtle interplay between the solution polarity and viscosity is believed to be responsible for the observed non-monotonic dependence of  $\alpha_{CT}/\alpha_{LE}$  on temperature. As expected, the change in reaction free energy ( $-\Delta G_r$ ) associated with the LE $\rightarrow$ CT conversion reaction in P4C is found to follow the trend of  $\alpha_{CT}/\alpha_{LE}$  with temperature at all LiClO<sub>4</sub> concentrations, the effects being maximum for ethyl acetate.

Time resolved studies indicate that the decay kinetics related to the TICT reaction of P4C is bi-exponential in nature at all LiClO<sub>4</sub> concentrations and temperatures (~270 K – 345 K), providing further support to the classical two state reversible reaction mechanism as proposed earlier with P4C in pure solvents.<sup>6</sup> We would like to mention here that a fast component, if present at higher temperatures, might have been missed due to the limited time resolution employed in our experiment. Except at higher electrolyte concentrations in ethyl acetate, the reaction is found to slow

down by a factor of  $\sim 5$  in ethyl acetate and  $\sim 3$  in acetonitrile and ethanol at all electrolyte concentrations for lowering the temperature from  $\sim 345$  K to  $\sim 270$  K. At higher electrolyte concentrations in ethyl acetate, temperature dependent dissociation of  $\text{LiClO}_4$  is believed to govern the reaction rate at temperatures higher than  $\sim 300$  K and below it the solution viscosity is assumed to dominate the rate of the reaction. Extensive dielectric relaxation studies of  $\text{LiClO}_4$  solutions in these solvents at different temperatures are proposed to estimate the concentrations of ion-pairs and solution dielectric constant so that a better understanding of the TICT reaction in electrolyte solutions of non-aqueous solvents could be generated. Activation energy determined from the temperature dependent studies of the TICT reaction of P4C in pure ethyl acetate, acetonitrile and ethanol is found to be in good agreement with the prediction of Maroncelli and coworkers.<sup>6</sup> In addition, a significant dependence of the activation energy on the electrolyte concentration in these solvents has been found. The present study reveals that the electrolyte concentration dependence of ICT reaction rate is *qualitatively* different in weakly polar solvent such as ethyl acetate from that in strongly polar solvent such as acetonitrile and ethanol. The data presented here also reveal that the step-wise increase of solvation energy via sequential addition of electrolyte induces the reaction in weakly polar solvents to crossover from the Marcus inverted region to the normal region.

## References and Notes

1. Braun, D.; Rettig, W. *Chem. Phys.*, **1994**, *180*, 231; *Chem. Phys. Lett.* **1997**, *268*, 110.
2. Rettig, W. *J. Phys. Chem.* **1982**, *86*, 1970.
3. Rettig, W. *Ber. Bunsen-Ges. Phys. Chem.* **1991**, *95*, 259.
4. Zachariasse, K. A.; Grobys, M.; von der Haar, T.; Hebecker, A.; Il'ichev, Y. V.; Jiang, Y.-B.; Morawski, O.; Kuhnle, W. *J. Photochem. Photobiol. A* **1996**, *102*, 59.
5. Grabowski, Z. R.; Rotkiewicz, K.; Rettig, W. *Chem. Rev.* **2003**, *103*, 3899.
6. Dahl, K.; Biswas, R.; Ito, N.; Maroncelli, M. *J. Phys. Chem. B*, **2005**, *109*, 1563.
7. Hicks, J.; Vandersall, M.; Babarogic, Z.; Eisenthal, K. B. *Chem. Phys. Lett.* **1985**, *116*, 18.
8. Pradhan, T.; Ghoshal, P.; Biswas, R. *J. Phys. Chem. A* **2008**, *112*, 915.
9. Rettig, W.; Fritz, R.; Braun, D. *J. Phys. Chem. A* **1997**, *101*, 6830.
10. Pradhan, T.; Biswas, R. *J. Phys. Chem. A* **2007**, *111*, 11514.
11. Pradhan, T.; Biswas, R. *J. Phys. Chem. A* **2007**, *111*, 11524.
12. Rettig, W. *J. Luminesc.* **1980**, *26*, 21.
13. Lippert, E.; Rettig, W.; Bonacic-Koutecky, V.; Heisel, F.; Mische, J. *Adv. Chem. Phys.* **1987**, *68*, 1.
14. Zachariasse, K. A.; Druzhinin, S. I.; Bosch, W.; Machinek, R. *J. Am. Chem. Soc.* **2004**, *126*, 1705.
15. Techert, S.; Zachariasse, K. A. *J. Am. Chem. Soc.* **2004**, *126*, 5593.
16. Zachariasse, K. A. *Chem. Phys. Lett.* **2000**, *320*, 8.
17. Akilan, C.; Hefter, G.; Rohman, N.; Buchner, R. *J. Phys. Chem. B* **2006**, *110*, 14961.
18. Ronne, C.; Thrane, L.; Astrand, P.-O.; Wallqvist, A.; Mikkelsen, K.V.; Keiding, S. R.; *J. Chem. Phys.* **1997**, *107*, 5319.
19. Chapman, C. F.; Maroncelli, M.; *J. Phys. Chem. B* **1991**, *95*, 9095.
20. Fee, R. S.; Milsom, J. A.; Maroncelli, M. *J. Phys. Chem.* **1991**, *95*, 5170.

21. Unfortunately, CT emission decays for all LiClO<sub>4</sub> concentrations at all temperatures in these three solvents could not be collected as it would take a very long time for gathering a reasonable peak count and acceptable statistics. However, a few were collected and analyzed.
22. Zwan, van der G.; Hynes, J. T. *Chem. Phys.* **1991**, *152*, 169.
23. Piotrowiak, P.; Miller, J.R. *J. Phys. Chem.* **1993**, *97*, 13052.
24. (a) Marcus, R. A. *J. Chem. Phys.* **1956**, *24*, 966. (b) Marcus, R. A. *Faraday Discuss. Chem. Soc.* **1960**, *29*, 21. (c) Marcus, R. A. *Annu. ReV. Phys. Chem.* **1964**, *15*, 155.
25. (a) McLendon, G.; Miller, J. R. *J. Am. Chem. Soc.* **1985**, *107*, 7811; (b) McLendon, G. *Acc. Chem. Res.* **1988**, *21*, 160.
26. (a) Scott, J. R.; Willie, A.; McLean, M.; Stayton, P. S.; Sligar, S. G.; Durham, B.; Millett, F. *J. Am. Chem. Soc.* **1993**, *115*, 6820; (b) Scott, J.R.; McLean, M.; Sligar, S. G.; Durham, B.; Millett, F. *J. Am. Chem. Soc.* **1994**, *116*, 7356.
27. Dutton, P. L.; Mosser, C. C. *Proc. Natl. Acad. Sci. U.S.A.* **1994**, *91*, 10247.
28. (a) Miller, J. R.; Calcaterra, L. T.; Closs, G. L. *J. Am. Chem. Soc.* **1984**, *106*, 3047; (b) Closs, G. L.; Calcaterra, L. T.; Green, N. J.; Penfield, K. W.; Miller, J. R. *J. Phys. Chem.* **1986**, *90*, 3673; (c) Closs, G. L.; Miller, J. R. *Science* **1988**, *240*, 440; (d) Liang, N.; Miller, J. R.; Closs, G. L. *J. Am. Chem. Soc.* **1990**, *112*, 5353.
29. Turro, C.; Zaleski, J.M.; Karabatsos, Y.M.; Nocera, D.G., *J. Am. Chem. Soc.* **1996**, *118*, 6060.
30. Yonemoto, E.H.; Riley, R.L.; Kim, Y. II; Atherton, S.J.; Schmehl, R.H.; Mallouk, T.E. *J. Am. Chem. Soc.* **1992**, *114*, 8081.
31. Larson, S.L.; Cooley, L.F.; Elliot, C.M.; Kelley, D.F. *J. Am. Chem. Soc.* **1992**, *114*, 9504.
32. Yonemoto, E.H.; Saupe, G.B.; Schmehl, R.H.; Hubig, S.M.; Riley, R.L.; Iverson, B.L.; Mallouk, T.E. *J. Am. Chem. Soc.* **1994**, *116*, 4786.
33. Atkins, P. W. *Physical Chemistry*; Oxford Univ. Press: 1994
34. Barthel, J. and Buchner, R. *Pure & Appl. Chem.* **1986**, *58*, 1077.
35. Buchner, R.; Hefter, G. *J. Solution. Chem.* **2002**, *31*, 521.

36. Barthel, J.; Kleebauer, M.; Buchner, R. *J. Solution. Chem.* **1995**, *24*, 1.
37. Wurm, B.; Munsterer, M.; Richardi, J.; Buchner, R.; Barthel, J. *J. Mol. Liq.* **2005**, *119*, 97.
38. Eberspacher, P.; Wismeth, E.; Buchner, R.; Barthel, J. *J. Mol. Liq.*, **2006**, *129*, 3.

## Chapter 5

### Excited State Intramolecular Charge Transfer Reaction in 4-(1-azetidinyI) benzonitrile: Solvent Isotope Effects

#### 5.1. Introduction

Isotope chemistry has been applied widely throughout the field of chemistry, from mechanistic studies of biochemical reactions to the determination of paleotemperatures from isotopic compositions of fossils<sup>1-2</sup>. Deuterium substitution in solvents is known to modify both the static and dynamic nature of the solvents. For example, D<sub>2</sub>O is more structured and ordered liquid than H<sub>2</sub>O due to stronger H-bond interactions in the deuterated water than in the normal species. In addition, the Debye relaxation times are slower in D<sub>2</sub>O, whereas the peak frequencies of the intermolecular librations and intramolecular vibrations lie at somewhat lower values than those in normal water. Solvation dynamics studies of isotope-substituted water<sup>3-4</sup> and other polar solvents have revealed that the isotope-substitution affects the long time part of solvation energy relaxation which results into a slowing down of the solvation rate by ~10-20%. Because the dynamics of solvent reorganization is important for reactions where the solvent motion is coupled to the reaction coordinate, a slowing down in the solvent dynamics is expected to modify the reaction rate accordingly. Electron transfer (ET) or charge transfer (CT) reactions are such reactions where the solvation processes influence the reaction dynamics significantly.

Some studies have already used deuterium-substituted solute to investigate the effects of isotope on charge transfer reaction.<sup>5</sup> Rotkiewicz<sup>6-7</sup> et al. have investigated the solute isotope effects on twisted intramolecular charge transfer (TICT) reactions by studying the fluorescence quantum yields, life times and the intersystem crossing yields. However, effects of isotopic substitution in solvents on reaction rates of intramolecular charge transfer reactions have not been investigated yet. In this

chapter, we investigate the solvent isotope effects on the rate and yield of a photo-induced intramolecular charge transfer reaction in a molecule where the charge transfer in the photo-excited molecule is believed to occur simultaneously with the twisting of the donor group around the central bond that connects the acceptor moiety. The TICT molecule that we have used in the present study is 4-(1-azetidiny) benzonitrile (P4C). The details of TICT mechanism has been discussed in chapter 1. Since the TICT reactions have been found to couple partially to the medium dynamics, one naturally asks the following question: what could be the effects of the observed ~10 – 20% slowing down of the long time solvation rate in deuterated solvents on the TICT reactions occurring in these solvents? More precisely, would the reaction rate in isotopically substituted solvents be slowed down accordingly? This is possible only when the twisting mode explores the full solvent redistribution time scale during the course of the TICT reaction. As the static dielectric constant ( $\epsilon_0$ ) and dielectric relaxation time do not change significantly upon isotope substitution, the reaction rate is expected to be largely insensitive to solvent isotope substitution.

The organization of the rest of the chapter is as follows. Sample preparation and measurement methods are described very briefly in the next section. Section 5.3 contains experimental results from our steady state and time resolved studies. The article then ends with concluding remarks in section 5.4.

## **5.2. Experimental**

Synthesis of 4-(1-azetidiny) benzonitrile (P4C), sample preparation, steady state and time resolved measurements have been given in chapter 2 and chapter 3. Estimation of spectral properties has also been discussed in earlier chapter.

## **5.3. Results & Discussion**

As isotopic substitution induces no or insignificant changes in the polarity of the solvents considered here, the absorption and emission characteristics of a polarity probe in the deuterated solvents are not expected to differ much from those in the

normal solvents. This is what is seen in the present study for all the solvents studied. Fig.5.1 shows the absorption and emission spectra of P4C in ethanol and deuterated ethanol and the type of isotope insensitivity observed here is also seen for acetonitrile and methanol. Similar insensitivity has also been reported earlier by Lee<sup>8</sup> et al with a non reactive probe in normal and deuterated methanol and acetonitrile. The other spectral characteristics such as the absorption and emission peak frequencies ( $\nu_x$ ,  $x = \text{LE or CT}$ ), spectral band-widths ( $\Gamma$ ) for both the LE and CT emission bands of P4C, and CT/LE area ratios ( $\alpha_{\text{CT}}/\alpha_{\text{LE}}$ ) in these solvents are summarized in Table 5.1. The CT/LE area ratio which is a measure of the reaction yield also remains insensitive as isotope substitution in solvent does not change the medium polarity ( $\epsilon_0$ ). Note, however, that the area ratio ( $\alpha_{\text{CT}}/\alpha_{\text{LE}}$ ) varies as the solvent is changed and the variation is roughly correlated with the direction in which the medium polarity increases. This is also reflected in the changes in the values of the equilibrium constant ( $K_{\text{eq}}$ ) and changes in reaction Gibbs free energy ( $-\Delta G_{\text{r}}$ ) for the LE  $\rightarrow$  CT reaction of P4C. Calculations of these quantities ( $K_{\text{eq}}$  and  $-\Delta G_{\text{r}}$ ) are described below.

The area ratio is related to the changes in reaction Gibbs free energy via the equilibrium constant by the equation 2.1. Note in Table 5.1 that the values of  $-\Delta G_{\text{r}}$  and  $K_{\text{eq}}$  of the reaction in deuterated methanol is slightly larger than those in normal methanol. Following the trend in dielectric relaxation parameters upon deuteration in water and also in the absence of dielectric relaxation data for these isotope-substituted solvents, we can only suggest that the small increase of these quantities is probably due to a slight increase in solvent polarity due to stronger H-bonds in deuterated methanol.

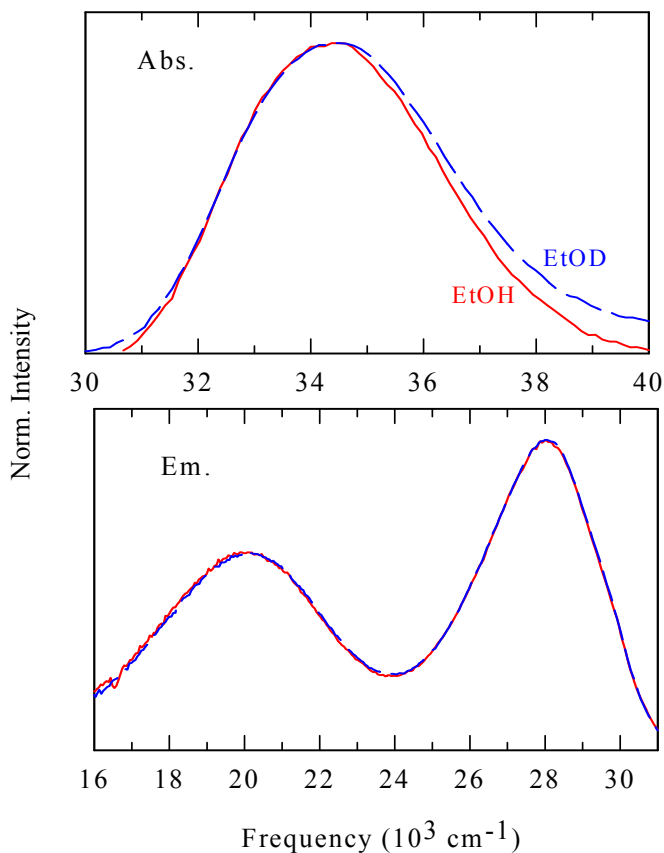


**Fig.5.1:** Absorption and emission spectra of 4-(1-azetidiny) benzonitrile (P4C) in deuterated and normal ethanol. Absorption spectra are shown in *upper panel* and emission spectra are shown in *lower panel*. Normal ethanol is represented by solid (red) and deuterated ethanol is represented by dashed (blue) lines. Similar effects of deuteration have also been found for acetonitrile and methanol.

**Table 5.1:** Solvent isotope effects on spectral properties, area ratios, equilibrium constants of changes in reaction free energies <sup>a</sup>

Solvents	$\nu_{\text{abs}}$	$\nu_{\text{LE}}$	$\nu_{\text{CT}}$	$\Gamma_{\text{abs}}$	$\Gamma_{\text{LE}}$	$\Gamma_{\text{CT}}$	$\alpha_{\text{CT}}/\alpha_{\text{LE}}$	$K_{\text{eq}}$	$-\Delta G_{\text{r}}$
CH <sub>3</sub> OH	34.47	27.76	19.60	4.42	1.53	4.18	1.35	3.85	3.34
CH <sub>3</sub> OD	34.47	27.77	19.61	4.43	1.53	4.18	1.42	4.04	3.46
CH <sub>3</sub> CH <sub>2</sub> OH	34.50	27.89	20.07	4.31	1.42	4.19	0.93	2.50	2.27
CH <sub>3</sub> CH <sub>2</sub> OD	34.69	27.90	20.15	4.56	1.42	4.09	0.91	2.42	2.19
CH <sub>3</sub> CN	34.57	27.44	20.05	4.32	1.33	3.72	0.57	1.45	0.93
CD <sub>3</sub> CN	34.55	27.45	20.07	4.25	1.34	3.60	0.56	1.44	0.91

a) Peak frequencies ( $\nu$ ) and band widths ( $\Gamma$ , fwhm) are in units of  $10^3 \text{ cm}^{-1}$ . Changes in reaction Gibbs free energy,  $-\Delta G_{\text{r}}$  is in units of KJ/mole. Note that the error

associated with peak frequency values is  $\pm 250 \text{ cm}^{-1}$  and that with band area is  $\sim 10\%$  of the reported value (a maximum of 4 measurements).

However, deuteration of ethanol and acetonitrile probably does not change the solvent polarity ( $\epsilon_0$ ) and therefore these quantities ( $-\Delta G_r$  and  $K_{eq}$ ) remain the same as in the normal solvents. Dielectric relaxation studies of isotope-substituted methanol, ethanol and acetonitrile are therefore required to explain this insensitivity in a more quantitative manner. Quantum yields ( $\Phi$ ), radiative and non radiative rates ( $k_x^{\text{rad}}$  and  $k_x^{\text{nr}}$ ) associated with LE and CT bands have been calculated for P4C in the normal and deuterated solvents using equation 2.2. Quantum yields of individual parts (LE and CT) for P4C molecule in deuterated and normal solvents have been determined and provided in Table 5.2.

**Table 5.2:** Solvent isotope effects on quantum yields, radiative and non-radiative rates<sup>a</sup>

Solvents	$\Phi_{\text{net}}$	$\Phi_{\text{LE}}$	$\Phi_{\text{CT}}$	$k_{\text{LE}}^{\text{rad}}$	$k_{\text{LE}}^{\text{nr}}$	$k_{\text{CT}}^{\text{rad}}$	$k_{\text{CT}}^{\text{nr}}$	$\langle \tau_{\text{LE}} \rangle (\text{ps})$	$\langle \tau_{\text{CT}} \rangle (\text{ps})$
CH <sub>3</sub> OH	0.017	0.007	0.010	5.11	7.02	0.85	0.87	141	1145
CH <sub>3</sub> OD	0.019	0.008	0.011	5.48	6.93	0.86	0.76	143	1299
CH <sub>3</sub> CH <sub>2</sub> OH	0.035	0.018	0.017	6.94	3.76	1.39	0.81	261	1210
CH <sub>3</sub> CH <sub>2</sub> OD	0.027	0.014	0.013	5.24	3.66	1.02	0.78	269	1264
CH <sub>3</sub> CN	0.04	0.026	0.014	4.71	1.80	0.93	0.63	542	1564
CD <sub>3</sub> CN	0.038	0.024	0.014	4.54	1.82	0.86	0.62	535	1589

a) The errors associated with the net quantum yield and the average life times (LE and CT) are respectively  $\sim 20\%$  and  $\sim 10\%$  (of reported values), estimated from a maximum of four measurements.

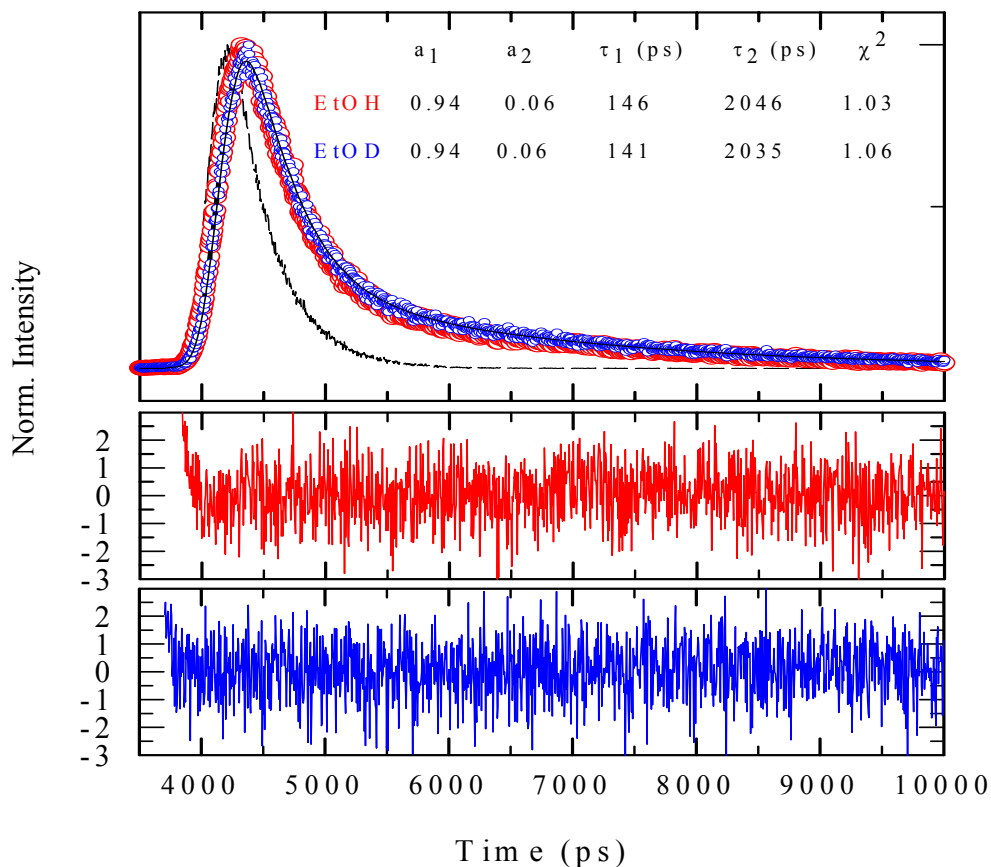
Error associated with the determination of quantum yields is  $\sim 20\%$  of each of the reported values. Quantum yields of P4C in deuterated solvents are nearly the same with that in normal solvents. Values for radiative ( $k^{\text{rad}}$ ), non radiative ( $k^{\text{nr}}$ ) and average life times ( $\langle \tau_{\text{avg}} \rangle$ ) can be determined by using our experimental data in the relations given in literature<sup>9</sup> and chapter 2 (Eq. 2.3, 2.6, 2.5 and 2.4). For individual parts, however we use the relations given in chapter 2. These quantities for P4C in the above solvent systems are calculated as discussed above and summarized in

Table 5.2. It is evident from this table that isotope substitution in solvent either has very small or negligible effects on quantum yields and radiative rates. However, there seems to be a small decrease in non-radiative rates in isotope-substituted solvents and this is probably because of the relatively stronger structure of the deuterated solvents. The average LE and CT lifetimes also do not change (a maximum of ~10% for CT life time in methanol) on isotope substitution of solvents. Interestingly, earlier studies<sup>6-7</sup> with dimethyl aminobenzonitril (DMABN) derivatives in deuterated water, methanol and ethanol reported much stronger isotope effects on fluorescence quantum yields and life times but no effects in acetonitrile.<sup>7,</sup>

10

Fig. 5.2 shows the LE emission decays of P4C in deuterated (blue circles) and normal (red circles) ethanol where the bi-exponential fit parameters are also presented. The weighted residuals are also shown in the lower panels of this figure (Fig. 5.2) whose random fluctuations over time indicate the adequacy of the bi-exponential function to fit the time dependent LE emission decays. We again mention here that the collected emission decays at wavelength near CT emission peaks could also be fitted with bi-exponential functions with same or similar time constants as found for the corresponding LE decays. For example, for P4C in methanol, fitting of CT emission decay with no constraints produces time constant 99 ps (rise time) and 1812 ps with  $\chi^2 = 0.97$ . This time constant (rise time) is thus very similar to the fast time constants (decay time, 96 ps) of the LE decay, indicating that these short time constants are essentially associated with the reaction rate. It is evident from Fig. 5.2 as well as from the listed fit parameters that deuterium substitution in ethanol has negligible effects on the rate of the LE  $\rightarrow$  CT reaction of P4C in these solvents. The decay parameters obtained for deuterated and normal methanol and acetonitrile also show the similar comparison. The relevant data are summarized in Table 5.3. As discussed earlier,<sup>11-13</sup> short time constant associated with the LE decay is regarded as the reaction time. The data in Table 5.3 indicate the isotope substitution neither changes the reaction time (short time constant) nor the amplitude of the associated component. This means that the reaction equilibrium

( $K_{eq} \propto a_{\text{short}}/a_{\text{long}}$ ) is not changed upon isotope substitution, which is also a finding in the steady state studies (see Table 5.1).



**Fig.5.2:** Two representative LE emission decays of P4C in deuterated (blue) and normal (red) ethanol. The data are represented by the circles, while the fit through the data are by the solid line. The instrument response function (IRF) is shown by the dashed line. The fit (bi-exponential) results are also provided in *inset* of *upper panel*. The LE peak count is  $\sim 3000$ . Residuals are shown in the *lower panel* (color code remains the same as in the upper panel).

The long time constants in alcohol solvents, however, increases by  $\sim 4\text{-}7\%$  upon deuteration, and is again probably due to the better stabilization of the excited state in the more structured isotope-substituted alcohols studied here. Data in Table 5.3

also indicates that deuterium substitution in acetonitrile has no effect on spectral properties as well as on the equilibrium constants and reaction kinetics.

**Table 5.3:** Bi-exponential fit parameters for LE emission decays: Solvent isotope effects

Solvent <sup>a</sup>	a <sub>1</sub>	a <sub>2</sub>	τ <sub>1</sub> (ps)	τ <sub>2</sub> (ps)	χ <sup>2</sup>
CH <sub>3</sub> OH	0.97	0.03	96	1804	0.98
CH <sub>3</sub> OD	0.97	0.03	94	1939	1.00
CH <sub>3</sub> CH <sub>2</sub> OH	0.94	0.06	146	2046	1.03
CH <sub>3</sub> CH <sub>2</sub> OD	0.94	0.06	141	2135	1.06
CH <sub>3</sub> CN	0.87	0.13	230	2579	0.95
CD <sub>3</sub> CN	0.87	0.13	230	2577	1.10

a) The error associated with the amplitude estimates is ~5% of the reported values.

#### 5.4. Conclusion

Solvent isotope effects on the reaction rate and yield of a twisted intramolecular charge transfer (TICT) reaction in deuterated methanol, ethanol and acetonitrile have been investigated in this chapter. Both the reaction rate and reaction yield have been found to have no effects from solvent isotope substitution. Other solute properties such as quantum yield, absorption and emission frequencies, line-widths and radiative rates also remain the same in deuterated solvents as those in the normal solvents. Non-radiative rates, however, appears to reduce by a few percent ( $\leq 10\%$ ) in the alcohols studied here. The long time constant associated with the LE and CT decays of the TICT molecule (P4C) also lengthened by a small amount (~5%) upon deuteration in methanol and ethanol, while deuteration in acetonitrile does not show any such effects. The average LE and CT lifetimes also show similar effects upon isotope substitution in solvents.

Even though the average solvation times in deuterated water and methanol have been found to be larger by ~10%, a proportionate slowing down of the TICT reaction rate in the deuterated solvents has not been observed here. Deuteration of solvents can affect a reaction in the following manner: (i) deuteration can slightly increase the static dielectric constant of a solvent which would reduce the reaction barrier

involved in these reactions. This will enhance slightly the reaction rate (static solvent effects). (ii) the more structured-ness in the deuterated solvents and less zero-point energy of O-D bonds, on the other hand, would slow down the rate of the solvent orientational polarization relaxation. The relatively slow solvent polarization relaxation would then make the reactive mode (here the twisting mode) more coupled to the solvent dynamical modes producing a relatively stronger dynamical solvent control (dynamic solvent effects) of the reaction. Therefore, the insensitivity of the TICT reaction rates to the isotope substitution of these solvents may be a resultant of these two opposing solvent effects. This is probably the reason that even though the average solvation times in many of these solvents increases upon deuteration, the reaction rate remains insensitive. However, dielectric relaxation studies of these deuterated solvents are required to provide a more quantitative justification to the above discussion.

## References

1. Iwase, E.; Tomioka, A.; Saigusa, H.; Yagi, M., *Phys. Chem. Chem. Phys.*, **2004**, *6*, 3852.
2. Weston, R.E., *Chem.Rev.*; **1999**, *99*, 2115.
3. Nandi, N.; Roy, S.; Bagchi, B., *J. Chem. Phys.* **1995**, *102*, 1390.
4. Zolotov, B.; Gan, A.; Fainberg, B.D.; Huppert, D., *J. Luminesce*, **1997**, *72-74*, 842.
5. Dresner, J.; Prochorow, J.; Sobolewski, A., *Chem. Phys. Lett.*, **1978**, *54*, 292.
6. Kohler, G.; Grabner, G.; Rotkiewicz, K., *Chem. Phys.* **1993**, *173*, 275.
7. Grabowski, Z.R.; Rotkiewicz, K.; Rettig, W., *Chem. Rev.*, **2003**, *103*, 3899.
8. Lee, S.H.; Lee, J.H.; Joo, T., *J. Chem. Phys.*, **1999**, *110*, 10969.
9. Dahl, K.; Biswas, R.; Ito, N.; Maroncelli, M. *J. Phys. Chem. B*, **2005**, *109*, 1563.
10. Siebrand, W., *J. Chem. Phys.* **1971**, *55*, 5843.
11. Pradhan, T.; Biswas, R., *J. Phys. Chem. A* **2007**, *111*, 11524.
12. Pradhan, T.; Ghoshal, P.; Biswas, R., *J. Phys. Chem. A* **2008**, *112*, 915.
13. Biswas, R., Rohman, N.; Pradhan, T.; Buchner, R., *J. Phys. Chem. A* **2008**, *112*, 9379.

## Chapter 6

### Excited State Intramolecular Charge Transfer Reaction in Binary Mixtures of Water and Alcohol

#### 6.1. Introduction

Alcohol-water binary mixtures have been studied extensively over the years in order to correlate the solution structure with the observed anomaly in several thermodynamic properties of this mixtures<sup>1-30</sup>. As a subtle balance between the hydrophobic and hydrogen bonding (H-bonding) interactions determines the solution structure and hence the properties, attempts have been made to understand how the hydrophobic interactions among the alkyl groups of the alcohol molecules and the H-bonding interactions among the hydroxyl groups (-OH groups) of water and alcohol molecules assist each other to retain the structure of the pure form of the respective species. Neutron diffraction<sup>7-8, 27</sup>, small angle X-ray scattering (SAXS)<sup>17-19</sup>, light scattering<sup>17,31-33</sup> and other experimental studies<sup>9, 12-13</sup> have indicated that microscopic phase separation and cluster formation dominate the mixing in alcohol-water systems. While the aggregation of alcohol molecules are often linked to the anomalous change in several thermodynamic properties, modifications in solution structure are believed to be responsible for the observed sharp change in the ultrasound absorption coefficient alcohol-water binary mixtures<sup>9, 34-35</sup>. Even though several experimental studies support the idea of formation of clathrate type structures between water and alcohol molecules at very low alcohol concentration, neutron diffraction studies with the lowest alcohol mole fraction have not found any evidence for such a structure.

Computer simulation studies<sup>21-24</sup> with realistic potentials has aided the experiments where the self-association of alcohol molecules and structural enhancement are studied by using the surface distribution function (SDF)<sup>36</sup> approach. Simulation studies with tertiary butanol (TBA) in water have suggested that the life-time of the

clusters formed through aggregation of 2-4 alcohol molecules in ~20-30 ps and undergo continual change inducing fluctuations in the micro- environments<sup>22</sup>. These studies have also examined the question whether water-cage encapsulates the alcohol molecules or the alcohol hydroxyl groups are incorporated in the water-cage by participating in the H-bonding network while leaving the methyl groups interacting through hydrophobic interaction. Theoretical studies based on the RISM (Reference Interaction Site Model) approach with modified closure relations have indicated strengthening of H-bonding between all species and also explained the non-monotonic alcohol mole fraction dependence of isothermal compressibility<sup>24, 37</sup>. According to these studies, alcohol molecule resides in the cavity in the H-bonding network created by the surrounding water molecules which, in turn, lowers the compressibility of the medium<sup>37</sup>. However, with further addition of alcohol, the tetrahedral network structure gradually converts to the zigzag chain structure of alcohol increasing the compressibility of the water-alcohol mixtures<sup>37</sup>.

Since microscopic phase separation is inherent in TBA-water mixtures<sup>7-8, 12, 18-25, 38-43</sup>, TICT reaction in TBA-water solutions are expected to be affected by such heterogeneity in solution structure. However, the micro-heterogeneity may be less pronounced in presence of a TICT molecule as a recent neutron diffraction study with ternary mixture composed of cyclohexene, TBA and water in 2:6:1 ratio indicate that the non-polar cyclohexene molecules are favorably solvated by the alkyl groups of the alcohol molecules where the trimolecular mixture appears to be more homogeneous than the binary TBA-water solutions<sup>44</sup>. Several studies have been done earlier with DMABN in alcohol-alkane mixtures where formation of alcohol-DMABN exciplex was believed to play key roles in regulating the CT emission decay<sup>45-48</sup>. Effects of structural modification upon the addition of alkane have not been stressed in these studies. Such a study with 4-(1-azetidynyl) benzonitrile (P4C) in water-TBA mixtures at different alcohol mole fractions are presented here for the first time to the best of our knowledge.

While studying the TICT reaction in P4C in aqueous solutions of TBA, one would like to ask the following questions. First, will the strengthening of water structure due to addition of alcohol at low concentration and the resultant heterogeneity be reflected as the TICT reaction is carried out at different mole fractions? More precisely, can the TICT reaction be used as a probe to investigate the sharp change in solution structure<sup>1-4</sup> that occurs at the water rich regime with a peak at TBA mole fractions  $\sim 0.04$ ? Second, will the equilibrium ground state solvation (as probed by the steady state absorption) be different from that of excited state (as probed by the steady state fluorescence emission)? Third, what would be the effects of such solution structural change on the rate of intramolecular charge transfer reaction occurring in TBA-water solutions? Fourth, what would be the effects of mole fraction dependent solution dynamics on TICT reaction occurring in TBA-water solutions? In this chapter we present the results on the excited state intramolecular charge transfer reaction of 4-(1-azetidiny) benzonitrile (P4C) in aqueous TBA solutions at several alcohol mole fractions where we have investigated some of the questions posed above. Interestingly, a bi-exponential function with two different time constants is found to sufficiently describe the decay kinetics of P4C at all TBA concentrations, as has been found earlier in electrolyte solutions<sup>49</sup>.

We also present here results from our investigation whether alcohol concentration induced structural transition can be probed by monitoring the fluorescence anisotropy of a non-reactive probe. C153 has been chosen as a non-reactive probe for our study since experimental studies and quantum mechanical calculations have indicated C153 as one of the best solvation probes normally used in such studies<sup>50-51</sup>. Ethanol and tertiary butanol (TBA) have been chosen since these alcohols are fully miscible with water at any proportion and at any temperature. More importantly, aqueous binary mixtures of these alcohols show well-structured peak when several thermodynamic properties are followed as a function of alcohol mole fraction<sup>1-5</sup>. Also, the values of the mole fraction at which the above-mentioned peak occurs vary sharply with the identity of the alcohol in the mixture.

The organization of the rest of the chapter is as follows. Experimental details are given in the next section. Section 6.3 contains experimental results from our steady state and time dependent studies with P4C molecules in aqueous solution of TBA with different TBA mole fractions and with C153 in TBA-water and ethanol-water mixtures. The chapter then ends with concluding remarks in Sec. 6.4.

## **6.2. Experimental Details**

### **6.2.1. Data Collection for TICT Reaction in P4C**

Synthesis of P4C molecule has already been described in chapter 2 and hence will not be discussed here. Tertiary butyl alcohol (TBA) was obtained from Aldrich and used as received. Ethanol was obtained from SRL, India. De-ionized water (Millipore) was used for preparing the aqueous solutions of alcohols (TBA or ethanol) at different mole fractions. The solutions were prepared by dissolving a measured amount of alcohol in 10ml volumetric flask followed by shaking the solution for a few minutes. Caution was exercised to ensure the accuracy of the mole fraction, particularly near the very low alcohol and water concentrations. As before (chapters 3, 4 and 5) time resolved fluorescence emission intensity decays were collected using time correlated single photon counting (TCSPC) technique based on a laser system (Lifespec-ps, Edinburgh, UK) that provided 299 nm light as excitation with IRF  $\sim$ 475 ps. The procedures for both the steady state and time resolved data collection and their subsequent analyses protocols remained the same as discussed in previous chapters.

### **6.2.2. Data Collection for Fluorescence Anisotropy Studies with C153**

Time resolved fluorescence anisotropy decays were also collected using the TCSPC technique with 409 nm light as excitation (IRF  $\sim$  75 ps). Emission decays with emission polarizer at magic angle were collected to obtain the average lifetime of C153 at different alcohol mole fractions in these mixtures. Subsequently, the collected emission decays were deconvoluted from the IRF and fitted to multi-exponential function using an iterative reconvolution algorithm<sup>52-53</sup>.

Time resolved fluorescence anisotropies,  $r(t)$ , were calculated from the collected and back ground subtracted parallel ( $I_{\parallel}(t)$ ) and perpendicular ( $I_{\perp}(t)$ ) decays by using the following well-known formula<sup>54</sup>

$$r(t) = \frac{I_{\parallel}(t) - GI_{\perp}(t)}{I_{\parallel}(t) + 2GI_{\perp}(t)}, \quad (6.1)$$

where  $G$  accounts for the differential sensitivity to the two polarizations which was obtained by tail matching the intensity decays  $I_{\parallel}(t)$  and  $I_{\perp}(t)$ . Note that the average value for  $G$  obtained by tail matching the relevant decays at times longer than the anticipated rotation time is  $1.15 \pm 0.05$ .

The time resolved anisotropy constructed from the collected emission decays by using Eq.6.1 then fitted to a bi-exponential function after deconvoluting from the IRF using an iterative reconvolution fitting program. The following form of the bi-exponential function was used for this purpose<sup>54</sup>

$$r(t) = r(0)[a_1 \exp(-t/\tau_1) + (1 - a_1) \exp(-t/\tau_2)], \quad (6.2)$$

where  $\tau_1$  and  $\tau_2$  in Eq.6.2 represent the time constants associated with the decays of the components constituting  $r(t)$ .  $r(0)$  denotes the initial anisotropy and was taken as 0.376 for fitting the time resolved anisotropies of C153 in all the mixtures studied here<sup>54</sup>. The alcohol mole fraction dependence of rotational motion of C153 in these binary polar mixtures is presented in terms of the average rotational correlation time,  $\langle \tau_{\text{rot}} \rangle = a_1 \tau_1 + (1 - a_1) \tau_2$ , which comes from the time integration of Eq.6.2 after normalizing with  $r(0)$ . Note that all the experiments were performed at room temperature,  $295 \pm 0.5$  K.

## 6.3. Results & Discussion

### 6.3.1. Results: Steady State Study with P4C

Absorption and emission spectra of P4C in TBA-water solutions at TBA mole fractions 0.01, 0.04, 0.1, 0.6 and that in pure TBA are shown in Fig.6.1. These TBA mole fractions are chosen so that the effects of gradual change in H-bonding structure (from tetrahedral-like network at low concentration to zigzag chain at higher mole fractions) on the stabilization of the ground and excited states of a fluorescent probe are represented. As already mentioned, aqueous TBA solutions with low TBA mole fractions are characterized by aggregation of TBA molecules via interactions among hydrophobic tertiary butyl ( $-CMe_3$ ,  $Me = CH_3$ ) groups where the alcoholic hydroxyl ( $-OH$ ) groups are incorporated into the water H-bonding cage that surrounds the TBA cluster. In concentrated TBA solution, both water and TBA molecules associate to form zigzag H-bonding chain structure similar to that in pure alcohol. While the anomaly in thermodynamic properties of aqueous TBA solution is the maximum at 0.04 TBA mole fraction, 0.10 corresponds to the transition composition from the TBA-TBA intermolecular contact to the TBA-water molecular association. One of the most interesting aspects of Fig.6.1 is that at low TBA mole fractions (up to  $\sim 0.1$ ), absorption spectrum of P4C shows red shift with the increase in TBA concentration, whereas emission spectrum shifts towards blue. At mole fractions higher than 0.1, both absorption and emission spectra show blue shift with TBA concentration as the average polarity of the medium decreases. The alcohol mole fraction dependence of absorption and emission spectra and their bandwidths (full width at half maximum) have been studied in detail and are summarized in Fig.6.2 where the peak frequencies of absorption and emission bands (both LE and CT) and spectral widths are shown as a function of TBA mole fraction. Several interesting aspects are to be noted in this figure. First, the absorption spectrum shows a red shift with the increase in alcohol concentration up to TBA mole fraction  $\sim 0.10$  and then blue shifts upon further addition of TBA. Contrastingly, the emission spectrum exhibits a continuous blue shift with TBA mole fraction in a fashion that

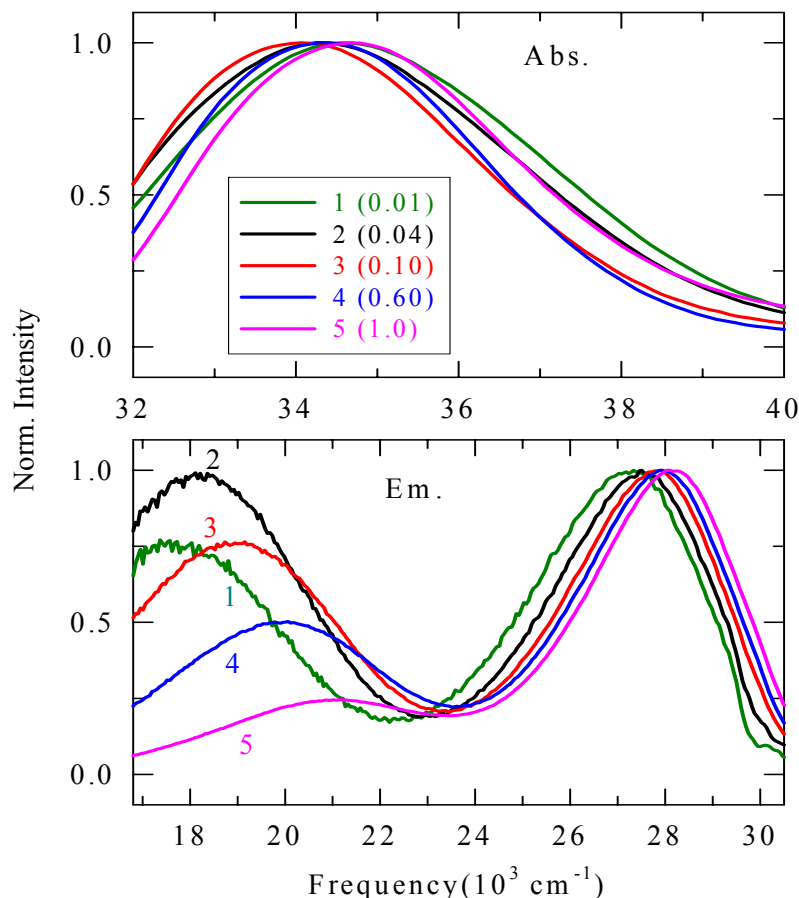


**Fig.6.1:** Absorption and emission spectra of 4-(1-azetidiny) benzonitrile (P4C) in different mole fractions of tertiary butyl alcohol of the mixture of water and tertiary butyl alcohol (TBA). *Upper panel* shows the absorption spectra and *lower panel* shows the emission spectra. The numbers in parenthesis indicate the TBA mole fraction in the TBA-water mixtures. Note that the absorption spectra are presented in a relatively narrower frequency scale in order to enhance the separation between spectra.

resembles the typical non-ideality in average polarity of such alcohol-water mixtures. Note that for the entire range of TBA concentration, the total blue shift for the CT band is  $\sim 2500 \text{ cm}^{-1}$ , whereas it is  $\sim 1000 \text{ cm}^{-1}$  for the LE band. Since addition of TBA in water facilitates formation of TBA clusters and enhances the H-bonding between all species, the microheterogeneity and the related structural modifications will affect the spectral properties of a dissolved solute. The enhanced H-bonding

structure at low TBA concentrations is further probed by a recent study on compressibility of TBA-water mixtures using the RISM theory<sup>37</sup> where realistic potentials have been used to represent both the species<sup>24,37</sup>. This theoretical study and comparisons with relevant experimental data have suggested that at low TBA concentration the cavity in the H-bonding network of water is occupied by the alkyl groups of the clustered TBA molecules and thereby reducing the compressibility of the solution<sup>37</sup>. Therefore, the reduced compressibility is an indicative of a more compact solvation environment surrounding the probe (P4C) molecule. This increased compactness due to the enhancement of local structure then naturally stabilizes the ground state energy level of the probe, leading to the observed red shift in the absorption spectrum. However, with further addition of TBA, tetrahedral-like network of H-bonding structure of water-rich solutions gradually converts to the chain-like alcohol structure at concentrated TBA solutions. Several studies<sup>7-8,12,18-25,38-43</sup> of TBA-water systems have revealed that such a structural transition occurs at TBA mole fraction  $\sim 0.10$ , a value at which the absorption peak frequency of P4C in the present study also shows a turn around. However, the question is then why emission frequency does not exhibit such a TBA mole fraction dependence? Simulation studies of TBA-water solutions have indicated that even though clusters of three or four TBA molecules are formed but undergo continual change on time scales of tens of picoseconds<sup>22</sup>. Since the stability times of these clusters (20-30 ps)<sup>22</sup> are many times smaller than the average life time of the excited state ( $>1$  ns) of the probe, the solvent environment surrounding the photo-excited probe undergoes a large number of relatively rapid fluctuations. These environmental fluctuations average out the subtle structural modification in dilute aqueous solutions of TBA allowing the solution polarity to primarily govern the emission transition energy.

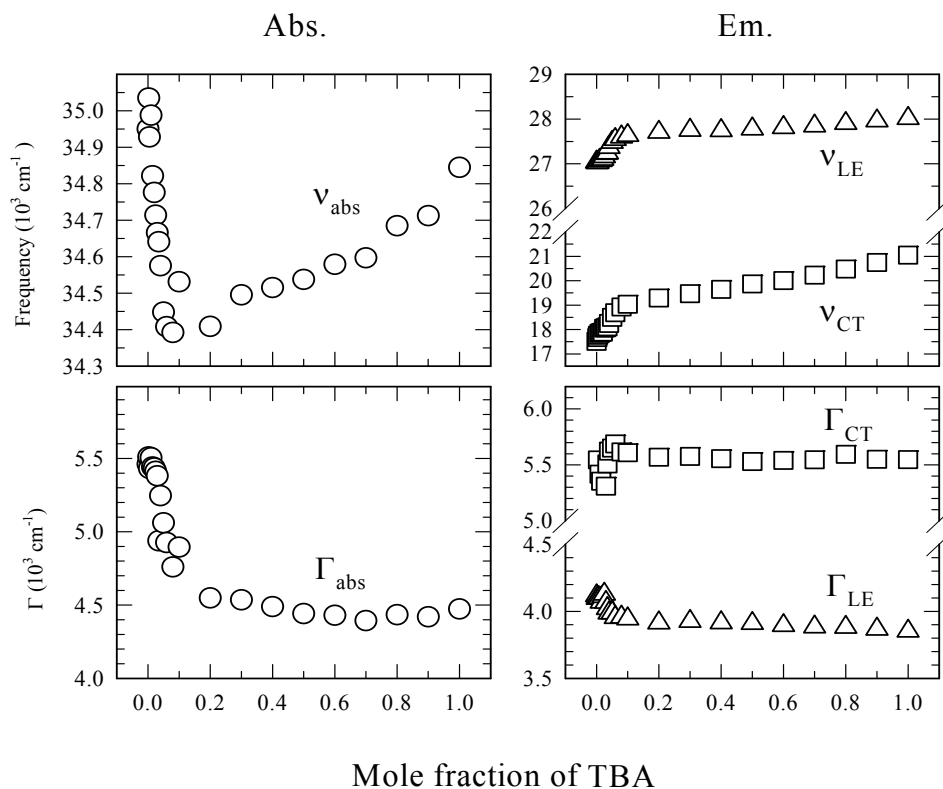


**Fig. 6.2:** Mole fraction dependence of absorption ( $\nu_{abs}$ ) and emission ( $\nu_{LE}$  and  $\nu_{CT}$ ) peak frequencies and line widths (full width at half maxima,  $\Gamma$ ) of the absorption spectra, LE bands and CT bands of 4-(1-azetidiny)benzonitrile (P4C) have been shown in water and TBA mixture. The open circles (in the *left panel*) represent absorption and open triangles and squares (in the *right panel*) represent the parameters associated with LE and CT bands of P4C. LE and CT peak frequencies ( $\nu_{LE}$  and  $\nu_{CT}$ ) have been obtained after deconvoluting the experimental emission spectra by broadening and shifting a reference spectrum with a Gaussian function (representing inhomogeneous solvent broadening).  $\Gamma_{LE}$  and  $\Gamma_{CT}$  are the full width at half maxima of LE and CT bands getting after deconvoluting of full experimental emission spectrum. The estimated uncertainty in frequencies and widths is  $\pm 300 \text{ cm}^{-1}$

Second interesting aspect of Fig.6.2 is the TBA mole fraction dependence of absorption and emission bandwidths of P4C. The absorption bandwidth (bottom-left panel) shows a sharp decrease with TBA mole fraction up to  $\sim 0.10$ . However,

the dependence of absorption bandwidth on TBA mole fraction is weaker in the range 0.10 – 1.0 and the total decrease in bandwidth in this range is only about 250  $\text{cm}^{-1}$  which is similar to frequency shift *versus* bandwidth behavior observed earlier with P4C in electrolyte solutions and also with a different solvation probe in neat solvents. The narrowing of absorption spectrum of P4C by  $\sim 1000 \text{ cm}^{-1}$  upon increasing the TBA concentration to  $\sim 0.10$  mole fraction is anomalously large and apparently contradicts the observations made in earlier studies<sup>50</sup>. As the spectral width in a binary mixture derives contributions from both the probe-solvent interaction strength and the heterogeneity in the surrounding solvent environment due to both density and concentration fluctuations, the narrowing of absorption spectrum may be regarded as a reflection of a novel interplay between the lowering of polarity and the loss of microscopic heterogeneity on each successive addition of TBA in water. The arguments given above may also be used to explain the narrowing of both the LE and CT emission bands between 0.10 – 1.0 TBA mole fractions. The blue shift with broadening in LE emission band and red shift with narrowing in the CT emission band have also been observed earlier for a non-reactive solvation probe coumarin 153 (C153) in pure solvents<sup>50</sup>. We would like to mention here that for C153 in hexane-alcohol binary mixtures, the emission bandwidth is found to increase up to alcohol mole fraction  $\sim 0.10$  and then decreases with further addition of alcohol<sup>55</sup>. This has been explained in terms of heterogeneity of solution structure<sup>55</sup>. However, no information is available in this study regarding the correlation between the red shift of the absorption spectrum and the absorption bandwidth.

Fig.6.3 depicts the TBA mole fraction dependence of the ratio between areas under the CT and LE emission bands of P4C in TBA-water solution. Note the area ratio shows a non-monotonic dependence on TBA concentration with a peak at TBA mole fraction  $\sim 0.04$ . This is the mole fraction of TBA where the maximum anomaly in thermodynamic properties as well as large increase in ultrasonic absorption<sup>9, 34-35</sup> and light scattering<sup>31, 33</sup> has been observed. The reasons for the anomalous increase in the area ratio (CT /LE) in dilute aqueous solutions of TBA can be understood by

examining the LE and CT emission bandwidths of P4C. The alcohol mole fraction dependent bandwidths presented in Fig.6.2 indicate that while the LE emission band narrows down upon addition of TBA, the width of the CT emission band increases up to TBA mole fraction  $\sim 0.04$  and then decreases. Therefore, the simultaneous broadening of the CT emission band with the narrowing of the LE band leads to the sharp increase of the area ratio (CT /LE) at  $\sim 0.04$  TBA mole fraction. As the CT state is primarily of  $L_a$  character and therefore more polar than the LE state ( $L_b$ )<sup>52</sup>, coupling of these states with the mole fraction dependent solution structure (environment) is likely to be different. This might be the reason for the observed difference in the mole fraction dependence of the LE and CT emission bandwidths. As before, we have measured quantum yield, radiative and non-radiative rates, and transition moments of P4C at different mole fractions of TBA in aqueous solution in order to investigate the effects of solution structure on these quantities. Refractive indices of the TBA-water solutions at different mole fractions of TBA have been measured ( $296.15 \pm 1K$ ) and summarized in Table 6.1. Quantum yields (net) of P4C determined at various mole fractions of TBA in aqueous solutions are shown in the upper panel of Fig.6.4. As expected, the mole fraction dependence of quantum yield is a non-ideal one and similar to that of LE and CT emission frequencies. Similar alcohol mole fraction dependence is also found for the quantum yields for the individual LE and CT bands (not shown here). Note that the quantum yield of P4C in pure TBA is very close to that in pure methanol ( $\Phi_{net} = 0.016$ )<sup>52</sup>.

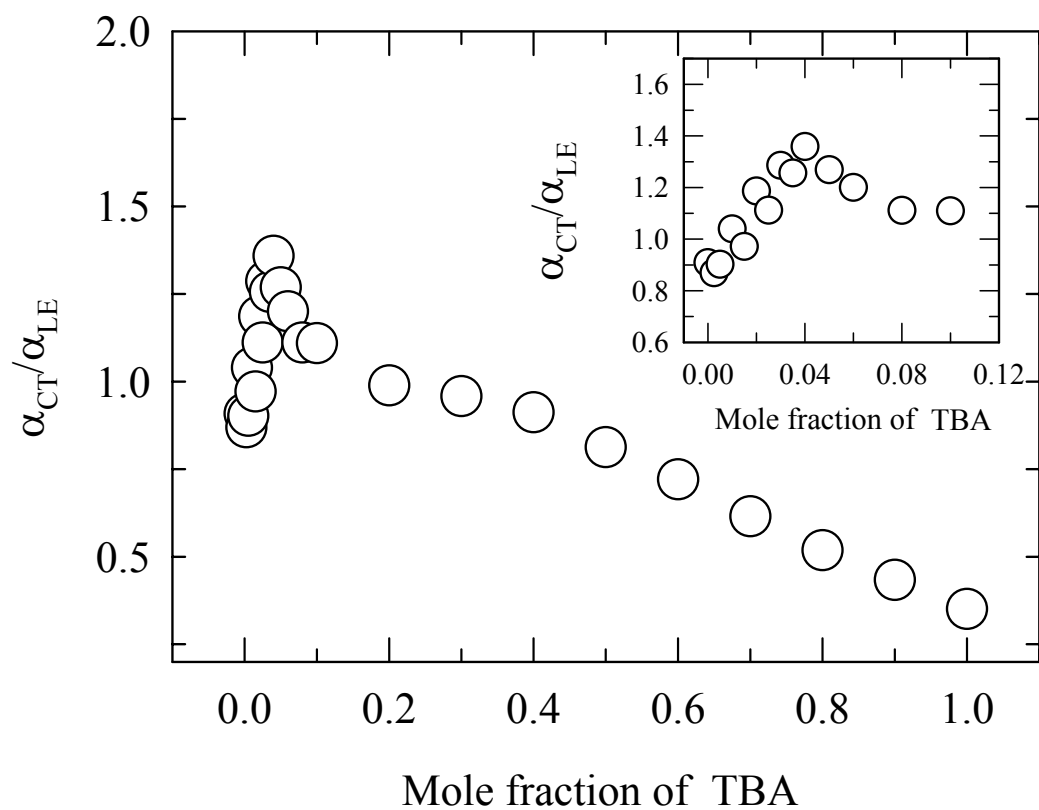


**Fig. 6.3:** Mole fraction dependence of formation of CT population in the mixture of TBA and water has been shown in this figure. The ratio ( $\alpha_{CT}/\alpha_{LE}$ ) between areas under the CT and LE bands are shown as a function of mole fraction of TBA. *Inset* shows  $\alpha_{CT}/\alpha_{LE}$  in the breaking region.

**Table 6.1:** Refractive indices and non-radiative rates associated with LE emission band of P4C in water-TBA mixtures at different TBA mole fractions

TBA Mole fraction	$n_s$	$k_{LE}^{nr}(10^9)/s$
0	1.331	31.40
0.0025	1.333	27.21
0.005	1.333	27.31
0.01	1.335	28.48
0.015	1.336	30.85
0.02	1.338	30.20
0.025	1.340	27.85
0.03	1.341	21.65
0.035	1.344	27.12
0.04	1.345	22.65
0.05	1.346	15.78
0.06	1.350	11.13
0.08	1.355	8.71
0.1	1.357	7.50
0.2	1.368	5.63
0.3	1.373	4.80
0.4	1.376	4.75
0.5	1.379	3.41
0.6	1.380	2.82
0.7	1.381	2.27
0.8	1.381	1.81
0.9	1.381	1.46
1	1.382	1.16

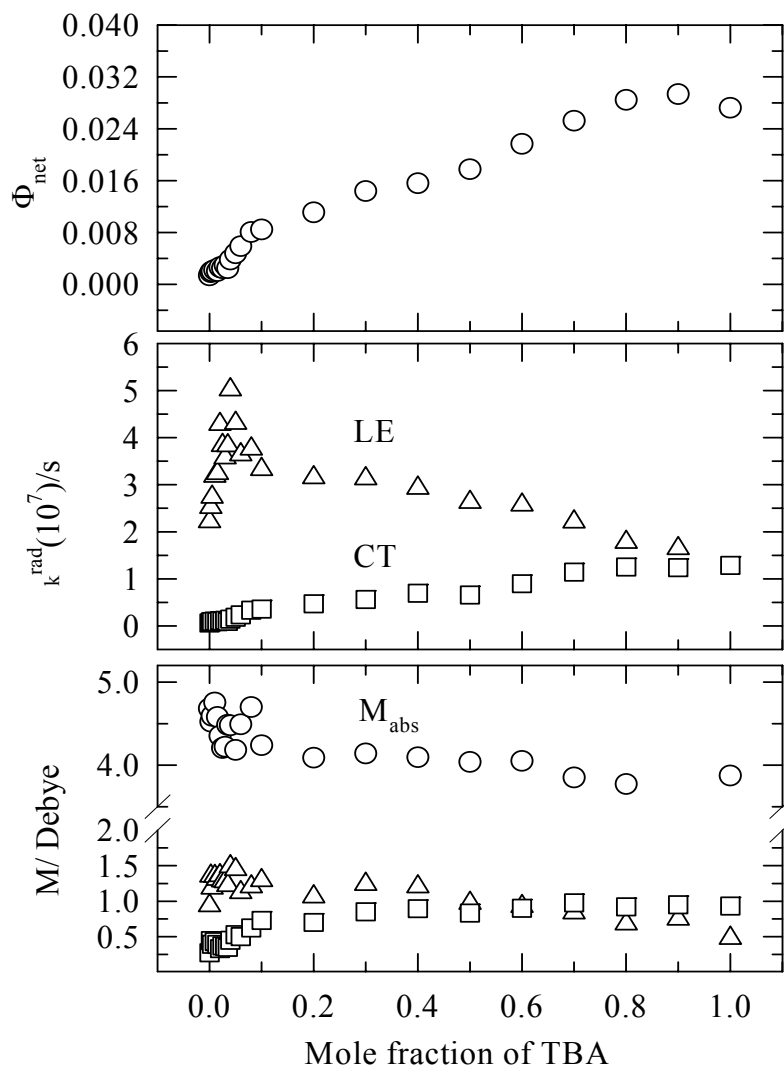


**Fig. 6.4.:** Mole fraction dependence of quantum yield ( $\Phi_{net}$ ), radiative rate( $k^{rad}$ ), absorption transition moment, emission(LE & CT) transition for P4C in water and TBA mixture have been shown in this figure. Open circles in the *upper panel* net quantum yield of P4C in the mixture. Open triangles and open squares in the *middle panel* indicate the radiative rate of P4C associated with LE and CT bands respectively. Open circles, open triangles and open squares in the *lower panel* indicate absorption transition moments, LE and CT transition moments respectively.

The calculated radiative rates for the LE and CT emission bands of P4C at different mole fractions of TBA in aqueous solution of TBA are shown in the middle panel of Fig. 6.4. The corresponding non-radiative rates for the LE emission band are

summarized in Table 6.1. The parameters necessary for the calculations of  $\langle\tau_{LE}\rangle$  and  $k_{CT}$  are obtained from the decay fits (shown later in Fig.6.6). The error bar for these radiative and non-radiative rates is  $\pm 25\%$  of the values reported here. It is interesting to note that  $k_{LE}^{rad}$  shows a peak at TBA mole fraction  $\sim 0.04$ , whereas  $k_{CT}^{rad}$  exhibits a typical non-ideal TBA mole fraction dependence. The fit parameters shown later in Fig. 6.6 indicates that there would be a minimum in  $\langle\tau_{LE}\rangle$  at TBA mole fraction  $\sim 0.04$  which is responsible for the observed peak in  $k_{LE}^{rad}$ .

Since the enhancement of solution structure at very low concentration of TBA significantly affects the absorption peak frequencies of the probe molecule, the absorption transition moment is also expected to show the effects of such structural modifications. The net absorption transition moment thus obtained for P4C in water-TBA mixtures by using Eq.2.8 are shown as a function of TBA mole fraction in the bottom panel of Fig.6.4. The maximum error bar associated with this calculation is  $\pm 15\%$ . The data in this figure (Fig. 6.4) seem to suggest that the TBA induced enhancement of the H-bonding structure have small but non-negligible effects on the net absorption transition moment of P4C. However, once the tetrahedral-like H-bonding network structure of water is disrupted and chain-like structure of alcohol appears upon further addition of TBA, the net absorption transition moment becomes almost insensitive to the TBA mole fraction beyond  $\sim 0.10$ . The near insensitivity of the net absorption transition moment of P4C on the average polarity of the medium has also been observed earlier in neat solvents<sup>52</sup> and also in electrolyte solutions<sup>56</sup>. All these observations probably indicate that the solution structure rather than the polarity of the medium dictates the absorption transition moment in solution phase. In order to investigate the effects of microheterogeneity and structural transition on emission moment, the TBA mole fraction dependence of emission transition moment for P4C in water-TBA solution has also been calculated (by using Eq.2.7) and shown in the bottom panel of Fig.6.4. It is interesting to note that the emission transition moment for the LE band does not show a sharp change upon increasing the alcohol concentration in the water rich region of the aqueous solution, even though the LE

radiative rate ( $k_{LE}^{rad}$ ) shows a peak at TBA mole fraction  $\sim 0.04$ . However, both the LE and CT emission transition moments exhibit near insensitivity to alcohol concentration beyond TBA mole fraction  $\sim 0.10$ . The non-radiative rates for the LE band at different TBA mole fractions have also been calculated and are summarized in Table 6.1. Note that the non-radiative rate for LE ( $k_{LE}^{nr}$ ) is very large in very dilute solutions of TBA which becomes comparable to that for P4C in methanol at TBA mole fraction  $\sim 0.10$ . It is probably the H-bonding network of water that facilitates the non-radiative relaxation processes and hence the non-radiative rates are very large for LE in the aqueous solution at TBA mole fraction  $< 0.05$ . This observation again suggests an appreciable role of solution structure in determining the non-radiative rate for an emission band.

### 6.3.2. Time Resolved Fluorescence Emission Studies with P4C

Time resolved emission decay measurements have been performed with P4C in water-TBA mixtures at 23 different TBA mole fractions in order to study the effects of TBA-induced structural transition and microscopic heterogeneity of water-TBA solutions on the rate of LE  $\rightarrow$  CT conversion reaction in P4C. As already mentioned in the Introduction, emission decays of P4C in water-TBA solution are bi-exponential with time at all TBA mole fractions. This is rather interesting because in water-TBA mixtures where microscopic heterogeneity governs the solution structure, a stretched exponential<sup>57</sup> rather than a simple bi-exponential function is expected to properly describe the decay kinetics. The fact that a time dependent bi-exponential function can sufficiently describe the decay kinetics of P4C in water-TBA mixtures is a reflection of rapid fluctuations in the immediate environment of the photo-excited P4C due to relatively faster lifetime of the TBA clusters. It may also be due to the fact that since a broader time resolution (FWHM of the IRF) is employed in this study, missing of faster components inhibits the detection of the subtle variation in the faster time scales. Representative bi-exponential fits to the emission decays collected at peak wavelengths of LE and CT bands of P4C at 0.60 mole fraction of TBA are shown in Fig.6.5 where fit parameters are also listed. Clearly, both the LE

and CT emission decays are bi-exponential as the residuals do not contain any non-random pattern<sup>58</sup> and values for the ‘goodness of fit parameter’ ( $\chi^2$ ) are close to 1.

Fig. 6.5 also demonstrates that when the fits are carried out without any constraints, time constants describing the CT emission decay are very similar to those required to fit the corresponding LE decays. As shown in the lower panel of Fig.6.5, ‘free’ fitting of CT emission decay at 0.60 TBA mole fraction produces time constants 220 ps (rise time) and 2100 ps with  $\chi^2 = 1.08$ . The time constant associated with the rise (rise time) is thus very similar to the fast time constant (decay time, 201 ps) of the LE decay indicating that these time constants are essentially associated with the average reaction rate<sup>52</sup> for the LE  $\rightarrow$  CT conversion reaction of P4C. Note here that fixing of the rise time to the fast decay time constant of LE emission decay (201 ps) or addition of a third exponential did not produce a better fit. As we would see soon that similar behavior has been observed at all TBA mole fractions. It is therefore interesting to note that self-association of TBA molecules in water-TBA mixtures has not induced any deviation from the biexponential kinetics observed earlier for P4C in neat solvents<sup>52</sup> and electrolyte solutions<sup>49</sup>. Therefore, the bi-exponential behavior of the decay kinetics for P4C in water-TBA mixtures also conform to the classical two state reversible reaction mechanism as described earlier. Note that in the present study the fast time constant is simply the average reaction time as the decays are all biexponential with time. The reaction time ( $\tau_{rxn}$ ) for P4C in water-TBA solutions are shown as a function of TBA mole fraction in the upper panel of Fig.6.6. The TBA mole fraction dependence of the reaction time therefore clearly reflects the non-ideality of the water-TBA binary mixture. The reaction time in pure TBA is  $\sim 300$  ps which is similar to that in pure 1-pentanol<sup>52</sup>. As the static dielectric constants ( $\epsilon_0$ ) of TBA and 1-pentanol are 12.5 and 13.9 respectively<sup>50</sup>, the similarity in reaction time probably indicates that the average polarity of the medium largely governs the LE  $\rightarrow$  CT conversion reaction in P4C.

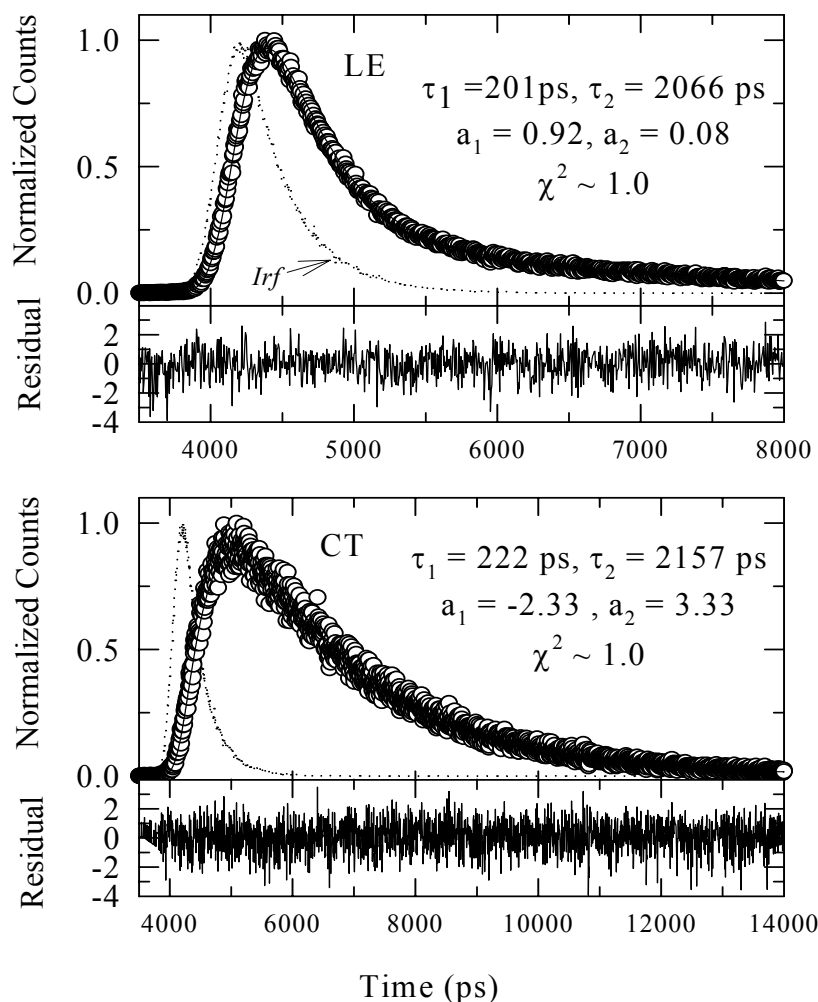


**Fig.6.5.** Representative LE emission decay (*upper panel*) and CT emission decay (*lower panel*) of P4C in the mixture of water and TBA at the mole fraction of 0.6 of TBA have been shown in this figure. The data are represented by the circles, while the fit through the data are by the solid line. The instrument response function is shown by the broken line. The fit (biexponential) results are also provided in the *upper panel* as well as in *the lower panel*. The LE peak count is  $\sim 3000$  and CT peak count is  $\sim 1000$ . Residuals are shown in the bottom of each panel ( $\pm 4$  full scale).

The fact that the average reaction time is  $\sim 6$  times faster in extremely dilute TBA solution than that in pure TBA provides further support to this conclusion as earlier studies<sup>59-60</sup> with DMABN in butyronitrile-octane and butanol-hexadecane mixtures

showed the rate being proportional to the polarity parameter  $E_T(30)$ . As the H-bonding network structure is believed to be strengthened upon addition of TBA in very dilute aqueous solutions, the increased ‘compactness’ (as reflected in the lowering of isothermal compressibility)<sup>37</sup> of the solvation environment may affect the rate of LE  $\rightarrow$  CT conversion reaction. The effects of such structural transition on the reaction rate should be reflected in the alcohol concentration dependence of  $\tau_{rxn}$  in the water-rich region of water-TBA mixtures. However, for the reasons already stated, the subtle variation in  $\tau_{rxn}$  with TBA concentration in the very dilute TBA solution could not be captured successfully. However, a closer look at these data seems to suggest a broad minimum in  $\tau_{rxn}$  at TBA mole fraction  $<0.05$ . Note that the values of  $\tau_{rxn}$  at these TBA mole fractions are much smaller than the effective resolution of our decay analysis method and are therefore likely to be associated with large uncertainties. However, these data are reproducible and the variation with alcohol concentration appears to be systematic. Therefore, the broad minimum at low TBA mole fraction may arise due to the TBA-induced compactness of the network structure which favors the formation of CT upon photo-excitation of P4C molecule. Note that steady state results presented in Fig.6.3 also bear the signature of such structural enhancement. Therefore, further studies with better time resolution is required to unravel the effects of structure enhancement on reaction rate in the very dilute aqueous solutions of TBA. The effects of enhanced solution structure are clearly observed when the time constant associated with the slower component of the emission decay is plotted as a function of TBA mole fraction. This is shown in the middle panel of Fig.6.6. Note the presence of a minimum in  $\tau_{slow}$  at TBA mole fraction  $\sim 0.04$ . The bottom panel of Fig.6.6 depicts the amplitudes as a function of TBA concentration obtained from the bi-exponential fits to the LE emission decays. The TBA mole fraction dependence of the amplitudes indicates that the LE  $\rightarrow$  CT conversion reaction is increasingly disfavored as the polarity of the medium is decreased with successive addition of TBA.

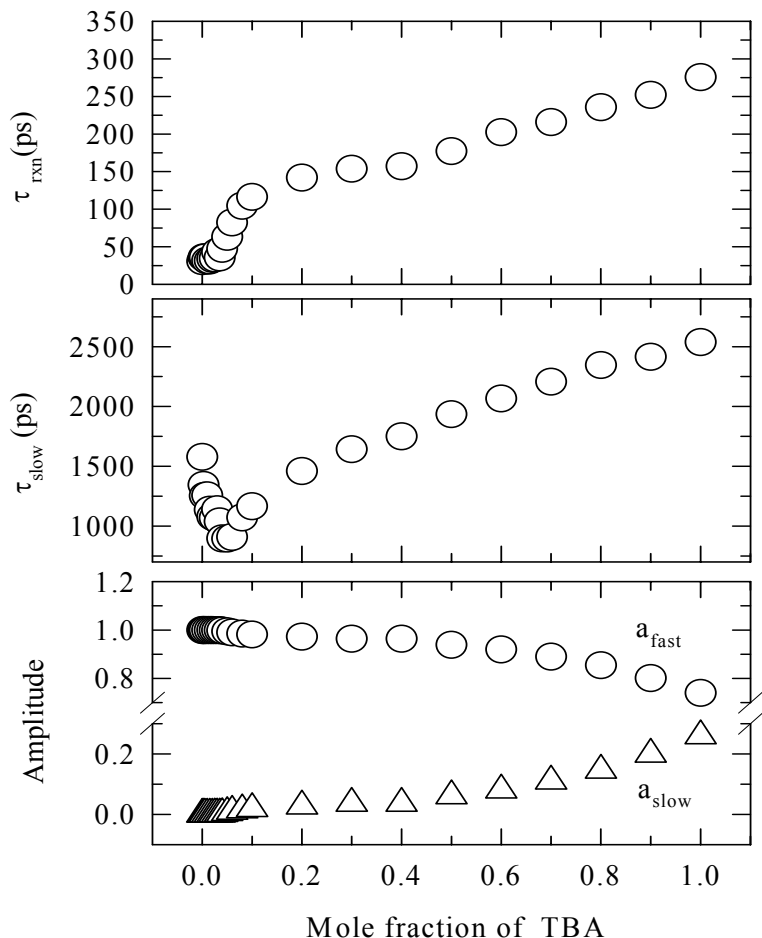


**Fig.6.6:** Mole fraction dependence of the reaction time ( $\tau_{\text{rxn}} = \tau_{\text{fast}}$ ), time constant associated with the slow component of the bi-exponential emission decay ( $\tau_{\text{slow}}$ ) and that of amplitudes ( $a_{\text{fast}}$  and  $a_{\text{slow}}$ ) associated with the LE  $\rightarrow$  CT conversion reaction of P4C in aqueous solutions of TBA. While the upper and middle panels show respectively the variation of  $\tau_{\text{rxn}}$  and  $\tau_{\text{slow}}$  with TBA mole fraction, the lower panel shows the same for the amplitudes obtained from bi-exponential fits to the collected emission decays.

Also, at the water-rich region, the overwhelming domination of the fast component ( $a_{\text{fast}}$ ) over the other one ( $a_{\text{slow}}$ ) suggests that the reaction is highly favorable due to the large value of change in reaction free energy ( $-\Delta G_r \propto \ln[a_{\text{fast}}/a_{\text{slow}}]$ )<sup>52</sup>. Note here

that even though the magnitude of  $a_{slow}$  is very small at TBA mole fractions  $<0.10$ , neglect of this does not produce a good fit (as indicated by  $\chi^2$  and non-random pattern of the residual).

### 6.3.3. Probing the Solution Structure Using a Non-reactive Probe, C153

Steady state fluorescence emission studies by using C153 in TBA-water solutions also produces the spectral features qualitatively similar to those found for the ICT molecule P4C. The steady state results are discussed in detail in Ref.61 and hence we will discuss here the fluorescence anisotropy data. Because the coupling of the solute rotation with the immediate environment controls the rotational diffusion of a solute, time resolved fluorescence anisotropy studies could be used to understand the nature of the coupling of the solute rotation with the dynamical solvent modes<sup>54</sup>. The time scale of the solvent modes, on the other hand, are governed by several factors, such as average polarity, structural correlations (and H-bonding network for associating liquids), heterogeneity in the environment, preferential solvation and inter-diffusion. Therefore, time resolved fluorescence anisotropy provides an opportunity to probe the microscopic heterogeneity of alcohol-water binary mixtures and the associated structural transition.

Time resolved fluorescence anisotropy decays of C153 in ethanol-water and TBA-water solutions have also been found to be bi-exponential with two distinctly different time constants at all TBA mole fractions. Representative bi-exponential fit to the constructed time resolved anisotropy from the collected parallel and perpendicular emission decays for C153 in TBA-water solution at 0.80 TBA mole fraction is shown in Fig.6.7. The nature of the residual (bottom panel) and the fit parameters listed in the upper panel indicate that a bi-exponential function is indeed required for adequate description of the  $r(t)$ . Except at extremely dilute ethanol concentrations, bi-exponential fits of similar quality have been obtained for all ethanol-water and TBA-water solutions studied here. Even though the single exponential fits to the  $r(t)$  decays at very low ethanol mole fractions (up to 0.10) have generated reasonable values for the ‘goodness of fit parameter’ ( $\chi^2$ ), the

residuals (not shown here) seem to indicate a presence of a second component. It is to be noted here that earlier studies of rotational anisotropy with different solute molecules in TBA-water mixtures have reported single exponential decay of  $r(t)$  with time at all TBA mole fractions<sup>10-11</sup>. However, it was argued later by Maroncelli and coworkers<sup>54</sup> that bi-exponential decay of  $r(t)$  is rather generic in nature and is dictated by the time dependence of the microscopic friction governing the rotational diffusion in solution. More precisely, the non-exponential nature of the microscopic friction experienced by the rotating solute renders the multi-exponential decay of the time resolved fluorescence anisotropy of C153 in these solutions<sup>54</sup>. Fig.6.8 depicts the alcohol mole fraction dependence of the fit parameters required to describe adequately the time resolved fluorescence anisotropies ( $r(t)$ ) obtained for C153 in ethanol-water and TBA-water solutions. While the time constants are shown in the left panels of this figure, the right panels describe the alcohol concentration dependence of the amplitudes associated with the  $r(t)$  decays. It is interesting to note in this figure that the long time constant ( $\tau_{long}$ ) and the amplitude associated with it ( $a_{long}$ ) increase initially and then saturate. The initial increase is particularly very sharp for TBA-water mixtures. The short time constant ( $\tau_{short}$ ) and the corresponding amplitude ( $a_{short}$ ), on the other hand, decrease upon increasing the alcohol mole fraction in the mixtures. The large difference between  $\tau_{short}$  and  $\tau_{long}$  may lead one to think that the bi-exponential decay of  $r(t)$  is originating from the rotational diffusion of C153 trapped in two different solvation environments – one which is predominantly enriched with alcohol molecules and the other with water molecules. Support for such a two state model for the solution structure of alcohol-water mixtures has also been provided earlier by light scattering studies<sup>17</sup>. As the tetrahedral network structure of water is strengthened upon addition of small quantity of alcohol in the water-rich region, the solution structure becomes more compact.

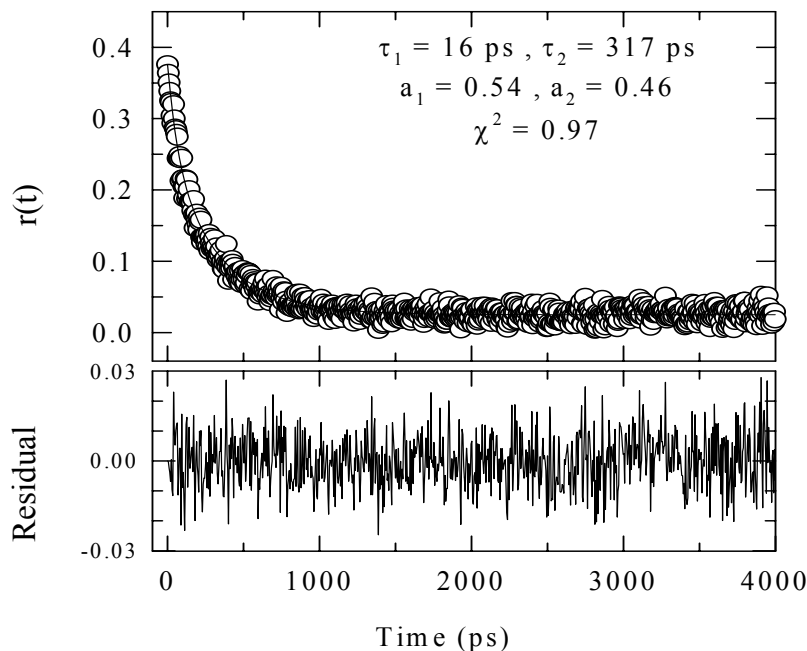


**Fig. 6.7:** Representative emission anisotropy decay (*upper panel*) of C153 in TBA-water mixture at 0.8 TBA mole fraction. While open circles represent the data, the solid line shows the fit through the data. Parameters obtained from bi-exponential fit to the data are also listed in the upper panel. The quoted  $\chi^2$  is actually the reduced  $\chi^2$ . Residuals (weighted) are shown in the *bottom panel*. Note that the fast time constant ( $\sim 15$  ps) is one-fifth of the FWHM of the IRF employed in our experiments and hence is at the detection limit. The standard error of estimate for the shorter time scale ( $\tau_{\text{short}}$ ) is about 30% of the quoted value at each alcohol mole fraction (due to limited time resolution) and the same for the long time scale ( $\tau_{\text{long}}$ ) is about 10% (of the quoted value). The standard error of estimate for the amplitudes, however, is approximately 5% (of the quoted value) at each alcohol mole fraction. Note here that the definitions for the standard error as well as those for reduced  $\chi^2$  and weighted residual are used as those described in the following reference: Bevington P R *Data Reduction and Error Analysis for the Physical Sciences*, McGraw-Hill: New York, 1969.

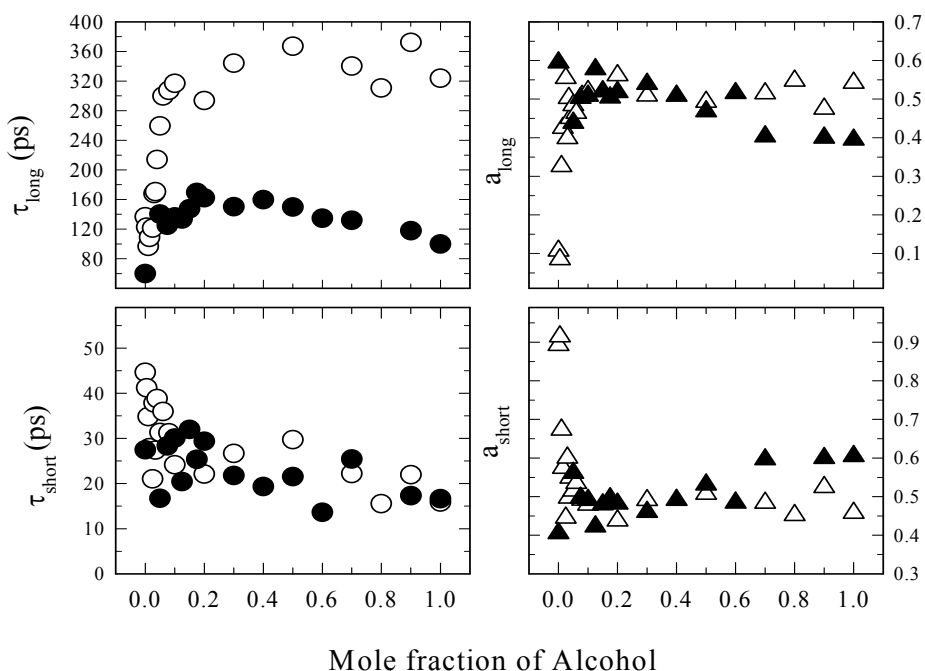


**Fig.6.8:** Alcohol mole fraction dependence of fit parameters required to adequately describe the experimental time resolved fluorescence anisotropy of C153 in TBA-water (open symbol) and ethanol-water (filled symbol) mixtures. Note that the time constants are shown in the *left panels* and the amplitudes in the *right panels*. The faster time constants obtained from the bi-exponential fits are represented by  $\tau_{\text{short}}$  and the slower ones by  $\tau_{\text{long}}$ . The corresponding amplitudes are represented respectively by  $a_{\text{short}}$  and  $a_{\text{long}}$ . The ‘goodness of fit parameter’ (reduced  $\chi^2$ ) for all these fits varies between 0.97 – 1.03. The standard errors of estimate are already described in Fig.6.7

The increased compactness of solution structure in the water rich region is also reflected in the lowering of isothermal compressibility<sup>37</sup> in the corresponding alcohol concentration range. The increase in structural compactness with alcohol concentration therefore leads to further slowing down of the long time constant with

concomitant increase in the amplitude of this component. Further addition of alcohol induces a transition in the solution structure from the tetrahedral network to zigzag chain-like molecular contacts giving rise to relatively more microscopically 'homogeneous' environment. This 'homogeneity' in the environment leads to the saturation of both the long time component and its amplitude at higher alcohol mole fraction. Now the next question: why the short time constant ( $\tau_{short}$ ) becomes smaller as the alcohol concentration is increased in the low mole fraction regime of alcohol in the mixture? This can be explained if we look at the mode coupling theory (MCT) analyses of density dependent microscopic friction on a translating solute in liquids<sup>62</sup>. According to the MCT, the enhanced solute-solvent collision frequency due to stronger structure at higher density leads to faster decay of time dependent friction on the solute<sup>62</sup>.

As the same structural features also enhance the viscosity of the medium due to stronger spatial correlations, the viscosity driven long-time decay of the microscopic friction becomes slower at later times<sup>62</sup>. Therefore, the structural enhancement makes the fast component faster and the slow component slower. This is probably the reason why the short time constant ( $\tau_{short}$ ) in the bi-exponential decay of  $r(t)$  for C153 in alcohol-water mixtures becomes smaller with alcohol mole fraction at very low alcohol concentration. The long time constant ( $\tau_{long}$ ) for ethanol-water mixture, however, shows a moderate decrease with increase in alcohol concentration at ethanol mole fraction  $>0.20$ . Since ethanol and water are nearly isoviscous solvents, the loss of water structure at higher ethanol concentration dominates the long time decay constant and  $\tau_{long}$  shows a decrease in this ethanol mole fraction range. For TBA-water mixture, on the other hand, the effects of viscosity rather than water structure controls the dynamics as the viscosity of TBA is approximately 5 times larger than that of water<sup>10-11</sup>. As a result,  $\tau_{long}$  in presence of TBA nearly saturates at higher alcohol mole fraction, whereas in presence of ethanol it shows a decrease with increasing ethanol mole fraction.

Fig.6.9 depicts the alcohol mole fraction dependence of average rotational correlation time,  $\langle \tau_{rot} \rangle$  for C153 in ethanol-water and TBA-water mixtures. Note that these times ( $\langle \tau_{rot} \rangle$ ) have been obtained from the fit parameters described in Fig.6.8.

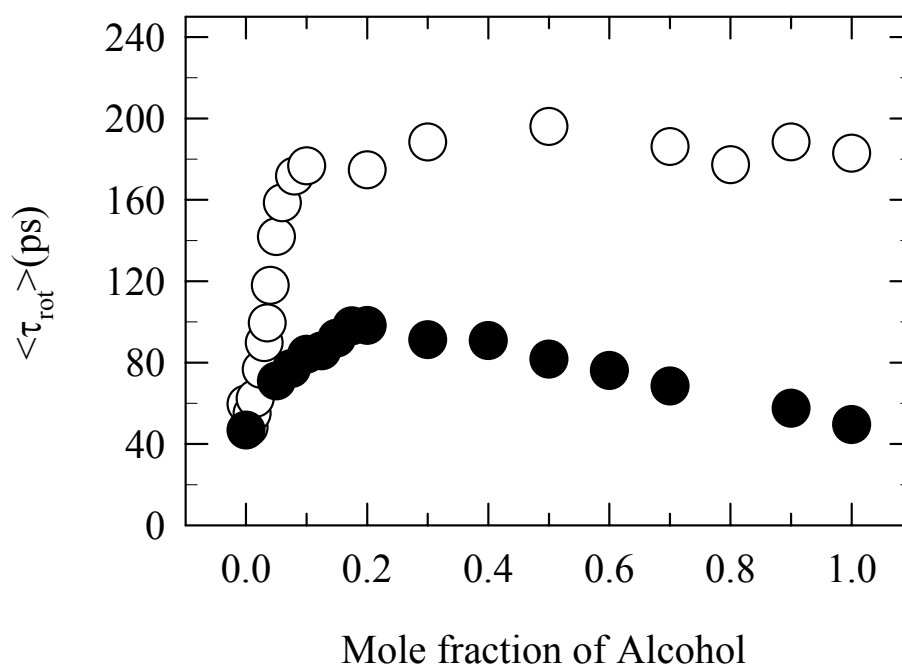


**Fig.6.9:** Alcohol mole fraction dependence of average rotational time ( $\langle \tau_{rot} \rangle$ ) for C153 in TBA-water and ethanol-water mixtures. While the open circles represent the data for TBA-water mixtures, filled circles denote those for ethanol-water mixtures.

The value of the  $\langle \tau_{rot} \rangle$  for C153 in pure ethanol shown in this figure (Fig.6.9) compares well with the literature value<sup>54</sup>. The most interesting aspect of this figure is the difference in slope of  $\langle \tau_{rot} \rangle$  with alcohol mole fraction for ethanol-water and

TBA-water mixtures. The stronger hydrophobic effect of TBA due to its bulkier tertiary butyl group is responsible for the increased orientational ordering (structure formation) of the water molecules leading to a sharp increase in the  $\langle \tau_{rot} \rangle$  for C153 in TBA-water mixture at very dilute TBA concentration. The sharp slope then transforms to an almost flat line at higher TBA concentration and this transformation occurs at a TBA mole fraction  $\sim 0.10$ . The slope for ethanol-water mixtures at low ethanol concentration is not as sharp because of less structure forming ability of ethanol molecules. Nevertheless, a change in slope with alcohol mole fraction is also visible here which occurs at ethanol mole fraction  $\sim 0.2$ . These values of alcohol mole fraction at which the slope changes, corroborate well with the literature values where structural transition is believed to occur in these alcohol-water mixtures.

#### **6.4. Conclusion**

Let us first summarize the main results of this chapter. While the absorption spectrum of P4C shows red shift with alcohol concentration in the TBA mole fraction regime 0.0 – 0.10 and then blue shifts with further addition of TBA in the aqueous solution, the emission spectrum exhibits continuous blue shift in the entire range of alcohol concentration. The non-ideality in solution polarity with alcohol mole fraction seems to be the main guiding factor for the emission shifts, whereas the absorption characteristics pick up also the effects of structural enhancement at very low TBA concentration. The relatively faster lifetime of the TBA clusters probably contributes to the ‘homogenization’ of the otherwise microscopically heterogeneous solution structure and hence the steady state fluorescence emission does not show any characteristics of the solution inhomogeneity. The spectral broadening and shifts for P4C with TBA mole fraction is found to be different from those in neat solvents and also in electrolyte solutions. The full width at half maximum (FWHM) of absorption spectrum is found to narrow with red shift in the range 0.0 – 0.10 mole fraction of TBA which is opposite in direction to that found in systems where simply the average polarity is changed<sup>50, 52, 56</sup>. The CT emission band also shows spectral broadening with blue shift in the same range (0.0 - 0.10) of TBA mole fraction which is contrary to the expectation based on earlier observations<sup>50, 52,</sup>

<sup>56</sup>. At TBA mole fraction higher than 0.10, the narrowing and shifts of the absorption and CT emission bands correlate well with the earlier results<sup>49-50</sup>. The LE emission band, however, narrows as it shifts towards higher energy upon addition of TBA and shows a non-ideal alcohol concentration dependence. The opposite alcohol mole fraction dependence of the LE and CT emission bandwidths in the very dilute aqueous solutions of TBA is mainly responsible for the sharp rise in the CT/LE area ratio at TBA mole fraction  $\sim 0.04$ .

Non-ideal alcohol mole fraction dependence is also found for quantum yield and transition moments for LE and CT emission bands. While the radiative rate associated with the LE emission band shows a small increase with TBA concentration in the very dilute solution, the CT radiative rate exhibits non-ideal TBA mole fraction dependence. The absorption transition moment is also found to show a small increase in the TBA mole fraction range 0.0 – 0.10. It would be worth noting that the non-monotonic dependence of quantum yield on solvent polarity has been observed earlier<sup>63</sup> with N,N-dimethylaminobenzonitrile (DMABN) molecule in binary mixtures of n-octane and propionitrile. The observed non-monotonic dependence of TICT emission on propionitrile concentration has been explained in terms of a competition between the formation of the TICT state and the decay through nonradiative pathways. Such an analysis might be attempted to learn more about the competing processes for this ring compound and its analogues in alcohol-water binary mixtures.

The time dependent decay of the emission intensity is found to be bi-exponential for all TBA mole fractions even though microscopic heterogeneity is one of the characteristics of water-TBA solutions. This demonstrates that the decay kinetics of P4C in water-TBA mixtures also conform to the two state model as envisaged earlier<sup>49, 52</sup>. The time constant associated with the slower component of the bi-exponential decay shows the effects of TBA-induced structural enhancement at very dilute solutions of TBA. However, at higher alcohol concentration  $\tau_{slow}$  shows the expected non-ideal TBA mole fraction dependence.

Structural effects have been found to play a significant role in determining the mole fraction dependence of the time constants as well as the amplitudes associated with the decay components of the time resolved fluorescence anisotropy in these binary mixtures. The sharp increase in the average rotational correlation time with alcohol concentration in the very dilute solution is explained in terms of structural modifications due to hydrophobic effects of alkyl groups attached to these alcohols. The novel interplay between solution structure and viscosity critically determines the effects of structural transition on the rotational motion of C153 in these alcohol-water mixtures. Since slow solvation dynamics due to preferential solvation in these binary mixtures is likely to play an important role in determining the rate of TICT reaction, study of solvation dynamics in these media is required in order to explore the dynamic solvent control of the reaction rates<sup>50, 64-76</sup>. Therefore, further studies with different TICT molecules using a better time resolution are required where effects on the TICT reaction of the novel interplay between the hydrophobic and H-bonding interactions governing the structure and dynamics in binary mixtures can be better understood.

## References

1. Franks, F.; Ives D J G *Q. Rev. Chem. Soc.* **1966**, *20*, 1.
2. Zeidler, M. D. **1973** In *Water, a Comprehensive Treatise*, edited by Franks, F., (Plenum, New York, 1973), *2*, 529.
3. Arnett, E. M.; McKlevey, D. R, *J. Am. Chem. Soc.* **1966**, *88*, 5031.
4. Arnett, E. M.; McKlevey, D. R, *J. Am. Chem. Soc.* **1965**, *87*, 1393.
5. Arnett, E.M; Bentrude, W. G.; Burke J. J.; Duggleby, P. M. *J. Am. Chem. Soc.* **1965**, *87*, 1541.
6. Beddard, G. S.; Doust, T.; Hudales, J, *Nature* **1981**, *294*, 145.
7. Dixit, S.; Crain, J.; Poon, W. C. K; Finney, J. L.; Soper, A. K.; *Nature* **2002**, *416*, 829.
8. Soper, A. K.; Finney, J. L.; *Phys. Rev. Lett.* **1993**, *71*, 4346.
9. Brai, M.; Kaatze, U. *J. Phys. Chem.* **1992**, *90*, 8946.
10. Dutt, G. B.; Doraiswamy, S. *J. Chem. Phys.* **1992**, *96*, 2475.
11. Dutt, G. B.; Doraiswamy, S.; Periasamy, N.; *J. Chem. Phys.* **1991**, *94*, 2475.
12. Murthy, S. S. N. *J. Phys. Chem. A* **1999**, *103*, 7927.
13. Wojkow, D.; Czarnecki, M. A.; *J. Phys. Chem. A* **2005**, *109*, 8218.
14. D'Angelo, M.; Onori, G.; Santucci, A. *J. Chem. Phys.* **1994**, *100*, 3107.
15. Egashira, K.; Nishi, N. *J. Phys. Chem. B* **1998**, *102*, 4054.
16. Nishikawa, K.; Iijima, T. *J. Phys. Chem.* **1993**, *97*, 10824.
17. Yoshida, K.; Yamaguchi, T.; *Z. Naturforsch. A* **2001**, *56*, 529.
18. Nishikawa, K.; Kodera, Y.; Iijima, T. *J. Phys. Chem.* **1987**, *91*, 3694.
19. Koga, Y. *Chem. Phys. Lett.* **1984**, *111*, 176.
20. Sato, T.; Buchner, R. *J. Chem. Phys.* **2003**, *119*, 10789.
21. Nakanishi, K.; Ikari, K.; Okazaki, S.; Touhara, H. *J. Chem. Phys.* **1984**, *80*, 1656.
22. Kusalik, P. G.; Lyubertsev, A. P.; Bergman, D. L.; Laaksonen, A. *J. Phys. Chem. B* **2000**, *104*, 9533.
23. Laaksonen, A.; Kusalik, P. G.; Svishchev, I. M. *J. Phys. Chem. A* **1997**, *101*, 5910.

24. Yoshida, K.; Yamaguchi, T.; Kovalenko, A.; Hirata, F. *J. Phys. Chem. B* **2002**, *106*, 5042.
25. Perera, A.; Sokolic, F.; Almasy, L.; Koga, Y. *J. Chem. Phys.* **2006**, *124*, 124515.
26. Ben-Naim, A. *J. Chem. Phys.* **1977**, *67*, 4884.
27. Bowron, D. T.; Finney, J. L. *J. Phys. Chem. B* **2007**, *111*, 9838.
28. Lisa, L.; Loon, V.; Minor, R. N.; Allen, H. C. *J. Phys. Chem. A* **2007**, *111*, 7346.
29. Hu, K.; Zhou, Y.; Shen, J.; Ji, Z.; Cheng, G. *J. Phys. Chem. B* **2007**, *111*, 10160.
30. Templeton, E. F. G.; Kenney-Wallace, G. A. *J. Phys. Chem.* **1986**, *90*, 5441.
31. Iwasaki, K.; Fujiyama, T. *J. Phys. Chem.* **1977**, *81*, 1908.
32. Iwasaki, K.; Fujiyama, T. *J. Phys. Chem.* **1979**, *83*, 463.
33. Euliss, G. W.; Sorensen, C. M. *J. Chem. Phys.* **1984**, *80*, 4767.
34. Kaatze, U.; Pottel, R.; Schmidt, P. *J. Phys. Chem.* **1988**, *92*, 3669; **1989**, *93*, 5623.
35. Kaatze, U.; Menzel, K.; Pottel, R. *J. Phys. Chem.* **1991**, *95*, 324.
36. Svishchev, I. M.; Kusalik, P. G. *J. Chem. Phys.* **1993**, *99*, 3049.
37. Omelyan, I.; Kovalenko, A.; Hirata, F. *J. Theo. Comput. Chem.* **2003**, *2*, 193.
38. Yamaguchi, T. *Pure Appl. Chem.* **1999**, *71*, 1741 and references therein.
39. Cinelli, S.; Onori, G.; Santucci, A. *Colloids Surf. A.* **1999**, *160*, 3 and references therein.
40. Bowron, D. T.; Finney, J. L.; Soper, A. K. *J. Phys. Chem. B.*, **1998**, *102*, 3551.
41. Bowron, D. T.; Moreno, S. D. *J. Chem. Phys.* **2002**, *117*, 3753.
42. Yoshida, K.; Yamaguchi, T. *Z. Naturforsch. A* 2001, *56*, 529.
43. Wojtkow, D.; Czarnecki, M. *J. Phys. Chem. A.* **2005**, *109*, 8218.
44. Bowron, D. T.; Moreno, S. D. *J. Phys. Chem. B* **2005**, *109*, 16210
45. Wang, Y.; Eissenthal, K. B. *J. Chem. Phys.* **1982**, *77*, 6076.

46. Kohler, G.; Rechthaler, K.; Rotkiewicz, K.; Rettig, W. *Chem. Phys.* **1996**, *207*, 85.
47. Meech, S. R.; Phillips, *Chem. Phys. Lett.* **1985**, *116*, 262.
48. Weisenborn, P. C. M.; Varma, C. A. G. O.; De Haas, M. P.; Warman, J. M. *Chem. Phys. Lett.* **1986**, *129*, 562.
49. Pradhan, T.; Biswas, R. *J. Phys. Chem.* **2007**, *111*, 11524.
50. Horng, M. L.; Gardecki, J. A.; Papazyan, A.; Maroncelli, M. *J. Phys. Chem. B* **1995**, *99*, 17311.
51. Reynolds, L.; Gardecki, J.; Frankland, S. J.; Horng, M. L.; Maroncelli, M. *J. Phys. Chem.* **1996**, *100*, 10337.
52. Dahl, K.; Biswas, R.; Ito, N.; Maroncelli, M. *J. Phys. Chem. B.* **2005**, *109*, 1563
53. Lewis, J. E.; Maroncelli, M. *Chem. Phys. Lett.* **1998**, *282*, 197.
54. Horng, M. L.; Gardecki, J. A.; Maroncelli, M. *J. Phys. Chem. A.* **1997**, *101*, 1030.
55. Cichos, F.; Willert, A.; Rempel, U.; von Borczyskowski, C. *J. Phys. Chem. A* **1997**, *101*, 8179.
56. Pradhan, T.; Biswas, R. *J. Phys. Chem.* **2007**, *111*, 11514
57. Arzhantsev, S.; Jin, H.; Ito, N.; Maroncelli, M. *Chem. Phys. Lett.* **2005**, *417*, 524.
58. Bevington, P. R. *Data Reduction and Error Analysis for the Physical Sciences*; McGraw-Hill: New York, 1969.
59. Hicks, J.; Vandersall, M.; Babarogic, Z.; Eienthal, K. B.; *Chem. Phys. Lett.* **1985**, *116*, 18.
60. Hicks, J. M.; Vandersall, M. T.; Sitzmann, E. V.; Eienthal, K. B.; *Chem. Phys. Lett.* **1987**, *135*, 413.
61. Pradhan, T.; Ghoshal, P.; Biswas, R. *J. Chem. Sci* **2008**, *120*, 275
62. Bagchi, B.; Bhattacharyya, S. *Adv. Chem. Phys.* **2001**, *116*, 67.
63. Nag, A.; Kundu, T.; Bhattacharyya, K. *Chem. Phys. Lett.* **1989**, *160*, 257.
64. Chandra, A.; Bagchi, B.; *J. Chem. Phys.* **1991**, *94*, 8367.

65. Luther, B.M.; Kimmel, J. R.; Levinger, N. E. *J. Chem. Phys.* **2002**, *116*, 3370.
66. Chandra, A. *Chem. Phys. Lett.* **1995**, *235*, 133.
67. Jarzeba, W.; Walker, G. C.; Johnson, A. E.; Barbara, P. F. *Chem. Phys.* **1991**, *152*, 57.
68. Gardecki, J. A.; Maroncelli, M. *Chem. Phys. Lett.* **1999**, *301*, 571.
69. Ladanyi, B. M.; Skaf, M. S. *J. Phys. Chem. A* **1996**, *100*, 18258.
70. Laria, D.; Skaf, M. S. *J. Chem. Phys.* **1999**, *111*, 300.
71. Day, T. J. F.; Patey, G. N. *J. Chem. Phys.* **1997**, *106*, 2782.
72. Day, T. J. F.; Patey, G. N. *J. Chem. Phys.* **1999**, *110*, 10937.
73. Yoshimori, A.; Day, T. J. F.; Patey, G. N. *J. Chem. Phys.* **1998**, *108*, 6378.
74. Yoshimori, A.; Day, T. J. F.; Patey, G. N. *J. Chem. Phys.* **1998**, *109*, 3222.
75. Mukherjee, S.; Sahu, K.; Roy, D.; Mondal, S. K.; Bhattacharyya, K. *Chem. Phys. Lett.* **2004**, *384*, 128.
76. Molotsky, T.; Huppert, D. *J. Phys. Chem. A* **2004**, *107*, 8449.

## Chapter 7

### Intramolecular Charge Transfer Reaction in Aqueous Reverse Micelles: Effects of Confined Environment

#### 7. 1. Introduction

Inverted or reverse micelles made of surfactant (charged or neutral), oil and a polar solvent (not any polar solvent) are clear, homogeneous and thermodynamically stable solutions.<sup>1-41</sup> In such multi-component mixtures, polar solvent molecules are trapped in a confinement created by the self-aggregation of the surfactant head groups, while the alkyl chain ('tail') of the surfactant molecules remain immersed in the bulk non-polar solvent (oil). Interestingly, surfactants with neutral or charged head groups<sup>35</sup> or even a mixture of surfactants with suitable combinations of polar and non-polar solvents in presence of a co-surfactant<sup>42</sup> have also been found to form reverse micelles. The anionic surfactant sodium bis(2-ethylhexyl)-sulfosuccinate (AOT) forms reverse micelles in presence of water and a nonpolar solvent (usually isooctane or heptane). In dilute aqueous solutions of AOT, the reverse micelle droplets are known to be spherical and the radius of the trapped water pool are given by  $r(^0A) \approx 2w_0$ , where  $w_0$  denotes the ratio between the molar concentration of water and the surfactant.<sup>5, 35</sup> As already mentioned in the Introduction, water in tiny volume plays a crucial role as a medium that controls the function and dynamics near biological membranes and active bio-molecular surfaces, reverse micelles typify biological model of a living cell. They are also promising candidates for synthesis of nanoparticles, drug transportation to a specified position and the subsequent delivery.

Confinement is known to severely affect the structure and dynamics of water molecules.<sup>1-43</sup> Experimental<sup>1-3</sup> and computer simulation<sup>27-29</sup> studies have revealed that the long time component of polar solvation energy relaxation is ~1000 times slower than that observed in the bulk water and also shows a pool size dependence.

Vibrational echo studies of water in nano-sized droplets have indicated the presence of a significant ultrafast component with a time constant of 30 – 50 fs in the decay of the frequency auto-correlation function.<sup>26</sup> Similar ultrafast decay has been either observed or estimated in solvent pools of quaternary microemulsions,<sup>9</sup> lecithin vesicles<sup>16</sup> and cationic reverse micelles.<sup>42</sup> Recently, photoinduced intramolecular charge transfer (ICT) reaction has been studied in aqueous and several non-aqueous AOT/heptane reverse micelles where the importance of the reverse micelle interface to control a ICT process are stressed.<sup>40-41</sup> However, no attempt, even at the semi-quantitative level, has been made so far to correlate the rate and yield of a reaction that possesses an activation barrier occurring in these ‘nano-reactors’ with the average polarity and dynamics of the confined pool. In this chapter we report such a study where photo induced intramolecular charge transfer reaction has been investigated in aqueous AOT/heptane reverse micelles at different pool sizes. As the polarity of a reaction medium plays a very important role in determining both the yield and the rate of a TICT reaction,<sup>43-45</sup> we have made a continuum model estimate of the average polarity (in terms of static dielectric constant,  $\epsilon_0$ ) of the nano-confinements in these microemulsions by following the steady state fluorescence emission of a non-reactive solvation probe.<sup>46</sup>

The molecule that we have used for studying the intramolecular charge transfer reaction is 4-(1-morpholenyl) benzonitrile and is designated as M6C in the SCHEME 2 (chapter1). The structural similarity between the M6C and 4-(1-piperidinyl)benzonitrile (P6C) molecules<sup>43-45</sup> have led us to assume that the photo-induced charge transfer reaction in M6C in polar media also occurs simultaneously with the twisting of the morpholenyl group around the central bond joining the benzonitril moiety. Therefore, the photo-induced charge transfer reaction in M6C may be termed as twisted intramolecular charge transfer (TICT) reaction. As shown in the SCHEME 3 (chapter 1), photo-excitation promotes M6C to the locally excited (LE) state in the first excited electronic surface ( $S_1$ ) which is relatively less polar and possesses charge distribution similar to that in the ground state. The photo-prepared LE state then either undergoes intramolecular charge transfer with the forward rate

constant  $k_f$  or comes back to the ground ( $S_0$ ) state with an average (radiative + non-radiative) rate constant ( $k_{LE}$ ). Likewise, the charge transferred (CT) state can go back to the LE state with a rate constant of  $k_r$  or populates the ground state via the radiative and non-radiative pathways with the average rate constant,  $k_{CT}$ . The activation barrier that separates the LE state from the more polar CT state is expected to be  $\sim 5k_B T$ ,<sup>45</sup> where  $k_B T$  denotes the Boltzmann constant times the absolute temperature. Since time scales in such low barrier reactions are typically in the picoseconds,<sup>47</sup> the slow solvent modes with a nanosecond time scale observed in these reverse micelles may occur even before the solvent reorganization is complete. In addition, the drastically reduced average dielectric constant of the nano-pool decreases the changes in reaction free energy ( $-\Delta G_r$ ) by substantially reducing the equilibrium constant ( $K_{eq}$ ) for the LE  $\rightarrow$  CT conversion reaction. Since interactions with the surfactant head groups render the nano-environment more rigid than the bulk polar solvent,<sup>2-3</sup> the twisting mode involved in the LE  $\rightarrow$  CT conversion reaction is also expected to experience more retardation. This, in turn, would reduce the rate of such a reaction. The reduction in dielectric constant, on the other hand, reduces the dielectric contribution to the total friction and hence assists the twisting. All these factors, therefore, lead to complicated environment effects on TICT reaction rate in reverse micelles.

The present chapter reports the following results. Quantum yield and radiative rate are found to decrease with the pool size, whereas the changes in reaction free energy and the non-radiative rate increase with the size of the reverse micelles. As expected, the formation of the CT state increases with pool size and the peak frequency of the CT emission band shifts towards lower energy. The time-resolved emission decays of M6C have been analyzed by using the kinetic framework employed earlier for studying the TICT reaction of several substituted benzonitril derivatives in normal solvents,<sup>45</sup> liquid mixtures<sup>48-50</sup> and electrolyte solutions.<sup>51-52</sup> Note that the emission decay of M6C in heptane at several wavelengths across the emission band has been found to be single exponential with only one time constant

of approximately 2 ns, which is very similar to the decay characteristic of a closely related compound P6C in several non-polar solvents.<sup>45</sup> For all pool sizes, the emission decay of M6C collected near the LE peak wavelength is found to be bi-exponential function of time with a shorter and a longer decay time constants. At a few pool sizes for which the CT emission decay could be collected,<sup>53</sup> the decay is characterized by a rise component (negative amplitude) associated with a shorter time constant (of the two time constants) and a longer decay time constant. Also, the time constant associated with fast component of the LE decay is found to be very similar with the rise time constant of the CT decay. As before, the shorter time constant is identified with the reaction time for the LE  $\rightarrow$  CT conversion reaction in M6C which decreases by a factor of 2 as the pool size swells up by a factor of 33. Most importantly, the reaction time in these confinements is in the range of 200 – 400 ps, which is 10 - 20 times slower than that for M6C in the moderately polar ( $\epsilon_0 \sim 10$ ) bulk solvents. The estimated dielectric constant at the largest aqueous pool size ( $w_0 \approx 37$ ) is found to be  $\sim 4$  times less than that of the bulk water. The dielectric relaxation measurements in these microemulsions at 0.5 M AOT indicate the presence of a Cole-Davidson type relaxation process with time constants in the range of 500 – 800 ps. This orientation relaxation time scale is therefore well-correlated with the slow reaction time scales (200 – 400 ps) found in the AOT/heptane/water reverse micelles.

The organization of the rest of the chapter is as follows. Experimental details are discussed in section 7.2, followed by results and discussion in section 7.3. Concluding remarks are given in section 7.4.

## 7.2. Experimental

4-(1-morpholenyl) benzonitrile (M6C) was synthesized by following the protocol given in the literature.<sup>54-55</sup> Approximately 1.5 g (12 mmol) 4-fluorobenzonitrile (Alfa Aesar, 99%) and the triple molar quantity of morpholine ( 4g, 46 mmol) (LOBA CHEMIE, India) were dissolved in 25 ml dimethyl sulfoxide (Aldrich) and stirred in

refluxed condition for 24 h at 365 K. The mixture was then cooled and poured into 500 ml water (Millipore) and the separated product by filtration was dried and recrystallized 3 times from cyclohexane (Merck, Germany). Purity of the compound was checked by thin layer chromatography and monitoring the excitation wavelength dependence of fluorescence emission in several bulk polar and non-polar solvents.

Bis-(2-ethylhexyl) sodium sulfosuccinate (AOT) ( $\geq 98\%$ , Fluka, Switzerland, purum and Sigma,  $\geq 99\%$ ) was used after vacuum drying for 24 h. Spectroscopic grade n-heptane (Merck,  $\geq 99.5\%$ ) were used after drying over molecular sieves and filtration. Solutions were made by dissolving a measured amount of solid AOT in n-heptane (heptane hereafter) by volumetric method. Subsequently, de-ionized water (Millipore) was added to the solution to obtain appropriate  $w_0$ , where  $w_0$  denotes the ratio of molar concentration of water to AOT. The concentration of AOT in all reverse micelles was maintained at 0.1 M. The mixtures were then gently stirred to obtain transparent, homogeneous and thermodynamically stable solutions.

The methods for sample preparation and spectroscopic data collection remain the same as described in previous chapters. The error associated with the spectral peak frequency determination is typically  $\pm 250 \text{ cm}^{-1}$  and that with the band area is  $\sim 10\%$  (of the reported value). Life time data for measuring radiative and non-radiative rates and time-resolved fluorescence emission intensity decay data for M6C in microemulsions were collected by using a time-correlated single photon counting apparatus (Lifespec, Edinburgh Instruments) with excitation wavelengths at 299 nm and an emission band pass of 8nm. The full width at half maximum of the instrument response function (IRF) was  $\sim 475 \text{ ps}$ . The decays were found to fit globally to a bi-exponential function of time with a short and a long time constants.<sup>56</sup>

### 7.3. Results & Discussion

#### 7.3.1. Estimation of the Average $\varepsilon_0$ of the Confined Pool in Aqueous Reverse Micelles

The following empirical relation is used to estimate the average  $\varepsilon_0$  of the solvent pools from the emission peak frequency ( $\nu_{em}$ ) of C153 dissolved in these microemulsions,<sup>57</sup>

$$\nu_{em} (10^3 \text{ cm}^{-1}) = 23.12 - 5.06[(\varepsilon_0 - 1)/(\varepsilon_0 + 2)] - 1.5 \left[ (n^2 - 1)/(n^2 + 2) \right], \quad (7.1)$$

where  $n$  denotes the refractive index of the solvent. Note that the above empirical relation and similar ones (for anthracene and its substituted derivatives) have been found earlier<sup>58-59</sup> to be successful in semi-quantitative estimation of the local density around an attractive solute in supercritical fluids. Here we assume the refractive index of the trapped pool as that of bulk water. A simple numerical inversion of the above relation with a given value of  $\nu_{em}$  then provides an estimate of the average  $\varepsilon_0$ . Note that for these microemulsions, the estimated value of  $\varepsilon_0$  corresponding to a value of  $\nu_{em}$  is *not* a unique one as the latter (emission peak frequency) shows excitation wavelength dependence in these microscopically heterogeneous systems.<sup>1-3,35</sup> Nevertheless, this approach provides a qualitative understanding of the confinement effects on the medium polarity and could be useful for assessing the pool size dependent environment effects on a chemical reaction.

The values of  $\varepsilon_0$  estimated by using Eq.7.1 are shown as a function of pool size ( $w_0$ ) in Fig. 7.1. Representative emission spectra of C153 in AOT/water reverse micelles at several pool sizes are provided in the Appendix 2 (Fig. A13).

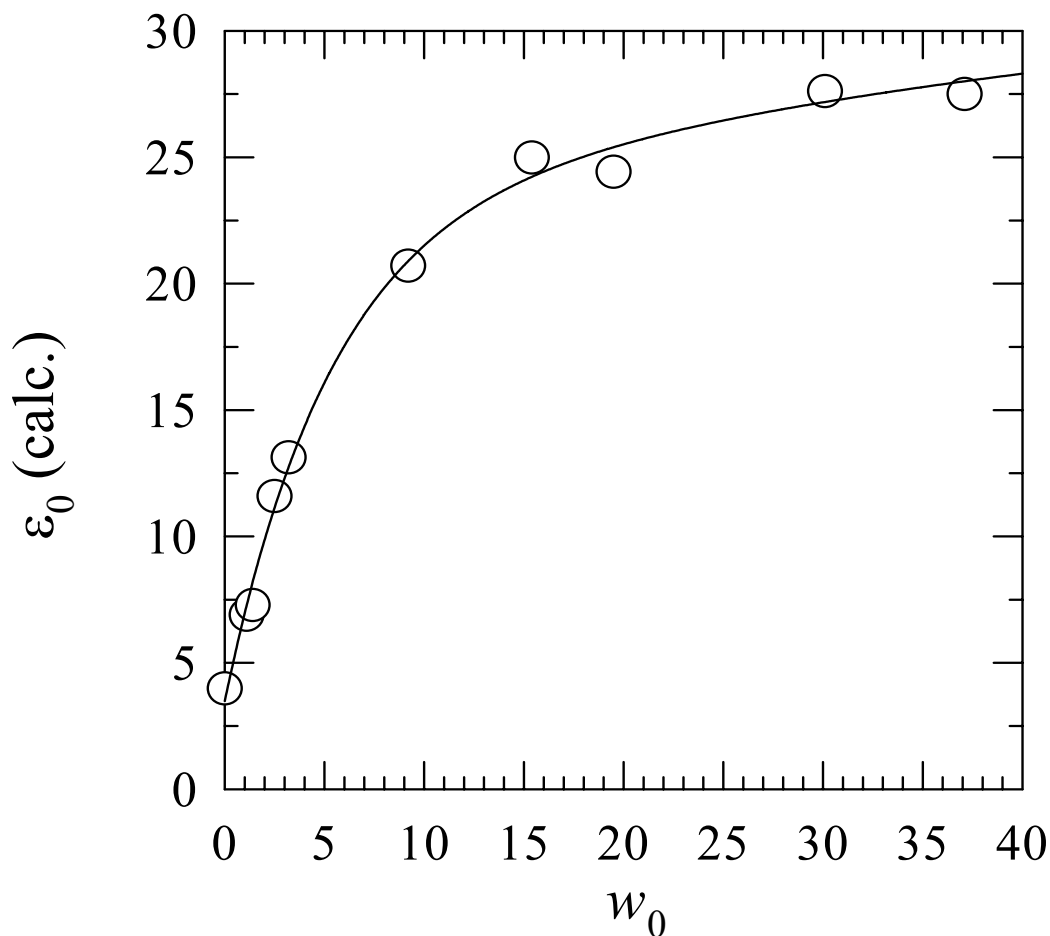


**Fig. 7.1:** Estimated values of static dielectric constant ( $\epsilon_0$ ) at different pool sizes ( $w_0$ ) as reported by the peak frequencies of the emission spectra of a non-reactive solvation probe in AOT/water/heptane reverse micelles. The pool size is controlled by varying the water concentration at a particular surfactant concentration (here AOT) in the microemulsion. That is,  $w_0 = [\text{water}]/[\text{AOT}]$ .

It is evident from Fig. 7.1 that the bulk dielectric constant of water decreases drastically upon confinement, which has also been predicted by a recent simulation study.<sup>60</sup> Also note that the dielectric constant of the confined pool increases as the size of the pool grows upon addition of water. At  $w_0 \approx 37$ , the dielectric constant is almost one-third of that of bulk water. The drastic reduction of the dielectric constant upon confinement may be connected to the substantial slowing down of the polar solvation dynamics in AOT/water reverse micelles<sup>1-3, 6-10</sup> as follows. The curvature

of the potential energy surface in which the polar solvation energy relaxes is determined by the longitudinal component of the wavevector ( $k$ ) dependent static dielectric constant  $\varepsilon_L(k)$  at its long wavelength limit.<sup>61-62</sup> As  $\varepsilon_0$  decreases, the curvature becomes flatter and consequently the relaxation becomes slower. Therefore, the solvent dynamics in response to a photo-excited probe becomes slower in AOT/water reverse micelles on, *at least*, two counts: they are the reduction of  $\varepsilon_0$  and the sluggish movements (both rotational and translational) of the solvent molecules due to the increase in microviscosity (or rigidity) upon confinement. Interestingly however, the dramatic slowing down of the long time component ( $\sim 1000$  times slower than in the bulk water) observed in the Stokes shift dynamics is absent in the vibrational echo decays and vibrational echo peak shift measurements.<sup>25-26</sup> Vibrational echo experiments report a pool-size dependent dynamics and, most importantly, reveal that the long time dynamics in the smallest pool is slowed down by a factor of 10 only, even though a large ultrafast component with a time constant of  $\sim 40$  fs is found to be present in the frequency-frequency correlation function (FFCF).<sup>26</sup> Simulation studies have interpreted the slow solvent dynamics in terms of electrostatic ion-solvent interactions<sup>27-28, 63</sup> although the echo experiments<sup>26</sup> assert that the geometric confinement rather than the ionic strength is responsible for the sluggish movement of the solvent particles inside the microemulsions. We therefore believe that the flattening of the surface curvature due to the drastic reduction of the average dielectric constant of water in concert with the slower solvent orientational relaxation render the dielectric response of the solvent to an excited solute probe  $\sim 1000$  times slower in confined environments than that in the bulk. Subsequently, the modified solvent dynamics contributes to the slowing down of a TICT reaction occurring inside the reverse micelles. Note the corresponding dielectric relaxation data reported in Ref.64 reveal that the time scale ( $\tau$  values) for  $w_0$  values ranging from 10 to 40 at AOT concentration 0.5 M is lying in the range of 600 – 800 ps. This time scale when inserted in a continuum model expression along with the values of  $\varepsilon_0$  and  $\varepsilon_\infty$ , produces longitudinal relaxation time scales for dipole solvation in the range of half-a-nanosecond.<sup>61-62</sup> This time scale is

strikingly similar to what has been observed in numerous solvation dynamics experiments in AOT/water/heptane reverse micelles.<sup>2-10</sup> In addition, the polarity estimated from the spectral shift has been found to be in good agreement with those from dielectric relaxation study (see, for detail, Ref. 64).

### **7.3.2. TICT Reactions in AOT/water/heptane Reverse Micelles: Steady State Fluorescence Study**

Representative absorption and emission spectra of M6C in reverse micelles at two different pool sizes and those in water and heptane are shown in Fig. 7.2. Relative to M6C in heptane, the broadening as well as red-shift in the absorption spectra in reverse micelles (upper panel, Fig. 7.2) clearly indicate that the solute (M6C) molecule is interacting with the polar environment inside these microemulsions. The absorption spectrum in water, however, shows the maximum broadening and largest shift due to larger solvent polarity ( $\epsilon_0 \approx 80$ ). The emission spectra shown in the lower panel (Fig. 7.2) indicate CT population increases as the pool size becomes larger. This is consistent with the data shown in Fig. 7.1 where estimated average polarity of the confined pool is found to increase with the pool size ( $w_0$ ). The emission spectra also seems to suggest that the LE $\rightarrow$ CT conversion reaction for M6C takes place almost irreversibly in water, whereas formation of CT is strongly disfavored in heptane. Also, there is a possibility that being soluble in heptane, M6C could also be partitioned into the heptane and micellar pseudophases and the two peaks in the emission profile might correspond to the emissions from these two different environments.<sup>35, 40</sup> However, the difference between these two peaks is  $\sim 8000 \text{ cm}^{-1}$  which is too large a shift for M6C to be caused by the polarity of the confined solvent pool. This is further supported by the emission spectra of M6C in bulk solvents with different values of  $\epsilon_0$  (Fig. A14, Appendix 2). Therefore, the emission spectra of M6C in reverse micelles shown in Fig. 7.2 are indeed representing emissions from the LE and CT states of the photo-excited molecule dissolved in the confined solvent pool. The pool size dependence of spectral peak

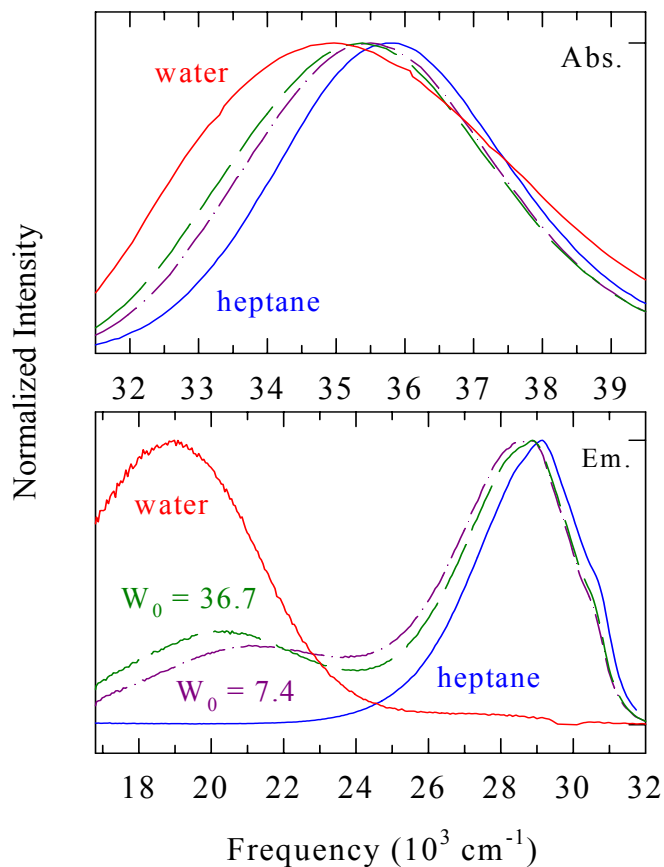


**Fig. 7.2:** Representative absorption (upper panel) and emission (lower panel) spectra of the TICT molecule M6C at two different values of  $w_0$  as well as those in heptane (blue) and water (red). The spectra at  $w_0 = 7.4$  are denoted by dashed-dot lines (pink) and those at  $w_0 = 36.7$  by dashed lines (dark green).

frequency and bandwidth of M6C is shown in Fig. 7.3 where the values at ‘zero’ water concentration are also shown (filled symbols). As expected, the absorption peak frequency (left-upper panel) shifts towards lower energy by  $\sim 200 \text{ cm}^{-1}$  as the pool size swells up by a factor of  $\sim 33$ . The absorption bandwidth (right-upper panel) also broadens by similar amount. Note that the red-shift in absorption spectrum with

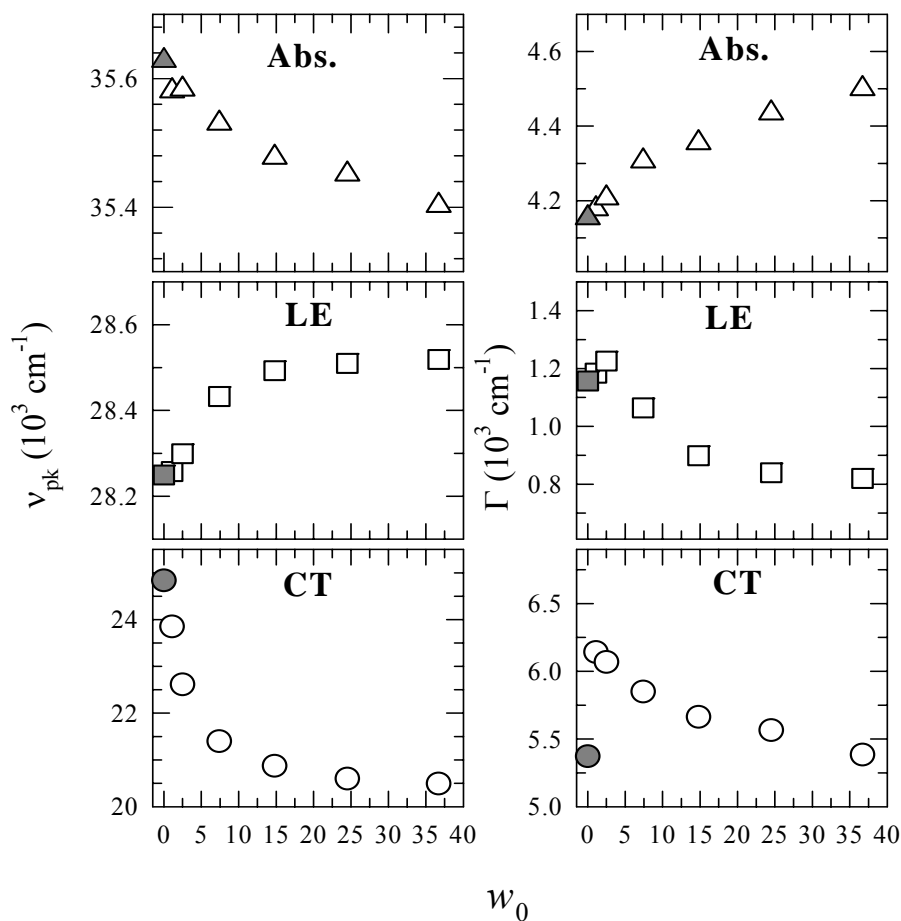


**Fig. 7.3:** Spectral peak frequencies ( $\nu_{pk}$ , left panels) and bandwidths ( $\Gamma$ , right panels) of M6C in AOT/water/heptane reverse micelles at different values of  $w_0$ . The filled symbols (grey) denote the values of these spectral quantities at  $w_0 \approx 0$ . Note that for the LE and CT emission bands, the widths ( $\Gamma$ ) represent the inhomogeneous widths.

concomitant broadening with solvent polarity has also been observed earlier for other ICT molecules and non-reactive probes in a number of different solution environments. The peak frequency for the LE emission band (left-middle panel) shows a blue-shift with the increase in  $w_0$ , which is counter-intuitive because the increase in average polarity with  $w_0$  is expected to shift the LE band towards lower energy.<sup>45-46</sup> Even though the total LE shift observed in the whole range of  $w_0$  is

merely  $250\text{ cm}^{-1}$ , the systematic nature of the variation may be real and we do not know the reasons for such a behavior. The pool size dependencies of the CT emission peak frequency and bandwidth are shown in the lower panels of Fig.7.3. Note here that the CT emission peak frequency at the first non-zero value of  $w_0$  (that is,  $w_0=1.1$ ) is about  $4500\text{ cm}^{-1}$  red-shifted from the LE peak frequency of M6C in heptane. This suggests that M6C is indeed interacting with the polar environment of the reverse micelles. Also, the CT band shows a red-shift of approximately  $4000\text{ cm}^{-1}$  for changing  $w_0$  from  $\sim 1$  to  $\sim 37$  and accompanies total narrowing of the bandwidth (inhomogeneous) of about  $750\text{ cm}^{-1}$ . The large amount of red-shift in the CT band indicates stronger solute-solvent polar interactions in the bigger solvent pools. The large value of the bandwidth at  $w_0 \approx 1$  indicates strong heterogeneity in the environment around the reactant molecule. The bandwidth, however, decreases with  $w_0$ , as the larger pool size leads to increased ‘homogenization’ of the environment. Note that the polarity dependence of the CT emission peak frequency and bandwidth for M6C in reverse micelles via  $w_0$  is also similar to those for a few TICT molecules in electrolyte solutions,<sup>51</sup> and non-reactive solvation probes in neat solvents.<sup>46</sup>

Next we turn our attention to the spectral properties observed in the microemulsions in the absence of any added water. More precisely, what does the values of peak frequencies (absorption and emission), bandwidths and other steady state properties (shown by the filled grey symbols) at  $w_0 \approx 0$  mean? There is always a finite possibility that a trace amount of water could be present as impurity in either heptane or in the surfactant (AOT is known to absorb moisture) or even in both that would lead to the formation of cavity with trapped water molecules in it. In such a scenario, the cavity radius may easily be in the range of  $2\text{-}3\text{ \AA}$  (approximately the size of an oxygen atom). Since the van der Waals radius of M6C is  $\sim 3.5\text{ \AA}$ ,<sup>45</sup> the cavity would be able to barely accommodate a M6C molecule. Consequently, the rotation of the donor moiety (the morpholenyl group in M6C) would be severely hindered due to the close proximity of the surfactant head groups to the molecule undergoing

reaction in such a narrow pore. The effects of the low polarity and severe spatial restriction at  $w_0 \approx 0$  are then likely to be manifested in several properties such as the stabilization energies (peak frequencies), formation of LE and CT populations, equilibrium constant and finally on the reaction rate. Interestingly, the spectral properties obtained at  $w_0 \approx 0$  is strongly related with those at other non-zero values of  $w_0$ , suggesting that average polarity of the confined pool could indeed be a good correlating property for TICT reactions in such confined media. Note, however, that the CT bandwidth at  $w_0 \approx 0$  is narrower by  $\sim 750 \text{ cm}^{-1}$  compared to that at  $w_0 \approx 1$  and almost the same at  $w_0 \approx 37$ . The presence of very few water molecules in the cavity at  $w_0 \approx 0$  cannot form multiple solvation layers and thus the extent of spatial heterogeneity in this pool size may not be large. This might be one of the probable reasons for the comparable bandwidths at these two extreme pool sizes. The pool size ( $w_0$ ) dependence of the CT/ LE area ratio ( $\alpha_{CT}/\alpha_{LE}$ ) for M6C in reverse micelles is presented in Fig. 7.4 (upper panel). The area under each band ( $\alpha_x$ ,  $x = \text{CT}$  or LE) has been calculated as discussed earlier.<sup>45</sup> Note here that the CT/LE ratio increases as the pool size becomes larger. This suggests that formation of CT state is increasingly favored as  $w_0$  grows larger with successive addition of water at a fixed surfactant concentration. Note the area ratio ( $\alpha_{CT}/\alpha_{LE}$ ) is 4 times larger at  $w_0 \approx 37$  than that at  $w_0 \approx 0$ . The fact that the CT population is  $\sim 10\%$  at  $w_0 \approx 0$  and none in heptane suggests that M6C is located either at the polar interface of the microemulsion or partially encapsulated inside the cavity. We would like to mention here that LE population also derives contribution from those M6C molecules which may be partitioned into the heptane phase.<sup>35, 40</sup> As the formation of CT population is severely inhibited in non-polar solvents like heptane, the growth of the CT/LE ratio with  $w_0$  is directly linked to the average polarity ( $\epsilon_0$ ) of the solvent pool encapsulated in these reverse micelles.

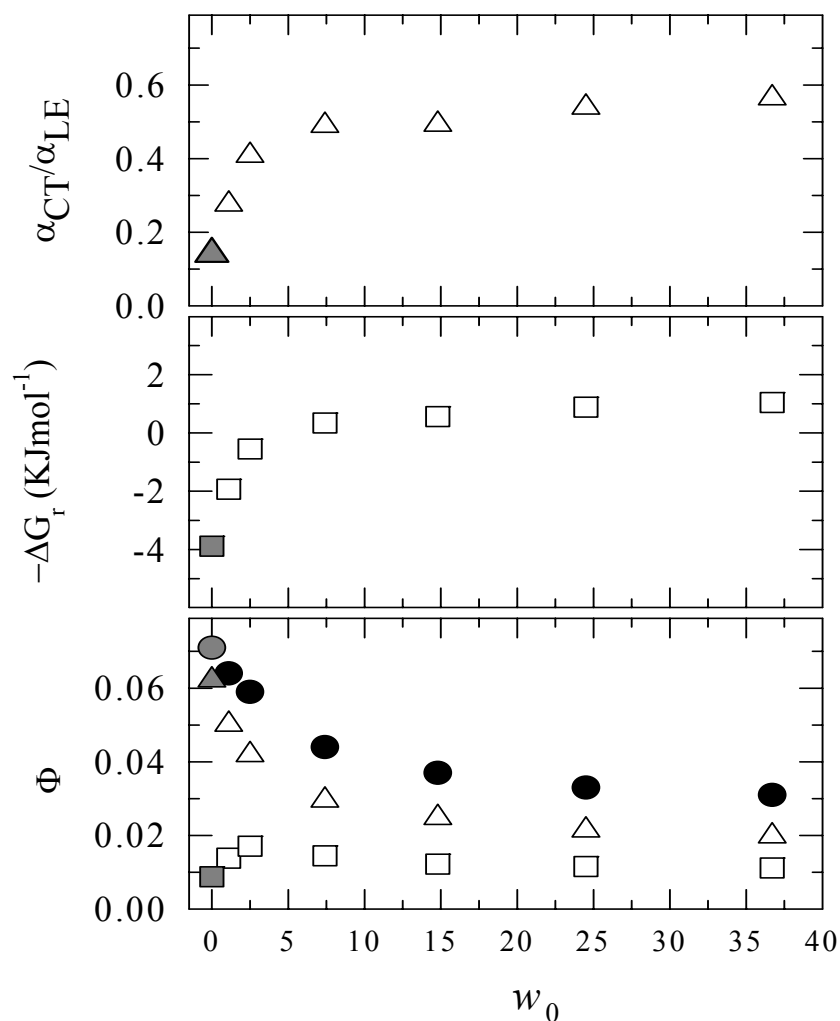


**Fig. 7.4:** The ratio between the areas under the CT and LE emission bands ( $\alpha_{CT}/\alpha_{LE}$ ), the change in reaction free energy ( $-\Delta G_r$ ) associated with the LE  $\rightarrow$  CT conversion and quantum yield ( $\Phi$ ) for M6C are shown as a function of  $w_0$ . For further discussion, see text.

The average polarity of the pool, however, cannot control entirely the formation of CT state as the confinement exerts restriction on the rotation of the donor group (morpholenyl group in M6C). The extra restriction arises from the enhanced rigidity of the solvent molecules due to confinement. The effects of the environmental rigidity is best understood when the CT/LE area ratio at a particular  $w_0$  is compared with that in bulk solvents with comparable dielectric constant. For example, the ratio ( $\alpha_{CT}/\alpha_{LE}$ ) at  $w_0 \approx 37$  is 0.56, whereas it is  $\sim 15$  in bulk propanol ( $\epsilon_0 \approx 20.5$ ).<sup>65</sup>

Therefore, in a polar pool with comparable  $\varepsilon_0$ , the area ratio for M6C is almost 27 times less than that in the bulk propanol.<sup>65</sup> As the area ratio is connected to the equilibrium constant ( $K_{eq}$ ) for the LE  $\rightarrow$  CT conversion reaction in M6C, this reduction in area ratio is translated to a lowering of  $K_{eq}$  by a factor of  $\sim 14$  at  $w_0 \approx 37$ . Subsequently, the change in reaction free energy ( $-\Delta G_r$ ) associated with the conversion reaction is calculated by using Eq.2.1 and shown as a function of pool size in the middle panel of Fig. 7. 4. As expected,  $-\Delta G_r$  is following the trend of  $\alpha_{CT}/\alpha_{LE}$  depicted in the upper panel of Fig. 7.4 Note that the pool size dependent  $-\Delta G_r$  varies from negative to positive values indicating that an unfavorable LE  $\rightarrow$  CT conversion reaction in smaller pool sizes becomes favorable in bigger microemulsion droplets. In fact, the equilibrium constant is  $\sim 7$  times larger at  $w_0 \approx 37$  than that at  $w_0 \approx 0$ . Note also that  $-\Delta G_r$  at  $w_0 \approx 37$  is approximately 7 times smaller than that in the bulk propanol, suggesting a substantial slowing down of the reaction upon confinement.

We have estimated quantum yield, radiative and non-radiative rates, and transition moments for M6C in all pool sizes. The equation 2.2 (chapter 2) has been used to determine the quantum yield. Values of net quantum yields as well as those for LE and CT emission bands for M6C calculated by using Eq. 2.2 are shown in the lower panel of Fig. 7.4. Note that both the net quantum yield and that associated with the LE band decrease as  $w_0$  increases, whereas the quantum yield for the CT band initially increases and then saturates with  $w_0$ . Interestingly, the pool size dependence of the quantum yields for M6C is similar to the electrolyte concentration dependence for several related compounds in electrolyte solutions studied earlier.<sup>50-51</sup> A partial restoration of the three dimensional H-bond network at higher  $w_0$  values is probably the reason for the observed decrease, since extensive H-bond network in water is known to augment the non-radiative relaxation channels. A recent study of TICT reaction in water-tertiary butanol (water-TBA) mixtures have also indicated that

partial destruction of H-bond network of water at higher TBA concentration leads to the increase in net quantum yield.<sup>50</sup> The net quantum yield of M6C at  $w_0 \approx 37$  is also found to be similar to those ( $\sim 0.045 \pm 0.01$ ) in some moderately polar bulk solvents such as ethyl acetate ( $\epsilon_0 = 6.02$ ) and tetrahydrofuran ( $\epsilon_0 = 7.58$ ).<sup>66</sup> The radiative ( $k_{LE}^{rad}$ ) and non-radiative ( $k_{LE}^{nr}$ ) rates have been determined by using the relations already discussed in chapter 2 for several values of  $w_0$  and are summarized in Table 7.1. The error bar associated with the calculation of these radiative and non-radiative rates is typically  $\pm 15\%$  about the values reported here. Since CT quantum yield is very small (lower panel, Fig. 7.4), the radiative rate for the CT emission band has not been calculated. Data in Table 7.1 indicate that while the radiative rate ( $k_{LE}^{rad}$ ) decreases with  $w_0$ , the non-radiative rate ( $k_{LE}^{nr}$ ) increases with the pool size.

**Table 7.1:** Pool size ( $w_0$ ) dependent radiative, non-radiative and absorption transition moments of M6C AOT/water/heptane reverse micelles.

$w_0$	$\mathbf{K}_{LE}^{rad} (10^7 \text{ s}^{-1})$	$\mathbf{K}_{LE}^{nr} (10^9 \text{ s}^{-1})$	$\mathbf{M}_{abs} (\text{D})$
0.0	3.097	0.467	3.6
1.1	3.003	0.569	3.5
2.5	2.653	0.607	3.2
7.4	2.067	0.680	3.6
14.8	1.754	0.690	3.3
24.5	1.587	0.724	3.6
36.7	1.531	0.757	3.8

The net absorption transition moments (by using Eq. 2.8) for M6C at various values of  $w_0$  are shown in Table 7.1. It is evident from this table that these absorption transition moments do not show any dependence on pool size which was also found for several TICT molecules in neat solvents,<sup>45</sup> electrolyte solutions<sup>51-52</sup> and water-TBA mixtures at higher alcohol mole fractions.<sup>50</sup>

### 7.3.3. Time Resolved Studies of TICT Reaction in Reverse Micelles: Pool Size Dependence

As already mentioned in the Introduction, emission decays of M6C in all pool sizes have been found to be bi-exponential with time. This is rather interesting because solvent dynamics being sluggish in confined environments, the reaction is expected to be not in the rapid solvent equilibration limit.<sup>45</sup> This would then lead to a deviation from the biexponential character of the time resolved emission intensity decay, questioning the validity of the classical two state reversible reaction mechanism as described earlier.<sup>45</sup> Also, because of the microscopic heterogeneity both in the solvent structure and dynamics as well as the solute distribution, a stretched exponential rather than a simple bi-exponential function is expected to be suitable for the decay kinetics. Representative bi-exponential fits to the emission decays collected at peak wavelength of LE at  $w_0 \approx 0$  and  $w_0 \approx 24$  are shown in Fig. 7.5 where fit parameters are also summarized. Clearly, the LE emission decays are bi-exponential with time as the residuals do not contain any non-random pattern and values for the ‘goodness of fit parameter’ ( $\chi^2$ ) are close to 1. While the shorter one between the two time constants obtained by fitting the LE emission decays at a given pool size is believed to be associated with the reaction time of the LE  $\rightarrow$  CT conversion reaction in M6C, the longer time constant reflects the average time for LE decay to the ground state. Note that the values of the longer time constant (2.1 ns and 1.8 ns) at these two pool sizes are similar to those found for another closely related TICT molecule, 4-(1-azetidiny)-benzotrile (P4C) in TBA-water solutions at higher TBA mole fractions.<sup>50</sup> The reaction time for the LE  $\rightarrow$  CT conversion reaction in M6C is  $\sim 250$  ps at  $w_0 \approx 24$  and  $\sim 1200$  ps at  $w_0 \approx 0$ . Note here that an unconstrained bi-exponential fit to the CT emission decay at  $w_0 \approx 24$  has also produced a rise time  $260 \pm 20$  ps and a long time constant of about 2 ns.

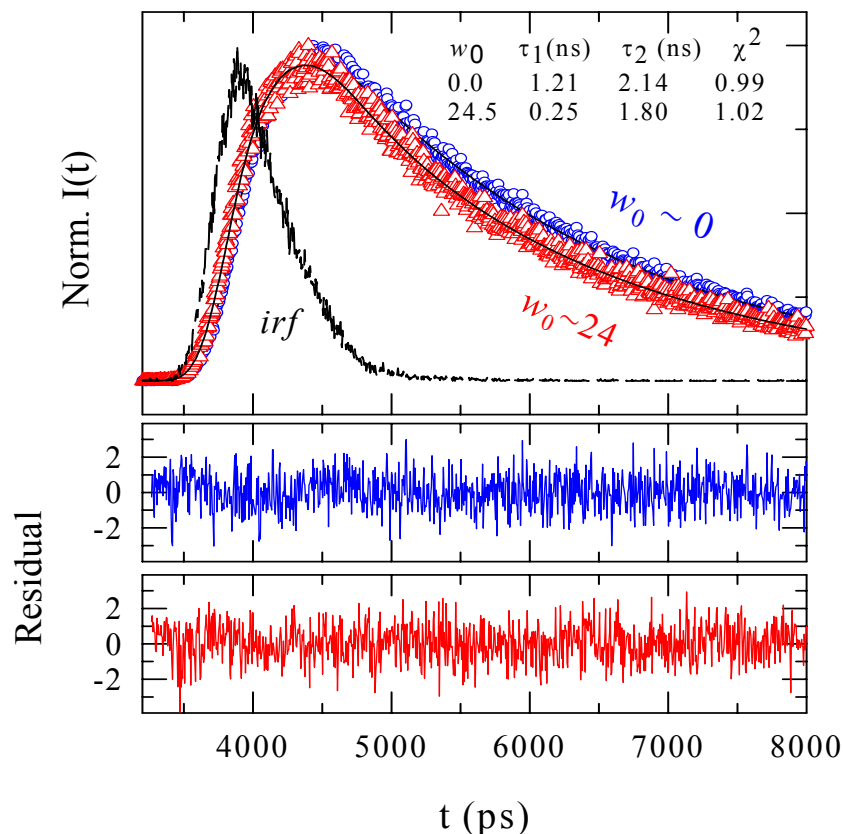


**Fig. 7.5:** Representative time resolved LE emission decays of M6C dissolved in AOT/water/heptane reverse micelles at two different pool sizes:  $w_0 \approx 0$  (blue circles) and at  $w_0 \approx 24$  (red triangles) along with time constants and chi-squared values obtained from bi-exponential fits (solid lines going through the symbols). The residuals (color-coded) for these pool sizes are shown in the lower panels. The amplitudes ( $a_1$  and  $a_2$ ) at  $w_0 \approx 0$  and  $w_0 \approx 24$  are (0.86, 0.14) and (0.71, 0.29), respectively. Note the LE emission decays were collected at wavelengths corresponding to the peak of the steady state emission spectra.

These values are very similar to the time constants found for the LE emission decay collected at this pool size ( $w_0 \approx 24$ ). This has also been observed in earlier studies with several closely related TICT molecules.<sup>45, 50, 52</sup> The shorter time constant is indeed then the reaction time for M6C in these confined environments. Note here

that if the LE emission decay at  $w_0 \approx 0$  is fitted to a single exponential, the fit worsens generating non-random patterns at shorter times of the total decay profile. However, the fit becomes smoother and the residual more regular if a bi-exponential function of time is used. Interestingly therefore, the bi-exponential behavior of the decay kinetics for M6C in AOT/water/heptane reverse micelles also conform to the classical two state reversible reaction mechanism as described by Maroncelli and coworkers<sup>45</sup>

The bi-exponential fit parameters required to fit the LE emission decays of M6C at seven pool sizes are shown in Fig.7.6 Note that in the present study the fast time constant is simply the reaction time as the decays are all bi-exponential with time. While the reaction times ( $\tau_{short}$ ) for M6C in reverse micelles obtained at different values of  $w_0$  are presented in the left panels, the amplitudes are shown in the right panels of Fig. 7.6. It is evident from the left-upper panel of Fig.7.6 that the reaction is 6 times faster at  $w_0 \approx 37$  than that at  $w_0 \approx 0$  with amplitude of the shorter component ( $a_{short}$ ) being  $\sim 3$  times more at the largest pool than that at the smallest one. As the pool size grows bigger, the reaction time decreases simultaneously with the increase in amplitude of the associated component ( $a_{short}$ ). The growth of the short component ( $a_{short}$ ) with pool size suggests that the reaction is becoming favorable due to larger change in reaction free energy ( $-\Delta G_r \propto \ln[a_{short}/a_{long}]$ ). Therefore, the pool size ( $w_0$ ) dependencies of both the reaction time and amplitude clearly reflect that the reaction is increasingly favored due to enhanced polarity and better mobility of the environment as the pool grows in size. Note that the reaction time at the largest pool is  $\sim 200$  ps and is strikingly close to that ( $\sim 190$  ps) of P6C in bulk decanol ( $\epsilon_0 = 7.2$ ) at room temperature. This similarity in reaction times indicates that probably both the environment rigidity (via viscosity) and average polarity play important roles for determining the rates of such reactions in a given environment. The reaction times shown in Fig 7.6

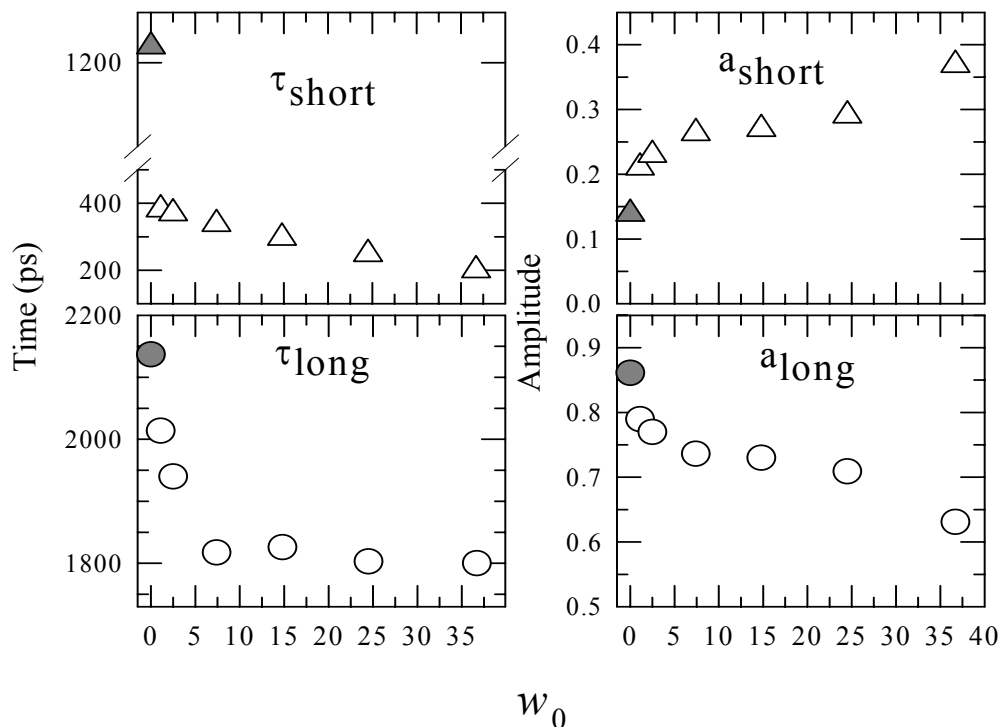


**Fig. 7.6:** Time constants ( $\tau_i$ ,  $i = short$  or  $long$ ) and amplitudes ( $a_i$ ) obtained after fitting the LE emission decays with bi-exponential function of time at different pool sizes ( $w_0$ ).  $\tau_{short}$  is assumed to be the reaction time ( $\tau_{rxn}$ ) for the LE  $\rightarrow$  CT conversion reaction in M6C.

for  $w_0$  values ranging from  $\sim 1$  to  $\sim 37$  are in the order of few hundreds of picosecond which are many times larger than that at bulk solvents of comparable polarities. For example, the LE  $\rightarrow$  CT conversion reaction for M6C in propanol at room temperature proceeds with a reaction time of approximately 25 ps, which is also similar to that obtained for P6C in the same solvent at similar condition.<sup>45</sup> The ratio between the reaction rate in reverse micelles and that in bulk propanol is shown as a function of pool size in Fig. 7.7. The slowing down of the reaction rate by a factor of 10 – 20 between  $w_0$  values  $\sim 1$  to  $\sim 37$  is partially linked to the slow orientational relaxation time scales of encapsulated water molecules in these reverse micelles.

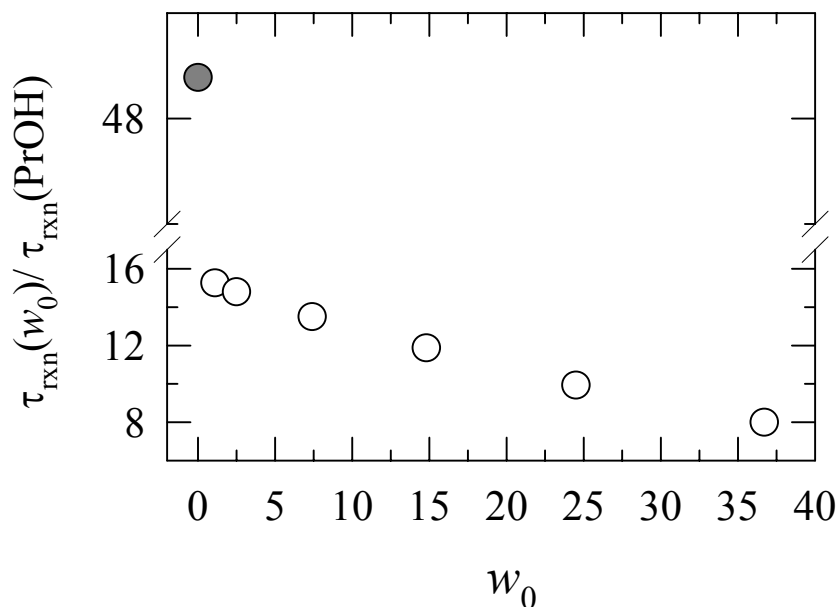


**Fig. 7.7:** The ratio between the reaction time for M6C at a given pool ( $\tau_{rxn}(w_0)$ ) and that in the bulk propanol ( $\tau_{rxn}(PrOH)$ ) is shown as a function of pool size,  $w_0$ .

The reduced polarity of the solvent pool also contributes significantly to the slowing down of the formation of the charge-transferred state. Note that the measured dielectric relaxation time quoted in Ref.64 leads to a longitudinal relaxation time scale ( $\tau_L$ ) in the range of 500 ps for dipolar solvation dynamics in AOT/water reverse micelles. It is therefore likely that the observed slow reaction times are a manifestation of slow solvent stabilization of the activated species as well as that of the charge-transferred product. Since the cavity size is barely enough for partially accommodating the M6C molecule along with a few water molecules at  $w_0 \approx 0$ , the rotation of the donating moiety becomes severely restricted. Also, a drastic reduction in the average polarity in such a small cavity may not be able to sufficiently stabilize the CT state. Consequently, the reaction rate at  $w_0 \approx 0$  becomes almost 50 times slower than that in bulk propanol.

## 7.4. Conclusion

The main results of the chapter are as follows. A new twisted intramolecular charge transfer (TICT) molecule has been synthesized and, photophysics and photochemistry studied at several pool sizes in AOT/water/heptane reverse micelles. The net quantum yield of M6C is found to decrease as the pool size grows in size, whereas the non-radiative rate increases. The absorption transition moment remains insensitive to the pool size. The pool size dependencies of these photophysical quantities appear to be similar to the alcohol mole fraction dependence of a closely related TICT molecule in TBA-water mixtures at higher TBA concentrations.<sup>50</sup> This similarity suggests the role of the three dimensional H-bond network structure of water in determining the photophysics of dissolved probes. The average static dielectric constants of the solvent pools have been estimated from the emission peak frequencies of a non-reactive probe dissolved in these microemulsions as well as from the permittivity measurements of reverse micelles using 0.5 M AOT. The estimated bulk dielectric constant in the confined environment is found to be drastically different from that of bulk water. The reduction in average polarity then leads to a less production of the charge transferred state in M6C upon photo-excitation. At the largest pool size ( $w_0 \approx 37$ ), the equilibrium constant ( $K_{eq}$ ) for the LE  $\rightarrow$  CT conversion reaction of M6C is found to be 15 times smaller than that in bulk propanol whose polarity is comparable to the estimated polarity at this pool size. The change in reaction free energy ( $-\Delta G_r$ ) are also found to be  $\sim 8$  times smaller than that in bulk propanol. Interestingly,  $-\Delta G_r$  changes sign (from negative to positive) with the increase in pool size, indicating that the reaction becomes more favorable in larger  $w_0$  values.

We have also investigated the effects of surfactant concentration on the LE  $\rightarrow$  CT reaction of M6C at two representative pool sizes –  $w_0 = 7.4$  and  $w_0 = 24.5$ . The steady state studies indicate that at both the pool sizes the absorption and LE peak frequencies show red-shift by  $400 - 600 \text{ cm}^{-1}$  upon changing the AOT concentration from 0.1 M to 0.5 M. However, the LE emission band is found to broaden by similar

amount. Interestingly, the CT shift is much smaller ( $\sim 100 \text{ cm}^{-1}$ ) and accompanies narrowing by about  $800 \text{ cm}^{-1}$  for increasing the AOT concentration to 0.5 M. The narrowing of the CT band is the direct effect of the increasing solute-environment interaction<sup>46</sup> at higher AOT concentration. The increase in AOT concentration also enhances the CT population relative to that of LE that leads to the enhancement of  $-\Delta G_{\text{r}}$  by a factor of 6 at  $w_0 = 7.4$  and  $\sim 4$  at  $w_0 = 24.5$  for changing the AOT concentration from 0.1 M to 0.5 M. The reaction rate, on the other hand, slows down by  $\sim 70\%$  at  $w_0 = 7.4$  and  $\sim 25\%$  at  $w_0 = 24.5$  for increasing the concentration from 0.1 M to 0.5 M. The stronger ion-dipole interactions leading to higher dielectric friction on the twisting mode as well as further reduced polarity at higher AOT concentration may be responsible for such a slowing down of the reaction rate. However, further studies with several other AOT concentrations and at different pool sizes are required to understand the surfactant concentration effects on such reactions.

Since these confined environments are known to possess strong spatial heterogeneity, the reaction rate is expected to be significantly coupled to the location of the TICT molecule inside the confined solvent pool. For example, if the relatively stronger ion-dipole interaction makes the TICT molecule reside near the interface created by the AOT head group and polar solvent molecules, the reaction rate would be largely dictated by the time scale and polarity of that locality. On the other hand, if strong dielectric screening and proper solvation drive the reactant molecule to go into the center of the pool, the enhanced mobility and increased polarity would render the reaction more facile and faster. In principle, one can resolve the spatial heterogeneity of reaction rate by selectively exciting the population via excitation wavelength dependence study. Such a study on vibrational dynamics of confined water molecules has recently been carried out where a moderate dependence on excitation wavelength is indicated.<sup>25-26</sup> Moreover, several recent studies<sup>1-10, 16</sup> have suggested the presence of a significant amount of ultrafast component in aqueous reverse micelles with time constant in the range of 30 – 50 fs. One wonders then how the ultrafast response would scale with the spatial heterogeneity and what would be

the effects of such ultrafast components on reactions which possess polar intermediates such as the TICT reaction? A coupled investigation of ultrafast solvation dynamics and reaction kinetics is therefore required to fully understand the environment effects on TICT reactions in these confined systems. A comparison among time scales measured in quaternary microemulsions,<sup>9</sup> lecithin vesicles,<sup>16</sup> catanionic<sup>42</sup> and AOT/water/heptane reverse micelles<sup>2-10</sup> suggests that solvent dynamics seems to be the fastest in the quaternary microemulsions and lecithin vesicles, and then sequentially comes catanionic and AOT/water/heptane reverse micelles. It would then be interesting to study whether a TICT reaction picks up the dynamical modes so neatly and the reaction rate is modified accordingly. Dynamical solvent control of TICT reaction in other molecules that possess higher activation energies in these confined environments might also be interesting.

## References and Notes

1. Levinger, N. E. *Science*, **2002**, *298*, 1722.
2. Bhattacharyya, K. *Acc. Chem. Res.* **2003**, *36*, 95 and references therein.
3. Ghosh, S.; Mandal, U.; Adhikari, A.; Dey, S.; Bhattacharyya, K. *Int. Rev. Phys. Chem.* **2007**, *26*, 421.
4. Luisi, P. L.; Straub, B. E.; Eds., *Reverse Micelles: Biological and Technological Relevance to Amphiphilic Structures in Apolar Media*, Plenum: New York, **1984**.
5. De, T.; Maitra, A.; *Adv. Colloid Interface Sci.*, **1995**, *59*, 95.
6. Baruah, B.; Roden, J. M.; Sedgwick, M.; Correa, N. M.; Crans, D. C.; Levinger, N. E. *J. Am. Chem. Soc.* **2006**, *128*, 12758.
7. Willard, D. M.; Riter, R. E.; Levinger, N. E. *J. Am. Chem. Soc.* **1998**, *120*, 4151.
8. Harpham, M. R.; Ladanyi, B.; Levinger, N. E. *J. Phys. Chem. B.* **2005**, *109*, 16891
9. Corbeil, E. M.; Levinger, N. E. *Langmuir* **2003**, *19*, 7264.
10. Correa, N. M.; Levinger, N. E. *J. Phys. Chem. B.* **2006**, *110*, 13050.
11. Rosenfeld, D. E.; Schmuttenmaer, C. A. *J. Phys. Chem. B* **2006**, *110*, 14309.
12. Vanables, D. S.; Huang, K.; Schmuttenmaer, C. A. *J. Phys. Chem. B* **2001**, *105*, 9132.
13. Boyd, J. E.; Briskman, A.; Sayes, C. M.; Mittelman, D. A.; Colvin, V. J. *Phys. Chem. B* **2002**, *106*, 6346.
14. Boyd, J. E.; Briskman, A.; Colvin, V. L.; Mittleman, D. M. *Phys. Rev. Lett.* **2001**, *87* 147401/1.
15. Zhong, Q.; Steinburst, D. A.; Carpenter, E. E.; Owrutsky, J. C. *Langmuir* **2002**, *18*, 7401.
16. Bursing, H.; Ouw, S.; Kundu, P.; Vohringer, P. *Phys. Chem. Chem. Phys.* **2001**, *3*, 2378.
17. Pileni, M. P.; Ed. *Structure and Reactivity in Reverse Micelles*; Elsevier: Amsterdam, **1989**; vol. 65.
18. Cho, C. H.; Chung, M.; Lee, J.; Nguyen, T.; Singh, S.; Vedamuthu, M.; Yao,

- S.; Zhu, S. B.; Robinson, G. W. *J. Phys. Chem.* **1995**, *99*, 7806.
19. Lundgren, J. S.; Heitz, M. P.; Bright, F. V. *Anal. Chem.* **1995**, *67*, 3775.
20. Das, S.; Datta, A.; Bhattacharyya, K. *J. Phys. Chem. A* **1999**, *101*, 3299.
21. Sarkar, N.; Das, K.; Datta, A.; Das, S.; Bhattacharyya, K. *J. Phys. Chem.* **1996**, *100*, 10523.
22. Datta, A.; Mandal, D.; Pal, S. K.; Bhattacharyya, K. *J. Phys. Chem. B* **1997**, *101*, 10221.
23. Riter, R. E.; Willard, D. M.; Levinger, N. E. *J. Phys. Chem. B* **1998**, *102*, 2705.
24. Moilanen, D. E.; Levinger, N. E.; Spry, D. B.; Fayer, M. D. *J. Amer. Chem. Soc.* **2007** *129*, 14311.
25. Tan, H-S. ; Piletic, I. R.; Fayer, M. D. *J. Chem. Phys.* **2005**, *122*, 174501.
26. Piletic, I. R.; Tan, H-S.; Fayer, M. D. *J. Phys. Chem. B* **2005**, *109*, 21273.
27. Faeder, J.; Ladanyi, B. M. *J. Phys. Chem. B* **2001**, *105*, 11148.
28. Faeder, J.; Ladanyi, B. M. *J. Phys. Chem. B* **2000**, *104*, 1033.
29. Bhattacharyya, K. ; Bagchi, B. *J. Phys. Chem. A* **2000**, *104*, 10603.
30. Salaniwal, S.; Cui, S. T. ; Cochran, H. D. ; Cummings, P. T. *Langmuir*, **2001**, *17*, 1773.
31. Salaniwal, S.; Cui, S. T. ; Cochran, H. D. ; Cummings, P. T. *Langmuir*, **2001**, *17*, 1784.
32. Salaniwal, S.; Cui, S. T. ; Cochran, H. D. ; Cummings, P. T. *Langmuir*, **1999**, *15*, 5188.
33. Senapati, S. ; Keiper, J. M. ; DeSimone, J. M. ; Wignall, G. D. ; Melnichenko, Y. B. ; Frielinghaus, H. ; Berkowitz, M. L. *Langmuir*, **2002**, *18*, 7371.
34. Mahiuddin, S.; Renoncourt, A.; Bauduin, P.; Touraud, D.; Kunz, W. *Langmuir* **2005**, *21*, 5259.
35. Silber, J. J.; Biasutti, A.; Abuin, E.; Lissi, E. *Adv. Colloid Interface Sci.* **1999**, *82*, 189.
36. Falcone, R. D.; Correa, N. M ; Biasutti, M. A.; Silber, J. J. *Langmuir*, **2002**, *18*, 2039.

37. Falcone, R. D.; Correa, N. M.; Biasutti, M. A.; Silber, J. J. *J. Colloid Interface Sci.* **2006**, *296*, 356.
38. Falcone, R. D.; Biasutti, M. A.; Correa, N. M.; Silber, J. J.; Lissi, E.; Abuin, E. *Langmuir*, **2004**, *20*, 5732.
39. Silber, J. J.; Falcone, R. D.; Correa, N. M.; Biasutti, M. A.; Abuin, E.; Lissi, E.; Campodonico, P. *Langmuir*, **2003**, *19*, 2067.
40. Novaira, M.; Biasutti, M. A.; Silber, J. J.; Correa, N. M.; *J. Phys. Chem. B*, **2007**, *111*, 748.
41. Novaira, M.; Moyano, F.; Biasutti, M. A.; Silber, J. J.; Correa, N. M.; *Langmuir*, **2008**, *24*, 4637.
42. Biswas, R.; Das, A. R.; Pradhan, T.; Tourad, D.; Kunz, W.; Mahiuddin, S. *J. Phys. Chem. B*. **2008**, *112*, 6620.
43. Grabowski, Z. R.; Rotkiewicz, K.; Rettig, W. *Chem. Rev.* **2003**, *103*, 3899.
44. Lippert, E.; Rettig, W.; Bonacic-Koutecky, V.; Heisel, F.; Mieche, J. A. *Adv. Chem. Phys.* **1987**, *68*, 1.
45. Dahl, K.; Biswas, R.; Ito, N.; Maroncelli, M. *J. Phys. Chem. B*, **2005**, *109*, 1563.
46. Horng, M.L.; Gardecki, J. A.; Papazyan, A.; Maroncelli, M. *J. Phys. Chem.* **1995**, *99*, 17311.
47. Zwan, van der G.; Hynes, J. T. *Chem. Phys.* **1991**, *152*, 169.
48. Hicks, J.; Vandersall, M.; Babarogic, Z.; Eisenthal, K. B. *Chem. Phys. Lett.*, **1985**, *116*, 18.
49. Hicks, J.; Vandersall, M. T.; Sitzmann, E. V.; Eisenthal, K. B. *Chem. Phys. Lett.*, **1987**, *135*, 413.
50. Pradhan, T.; Ghoshal, P.; Biswas, R. *J. Phys. Chem. A*. **2008**, *112*, 915.
51. Pradhan, T.; Biswas, R. *J. Phys. Chem. A*. **2007**, *111*, 11514.
52. Pradhan, T.; Biswas, R. *J. Phys. Chem. A*. **2007**, *111*, 11524.
53. The CT emission decays could not be collected for all pool sizes due to the very low CT quantum yield.
54. Rettig, W. *J. Luminesc.* **1980**, *26*, 21.
55. Rettig, W. *J. Phys. Chem.* **1982**, *86*, 1970.

56. Krishna, M. M. G. *J. Phys. Chem. A* **1999**, *103*, 3589.
57. Biswas, R.; Lewis, J. E.; Maroncelli, M. *Chem. Phys. Lett.* **1999**, *310*, 485.
58. Lewis, J. E.; Biswas, R.; Robinson, A. G.; Maroncelli, M. *J. Phys. Chem. B* **2001**, *105*, 3306.
59. Song, W.; Biswas, R.; Maroncelli, M. *J. Phys. Chem. A* **2000**, *104*, 6924.
60. Senapati, S.; Chandra, A. *J. Phys. Chem. B* **2001**, *105*, 5106.
61. Bagchi, B.; Biswas, R. *Adv. Chem. Phys.* **1999**, *109*, 207.
62. Bagchi, B.; Chandra, A. *Adv. Chem. Phys.* **1991**, *80*, 1.
63. Balasubramanian, S.; Bagchi, B. *J. Phys. Chem. B* **2001**, *105*, 12529.
64. Biswas, R.; Rohman, N.; Pradhan, T.; Buchner, R. *J. Phys. Chem. B* **2008**, *112*, 9379
65. See the tabulated values supplied along with Fig. A14 in Appendix2
66. The values for the net quantum yield of M6C in ethyl acetate and tetrahydrofuran respectively are  $(0.040 \pm 0.05)$  and  $(0.042 \pm 0.05)$  (unpublished data)

## Chapter 8

### **Spectroscopic Studies of Catanionic Reverse Microemulsion: Correlation with the Superactivity of Horseradish Peroxidase Enzyme in a Restricted Environment**

#### **8.1. Introduction**

As already discussed in the previous chapter, an aqueous reverse microemulsion, which is a thermodynamically stable liquid made up of surfactant(s), cosurfactant, oil and water typifies biological model of a living cell<sup>1</sup>. In this system water molecules are confined in a reaction vessel of nanometer dimension, dispersed in a continuous oil medium. The behaviour of water molecules inside the pool is similar in many aspects with water molecules bound to biological systems and in other restricted environments.<sup>1-34</sup>

We have already found that the size of the water pool can be tailor-made by controlling the water to surfactant ratio for making microemulsions mimic a biological system or any other restricted environment. Literature shows that reverse microemulsions containing sodium bis(2-ethylhexyl) sulfosuccinate (aerosol-AT or commonly AOT), an anionic amphiphile, have frequently been taken as a biological model in contrast to cationic or mixed amphiphiles.<sup>1-3</sup> However, a biological system contains not only anionic or uncharged components but also positively charged molecules. Therefore, catanionic reverse microemulsions appear to be a better model for many biological systems.<sup>34</sup>

A catanionic reverse microemulsion as a reaction medium is rarely used<sup>34-38</sup> except for solubilization and phase behaviour studies<sup>39-43</sup>. The first example for the enzyme activity in a catanionic reverse microemulsion has appeared in 2005, which demonstrates that at a certain composition of sodium dodecyl sulphate (SDS) and

dodecyltrimethylammonium bromide (DTAB), this catanionic microemulsion exhibits enzymatic superactivity<sup>34</sup> at a DTAB to total surfactant ratio of 15 % even though DTAB has a negative effect on enzymes.<sup>44</sup> Interestingly, the enzymatic activity in this catanionic microemulsion is up to a DTAB mole fraction of 0.15, in comparison to microemulsions containing only SDS as the surfactant.<sup>45</sup> All these results are somewhat surprising since DTAB even at  $\leq 10^{-2}$  M strongly inhibits the enzyme activity.<sup>44</sup> The cosurfactant (n-hexanol) has also negative effect on the enzymatic activity, which is probably due to the denaturation of the enzyme structure by the alcohol.<sup>46-47</sup> Therefore, the superactivity of the enzyme might be related to a just *optimum* level of hydration, which is supplied by the finite-sized water pool confined in this reverse microemulsion. It seems that DTAB resides at the oil-water interface and therefore minimizes the poisoning of the enzyme due to limited contact. Another reason for the superactivity of the enzyme could be that the pH inside the droplets of the SDS/DTAB microemulsions is close to the critical value of 4.5, at which the initial velocity of the enzymatic activity is maximum. Note that the pure buffer has a pH value of 5.<sup>34</sup>

Recently, several experimental,<sup>48-50</sup> computer simulation<sup>51-52</sup> and theoretical studies<sup>53-55</sup> have indicated the role of structure and dynamics of water molecules near to a biological surface in determining the functional activity of that moiety. Very recently, Abecassis et al.<sup>56</sup> have studied the microstructure and phase behaviour of a 'true' catanionic reverse microemulsion and concluded that the surface charge of a catanionic microemulsion plays a significant role for the microstructure, which can be tailor-made. In fact, there has been a great deal of interest in correlating the function of protein molecules with the dynamics of water molecules surrounding it.<sup>48-50</sup> Since the three dimensional hydrogen bonding network structure of water molecules near to a biologically active site and those in a confinement are expected to be strongly modified, both the polarity and dynamics of these molecules are likely to be very different from those in the bulk. In addition, the hydration layers surrounding an active site or a dipolar probe in a finite size confinement are microscopically heterogeneous (both structurally and dynamically) due to binding

via electrostatic and other specific interactions.<sup>1-3, 6-16</sup> These interactions render the water dynamics much slower but cannot make too sluggish to stop the functional activity of that particular protein or enzyme. The role of this heterogeneity and dynamics in keeping a protein or enzyme functional is an aspect of constant debate and discussion. Since the reduced polarity of confined solvent has been found to considerably affect the rate of a TICT reaction in reverse micelles (previous chapter), an enzymatic reaction is also likely to be significantly affected if carried out in microemulsions.

In this chapter, we are studying the average polarity and dynamics of the confined solvent pool inside cationic reverse microemulsions formed by mixing five components: SDS, DTAB, dodecane, n-hexanol and water (present as buffer). Various components of this mixture are varied in order to change the size of the droplets formed. The hydrodynamic diameters of these reverse microemulsion droplets have been determined by using the DLS technique. The average polarity and the dynamics of the confined solvent pool inside these droplets have been probed via steady state and time resolved fluorescence emission spectroscopy. Anisotropy studies have been carried out to gain a qualitative idea about the rigidity of the confined solvent pool. Subsequently, an attempt has been made to correlate the DLS and spectroscopic results with the enzymatic activity of horseradish peroxidase<sup>57</sup> obtained earlier in these microemulsions.<sup>34</sup>

The organization of the rest of the chapter is as follows. Experimental details including materials, experimental techniques and analyses methods have been described briefly in the next section. Section 8.3 contains the results and discussion. The paper then ends with concluding remarks in Section 8.4.

## **8.2. Experimental Details**

**8.2.1. Materials.** Sodium dodecyl sulfate ( $\geq 99\%$ , SRL, India), dodecyltrimethylammonium bromide ( $>99\%$ , Aldrich, Germany), n-hexanol ( $> 98\%$ ,

Acros Organics, USA), and n-dodecane (>99%, Aldrich, Germany) were used without further purification. A buffer of pH 5 consisting of 0.009 mol L<sup>-1</sup> citric acid monohydrate (99.5%, Qualigens, India) and 0.016 mol L<sup>-1</sup> sodium citrate dihydrate (>99%, BDH, India) were used for preparation of microemulsion and maintaining pH. Double-distilled water was used to prepare the solutions.

**8.2.2. Preparation of Microemulsion.** We have three series of cationic microemulsions. In the first series, DTAB was varied (1.576, 2.222, 2.828 and 3.434 %) by keeping the total surfactant (SDS+DTAB) composition at 20.2 % and cosurfactant (n-hexanol) at 20.2 %, n-dodecane 37.6 % and buffer at 22 %. Under this series the microemulsions are designated as ME10, ME11, ME12 and ME13, respectively. In the second series of microemulsions, composition of n-hexanol was varied (20.2, 22, 25, 28.9 and 30 %) taking the composition of ME10 as the base value and the total composition of n-hexanol and n-dodecane was kept at 57.8 %. The microemulsions are designated as ME10, ME14, ME15, ME16 and ME17. In the third series, buffer composition was varied (22, 20, 18, 15 and 10 %) keeping the total composition of buffer and n-dodecane at 59.6% and the microemulsions are designated as ME10, ME18, ME19, ME20 and ME21. Composition of different components is in % w/w with respect to total microemulsion composition. In all three series of microemulsions ME10 is common. Addition of calculated amounts of the components followed by stirring produced the samples, which were transparent to the bare eyes. Table 8.1 summarizes the sample (cationic reverse microemulsions) composition.

**TABLE 8.1: Compositions of Microemulsions (ME). The numbers are the code numbers started from ME10 to ME21**

(a) Variation of SDS to DTAB ratio for a total surfactant content of 22.2%.

Sl No	Code No	Weight fraction of SDS (= SDS/(SDS+DTAB))
1	ME13	0.830
2	ME12	0.860
3	ME11	0.890
4	ME10	0.9221

(b) Variation of hexanol to dodecane ratio for a total composition (hexane + dodecane) of 57.8%

Sl No	Code No	n-hexanol w/w %
1	ME10	20.20
2	ME14	22.00
3	ME15	25.00
4	ME16	28.90
5	ME17	30.00

(c) Variation of buffer to dodecane ratio for a total content (buffer + dodecane) of 59.6 %

Sl No	Code No	Buffer w/w %
1	ME21	10.00
2	ME20	15.00
3	ME19	18.00
4	ME18	20.00
5	ME10	22.00

**8.2.3. Spectroscopic Experiments.** In a typical steady-state absorption and emission run, coumarin 153 (C153) was added to a microemulsion (concentration  $< 10^{-5}$  M) and the spectra were recorded with an UV-Visible Spectrophotometer (UV-2450, Shimadzu). An optically clean quartz cell with 1 cm optical path length was used for recording the spectra. Subsequently, the absorbance of the samples was adjusted (via dilution) to  $\sim 0.10$  and emission spectra were collected with a Fluoromax-3, Jobin-Yvon. For each emission scan, the peak wavelength of the corresponding absorption spectrum was used as an excitation wavelength. Absorption and emission peak frequencies were calculated as *average* of the peak frequencies obtained by fitting

the upper half of the spectrum (absorption or emission) with an inverted parabola, first moment and the arithmetic mean of the frequencies at half intensities on both blue and red ends of the spectrum<sup>58-59</sup>. This averaging takes care off the asymmetric movement of the spectral band as the sample composition changes.

The solvation dynamics in these media was followed by monitoring the peak shift in the time resolved emission spectrum (TRES) of an excited probe (C153 in this case) constructed from a series of 18–22 emission decays at equally spaced wavelengths across the steady state emission spectrum of the dissolved probe.<sup>60</sup> The decays (magic angle) were collected via time correlated single photon counting (TCSPC) method by using 409 nm light as excitation. The excitation wavelength (409 nm) for the time resolved emission studies was kept fixed for all the samples. The full-width at half maximum (FWHM) of the instrument response function (IRF) with this excitation source was approximately 75 ps. The collected decays were deconvoluted from the IRF and fitted to multi-exponential function using an iterative reconvolution algorithm. Such fitting enables one to capture relaxation processes with time scales in the range of ~15 ps. Note that this resolution might miss the relatively faster component of the solvent response but is expected to capture the long time dynamics well. Subsequently, time dependent progress of solvation was expressed in terms of solvent response function<sup>60</sup>,  $S(t) = \frac{\nu(t) - \nu(\infty)}{\nu(0) - \nu(\infty)}$ , where  $\nu(t)$  denotes the peak

frequency of the emission spectrum at a certain time (t) after the laser-excitation of the probe and  $\nu(0)$  represents the emission peak frequency immediately after excitation (with the same environment configuration as in the ground state).<sup>60</sup>  $\nu(\infty)$  is the peak frequency of the emission spectrum of the excited probe at sufficiently long time when the reorganization of the environment is supposed to be completed. Therefore,  $\nu(\infty)$  should be equal to the peak frequency of the steady state emission spectrum of the same probe. Even though this would be the case for most of the solvents at ambient condition and at higher temperatures,  $\nu(\infty)$  might differ (by at most 300 cm<sup>-1</sup>) from the steady state value in systems where lowering the temperature or geometric confinement slows down the solvent motions

substantially.<sup>60</sup> The average solvation time,  $\langle \tau_s \rangle$ , was determined from  $S(t)$  as follows,  $\langle \tau_s \rangle = \int_0^{\infty} dt S(t)$ . Subsequently, the missing component of the fast initial decay of  $S(t)$  was determined by estimating the time-zero spectrum<sup>61</sup> from the following relation<sup>29,62</sup>,  $\nu_{em}(t=0) \approx \nu_{abs} - [\nu_{abs} - \nu_{em}]^{\text{nonpolar}}$ . Here  $\nu_{abs}$  is the absorption peak frequency of C153 in a given microemulsion. The absorption and emission peak frequencies of C153 in non-polar medium were taken as those obtained for C153 in heptane. Ideally, these values should be obtained from the hypothetical microemulsion where non-polar solvent alone constitutes the encapsulated solvent pool.

Time resolved fluorescence anisotropies,  $r(t)$ , were calculated from the collected parallel ( $I_{\parallel}(t)$ ) and perpendicular ( $I_{\perp}(t)$ ) decays by using the relation already described in chapter 6 (Eq. 6.1). The time resolved anisotropy constructed from the collected emission decays was then fitted to a bi-exponential function (Eq.6.2, chapter 6) after deconvoluting from the IRF using an iterative reconvolution-fitting program. The average rotational correlation time was determined as follows,  $\langle \tau_r \rangle = a_1 \tau_1 + (1 - a_1) \tau_2$ , where  $a_i$ s ( $i = 1$  and  $2$ ) and  $\tau_i$ s are the amplitudes and time constants obtained from the bi-exponential fitting of normalized  $r(t)$ .

**8.2.4. DLS Experiment.** The hydrodynamic diameters of the microemulsion droplets of different compositions were measured by using the dynamic light scattering (DLS) technique and by employing a 4 mW He-Ne laser (Nano S, Malvern, France) equipped with a thermostated sample chamber. The scattering intensity data were processed (using the software supplied with the instrument) to obtain the hydrodynamic diameter ( $R_h$ ). The hydrodynamic diameter ( $R_h$ ) of the microemulsion droplets is estimated from the intensity auto-correlation function by using the relation,  $R_h = \frac{k_B T}{3\pi\eta D}$ , where  $k_B T$  denotes, as usual, the Boltzmann constant ( $k_B$ ) times the absolute temperature ( $T$ ) and  $\eta$  the medium viscosity.  $D$  is the

translational diffusion coefficient of the droplet, which was determined from the intensity auto-correlation data.

### 8.3. Results and Discussion

**8.3.1. Distribution of C153 in Microemulsion.** As mentioned in the experimental section, the systems considered in this study contain five major components: SDS/DTAB/n-hexanol/buffer/n-dodecane. Since these systems (microemulsion) are microscopically heterogeneous, the probe molecule (C153) is likely to be distributed among the components constituting the microemulsion at a given composition, which will induce an excitation wavelength dependence of the emission spectrum of C153. Figure 8.1 shows the emission spectra of C153 in water, n-hexanol and heptane along with the one in microemulsion (ME13). While the emission spectrum of C153 in heptane shows vibrational features, the corresponding one in water is devoid of any structure because of stronger solute-solvent dipolar interaction. Also, the emission spectrum in water is noisy due to very low solubility of C153 in water. Interestingly, the peak frequency of the emission spectrum,  $\nu_{em}$ , of C153 in hexanol (static dielectric constant,  $\epsilon_0 \approx 12$ ) is red-shifted by about  $3500 \text{ cm}^{-1}$  relative to that in heptane ( $\epsilon_0 \approx 2$ ) but blue-shifted by only about  $600 \text{ cm}^{-1}$  from that in water ( $\epsilon_0 \approx 80$ ). This indicates that a change from non-polar to moderately polar solvent stabilizes the excited state of a dipolar probe significantly. Further enhancement in  $\epsilon_0$ , however, does not induce a linear increase in the stabilization energy as the solvent density does not differ appreciably.<sup>58-59,63</sup> The emission spectrum of C153 in microemulsion is red-shifted by  $\sim 400 \text{ cm}^{-1}$  compared to that in hexanol, indicating an environment slightly more polar than bulk hexanol.

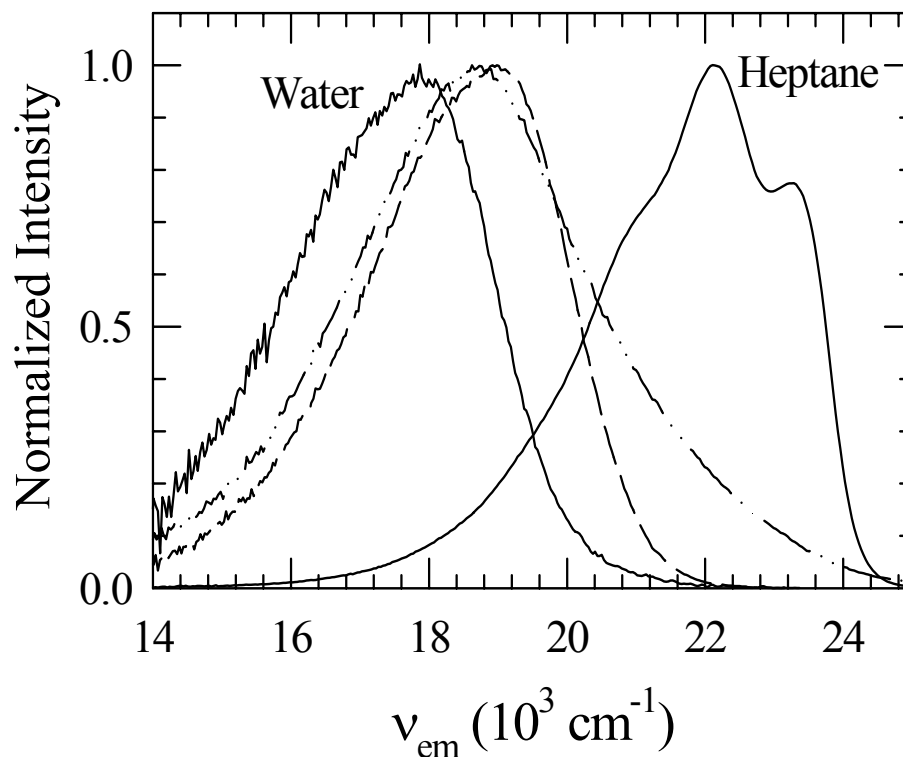


**Fig. 8.1:** Emission spectra of C153 in water (solid line), microemulsion at 0.830 weight fraction of SDS content (dash-dot-dot line), hexanol (dashed line) and heptane (solid line). All emission spectra are obtained after exciting at 409 nm.

When  $\nu_{em}(10^3 \text{ cm}^{-1}) \approx 18.6$  is used as a value for the emission peak frequency of C153 in this microemulsion in a continuum model expression<sup>58,64</sup>, the average static dielectric constant is found to be  $\sim 16$ , which is close to that of cyclohexanone.<sup>60</sup> Interestingly, fluorescence studies of AOT/isooctane/water reverse micelles have also indicated a drastic reduction of average polarity of water<sup>29</sup> and other non-aqueous solvents<sup>63</sup> upon confinement from the bulk values. Note also that the emission spectrum from the microemulsion is relatively broader, indicating the environmental inhomogeneity in the system. Therefore, the emission spectrum from the microemulsion is arising mostly from C153 dissolved in the polar solvent pool trapped inside the reverse micelle-like aggregation. The trapped solvent pool may

also contain some amount of hexanol as well since the latter is partially miscible in water.

Because microscopic heterogeneity is rather generic for these complex systems, the fluorescence emission from the dissolved probe is expected to show significant excitation wavelength dependence. This is shown in Fig. 8.2. Note that the full width at half maxima (FWHM), shown in the upper panel, narrows by about  $500\text{ cm}^{-1}$  as the excitation wavelength changes from 378 nm to 460 nm, whereas the emission peak frequency shows a red shift by about  $1000\text{ cm}^{-1}$  in the same excitation wavelength range. This red-shift together with the shrinking of the band-width of the emission spectrum clearly reflects the distribution of C153 in various solvent components (polar and non-polar) as well as those in different layers in the solvent pool trapped inside the microemulsion droplets. The polarity of the trapped solvent pool affects the fluorescence emission of C153 in a manner similar to that in bulk polar solvents (red shift in the emission spectrum with simultaneous narrowing of the bandwidth as the solvent polarity increases),<sup>60</sup> the observed narrowing of the emission spectrum probably indicates that as the excitation wavelength becomes longer, the C153 population trapped in relatively more ‘homogeneous’ and polar environment is excited more selectively. If this is true then the relative Stokes shift,  $\Delta\Delta\nu = (\nu_{\text{abs}} - \nu_{\text{em}})_{\text{polar}} - (\nu_{\text{abs}} - \nu_{\text{em}})_{\text{nonpolar}}$ <sup>58-60</sup> due to polar interaction *alone* should increase with the increase in the excitation wavelength. A near linearity of  $\Delta\Delta\nu$  with  $\lambda_{\text{exc}}$  is found in the present study<sup>65</sup> that also reflects the spatial distribution of C153 molecules in these microemulsions. Note that similar heterogeneous distribution of environment around a dissolved probe has also been observed earlier in AOT/water reverse micelles<sup>3,26</sup> and ionic liquids<sup>66</sup>.

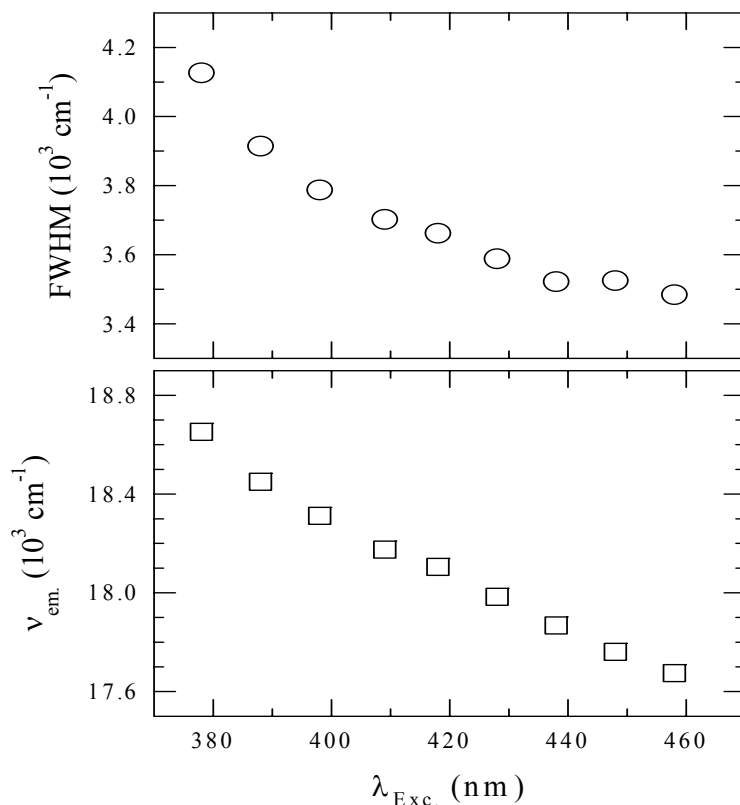


**Fig. 8.2:** Excitation wavelength ( $\lambda_{exc}$ ) dependence of the full width at half maximum (FWHM) of the emission spectrum (*upper panel*) and emission peak frequency (*lower panel*) of C153 in microemulsion (ME13) at 0.830 weight fraction of SDS content. Note that the narrowing of FWHM as  $\lambda_{exc}$  shifts towards lower energy indicates more ‘homogeneous’ environment being probed with larger  $\lambda_{exc}$  inside a catanionic microemulsion droplet at a given composition. The emission peak frequency of C153 in the ME13 microemulsion shows a red shift as the excitation wavelength increases. Note the concomitant narrowing of the fluorescence emission spectrum with the red shift of emission peak frequency. This correlation between the emission peak frequency and the emission bandwidth is similar to earlier studies where emission of C153 in pure polar solvents shows simultaneous narrowing with red shift as the polarity of the solvent increased. This indicates that the relative Stokes shift,  $\Delta\Delta\nu = [\nu_{abs} - \nu_{em}]_{polar} - [\nu_{abs} - \nu_{em}]_{nonpolar}$ , will also increase for this system as a function of  $\lambda_{exc}$ . This may be interpreted as more polar region being probed with larger  $\lambda_{exc}$ . The error associated with the frequency values reported here is  $\pm 250 \text{ cm}^{-1}$ .

**8.3.2. Solubilization of n-Hexanol and Enzymatic Activity:** The activity of enzyme in a microemulsion is substantially influenced by the composition of the interface. Therefore, incorporation of alcohol molecules as co-surfactant at the oil-

water interface is likely to affect the enzyme activity inside the microemulsion droplets. Generally, alcohol molecules with more than four carbon atoms in its alkyl group are known to be a good cosurfactant and hence n-hexanol is a good cosurfactant for the cationic microemulsion studied here.<sup>67-68</sup> The upper panel Fig. 8.3 demonstrates that with the increase of n-hexanol in the microemulsion at a fixed SDS/(SDS+DTAB) weight fraction and buffer content the hydrodynamic diameter of the droplet increases. It is evident from this figure that the increase in n-hexanol leads to a swelling that increases the hydrodynamic diameter of the droplets. Interestingly, the enzymatic activity of horseradish peroxidase (HRP), shown in the same panel, also decreases as the droplet size increases upon addition of n-hexanol. Since the HRP activity in different n-alcohols-citrate buffer saturated solutions is reported to be significantly lower,<sup>45-47</sup> the present results demonstrate that the HRP activity at the interface is strongly reduced by n-hexanol. The following reasons may be responsible for the weakening of the HRP activity at the interface. First, the denaturant property of n-hexanol molecules present at the interface is likely to reduce the activity of the enzyme. Second, there could be a structural transition<sup>43</sup> of the spherical (assumed) microemulsion droplets at higher concentration of n-hexanol to aspherical nanostructures where the confined fluid might not be able to optimally hydrate the enzyme for its activity.

**8.3.3 Polarity of the Confined Fluid and its Dynamics.** As the polarity of a medium plays a crucial role in determining the reaction rate and yield, one would like to know the average polarity of the polar solvent inside the pool of the microemulsion droplets. Also, since the polarity of a fluid and its structure determines the time scale of the environment reorganization around an excited solute, the study of solvation dynamics may supply useful information for correlating the medium dynamics with the enzymatic activity of HRP in the cationic microemulsion. Solvation dynamics of laser excited C153 dissolved in these microemulsions have been measured with different hexanol content (20.2-30%, Table 8.1b).

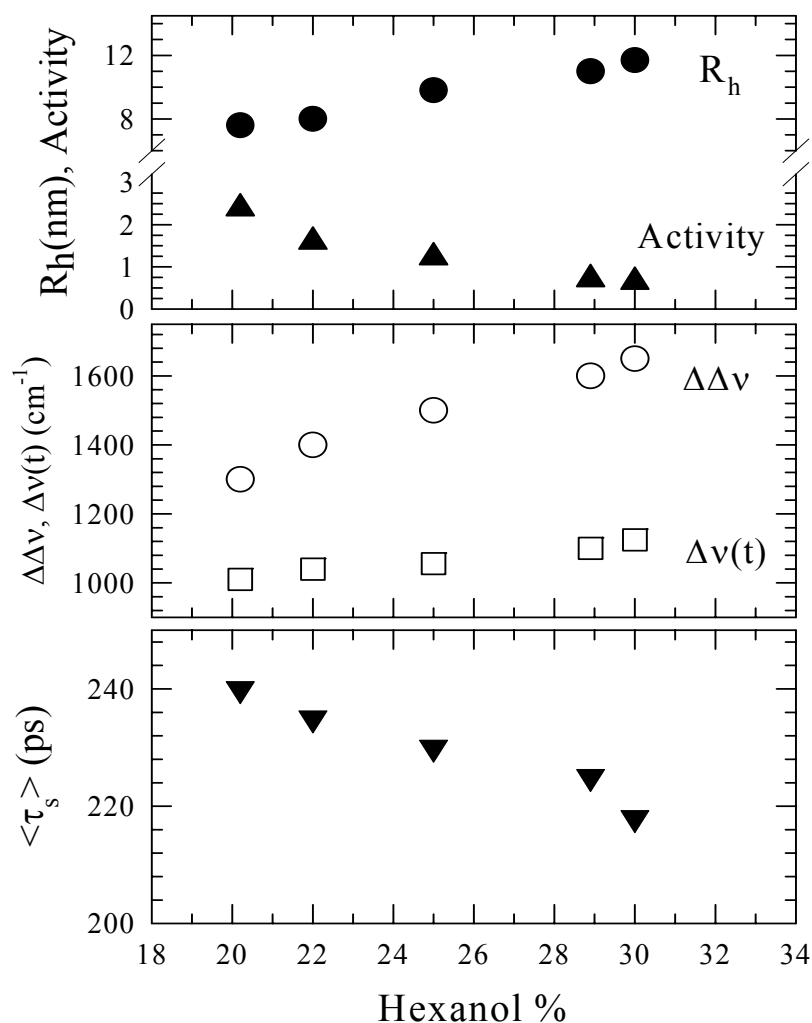


**Fig. 8.3:** Variation of hydrodynamic diameter,  $R_h$ , enzyme activity of horseradish peroxidase (Activity), relative Stokes shift,  $\Delta\Delta v$ , Stokes shift observed in our time resolved experiments,  $\Delta v(t) = v(0) - v(t)$ , and average solvation time,  $\langle \tau_s \rangle$ , as a function of hexanol concentration for C153 in microemulsion at 0.92 weight fraction of SDS and 22 % (w/w) of buffer content. Note that at various hexanol concentrations, the hydrodynamic diameter (solid circle) and enzyme activity (solid triangle) are shown in the *upper panel*, the relative Stokes shift (open circle) and Stokes shift from time resolved experiments (open squares) in the *middle panel* and the average solvation time in the *lower panel*. Note that the enzymatic activity data have been taken from Ref. 34.

The time dependent Stokes shift,  $\Delta v(t)$ <sup>69</sup>, observed for these samples are shown as a function of hexanol content in the middle panel (open squares) of Fig.8.3. The

relative Stokes shifts,  $\Delta\Delta\nu$ , obtained for these systems from the steady state absorption and fluorescence emission measurements are also shown in the same panel. The magnitudes of both  $\Delta\Delta\nu$  and  $\Delta\nu(t)$  for these microemulsions indicate that the average dielectric constants of the confined environments of the microemulsion droplets are in the range of 10–20.<sup>60</sup> Note that the molecular dynamics simulations<sup>51</sup> and experimental studies<sup>3,63</sup> of AOT/water reverse micelles have also indicated similar polarity of the confined water pool.

The decay of  $S(t)$  in all these systems are found to be a bi-exponential function of time. It is likely that fast components with time scales shorter than 15 ps might have been missed due to the limited time resolution employed in our experiments. We will come back to this point later. However, this limitation is not likely to affect the qualitative understanding of the average solvation time scales in these complex environments. The average solvation time,  $\langle\tau_s\rangle$ , obtained from the time resolved measurements for these systems are shown as a function of n-hexanol content in the bottom panel of Fig. 8.3. Note that the variation in  $\langle\tau_s\rangle$  is small (within 220–240 ps) for the change in droplet diameter from 8 to 12 nm. Similar weak dependence of  $\langle\tau_s\rangle$  on droplet size has been observed earlier in quaternary microemulsions<sup>9,70</sup>. Since hexanol is miscible with dodecane, the solvation dynamics may derive a slow component from the preferential solvation of the excited probe. Such a study in binary mixtures of hexanol/isooctane mixture reports  $\langle\tau_s\rangle$  in the nano-second range<sup>70</sup>. As dodecane is larger in size than isooctane, the average solvation time for hexanol/dodecane binary mixtures is also expected to be at least in the same range. Therefore, the time scales (220 - 240 ps) are likely to be associated with solvation dynamics in these catanionic micromulsions. However, even within this small range of diameter change  $\langle\tau_s\rangle$  shows a very small decrease. This is consistent with the current understanding of solvation dynamics in confined media, where solvent molecules are believed to be more mobile in a larger solvent pool.<sup>1-29</sup> Nevertheless, the average solvation time found for these systems is in the expected range for microemulsions<sup>2-3,7</sup> and the dielectric constant of water decreases drastically upon

confinement in the microemulsion droplet. Also, the tetrahedral hydrogen bonding network structure of water is partially modified in trapped water within the nano-sized droplets. This, in turn, is likely to modify the bulk de-mixing behavior of water-hexanol mixtures. The weak dependence of average solvation time ( $\langle\tau_s\rangle$ ) on hexanol concentration may, however, arise due to the non-detection of the ultrafast dynamics of the confined polar pool in these microemulsions. It might be that nearly all of the initial fast energy relaxation via the collective solvent mode (small amplitude motion of the hydrogen bonded network in water) is missed due to the limited time resolution employed in our experiments, leaving only the diffusive dynamics at relatively longer time to be detected. Since water constitute an important component (as buffer) in all the microemulsions studied, there is a definite possibility that we have missed *completely* the ultrafast dynamics that might have been present in these catanionic reverse micelles. The analyses by using the Fee-Maroncelli method<sup>61</sup> seems to suggest that the missing portion could be as large as 50% of the total decay of the solvent response function measured for all the microemulsions considered here. Naturally therefore, the average solvation time ( $\langle\tau_s\rangle$ ) shows a weak dependence or even *insensitivity* to the size of the microemulsion droplets.

**8.3.4. Influence of Surfactant and Buffer on the Droplet Size and Dynamics.** We have varied the weight fraction of SDS [i.e., SDS/(SDS+DTAB)] from 0.830% to 0.9221% (Table 8.1a) to examine its effect on the HRP enzyme activity. The HRP activity has been found to increase with the increase in SDS content.<sup>34</sup> The effect of SDS on the droplet size is shown in the upper panel of Fig. 8.4. Note that the dependence of droplet size and its correlation with the HRP activity is similar to what has been found when n-hexanol concentration was varied (activity inversely proportional to droplet size). Also note that the HRP activity is the maximum, when the droplet size is minimum (~8 nm in the present study). With the increase in SDS, cosurfactant (n-hexanol in this case) should be gradually replaced by it in the interface. This would enhance the electrostatic attraction between the counter charged surfactants leading to a decrease in the total surface area. As a result, the

percolation of n-hexanol into the confined solvent pool should also decrease, which, in turn, would enhance the activity of HRP. This is probably the reason for the increase in HRP activity with the increase in SDS content (filled triangles in the upper panel of Fig. 8.4). The polarity of the solvent pools inside the microemulsion droplets has also been probed and presented in the middle panel of Fig. 8.4. Clearly,  $\Delta\Delta\nu$  and  $\Delta\nu(t)$  are again similar in magnitudes to those presented in Fig. 8.3. The decrease in both these quantities upon increasing the SDS content reflects the reduced pool size and correlates well with DLS results. The average solvation time,  $\langle\tau_s\rangle$ , presented in the bottom panel of Fig. 8.4, shows a small increase with the increase in SDS content. It is interesting, however, that the average solvation time changes very little upon increasing the SDS fraction from 0.83 to 0.92, while the hydrodynamic diameter reduces by a factor of  $\sim 3$  in the same SDS range (upper panel). Since successive addition of SDS increasingly ejects out n-hexanol from the interstitial spaces and brings the other surfactant molecules with counter charge closer through the electrostatic attraction, the droplet size becomes smaller. Here also the estimated missing component of the ultrafast dynamics ranges between 45 – 55 %. This may be one of the reasons for the observed weak dependence of average solvation time on SDS fraction. The effects of buffer (water) on the droplet size and solvation dynamics are shown in Fig. 8.5. The enzyme activity is known to show the maximum activity when it is properly hydrated.<sup>71-73</sup> Since the increase in buffer concentration is in line with an increased water content of the medium, the enzyme activity is expected to increase. This is indeed the result, which is shown in the upper panel of Fig. 8.5. However, the droplet size decreases by approximately a factor of 2 upon increasing the buffer from 10 to 15 % and then becomes almost insensitive to further increase in buffer concentration. As the buffer content increases, the relative amount of hexanol at the interface decreases, even though the critical micellar concentrations for all the surfactants in the solution are maintained.

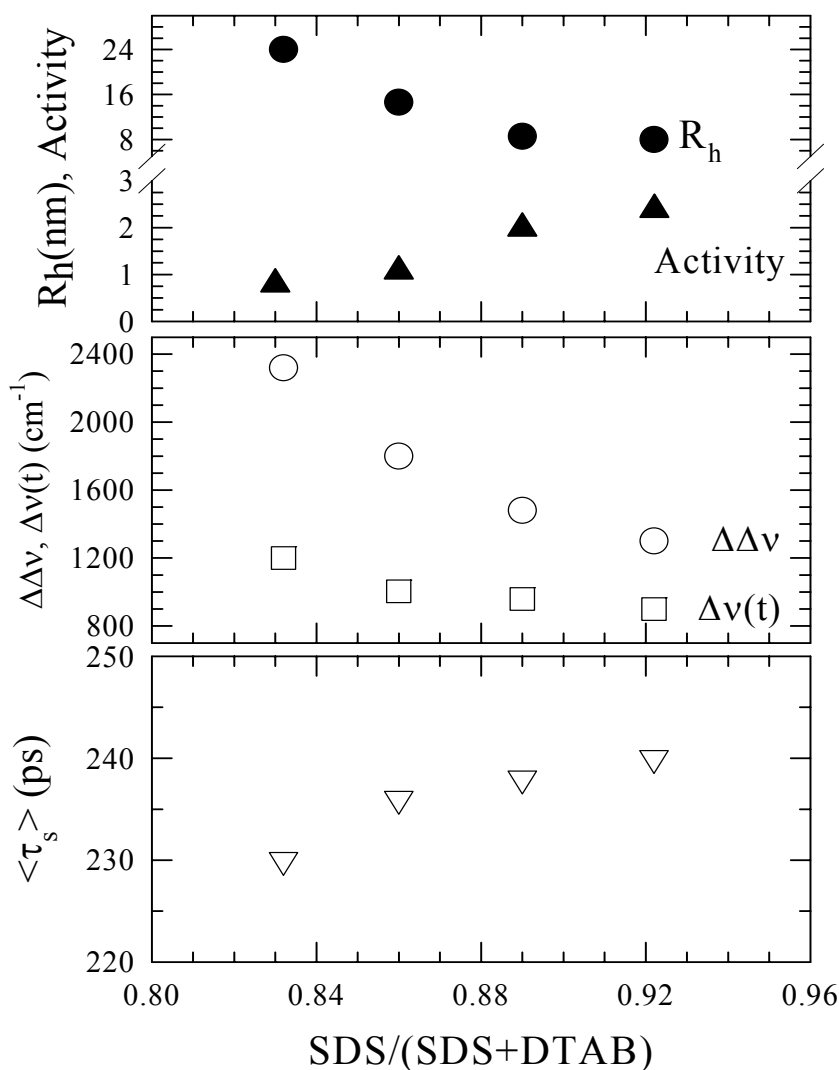


**Fig. 8.4:** Effects of SDS weight fraction (Table 8.1a) on the hydrodynamic diameter,  $R_h$ , enzyme activity of horseradish peroxidase (Activity), relative Stokes shift,  $\Delta\Delta v$ , Stokes shift observed in our time resolved experiments,  $\Delta v(t) = v(0) - v(t)$ , and average solvation time,  $\langle\tau_s\rangle$ , for C153 in microemulsion at 22.0 and 20.2 % weight fractions of buffer and hexanol, respectively. The other representations remain the same as in Fig. 8.3. Enzymatic data are from Ref. 34. For details, see text.

The dilution of cosurfactant (n-hexanol) is actually decreasing its localization into the reverse micelle film. This is responsible for the initial decrease in the hydrodynamic diameter of the droplets. The decrease in n-hexanol concentration

assists HRP activity by both reducing the probability of alcohol poisoning of the enzyme and also supplying more number of water molecules for the enzyme to hydrate properly. The buffer concentration dependencies of the relative Stokes shift,  $\Delta\Delta\nu$ , and the average solvation time,  $\langle\tau_s\rangle$ , are shown respectively in the middle and bottom panels of Fig. 8.5. As expected, the magnitude of  $\Delta\Delta\nu$  decreases as the droplet size is reduced. The time dependent Stokes shift,  $\Delta\nu(t)$ , also shows a similar behavior. The magnitudes of  $\Delta\Delta\nu$  and  $\Delta\nu(t)$  again suggest that the average polarity (in terms of  $\epsilon_0$ ) inside these cationic microemulsions ranges between 10 – 20. The amplitude of the missing component of the ultrafast dynamics is estimated to be in the range of 50 – 60%. As in the earlier cases, this may be the reason for the observed weak dependence of the average solvation time on the buffer concentration and hence, on the size of the microemulsion droplets.

**8.3.5. Solute Dynamics: Time-resolved Fluorescence Anisotropy Study.** The time dependent fluorescence anisotropy decay of C153 in these cationic microemulsions has been measured at the emission peak (~535 nm) for different microemulsions. As already mentioned, the decays are found to be bi-exponential functions of time, giving rise to two rotational time constants,  $\tau_1$  and  $\tau_2$ , for these microemulsions. Quite understandably, the short time constant, which is associated with the rotational motion of the dissolved probe (C153), should become shorter as the droplet size increases and the environment becomes less rigid. The long one, on the other hand, represents the global motion of the droplet and, therefore, should become longer as the droplet size increases. The values of the decay parameters are given in Table 8.2 for two terminal compositions for each series summarized in Table 8.1.

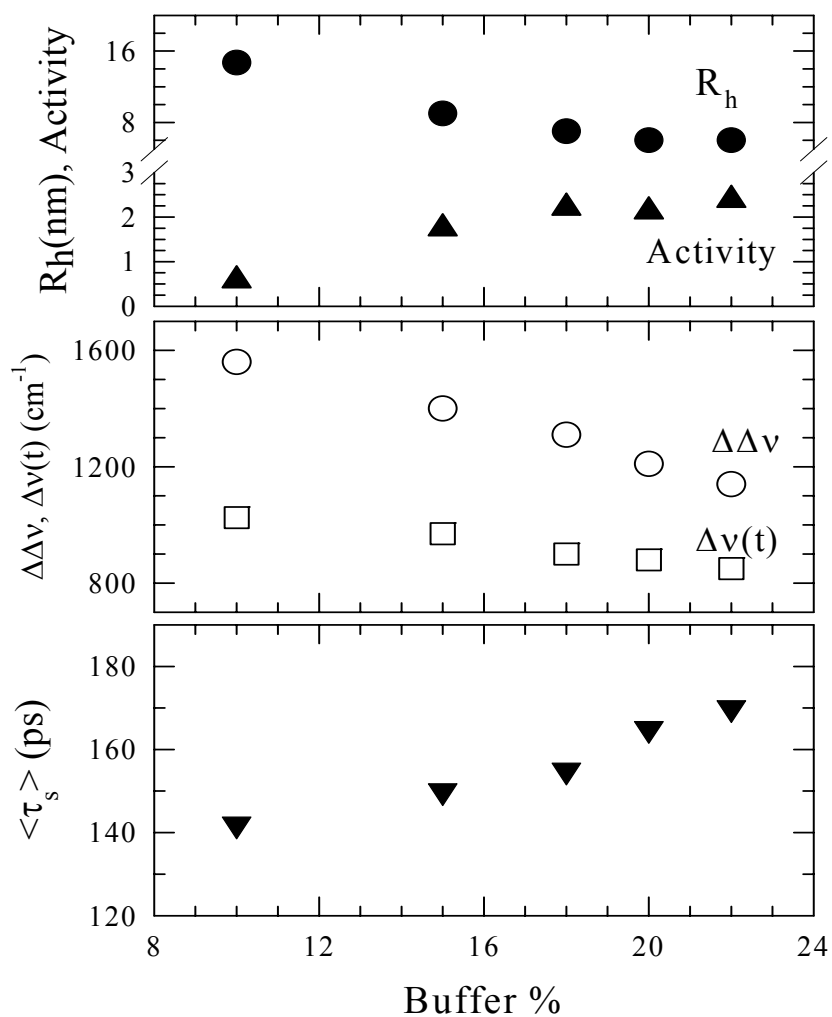


**Fig. 8.5:** Effects of buffer composition (Table 8.1c) on the hydrodynamic diameter,  $R_h$ , enzyme activity of horseradish peroxidase (Activity, Ref. ??), relative Stokes shift,  $\Delta\Delta v$ , Stokes shift observed in our time resolved experiments,  $\Delta v(t) = v(0) - v(t)$ , and average solvation time,  $\langle \tau_s \rangle$ , for C153 in microemulsion at 0.9221 and 20.2 weight fractions of SDS and buffer, respectively. The other representations remain the same as in Fig. 8.3.

**Table 8.2: Anisotropy decay parameters for C-153 in microemulsions for extreme compositions for SDS, Hexanol and Buffer excited at 409 nm. Corresponding hydrodynamic diameter ( $R_h$ ) are also shown. Compositions of the microemulsions are mentioned in Table 8.1.**

Microemulsion Samples	$R_h$ (nm)	$a_1$	$\tau_1$ (ps)	$a_2$	$\tau_2$ (ps)	$\langle\tau_r\rangle$ (ps)
ME-13	24	0.70	25	0.30	447	152
ME-10	8	0.66	26	0.34	348	135
ME-17	12	0.66	28	0.34	419	161
ME-21	16	0.67	29	0.33	389	148

Note that in these systems the anisotropy decay associates with a fast component,  $\tau_1$ , of  $\sim 30$  ps ( $\sim 70\%$ ) and a slow component,  $\tau_2$ , of  $\sim 400$  ps ( $\sim 30\%$ ). These well-separated time scales are indicative of two types of rotational motions involving C153, which are decoupled from each other. This is the typical behavior of our fluorescence anisotropy study for cationic microemulsions at all compositions, which were seen earlier in reverse micelles<sup>2-3</sup> and also in quaternary microemulsions.<sup>70</sup> The average rotational correlation time,  $\langle\tau_r\rangle$ , has been determined for all these cationic microemulsions and is presented in Fig. 8.6. The upper panel of Fig. 8.6 indicates that  $\langle\tau_r\rangle$  increases as the n-hexanol concentration increases. We have already seen (Fig. 8.3) that the hydrodynamic diameter of the droplets increases with the n-hexanol concentration. Therefore, the fluorescence anisotropy results for these microemulsions correlate well with the DLS results. However,  $\langle\tau_r\rangle$  does not show a linear increase with n-hexanol concentration as observed for droplet diameter. This is because the swelling of the droplet affects the two time constants in a manner opposite to each other. As expected, the short time constant dominates at small droplet size whereas the longer time constant dictates the magnitude of  $\langle\tau_r\rangle$  at larger droplet diameters. The variation of  $\langle\tau_r\rangle$  with SDS concentration and buffer percentage in the micro-emulsions is also shown respectively in the middle and bottom panels of Fig. 8.6. The average rotational correlation times for these systems also correlate well with the DLS data.

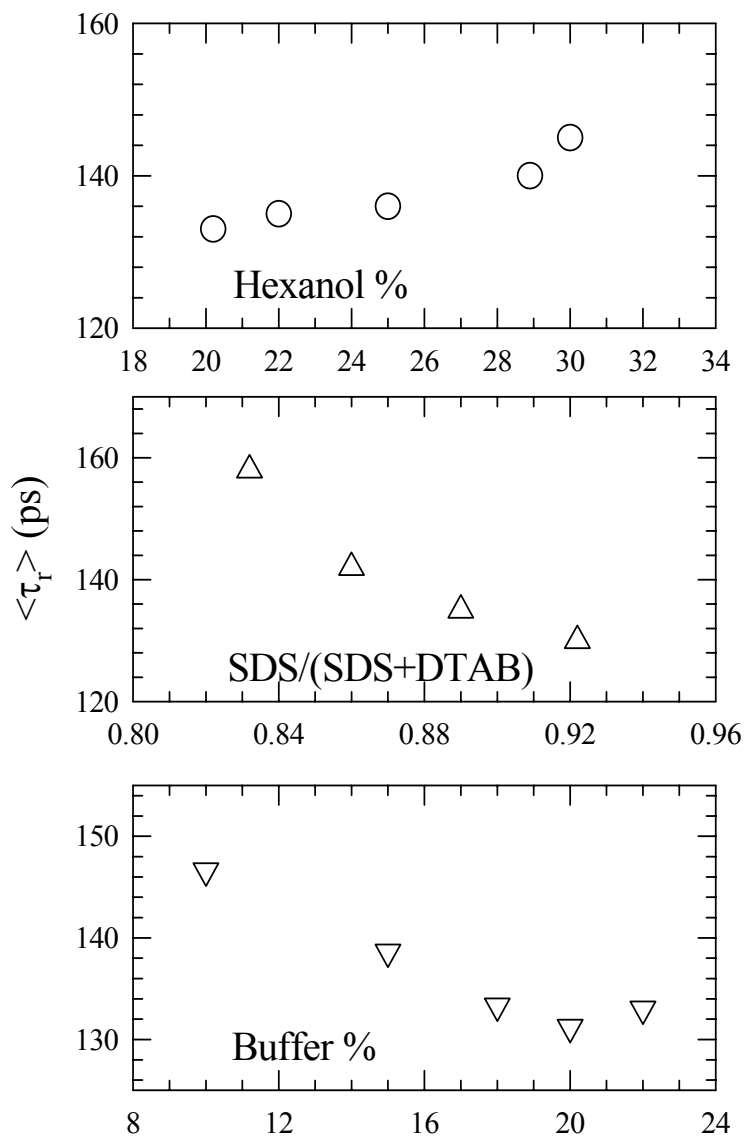


**Fig. 8.6:** Upper panel: Hexanol composition (Table 8.1*b*) dependence of the average rotational time,  $\langle \tau_r \rangle$ , of C153 in microemulsions at 0.92 weight fraction of SDS. Middle panel: Variation of  $\langle \tau_r \rangle$  for C153 with SDS weight fraction at 22.0 % weight fraction of buffer. Lower panel: Dependence of  $\langle \tau_r \rangle$  on buffer concentration (in percentage) in microemulsion at 0.9221 weight fraction of SDS. Note that in all cases the anisotropy decay has been found to be bi-exponential with time and  $\langle \tau_r \rangle$  has been obtained by using the formula as discussed in the text.

It is interesting to observe that while the longest  $\langle \tau_r \rangle$  corresponds with the lowest HRP activity and the smallest  $\langle \tau_s \rangle$  for microemulsions obtained by varying the

hexanol concentration, the maximum activity and the largest  $\langle\tau_s\rangle$  occurs at SDS fraction and buffer percentage where  $\langle\tau_r\rangle$  is the lowest. This correlation between the enzyme activity and, the average rotational and solvation times probably indicates that the enzyme activity is related with the slow dynamical modes of the medium. This is however in contrast to what has observed for protein functionality in bulk water where slowing down of hydration dynamics has led to the suppression of enzyme activity<sup>74</sup>. Another feature to note in Fig.8.6 that the average rotational times for C153 in all these microemulsions fall in the range of 120 – 160 ps where the underlying anisotropy decays are bi-exponential in time. Time resolved anisotropy studies of C153 in bulk polar solvents have shown that anisotropy decays are generally non-exponential and possess a fast component with time constant  $\sim 20$  ps for solvents with values of  $\epsilon_0$  in the range 10 – 20 and a longer time constant in the range of 100 – 200 ps (particularly for a few medium-sized alcohols)<sup>75</sup>. The representative data in Table 8.2 also indicate the presence of fast components with similar time constants for C153 in microemulsions at different compositions. However, the fast time constant remains insensitive to the size of the microemulsions. Similar insensitivity to droplet size has also been observed earlier with a different dipolar probe in quaternary microemulsions<sup>70</sup>. As analyzed for average solvation time, this may also arise due to the missing of a component in  $r(t)$  faster than our detection limit. The long time constant scales approximately with the size of the hydrodynamic diameter of the microemulsions.<sup>76</sup> Therefore, the average rotational correlation times are most likely those of C153 trapped inside the microemulsions.

#### **8.4. Conclusion**

Enzymatic activity studies are a valuable tool to investigate local structures and compositions in confined media. However, these studies are not detailed enough to reveal local polarities and dynamics of the nano-droplets in the highly complex catanionic SDS/DTAB reverse microemulsion systems. In the present chapter we are able to generate some further understanding of the restricted environment/nanoenvironment that correlates with the previous result of HRP activity<sup>34</sup>. It is

found that the activity of HRP becomes the maximum when the dynamical modes of the environment become the slowest. We believe that n-hexanol increases the interfacial fluidity of the microemulsion, hence its percolation. The other experimental findings also support this model along with the enzymatic activity study. So, these systems can be used to get controlled enzyme activity, as we can monitor the internal environment by changing the fluidity. As a result we think that we can now specifically design useful media for organic synthesis reactions, as the polarity of the core pseudo-phase can be externally monitored. Our systems contain a cationic surfactant (DTAB), which normally has an inhibition influence on the enzyme activity. But the cationic-anionic interaction suppresses this inhibition effect, which also suggests that the DTAB molecules are not free in these systems, but located in the interfacial film of the microemulsions. Therefore, further studies are required to fully explore various aspects of these mixed surfactant microemulsions.

## References and Notes

1. Levinger, N. E. *Science*, **2002**, 298, 1722.
2. Bhattacharyya, K. *Acc. Chem. Res.* **2003**, 36, 95 and references therein.
3. Ghosh, S.; Mandal, U.; Adhikari, A.; Dey, S.; Bhattacharyya, K. *Int. Rev. Phys. Chem.* **2007**, 26, 421.
4. Luisi, P. L.; Straub, B. E.; Eds., *Reverse Micelles: Biological and Technological Relevance to Amphiphilic Structures in Apolar Media*, Plenum: New York, **1984**.
5. De, T.; Maitra, A.; *Adv. Colloid Interface Sci.*, **1995**, 59, 95.
6. Baruah, B.; Roden, J. M.; Sedgwick, M.; Correa, N. M.; Crans, D. C.; Levinger, N. E. *J. Am. Chem. Soc.* **2006**, 128, 12758
7. Willard, D. M.; Riter, R. E.; Levinger, N. E. *J. Am. Chem. Soc.* **1998**, 120, 4151.
8. Harpham, M. R.; Ladanyi, B.; Levinger, N. E. *J. Phys. Chem. B.* **2005**, 109, 16891
9. Corbeil, E. M.; Levinger, N. E. *Langmuir* **2003**, 19, 7264.
10. Correa, N. M.; Levinger, N. E. *J. Phys. Chem. B.* **2006**, 110, 13050.
11. Rosenfeld, D. E.; Schmuttenmaer, C. A. *J. Phys. Chem. B* **2006**, 110, 14309.
12. Vanables, D. S.; Huang, K.; Schmuttenmaer, C. A. *J. Phys. Chem. B* **2001**, 105, 9132.
13. Boyd, J. E.; Briskman, A.; Sayes, C. M.; Mittelman, D. A.; Colvin, V. J. *Phys. Chem. B* **2002**, 106, 6346
14. Boyd, J. E.; Briskman, A.; Colvin, V. L.; Mittleman, D. M. *Phys. Rev. Lett.* **2001**, 87 147401/1.
15. Zhong, Q.; Steinburst, D. A.; Carpenter, E. E.; Owrutsky, J. C. *Langmuir* **2002**, 18, 7401.
16. Bursing, H.; Ouw, S.; Kundu, P.; Vohringer, P. *Phys. Chem. Chem. Phys.* **2001**, 3, 2378.
17. Pileni, M. P.; Ed. *Structure and Reactivity in Reverse Micelles*; Elsevier: Amsterdam, **1989**; vol. 65.

18. Cho, C. H.; Chung, M.; Lee, J.; Nguyen, T.; Singh, S.; Vedamuthu, M.; Yao, S.; Zhu, S. B.; Robinson, G. W. *J. Phys. Chem.* **1995**, *99*, 7806.
19. Lundgren, J. S.; Heitz, M. P.; Bright, F. V. *Anal. Chem.* **1995**, *67*, 3775.
20. Das, S.; Datta, A.; Bhattacharyya, K. *J. Phys. Chem. A* **1999**, *101*, 3299.
21. Sarkar, N.; Das, K.; Datta, A.; Das, S.; Bhattacharyya, K. *J. Phys. Chem.* **1996**, *100*, 10523.
22. Datta, A.; Mandal, D.; Pal, S. K.; Bhattacharyya, K. *J. Phys. Chem. B* **1997**, *101*, 10221.
23. Riter, R. E.; Willard, D. M.; Levinger, N. E. *J. Phys. Chem. B* **1998**, *102*, 2705.
24. Moilanen, D. E.; Levinger, N. E.; Spry, D. B.; Fayer, M. D. *J. Amer. Chem. Soc.* **2007** *129*, 14311.
25. Tan, H-S. ; Piletic, I. R.; Fayer, M. D. *J. Chem. Phys.* **2005**, *122*, 174501.
26. Piletic, I. R.; Tan, H-S.; Fayer, M. D. *J. Phys. Chem. B* **2005**, *109*, 21273.
27. Faeder, J.; Ladanyi, B. M. *J. Phys. Chem. B* **2001**, *105*, 11148.
28. Faeder, J.; Ladanyi, B. M. *J. Phys. Chem. B* **2000**, *104*, 1033.
29. Bhattacharyya, K. ; Bagchi, B. *J. Phys. Chem. A* **2000**, *104*, 10603.
30. Salaniwal, S.; Cui, S. T. ; Cochran, H. D. ; Cummings, P. T. *Langmuir*, **2001**, *17*, 1773.
31. Salaniwal, S.; Cui, S. T. ; Cochran, H. D. ; Cummings, P. T. *Langmuir*, **2001**, *17*, 1784.
32. Salaniwal, S.; Cui, S. T. ; Cochran, H. D. ; Cummings, P. T. *Langmuir*, **1999**, *15*, 5188.
33. Senapati, S. ; Keiper, J. M. ; DeSimone, J. M. ; Wignall, G. D. ; Melnichenko, Y. B. ; Frielinghaus, H. ; Berkowitz, M. L. *Langmuir*, **2002**, *18*, 7371.
34. Mahiuddin, S.; Renoncourt, A.; Bauduin, P.; Touraud, D.; Kunz, W. *Langmuir* **2005**, *21*, 5259.
35. Shi, H. T.; Qi, L.M.; Ma, J. M., Cheng, H. M. *Chem. Commun.* **2002**, 1704.
36. Shi, H. T.; Qi, L.M.; Ma, J. M., Cheng, H. M.; Zhu, B. Y. *Adv. Mater.* **2003**, *15*, 1647.

37. Shi, H. T.; Wang, X. H.; Zhao, N. N.; Qi, L.M.; Ma, J. M., *J. Phys. Chem. B* **2006**, *110*, 748.
38. López-Quinteta, M. A.; Tojo, C.; Blanco, M. C.; García-Rio, L.; Leis, J. R. *Curr. Opin. Colloid Interface Sci.* **2004**, *9*, 264.
39. Khan, A.; Marques, E. In *Specialist Surfactant*; Robb, I., Ed.; Blackie Academic and Professional: London, 1997, Chapter 3 and references therein.
40. Jokela, P.; Jonsson, B.; Khan, A. *J. Phys. Chem.* **1987**, *91*, 3291.
41. Li, X.; Ueda, K.; Kunieda, H. *Langmuir* **1999**, *15*, 7973.
42. Li, X.; Kunieda, H. *Curr. Opin. Colloid Interface Sci.* **2003**, *8*, 327 and references therein.
43. Abécassis, B.; Testard, F.; Arleth, L.; Hansen, S.; Grillo, I.; Zemb, T. *Langmuir*, **2006**, *22*, 8017.
44. Pinna, C.; Bauduin, P.; Touraud, D.; Monduzzi, M.; Ninham, W. B.; Kunz, W. *J. Phys. Chem. B* **2005**, *109*, 16511.
45. Bauduin, P.; Touraud, D.; Kunz, W.; Savelli, M.P.; Ninham, B.W. *J. Colloid Interface Sci.* **2005**, *292*, 244.
46. Cinelli, S.; Onori, G.; Santucci, A. *Colloids Surf. A. Physicochem. Eng. Aspects* **1999**, *160*, 3.
47. Shimizu, S.; Shimizu, K. *J. Am. Chem. Soc.* **1999**, *121*, 2387.
48. Pal, S. K.; Peon, J.; Bagchi, B.; Zewail, A. H. *J. Phys. Chem. B.* **2002**, *106*, 12376.
49. Pal, S. K.; Zewail, A. H. *Chem. Rev.* **1999**, *104*, 2099.
50. Halder, M.; Mukherjee, P.; Bose, S.; Hargrove, M. S.; Song, X.; Petrich, J. *W. J. Chem. Phys.* **2007**, *127*, 055101.
51. Balasubramanian, S.; Bagchi, B. *J. Phys. Chem. B* **2001**, *105*, 12529.
52. Senapati, S.; Chandra, A. *J. Phys. Chem. B* **2001**, *105*, 5106.
53. Nandi, N.; Bagchi, B. *J. Phys. Chem. B* **1997**, *101*, 10954.
54. Nandi, N.; Bhattacharyya K.; Bagchi, B. *Chem. Rev.* **2000**, *100*, 2013.
55. Prakash, M. K.; Marcus, R. A. *J. Phys. Chem. B* **2008**, *112*, 399.
56. Abécassis, B.; Testard, F.; Arleth, L.; Hansen, S.; Grillo, I.; Zemb, T. *Langmuir*, **2007**, *23*, 9983.

57. Das, T. K.; Mazumdar, S. *Eur. J. Biochem.* **1995**, *227*, 823.
58. Biswas, R.; Lewis, J. E.; Maroncelli, M. *Chem. Phys. Lett.* **1999**, *310*, 485.
59. Lewis, J. E.; Biswas, R.; Robinson, A. G.; Maroncelli, M. *J. Phys. Chem. B.* **2001**, *105*, 3306.
60. Horng, M.L.; Gardecki, J. A.; Papazyan, A.; Maroncelli, M. *J. Phys. Chem.* **1995**, *99*, 17311.
61. Fee, R. S. ; Maroncelli, M. *Chem. Phys.* **1994**, *183*, 235.
62. Sen, S.; Dutta, P.; Sukul, D.; Bhattacharyya, K. *J. Phys. Chem. A*, **2002**, *106*, 6017.
63. Biswas, R. (unpublished data).
64. The following correlation is used to estimate the dielectric constant of ME13 from the emission frequency of C153:  

$$\nu_{\text{em}}(10^3 \text{ cm}^{-1}) = 23.12 - 5.06[(\epsilon_0 - 1)/(\epsilon_0 + 2)] - 1.5 \left[ (n^2 - 1)/(n^2 + 2) \right],$$
 where refractive index ( $n$ ) of the medium is assumed to be that of bulk water. For details, see Refs. 58 and 59.
65. In order to calculate  $\Delta\Delta\nu$  for a probe in a given medium, one needs the absorption and emission peak frequencies of that probe in a non-polar bulk solvent and the absorption peak frequency of the probe dissolved in that medium. These values remain unchanged during the excitation wavelength dependence study of emission peak frequency of the probe in that medium. Consequently, the linear dependence of emission peak frequency on excitation wavelength ( $\lambda_{\text{exc}}$ ) is reflected in the correlation of  $\Delta\Delta\nu$  versus  $\lambda_{\text{exc}}$ .
66. Jin, H.; Li, X.; Maroncelli, M. *J. Phys. Chem. B* **2007**, *111*, 13473.
67. Clause, M.; Nicolas-Morgantini, L.; Zradba, A.; Touraud, D. *Water-ionic Surfactant-Alkanol-Hydrocarbon System: Influence of Certain Constitution and Composition Parameters upon the Realm-of Existence and Transport Properties of Microemulsion Type Media*. Surfactant Science Series 24 (Microemulsion Systems), **1987**, p. 15-66.
68. Ray, S.; Moulik, S. P. *J. Colloid Interface Sci.* **1995**, *173*, 28.

69. The time dependent Stokes shift is calculated as follows:  $\Delta\nu(t) = \nu_{t=0}^{\text{obs}} - \nu_{t=\infty}$ .
- That is, the difference between the emission peak frequencies at  $t=0$  as observed in our experiment and that after the solvent relaxation is complete.
70. Hazra, P.; Chakrabarti, D.; Chakraborty, A.; Sarkar, N. *Chem. Phys. Lett.* **2003**, *382*, 71.
71. Avramiotis, A.; Papadimitriou, V.; Cazianis, C. T.; Xenakis, A. *Colloids Surf. A: Physicochem. Eng Aspects* **1998**, *144*, 295.
72. Rees, G. D.; Robinson, B. H. *Biotechnol. Bioeng.* **1995**, *45*, 344.
73. Ayala, G.; Mendoza-Hernandez, G. *Biochem. Int.* **1990**, *22*, 717.
74. Pal, S. K.; Peon J.; Zewail, A. H. *Proc. Natl. Acad. Sc. (USA)* **2002**, *99*, 15297.
75. Horng, M.L.; Gardecki, J. A. ; Maroncelli, M. *J. Phys. Chem.* **1997**, *101*, 1030.
76. As the compositions of the microemulsions are different and hence the extent of solute-medium coupling differs, the scatters in the data (between ME-17 and ME-21) are expected.

## Chapter 9

### Concluding Remarks and Future Problems

In this Thesis we have studied medium effects on excited state intramolecular charge transfer reaction in electrolyte solutions, binary mixtures and confined environments using fluorescence steady state and time resolved spectroscopy. Solvent dynamical as well as structural effects that coupled with the reactive mode have been explored by following the reaction rate and equilibrium constants. Since concluding remarks are provided at the end of each of the chapters, we refrain from adding a separate chapter containing the general conclusion. However, there remain several interesting problems that should be studied in order to enhance and/ or compliment the understanding of medium effects on TICT reaction which has been generated by the work presented here. We therefore take this opportunity to discuss several interesting unsolved problems that may be studied in future.

#### **9.1. Anion dependence on excited state intramolecular charge transfer reaction**

Effect of electrolyte concentration and size of cations on charge transfer reaction has been discussed in chapter 2 and 3. Anions are known to interact differently with the solvent than the positively charged ions<sup>1</sup>. Anion dependence of the electrolyte on charge transfer reactions may therefore be interesting. One would also like to investigate what kind of association between an ion and a TICT molecule leads to the change in reaction rate. Computer simulation studies in close conjunction with experiments can be helpful to bring out the microscopic details of the reactant-ion interactions and the subsequent modification of the reaction rate.

## **9.2. Non-monotonic electrolyte concentration dependence of reaction rate by ZH theory**

We have applied Zwan-Hynes theory <sup>2-3</sup> to calculate reaction rate for moderate to high electrolyte concentration in ethyl acetate and a very good agreement with the theory and experiments have been observed (Chapter 2). Interestingly, at very low electrolyte concentrations a strong non-monotonic electrolyte concentration dependence of reaction rate in ethyl acetate and relatively a weaker dependence in acetonitrile and ethanol (Chapter 3) have been found. It could be interesting to explore whether the ZH theory could reproduce the observed non-monotonic electrolyte concentration dependence. This might be a possibility since the electrolyte friction calculated by the ZH theory depends strongly on the average solvation time. Since the average solvation time is larger in very dilute electrolyte solutions where the dissociation (of the electrolyte) is nearly complete, the friction would be large in this limit, leading to a decrease in the rate constant. If the average solvation time depends non-monotonically on electrolyte concentration then ZH theory would also be predicting a non-monotonic dependence. This should be tested against experiments.

## **9.3. Exploring non-Arrhenius temperature dependence of the TICT reaction rate**

We have observed non-Arrhenius temperature dependence of the TICT reaction rate at higher electrolyte concentration in ethyl acetate at higher temperature. This is probably due to rapid change in dielectric constant of the solution with change in temperature. However, this is purely speculative in the absence of any conductometric and dielectric relaxation studies of ethyl acetate containing high LiClO<sub>4</sub> concentrations at various temperatures which should be carried out to understand it properly. The activation energy found in pure ethanol is about  $1.5 k_b T$  less than the average of those in pure ethyl acetate and acetonitrile. Whether this difference in activation energy between the polar protic and polar aprotic solvents is

due to the H-bonding cannot be ascertained from the present study as answer to this question requires further studies with several other associating solvents.

#### **9.4. Interplay between hydrophobic and H-bonding interactions in TBA-Water binary mixtures**

Excited state intramolecular charge transfer reaction in TBA-Water mixtures has already been discussed in chapter 6. We have seen there the subtle interplay between hydrophobic and H-bonding interactions with varying compositions. But a total understanding of reaction rates with varying composition is not complete due to limited time resolution available to us. Since slow solvation dynamics due to preferential solvation in these binary mixtures is likely to play an important role in determining the rate of TICT reaction, study of solvation dynamics in these media is required in order to better explore the dynamic solvent control of the reaction rates<sup>4-18</sup>. Another interesting study would be the temperature dependence of the TICT reaction in the 0.04 mole fraction TBA-water solution. This system has recently<sup>19</sup> been shown to display significant meso-scale molecular aggregation and de-aggregation as the temperature of the solvent is increased from room temperature to ~383 K.

#### **9.5. Excited state intramolecular charge transfer reaction in non-aqueous reverse micelle: electrolyte concentration dependence**

In chapter 3 we observed that the average reaction time for the LE → CT conversion in P4C has been found to increase with electrolyte concentration in the low electrolyte concentration range ( $\leq 0.10$  moles-litre<sup>-1</sup>) which, upon further increase of concentration, decreases, giving rise to a non-monotonic electrolyte concentration dependence of the reaction rate. The non-monotonic nature is found to be the strongest for ethyl acetate ( $\epsilon_0 \sim 6$ ) and weakest for ethanol ( $\epsilon_0 \sim 24$ ), even though the electrolyte-induced increase in reaction rate at higher concentration is the highest in ethanol. This indicates that low polarity in solution is probably responsible for producing non-monotonic dependence in reaction rate. Since it is known that confinement reduces drastically the bulk polarity of a polar medium<sup>20</sup>, addition of

electrolyte in such an environment can lead to a strong non-monotonic electrolyte concentration dependence of reaction rate as observed in ethyl acetate<sup>21</sup>. The friction versus solvation model could be studied by investigating the reaction rate in confined environments in presence of electrolyte.

### **9.6. Probing medium dynamics by charge transfer reaction in catanionic reverse micelle**

It has been observed in chapter 8 that average solvation and rotational times are nearly independent of microemulsion droplet size where missing of fast components is thought to be responsible for the observed insensitivity. Further investigation with better time resolution is definitely required to understand the origin of this insensitivity. At a comparable droplets size, a comparison between the time scales observed in the present study for catanionic reverse micelles, those reported in Ref. 22 for quaternary microemulsions, and in AOT/water reverse micelles<sup>23-24</sup> seems to suggest that dynamically the solvent pool inside the quaternary microemulsions and AOT/water reverse micelles are respectively the fastest and slowest, whereas the catanionic pool stays in between. This may be due to different type of interactions of water molecules with the surfactant and surfactant mixtures constituting the microemulsions. Vibrational echo experiments<sup>25-26</sup> could be employed to investigate the difference in the nature of interactions between water molecules and surfactants, particularly near the inner surface of the microemulsions. Also, excitation wavelength dependence study of both solvation and rotational dynamics in the catanionic microemulsions may be very interesting. Simple chemical reactions such as intramolecular charge transfer or isomerization reactions in these medium could be studied in order to investigate the effects of slow medium dynamics.

### **9.7. Charge transfer reaction in DTN in electrolyte solutions**

We have already discussed in Chapter 2 the effects of electrolytes on excited state intramolecular charge transfer reaction in TICT molecules. DTN (4-N,N-dimethylamino-4'-cyanodiphenylacetylene) is a neutral molecule and strongly dipolar in its ground and excited states. One interesting aspect of DTN is that the electronic structure calculations indicate that the LE to CT process in DTN is

probably not of a TICT type<sup>27</sup>. The reaction in DTN is therefore not linked to the twisting as in PnC series. So it will be interesting to examine the solute DTN in electrolyte solutions. However, charge transfer is very rapid in DTN<sup>28</sup> and one therefore expects a small effect of electrolyte. Even if this is true, it will be interesting to use DTN as a probe of what happens subsequent to charge transfer. We want to look at how the CT band, subsequent to formation, moves as a response to the extra stabilization provided by the ion motions. What is more interesting here is that the elongated shape of DTN places its rotational diffusion time in most solvents close to the ionic relaxation time scale.<sup>29</sup> It will therefore be of interest to use emission anisotropy measurements to explore the nature of rotational motion of DTN in electrolyte solutions.

### **9.8. Effects of Mixed electrolytes on excited state intramolecular charge transfer reaction**

When two or more electrolytes are mixed with each other in solid state or they are dissolved in a polar solvent, the composition is called mixed electrolytes or mixed electrolyte solutions. When two or more electrolytes are added in a solvent, physiochemical properties of the solution change. In addition, vapor pressure, Gibbs free energy, viscosity, activity co-efficient, conductivity of the solution change due to adding mixed electrolytes<sup>30-38</sup>. Diffusion co-efficient of the ions present in the solution also changes appreciably. Depending upon the ionic potential (charge/radius) and ionic ratios between the different ions, one type of ion behaves differently in presence of the others to a particular reaction or physiological properties. For example, study of sodium (NaCl) intake and urinary excretion of sodium in presence of potassium (KCl) by Park<sup>39</sup> et al can be mentioned. According to this study they concluded that mixed NaCl-KCl salt diet decreased the intake of Na, and increased intake of K. In this context, one relevant question comes: *Is it possible for an ion (e.g.  $K^+$ ) act as a replacement of another ion (e.g.  $Na^+$ ) to a particular reaction (process), especially for biological reactions (process) which are sensitive to ion-specificity? Or one retards the action of the others? Or they do simultaneously the same action helping each other?* Answers are unknown to us as

extensive basic research towards this direction has not been performed yet. We want to address this question by measuring solvation dynamics, rotational dynamics of a non reactive probe and by intramolecular charge transfer reactions in this mixed electrolyte solutions where the questions of ion-specificity would be addressed to at both static and dynamic levels.

## References

1. Kay, R. L.; Evans, D. F.; *J. Phys. Chem.* **1966**, *70*, 2325.
2. Zwan, van der G.; Hynes, J. T. *Chem. Phys.* **1991**, *152*, 169.
3. Hynes, J. T. Charge -Transfer Reactions and Solvation Dynamics In Ultrafast Dynamics of Chemical Systems; Simon, J. D., Ed.; Kluwer: Dordrecht, 1994; p.345.
4. Cichos, F.; Willert, A.; Rempel, U.; von Borczyskowski, C. J. *Phys. Chem. A* **1997**, *101*, 8179
5. Cichos, P.; Brown, R.; Rempel, U.; von Borczyskowski, C. J. *Phys. Chem. A* **1999**, *103*, 2506.
6. Luther, B. M.; Kimmel, J. R.; Levinger, N. E. *J. Chem. Phys.* **2002**, *116*, 3370.
7. Chandra, A.; Bagchi, B. *J. Chem. Phys.* **1991**, *94*, 8367.
8. Chandra, A. *Chem. Phys. Lett.* **1995**, *235*, 133.
9. Jarzeba, W.; Walker, G. C.; Johnson, A. E.; Barbara, P. F. *Chem. Phys.* **1991**, *152*, 57.
10. Gardecki, J. A.; Maroncelli, M. *Chem. Phys. Lett.* **1999**, *301*, 571.
11. Ladanyi, B. M.; Skaf, M. S. *J. Phys. Chem. A* **1996**, *100*, 18258.
12. Laria, D.; Skaf, M. S. *J. Chem. Phys.* **1999**, *111*, 300.
13. Day, T. J. F.; Patey, G. N. *J. Chem. Phys.* **1997**, *106*, 2782.
14. Day, T. J. F.; Patey, G. N. *J. Chem. Phys.* **1999**, *110*, 10937.
15. Yoshimori, A.; Day, T. J. F.; Patey, G. N. *J. Chem. Phys.* **1998**, *108*, 6378.
16. Yoshimori, A.; Day, T. J. F.; Patey, G. N. *J. Chem. Phys.* **1998**, *109*, 3222.
17. Molotsky, T.; Huppert, D. *J. Phys. Chem. A* **2004**, *107*, 8449.
18. Mukherjee, S.; Sahu, K.; Roy, D.; Mondal, S. K.; Bhattacharyya, K. *Chem. Phys. Lett.* **2004**, *384*, 128.
19. Bowron, D. T.; Finney, J. L. *J. Phys. Chem. B* **2007**, *111*, 9838.
20. Biswas, R., Rohman, N., Pradhan, T., Buchner, R. *J. Phys. Chem. B* **2008**, *112*, 9379
21. Pradhan, T.; Biswas, R. J. Solution. Chem. 2008, xxx, xxx (in press)
22. Corbeil, E. M.; Levinger, N. E. *Langmuir* **2003**, *19*, 7264.

23. Bhattacharyya, K. *Acc. Chem. Res.* **2003**, *36*, 95 and references therein.
24. Ghosh, S.; Mandal, U.; Adhikari, A.; Dey, S.; Bhattacharyya, K. *Int. Rev. Phys. Chem.* **2007**, *26*, 421.
25. Tan, H-S. ; Piletic, I. R.; Fayer, M. D. *J. Chem. Phys.* **2005**, *122*, 174501.
26. Piletic, I. R.; Tan, H-S.; Fayer, M. D. *J. Phys. Chem. B* **2005**, *109*, 21273.
27. M. Maroncelli, private communications
28. J. Gardecki, Ph.D Thesis, Pennsylvania State University
29. Y. Hirata, Y. Kanemoto, T. Okada and T. nomoto, *J. Mol. Liq.* **1995**, *65/66*, 421.
30. Yamaguchi, S; Fukatsu, N., *Yoyuen Oyobi koon Kagaku*, **1993**, *36*, 21.
31. Mithlesh; Singh, M., *J. Indian Chem. Soc.*, **2006**, *83*, 803.
32. May, P.M., *Marine Chemistry*, **2006**, *99*, 62.
33. Kumar, A., *J. Phys. Chem.. B*, **2005**, *109*, 11743.
34. Patel, K.J.; Dhondge, S.S.; Manwalkar, S.M., *Indian J. Chem.*, **1995**, *34A*, 950
35. Hao, L.; Leaist, D. G., *J. Sol. Chem.*, **1995**, *24*, 523
36. Singh, R.; Singh, A.K.; Upadhyay, G.S., *Asian J. Chem.*, **1992**, *4*, 105.
37. Hsu, H.L.; Wu, Y.C; Lee, L.S., *J. Chem. Eng. Data*, **2003**, *48*, 514.
38. Ramana, G.V.; Rajagopal, E; Murthy, N.M., *Acoustics Letters*, **2001**, *24*, 244.
39. Park, S.J.; Paik, H.Y.; Lee, S.Y, *Hanguk Yongyang Hakhoeehi*, **2007**, *40*, 500.

# Appendices

## Appendix 1

### Kinetic Framework for Charge Transfer Reaction

#### 1. Time dependent LE Population

Scheme 3 in Chapter 1 indicates that the emission decays are bi-exponential functions of time. In some cases the decays observed in the LE region are more complex than bi-exponential functions and need sums of three or more exponential to fit the decays. In that cases the assumption of time independent rate constants breaks down. We can assume forward reaction involves a time-dependent rate constant for that cases but for simplicity to derive time dependent LE population we assume forward rate constants are time independent and can write the following differential relations,

$$\frac{d[LE]}{dt} = -k_{LE}[LE] - k_f[LE] + k_r[CT] \quad (1)$$

$$\frac{d[CT]}{dt} = -k_{CT}[CT] - k_r[CT] + k_f[LE] \quad (2)$$

$[LE(t)]$  can be obtained by solving equation (1).

Differentiating both sides of equation (1) we get,

$$\frac{d^2[LE]}{dt^2} = -k_{LE} \frac{d[LE]}{dt} - k_f \frac{d[LE]}{dt} + k_r \frac{d[CT]}{dt}$$

$$= -(k_{LE} + k_f) \frac{d[LE]}{dt} + k_r (-k_{CT}[CT] - k_r[CT] + k_f[LE]) \quad (3)$$

(Putting  $\frac{d[CT]}{dt}$  from equation (2))

Substituting  $k_r[CT]$  in equation (3) by  $\frac{d[LE]}{dt} + k_{LE}[LE] + k_f[LE]$  from equation (1)

we get,

$$\frac{d^2[LE]}{dt^2} = -(k_{LE} + k_f + k_{CT} + k_r) \frac{d[LE]}{dt} - (k_{LE}k_{CT} + k_{LE}k_r + k_fk_{CT})[LE]$$

Therefore,

$$\frac{d^2[LE]}{dt^2} + (k_{LE} + k_f + k_{CT} + k_r) \frac{d[LE]}{dt} + (k_{LE}k_{CT} + k_{LE}k_r + k_fk_{CT})[LE] = 0 \quad (4)$$

Let,

$$y = [LE]$$

$$x = t$$

$$P = k_{LE} + k_{CT} + k_f + k_r$$

$$Q = k_{LE}k_{CT} + k_{LE}k_r + k_fk_{CT}$$

Now, equation (4) becomes

$$\frac{d^2y}{dx^2} + P \frac{dy}{dx} + Qy = 0 \quad (5)$$

This is a second order differential equation.

Let,  $y = Ae^{\lambda x}$

Then, equation (5) becomes

$$\frac{d^2(Ae^{\lambda x})}{dx^2} + P \frac{d(Ae^{\lambda x})}{dx} + Q Ae^{\lambda x} = 0$$

$$\text{or, } A\lambda^2 e^{\lambda x} + P A \lambda e^{\lambda x} + Q A e^{\lambda x} = 0$$

$$\text{or, } A e^{\lambda x} (\lambda^2 + P\lambda + Q) = 0$$

As  $y \neq 0$ ,  $\lambda^2 + P\lambda + Q$  must be zero

Therefore,

$$\lambda^2 + P\lambda + Q = 0 \quad (6)$$

By solving equation (6) we get,

$$\lambda = \frac{-P \pm \sqrt{P^2 - 4Q}}{2}$$

$$\text{i.e. } \lambda_1 = \frac{-P + \sqrt{P^2 - 4Q}}{2} \text{ and } \lambda_2 = \frac{-P - \sqrt{P^2 - 4Q}}{2}$$

Therefore,

$$y = C_1 \exp\left(\frac{-P + \sqrt{P^2 - 4Q}}{2} x\right) + C_2 \exp\left(\frac{-P - \sqrt{P^2 - 4Q}}{2} x\right)$$

Where,  $C_1$  and  $C_2$  are the constants.

$$\therefore [LE(t)] = C_1 \exp\left(\frac{-P + \sqrt{P^2 - 4Q}}{2} t\right) + C_2 \exp\left(\frac{-P - \sqrt{P^2 - 4Q}}{2} t\right) \quad (7)$$

## 2. Time Dependent CT Population

Using equation (7) we can obtain  $[CT(t)]$  by solving equation (2)

Putting the value of  $[LE(t)]$  in equation (2) we get,

$$\frac{d[CT]}{dt} + (k_{CT} + k_r)[CT] = k_f(t) \left\{ C_1 \exp\left(\frac{-P + \sqrt{P^2 - 4Q}}{2} t\right) + C_2 \exp\left(\frac{-P - \sqrt{P^2 - 4Q}}{2} t\right) \right\} \quad (8)$$

Integral Factor (I.F) for the above equation is,  $\exp\left\{\int (k_{CT} + k_r) dt\right\} = \exp(k_{CT} + k_r)t$

Multiplying the above equation by I.F we get,

$$\begin{aligned}
& \exp[(k_{CT} + k_r)t] \frac{d[CT]}{dt} + \exp[(k_{CT} + k_r)t] (k_{CT} + k_r) [CT] \\
& = k_f(t) \left\{ C_1 \exp\left(\frac{-P + \sqrt{P^2 - 4Q}}{2} t\right) + C_2 \exp\left(\frac{-P - \sqrt{P^2 - 4Q}}{2} t\right) \right\} \exp[(k_{CT} + k_r)t] \\
& \text{or, } d\{[CT] \exp(k_{CT} + k_r)t\} = k_f \left\{ C_1 \exp\left(\frac{-P + \sqrt{P^2 - 4Q}}{2} t\right) + C_2 \exp\left(\frac{-P - \sqrt{P^2 - 4Q}}{2} t\right) \right\} \exp[(k_{CT} + k_r)t] dt
\end{aligned} \tag{9}$$

Integrating both sides of the above equation we get,

$$\begin{aligned}
[CT] \exp[(k_{CT} + k_r)t] & = k_f \left[ \frac{C_1}{\frac{-P + \sqrt{P^2 - 4Q}}{2} + (k_{CT} + k_r)} \exp\left\{\frac{-P + \sqrt{P^2 - 4Q}}{2} + (k_{CT} + k_r)\right\}t \right] + \\
& \left[ \frac{C_2}{\frac{-P - \sqrt{P^2 - 4Q}}{2} + (k_{CT} + k_r)} \exp\left\{\frac{-P - \sqrt{P^2 - 4Q}}{2} + (k_{CT} + k_r)\right\}t \right] + C
\end{aligned}$$

Where, C is the integrating constant.

When  $t=0$ ,  $[CT] = 0$

Therefore,

$$\begin{aligned}
C & = -k_f \left[ \frac{C_1}{\frac{-P + \sqrt{P^2 - 4Q}}{2} + (k_{CT} + k_r)} + \frac{C_1}{\frac{-P - \sqrt{P^2 - 4Q}}{2} + (k_{CT} + k_r)} \right] \\
\therefore [CT(t)] & = A \exp\left(\frac{-P + \sqrt{P^2 - 4Q}}{2} t\right) + B \exp\left(\frac{-P - \sqrt{P^2 - 4Q}}{2} t\right) - C \exp(-(k_{CT} + k_r)t) \tag{10}
\end{aligned}$$

Where,

$$A = \left[ \frac{k_f C_1}{\frac{-P + \sqrt{P^2 - 4Q}}{2} + (k_{CT} + k_r)} \right]$$

$$B = \left[ \frac{k_f C_2}{\frac{-P - \sqrt{P^2 - 4Q}}{2} + (k_{CT} + k_r)} \right]$$

$$C = -k_f \left[ \frac{C_1}{\frac{-P + \sqrt{P^2 - 4Q}}{2} + (k_{CT} + k_r)} + \frac{C_1}{\frac{-P - \sqrt{P^2 - 4Q}}{2} + (k_{CT} + k_r)} \right]$$

### 3. Quantum Yields from Radiative Rate Constants

Under the assumption of no CT excitation, the populations of the LE and CT states at a time  $t$  after excitation, their respective emission intensities  $I_{LE}(t)$  and  $I_{CT}(t)$  are given by well known relations<sup>1-2</sup>.

$$I_{LE}(t) \propto k_{LE}^{rad} \frac{[LE(t)]}{[LE(0)]} = k_{LE}^{rad} \frac{1}{\lambda_1 - \lambda_2} \left\{ (Y - \lambda_2) e^{-\lambda_2 t} + (\lambda_1 - Y) e^{-\lambda_1 t} \right\} \quad (11)$$

$$I_{LE}(t) \propto k_{LE}^{rad} \frac{[CT(t)]}{[LE(0)]} = k_{CT}^{rad} \frac{k_f}{\lambda_1 - \lambda_2} \left\{ e^{-\lambda_2 t} - e^{-\lambda_1 t} \right\} \quad (12)$$

Where,  $X = k_{LE} + k_r$  and  $Y = k_{CT} + k_r$ ,

$$\lambda_1 = \frac{-P + \sqrt{P^2 - 4Q}}{2} \quad \text{and} \quad \lambda_2 = \frac{-P - \sqrt{P^2 - 4Q}}{2}$$

$k_{LE}^{rad}$  and  $k_{CT}^{rad}$  are respectively radiative rate constants for LE and CT states.

Quantum yield for LE and CT can be obtained from equations (11) and (12).

If quantum yield for LE and CT are represented by respectively  $\Phi_{LE}$  and  $\Phi_{CT}$  then

$$\begin{aligned}
 \Phi_{LE} &= \int I_{LE}(t) dt = \int_0^{\infty} \frac{k_{LE}^{rad}}{\lambda_1 - \lambda_2} \left\{ (Y - \lambda_2) e^{-\lambda_2 t} + (\lambda_1 - Y) e^{-\lambda_1 t} \right\} dt \\
 &= \frac{k_{LE}^{rad}}{\lambda_1 - \lambda_2} \left[ \frac{(Y - \lambda_2) e^{-\lambda_2 t}}{-\lambda_2} + \frac{(\lambda_1 - Y) e^{-\lambda_1 t}}{-\lambda_1} \right]_0^{\infty} \\
 &= \frac{k_{LE}^{rad} Y}{\lambda_1 \lambda_2} \\
 &= \frac{k_{LE}^{rad} (k_{CT} + k_r)}{k_{LE} k_{CT} + k_{LE} k_r + k_{CT} k_f} \tag{13}
 \end{aligned}$$

Similarly we get,

$$\Phi_{CT} = \frac{k_{CT}^{rad} k_f}{k_{LE} k_{CT} + k_{LE} k_r + k_{CT} k_f} \tag{14}$$

#### 4. Relation between Quantum yields and Equilibrium Constants

From equation (13) and (14) we get,

$$\frac{\Phi_{CT}}{\Phi_{LE}} = \left( \frac{k_{CT}^{rad}}{k_{LE}^{rad}} \right) \frac{k_f}{k_{CT} + k_r} \tag{15}$$

Near to room temperature, the excited state reactions of the PnC solutes are generally rapid compared to the LE and CT decay rates. If one therefore assumes that

$k_f, k_r \gg k_{LE}, k_{CT}$  then

$$\frac{\Phi_{CT}}{\Phi_{LE}} = \left( \frac{k_{CT}^{rad}}{k_{LE}^{rad}} \right) \frac{k_f}{k_r}$$

$$= \left( \frac{k_{CT}^{rad}}{k_{LE}^{rad}} \right) K_{eq} \quad (16)$$

Where  $K_{eq} = \frac{k_f}{k_r}$ , equilibrium constant

## 5. Derivations of rate equations near room temperature

Near room temperature, excited state reactions are very rapid compared to LE and

CT decay rates, i.e. one can assume  $k_f, k_r \gg k_{LE}, k_{CT}$ , then

$$\lambda_2 - \lambda_1 = k_f + k_r$$

$$\lambda_1 = \frac{1}{2}(k_{LE} + k_{CT})$$

$$\lambda_2 = k_f + k_r$$

$$Y - \lambda_2 = k_f$$

$$\lambda_1 - Y = k_r$$

Equations (11) and (12) become as follows;

$$I_{LE}(t) \propto k_{LE}^{rad} \frac{1}{1 + K_{eq}} \{ e^{-k_{dec}t} + K_{eq} e^{-k_{rxn}t} \} \quad (17)$$

$$I_{CT}(t) \propto k_{CT}^{rad} \frac{K_{eq}}{1 + K_{eq}} \{ e^{-k_{dec}t} - e^{-k_{rxn}t} \} \quad (18)$$

Where  $k_{rxn} = k_f + k_r$  and  $k_{dec} = \frac{1}{2}(k_{LE} + k_{CT})$

## 6. Determination of $[CT(t)]$ assuming $[LE(t)]$ is multiexponential

From equation (1) we get,

$$k_f [LE] = -k_{LE} [LE] + k_r [CT] - \frac{d[LE]}{dt} \quad (19)$$

From equation (2) and (16) we get,

$$\frac{d[CT]}{dt} = -k_{CT} [CT] - k_{LE} [LE] - \frac{d[LE]}{dt} \quad (20)$$

Assuming that  $[LE(t)]$  is characterized using a multiexponential form:

$[LE(t)] = \sum_i a_i \exp(-r_i t)$  we can obtain  $[CT(t)]$  by solving equation (20) in the

following way.

$$\begin{aligned} \frac{d[CT]}{dt} &= -k_{CT}[CT] - k_{LE} \sum_i a_i \exp(-r_i t) - \frac{d}{dt} \sum_i a_i \exp(-r_i t) \\ &= -k_{CT}[CT] + \sum_i a_i r_i \exp(-r_i t) - k_{LE} \sum_i a_i \exp(-r_i t) \end{aligned}$$

$$\text{Or, } \frac{d[CT]}{dt} + k_{CT}[CT] = \sum_i (r_i - k_{LE}) \exp(-r_i t) \quad (21)$$

$$I.F. = \exp\left(\int k_{CT} dt\right) = \exp(k_{CT} t)$$

Multiplying both sides of equation (21) by I.F we get,

$$\exp(k_{CT} t) \frac{d[CT]}{dt} + \exp(k_{CT} t) k_{CT} [CT] = \exp(k_{CT} t) \sum_i (r_i - k_{LE}) \exp(-r_i t)$$

$$\text{or, } d[[CT] \exp(k_{CT} t)] = \sum_i (r_i - k_{LE}) \exp(k_{CT} - r_i) t dt \quad (22)$$

Integrating both sides of equation (22) we get,

$$[CT] \exp(k_{CT} t) = \sum_i \frac{(r_i - k_{LE}) a_i}{(k_{CT} - r_i)} \exp(k_{CT} - r_i) t + C \quad (23)$$

Where, C is the integrating constant.

When  $t=0$ ,  $[CT] = 0$

Putting  $[CT] = 0$  in equation (23) we get,

$$C = \sum_i a_i \frac{(r_i - k_{LE})}{(r_i - k_{CT})} \quad (24)$$

Putting the value of C from equation (24) in equation (23) we get,

$$[CT] = \sum_i \frac{(r_i - k_{LE})}{(k_{CT} - r_i)} a_i \exp(-r_i t) + \sum_i a_i \frac{(r_i - k_{LE})}{(r_i - k_{CT})} \exp(-k_{CT} t)$$

$$\text{Or, } [CT(t)] = \sum_i b_i \exp(-k_{CT} t) + \sum_i (-b_i) \exp(-r_i t) \quad (25)$$

$$\text{Where, } b_i = \sum \frac{(r_i - k_{LE})}{(r_i - k_{CT})} a_i$$

## References

1. Dahl, K.; Biswas, R.; Ito, N.; Maroncelli, M. *J. Phys. Chem. B*, **2005**, *109*,1563
2. Laws, W. R.; Brand, L. J. *Phys. Chem.* 1979, *83*, 795

## Appendix 2

**Table A1: LiClO<sub>4</sub> Concentration Dependence of C153 in Ethyl Acetate and Acetonitrile**

(A) Spectral properties of C153 in Ethyl Acetate + LiClO<sub>4</sub> Solution <sup>a)</sup>

Conc (M)	n (ref. index)	$\nu_{\text{abs}}$	$\Gamma_{\text{abs}}$	$\nu_{\text{em}}$	$\Gamma_{\text{em}}$	$k_{\text{net}}^{\text{rad}}$	$k_{\text{net}}^{\text{nr}}$	$M_{\text{em}}$
0.0	1.368	24.76	4.31	19.35	3.78	1.26	7.50	4.9
0.005	1.368	24.63	3.94	19.36	3.89	1.27	7.46	4.9
0.01	1.368	24.63	3.99	19.29	3.94	1.27	7.80	4.9
0.025	1.368	24.63	4.02	19.11	4.06	1.32	8.07	5.0
0.05	1.368	24.57	4.01	18.90	4.13	1.42	9.48	5.3
0.075	1.368	24.55	4.00	18.76	4.18	1.37	10.30	5.3
0.1	1.369	24.58	4.03	18.67	4.13	1.35	10.16	5.3
0.25	1.371	24.48	4.18	18.18	3.73	1.16	9.47	5.2
0.5	1.374	24.31	4.36	18.11	3.59	1.15	10.15	5.1
0.75	1.378	24.08	4.19	18.00	3.55	1.13	10.04	5.1
1.0	1.382	23.93	4.14	17.93	3.65	1.07	10.26	5.0
1.5	1.387	23.62	4.16	17.82	3.65	1.06	11.05	5.0
2.0	1.392	23.43	4.12	17.73	3.63	1.05	11.83	5.2
2.5	1.395	23.20	4.09	17.64	3.62	1.09	13.34	5.1
3.0	1.395	23.12	4.19	17.56	3.58	1.00	14.85	4.8

(B) Spectral properties of C153 in Acetonitrile + LiClO<sub>4</sub> Solution

Conc (M)	n (ref. index)	$\nu_{\text{abs}}$	$\Gamma_{\text{abs}}$	$\nu_{\text{em}}$	$\Gamma_{\text{em}}$	$k_{\text{net}}^{\text{rad}}$	$k_{\text{net}}^{\text{nr}}$	$M_{\text{em}}$
0.0	1.338	24.21	4.12	18.53	3.64	1.24	5.56	5.3
0.005	1.339	24.18	4.07	18.50	3.66	1.24	5.83	5.3
0.01	1.339	24.38	4.42	18.45	3.67	1.23	6.04	5.3
0.025	1.340	24.08	4.19	18.38	3.69	1.25	6.42	5.4
0.05	1.340	24.22	4.17	18.38	3.74	1.24	6.67	5.4
0.075	1.341	24.34	4.63	18.24	3.65	1.22	6.87	5.4
0.1	1.341	24.23	4.21	18.18	3.65	1.21	7.09	5.4
0.25	1.343	24.74	4.03	18.11	3.71	1.19	7.60	5.4
0.5	1.346	24.28	4.50	17.99	3.63	1.17	8.16	5.4
0.75	1.349	23.97	4.49	17.86	3.62	1.09	9.27	5.2
0.9	1.352	23.73	4.32	17.77	3.61	1.07	9.90	5.2
1.0	1.353	23.83	4.88	17.72	3.59	0.92	11.29	4.9

a) Peak frequencies ( $\nu$ ) and band widths ( $\Gamma$ , fwhm) are in the unit of  $10^3 \text{ cm}^{-1}$ .  $k^{rad}$  and  $k^{nr}$  are in the units of  $10^7 \text{ s}^{-1}$  and  $10^8 \text{ s}^{-1}$  respectively)  $M_{em}$  represents emission transition moment (in Debye unit)

**Table A2: Ion Size Dependence of TICT molecules in 0.5(M) Perchlorate Solutions of Acetonitrile <sup>a)</sup>**

**(A) Spectral properties and area ratio: P4C**

Ion	$z/r_{ion}$	$\nu_{abs}$	$\Gamma_{abs}$	$\nu_{LE}$	$\Gamma_{LE}^{inh}$	$\nu_{CT}$	$\Gamma_{CT}^{inh}$	$\frac{\alpha_{CT}}{\alpha_{LE}}$
Na <sup>+</sup>	0.980	34.30	4.22	27.33	1.39	19.38	3.61	0.93
Li <sup>+</sup>	1.351	34.67	4.19	27.40	1.40	19.15	3.70	0.86
Sr <sup>+2</sup>	1.724	34.11	4.39	27.15	1.12	18.87	3.16	1.31
Ca <sup>+2</sup>	2.000	34.16	4.43	27.31	1.39	18.52	3.81	1.18
Mg <sup>+2</sup>	2.780	33.96	4.71	27.23	1.12	19.33	3.04	0.82

**(B) Spectral properties and area ratio: P5C**

Ion	$\nu_{abs}$	$\Gamma_{abs}$	$\nu_{LE}$	$\Gamma_{LE}^{inh}$	$\nu_{CT}$	$\Gamma_{CT}^{inh}$	$\frac{\alpha_{CT}}{\alpha_{LE}}$
Na <sup>+</sup>	33.74	4.13	27.54	1.65	19.37	3.8	13.29
Li <sup>+</sup>	33.63	4.22	27.62	1.95	19.28	3.84	11.5
Sr <sup>+2</sup>	33.39	4.27	27.17	2.06	19.02	3.54	12.32
Ca <sup>+2</sup>	33.47	4.29	27.61	2.06	18.72	3.89	9.96
Mg <sup>+2</sup>	33.25	4.58	27.41	1.50	19.32	3.76	13.29

**(C) Spectral properties and area ratio: P6C**

Ion	$\nu_{abs}$	$\Gamma_{abs}$	$\nu_{LE}$	$\Gamma_{LE}^{inh}$	$\nu_{CT}$	$\Gamma_{CT}^{inh}$	$\frac{\alpha_{CT}}{\alpha_{LE}}$
Na <sup>+</sup>	33.67	4.26	26.28	1.70	20.06	3.88	49.0
Li <sup>+</sup>	33.55	4.31	26.61	2.05	19.88	3.93	43.6
Sr <sup>+2</sup>	33.40	4.37	26.80	1.50	19.63	3.35	49.0
Ca <sup>+2</sup>	33.45	4.38	26.80	1.50	19.28	4.19	54.6
Mg <sup>+2</sup>	33.22	4.58	25.58	1.87	20.01	3.97	49.0

a) Units are same as those in Table A1.  $\frac{\alpha_{CT}}{\alpha_{LE}}$  denotes the ratio of the areas under CT and LE emission bands .

**Table A3: Ion Size Dependence of C153 in 0.5(M) Perchlorate Solutions of Ethyl Acetate and Acetonitrile<sup>a</sup>**

**(A) Ethyl Acetate**

Ion	n (ref. index)	$v_{\text{abs}}$	$\Gamma_{\text{abs}}$	$v_{\text{em}}$	$\Gamma_{\text{em}}$	$k_{\text{net}}^{\text{rad}}$	$k_{\text{net}}^{\text{nr}}$	$M_{\text{em}}$	$\Phi$
Na <sup>+</sup>	1.374	24.39	4.11	18.17	3.94	0.95	9.51	4.6	0.50
Li <sup>+</sup>	1.374	24.31	4.36	18.11	3.59	1.15	10.15	5.1	0.53
Sr <sup>+2</sup>	1.386	24.19	4.75	17.87	3.56	0.94	11.48	4.7	0.45
Ca <sup>+2</sup>	1.382	24.08	4.29	17.72	3.54	1.02	12.43	4.9	0.45
Mg <sup>+2</sup>	1.381	24.01	5.82	18.16	3.82	0.91	13.10	4.5	0.41

**(B) Acetonitrile**

Ion	n (ref. index)	$v_{\text{abs}}$	$\Gamma_{\text{abs}}$	$v_{\text{em}}$	$\Gamma_{\text{em}}$	$k_{\text{net}}^{\text{rad}}$	$k_{\text{net}}^{\text{nr}}$	$M_{\text{em}}$	$\Phi$
Na <sup>+</sup>	1.346	24.14	4.28	18.09	3.68	1.09	7.54	5.1	0.59
Li <sup>+</sup>	1.346	24.28	4.50	17.99	3.63	1.17	8.16	5.4	0.59
Sr <sup>+2</sup>	1.361	23.48	4.36	17.68	3.54	1.09	10.11	5.3	0.52
Ca <sup>+2</sup>	1.356	23.37	4.04	17.58	3.48	1.20	10.25	5.6	0.54
Mg <sup>+2</sup>	1.355	22.92	4.89	17.74	3.67	1.06	11.46	5.1	0.48

<sup>a</sup>) Units are same as in Tables A1 and A2.  $\Phi$  represents quantum yield.

**Table A4: Peak frequency and widths associated with LE band <sup>a</sup>**

Ethyl Acetate			Ethanol			Acetonitrile		
Conc.	$\nu_{LE}$	$\Gamma_{LE}$	Conc.	$\nu_{LE}$	$\Gamma_{LE}$	Conc.	$\nu_{LE}$	$\Gamma_{LE}$
0	27.86	1.12	0	27.96	1.33	0	27.45	1.35
0.005	27.85	1.14	0.005	27.96	1.34	0.005	27.44	1.35
0.01	27.86	1.11	0.01	27.95	1.34	0.01	27.44	1.36
0.025	27.84	1.14	0.025	27.95	1.34	0.025	27.44	1.34
0.05	27.84	1.12	0.05	27.94	1.35	0.05	27.44	1.35
0.1	27.81	1.13	0.075	27.93	1.38	0.075	27.44	1.34
0.25	27.77	1.13	0.1	27.92	1.38	0.1	27.43	1.39
0.5	27.71	1.16	0.25	27.90	1.43	0.25	27.42	1.38
0.75	27.66	1.21	0.5	27.86	1.43	0.5	27.40	1.40
1.0	27.64	1.21	0.75	27.86	1.44	0.75	27.39	1.41
1.5	27.60	1.23	1.0	27.84	1.47	0.9	27.38	1.40
2.0	27.58	1.25	1.5	27.85	1.68	1.0	27.38	1.40
2.5	27.60	1.26	2.0	27.78	1.65			
3.0	27.61	1.28	2.5	27.86	1.55			
			3.0	27.85	1.37			
			3.5	27.84	1.32			
			4.0	27.88	1.39			
			4.5	27.90	1.19			
			5.0	27.94	1.20			

<sup>a</sup>Peak frequencies ( $\nu_{LE}$ ) and band widths ( $\Gamma_{LE}$ ) are in units of  $10^3 \text{ cm}^{-1}$

**Table A5:** P4C in Ethanol + LiClO<sub>4</sub> Solutions: Steady State Spectroscopic Properties <sup>a</sup>

Conc.(M)	T(K)	$\nu_{abs}$	$\Gamma_{abs}$	$\nu_{LE}$	$\nu_{CT}$	$\Gamma_{LE}$	$\Gamma_{CT}$
0.0	274.05	34.39	4.27	27.90	19.70	1.16	4.03
	287.75	34.43	4.32	27.89	19.92	1.38	4.12
	301.15	34.44	4.31	27.88	20.15	1.45	4.02
	314.95	34.49	4.40	27.87	20.25	1.61	4.41
	329.05	34.51	4.40	27.87	20.44	1.66	4.66
	343.45	34.55	4.43	27.86	20.63	1.77	4.85
0.1	274.05	34.39	4.42	27.78	19.49	0.51	3.40
	287.75	34.40	4.39	27.77	19.62	0.64	3.93
	301.15	34.44	4.44	27.77	19.80	0.85	4.04
	314.95	34.47	4.46	27.76	19.99	0.78	4.19
	329.05	34.48	4.46	27.70	20.11	0.98	4.08
	343.45	34.50	4.49	27.70	20.25	1.13	4.29
1.0	274.05	34.12	4.48	27.76	18.69	0.48	4.01
	287.75	34.12	4.42	27.77	19.19	1.31	3.48
	301.15	34.16	4.42	27.74	19.33	1.45	3.62
	314.95	34.27	4.58	27.71	19.46	1.54	3.78
	329.05	34.30	4.61	27.68	19.57	1.76	3.98
	343.45	34.28	4.53	27.66	19.71	1.99	4.19
3.0	274.05	33.74	4.37	27.92	18.71	1.60	3.75
	287.75	33.78	4.39	27.87	18.80	1.82	4.03
	301.15	33.77	4.36	27.84	18.99	1.90	3.92
	314.95	33.80	4.39	27.79	19.15	2.02	3.94
	329.05	33.88	4.49	27.80	19.25	2.03	4.06
	343.45	33.90	4.50	27.70	19.40	2.20	4.18

<sup>a</sup> Peak frequencies ( $\nu$ ) and band widths ( $\Gamma$ , fwhm) are in the unit of  $10^3 \text{ cm}^{-1}$ .

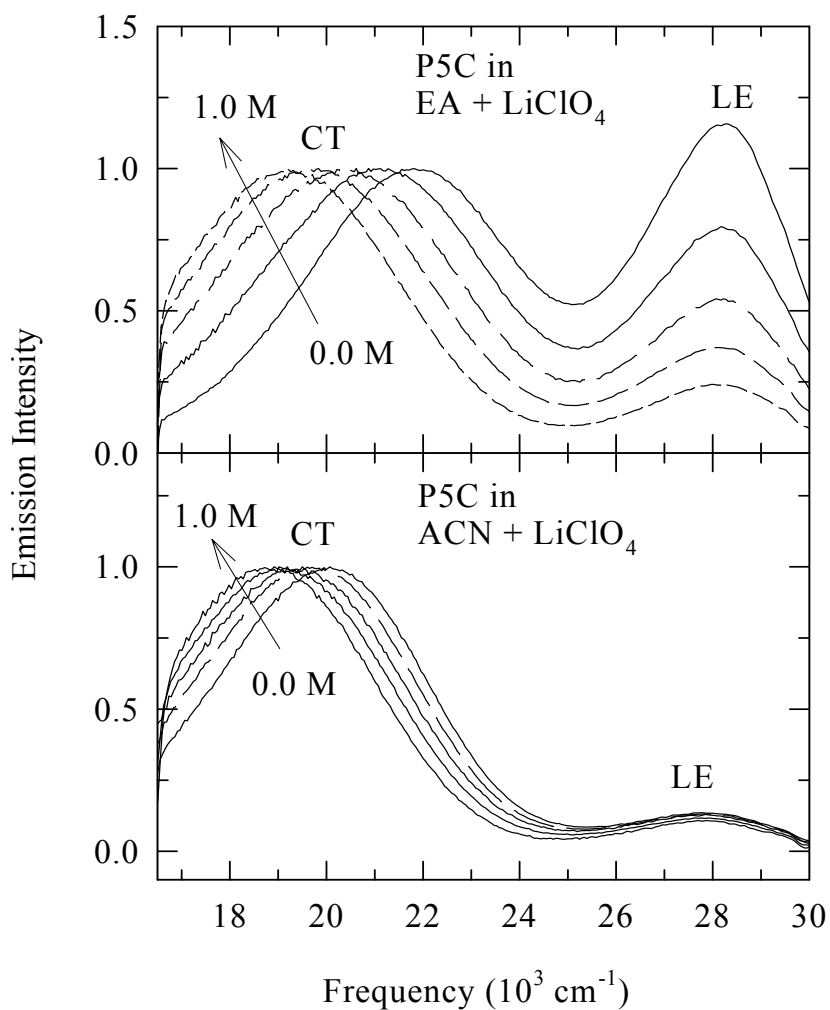


**Fig. A1:** Fluorescence emission spectra of P5C in several concentrations of  $\text{LiClO}_4$  in ethyl acetate (upper panel) and acetonitrile (lower panel). Spectra shown in this figure correspond to the following  $\text{LiClO}_4$  concentrations (M) in ethyl acetate and acetonitrile: 0.0, 0.1, 0.25, and 0.5, 1.0, respectively. Note here that we have shown spectra in ethyl acetate with  $\text{LiClO}_4$  only upto 1.0 M even though we could go upto 2.5 M.

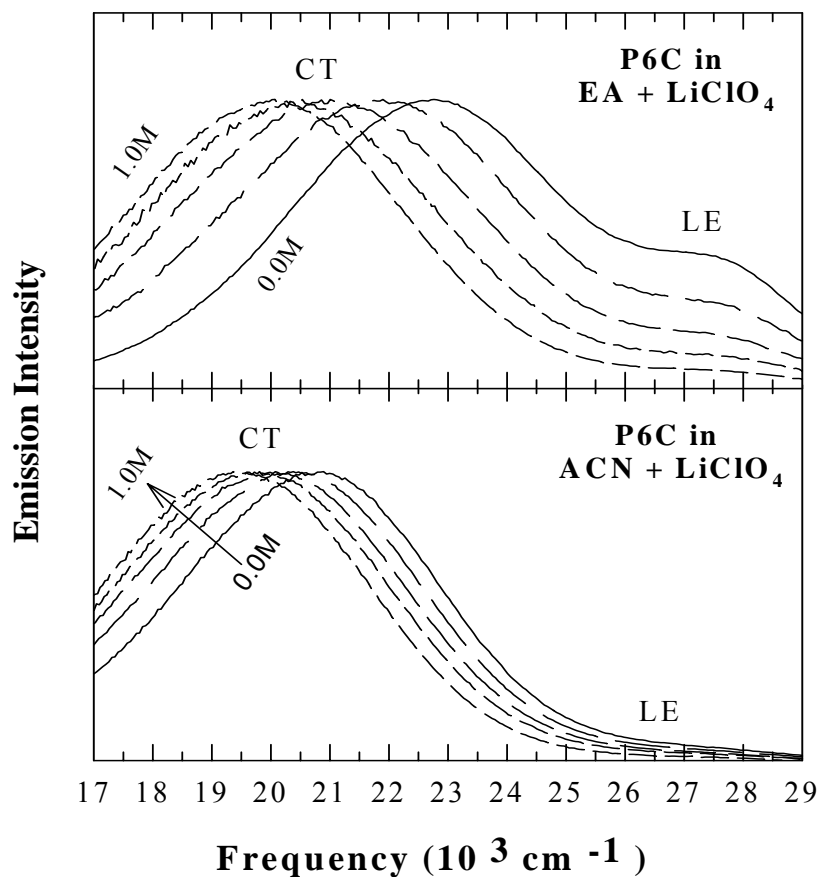


**Fig. A2:** Fluorescence emission spectra of P6C in several concentrations of LiClO<sub>4</sub> in ethyl acetate (upper panel) and acetonitrile (lower panel). The spectra shown here correspond to the following LiClO<sub>4</sub> concentrations (M): 0.0, 0.1, 0.25, 0.5, 1.0, respectively. Note that we have shown spectra in ethyl acetate with LiClO<sub>4</sub> only upto 1.0 M even though we could go upto 2.5 M.

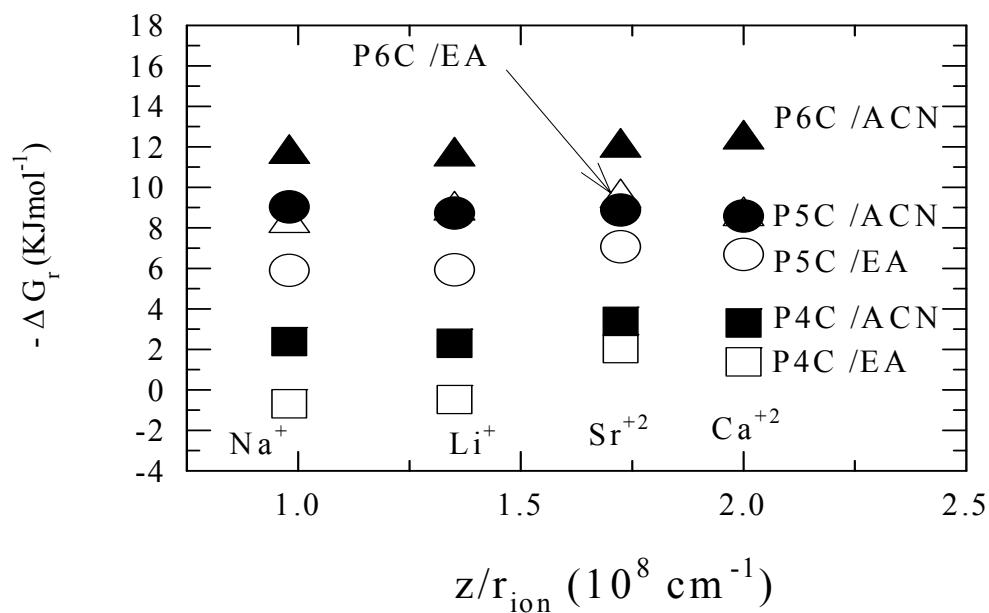


**Fig. A3:** Ion size dependence of change in reaction free energy ( $-\Delta G_r$ ) for LE $\rightarrow$ CT conversion in ethyl acetate (open symbols) and acetonitrile (filled symbols). Note that  $\text{Mg}^{+2}$  has not been shown in this figure. Values (in proper unit) of  $-\Delta G_r$  in presence of  $\text{Mg}^{+2}$  in ethyl acetate for P4C, P5C and P6C are respectively  $-0.82$ ,  $6.03$ ,  $8.90$ . Corresponding values in acetonitrile are  $2.06$ ,  $9.02$  and  $11.47$ .

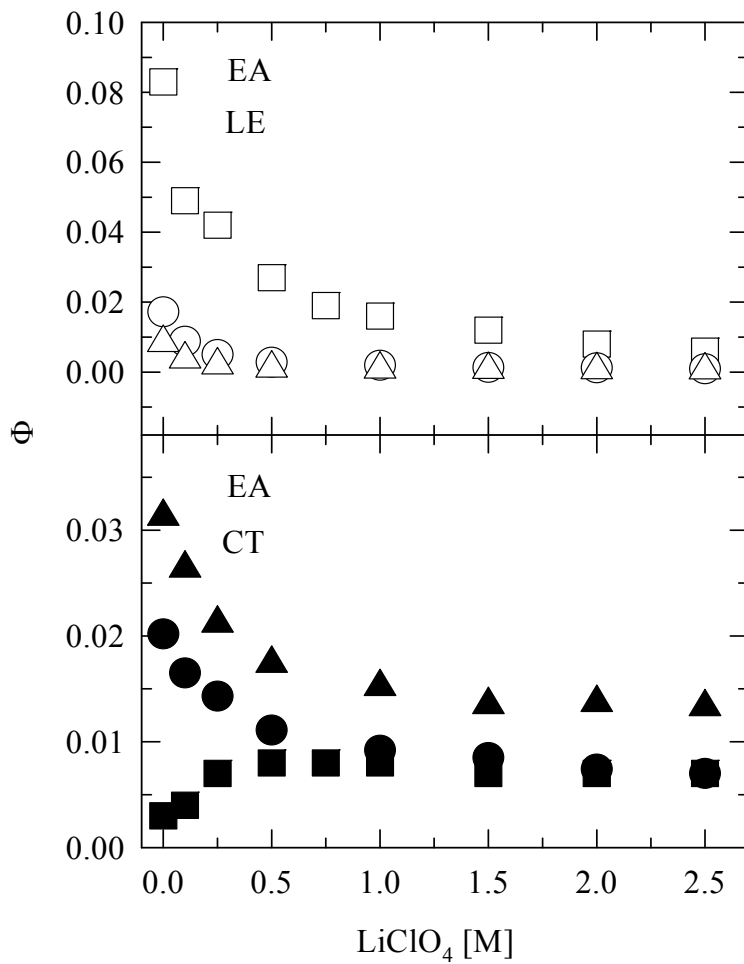


**Fig. A4:** Upper panel (open symbols) shows the quantum yield for the LE bands and lower panel (filled symbols) for CT bands in EA at different  $\text{LiClO}_4$  concentrations. Squares, circles and triangles represent electrolyte concentration dependent quantum yields of P4C, P5C and P6C, respectively. Estimated errors for these calculations are within  $\pm 10\%$  about the average for most of the cases.

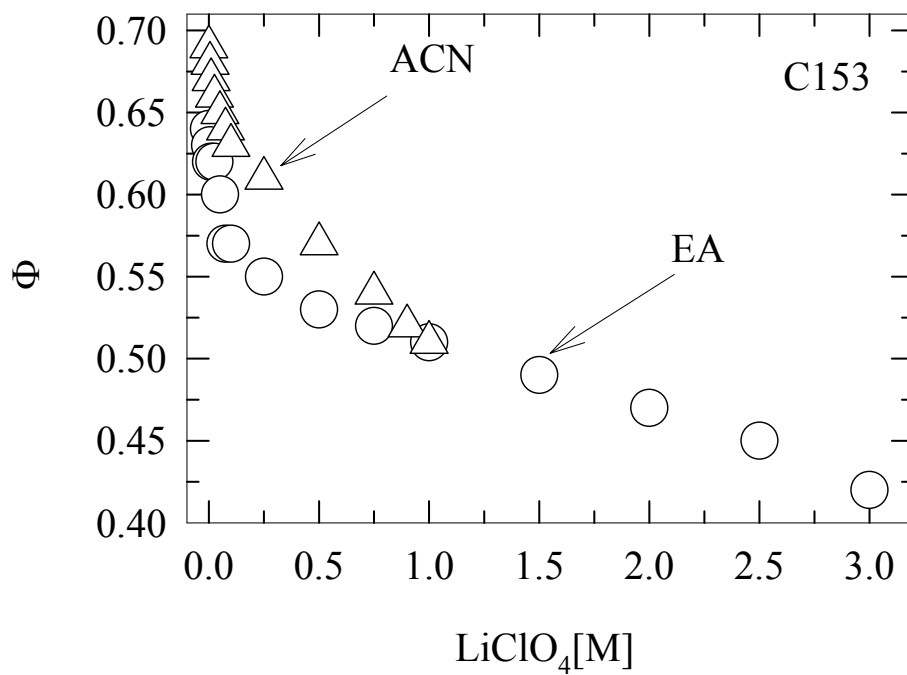


**Fig. A5:** Electrolyte (LiClO<sub>4</sub>) concentration dependence of quantum yield ( $\Phi$ ) for C153 in ethyl acetate and acetonitrile. Open circles and open triangles represent quantum yields of C153 in ethyl Acetate and acetonitrile, respectively. Estimated errors for these calculations are within  $\pm 10\%$  about the average for most of the cases.

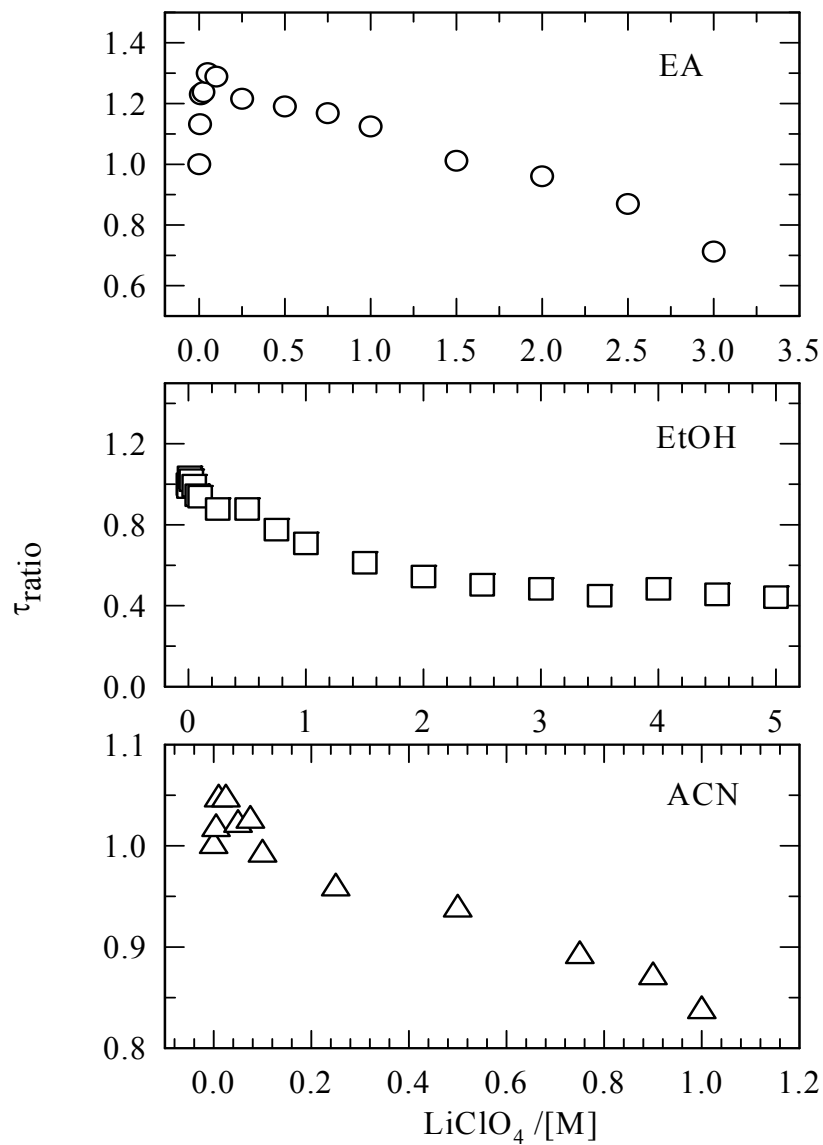


**Fig.A6:** The ratio between average reaction times obtained in presence and absence of electrolyte ( $\tau_{ratio} = \tau_{rxn}(M)/\tau_{rxn}(M=0)$ ) is shown as a function of  $\text{LiClO}_4$  concentration in ethyl acetate (upper panel), ethanol (middle panel) and acetonitrile (lower panel).

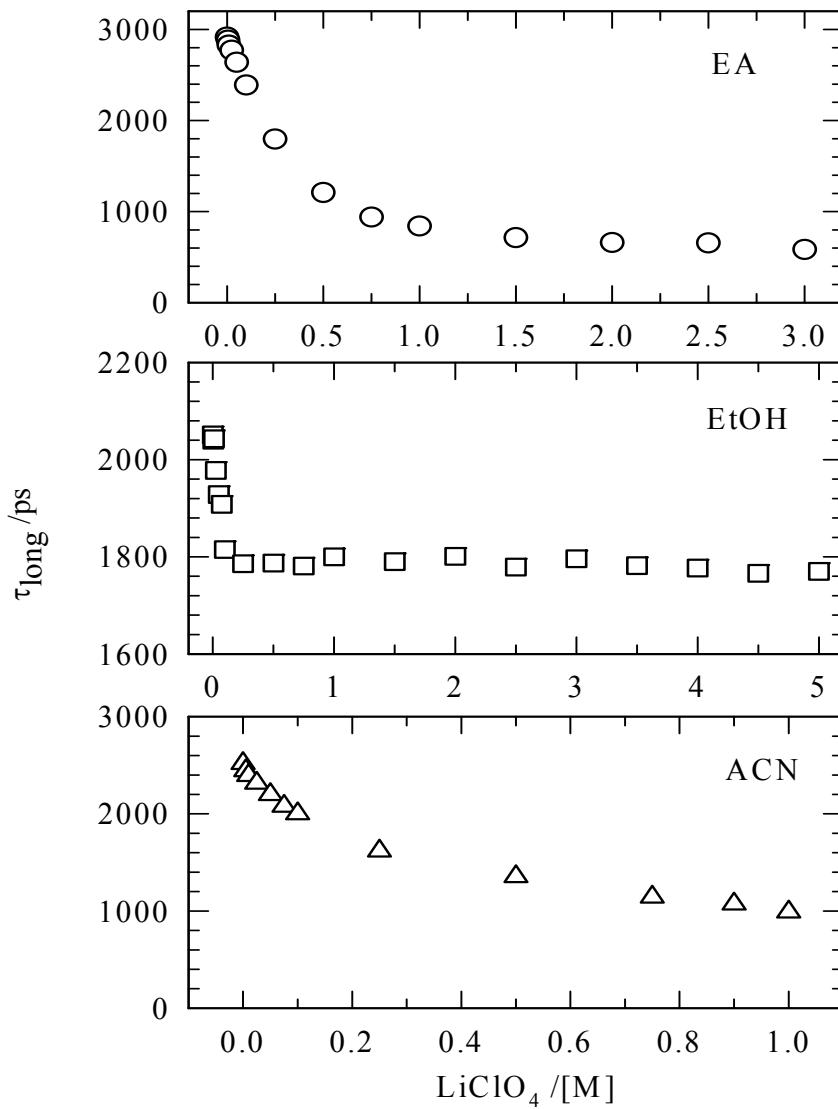


**Fig.A7:** Electrolyte concentration dependence of long time constant associated with the slow component of the bi-exponential LE emission decay ( $\tau_{long}$ ) of P4C in ethyl acetate (circles), ethanol (squares) and acetonitrile (triangles) have shown respectively in upper, middle and lower panels.

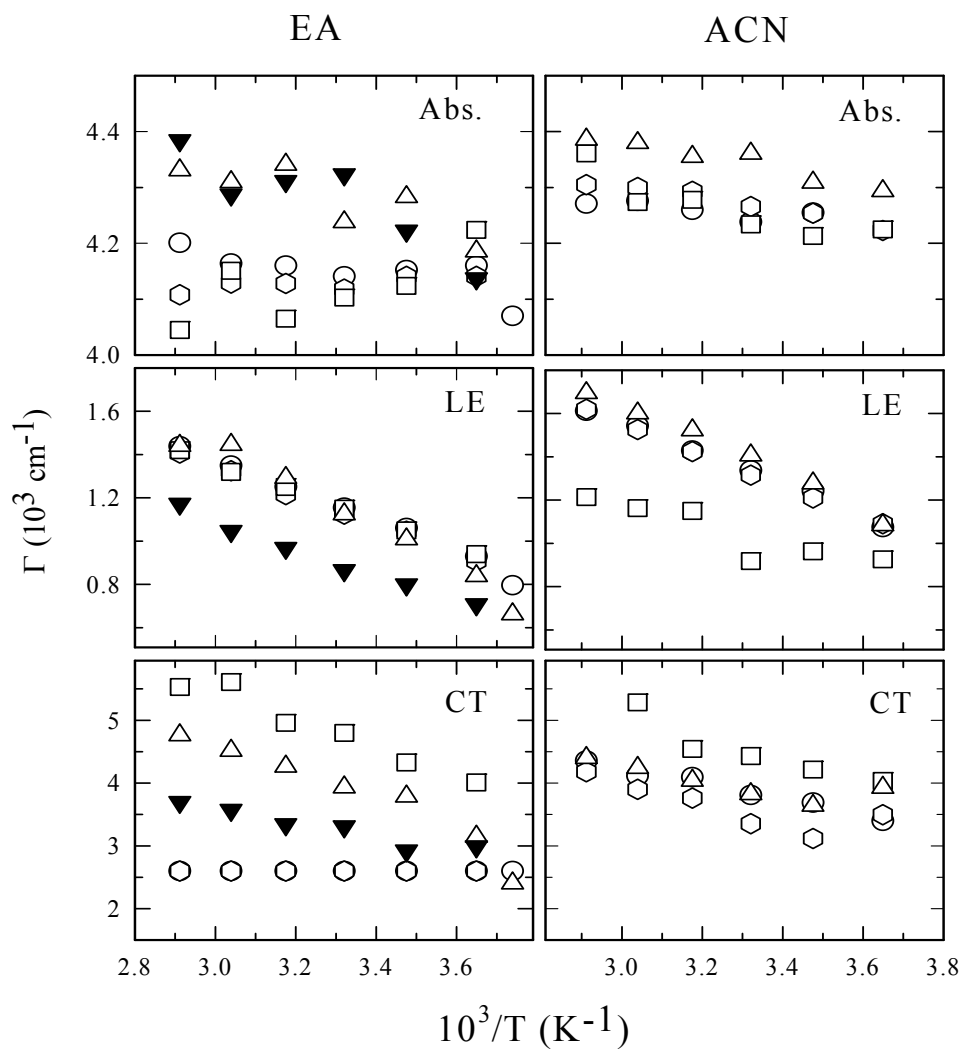


**Fig. A8.** Temperature dependent spectral bandwidths (full width at half maxima,  $\Gamma$ ) of the absorption spectra, and inhomogeneous widths of LE and CT emission bands of 4-(1-azetidynyl) benzonitrile (P4C) in ethyl acetate (left panel, 'EA') and acetonitrile (right panel, 'ACN') in presence of LiClO<sub>4</sub> at various concentrations. The circles, hexagons, squares, triangles, filled inverted triangles represent respectively the data at LiClO<sub>4</sub> concentrations (M) 0.0, 0.01, 0.10, 0.50, 1.0 in ethyl acetate and acetonitrile.

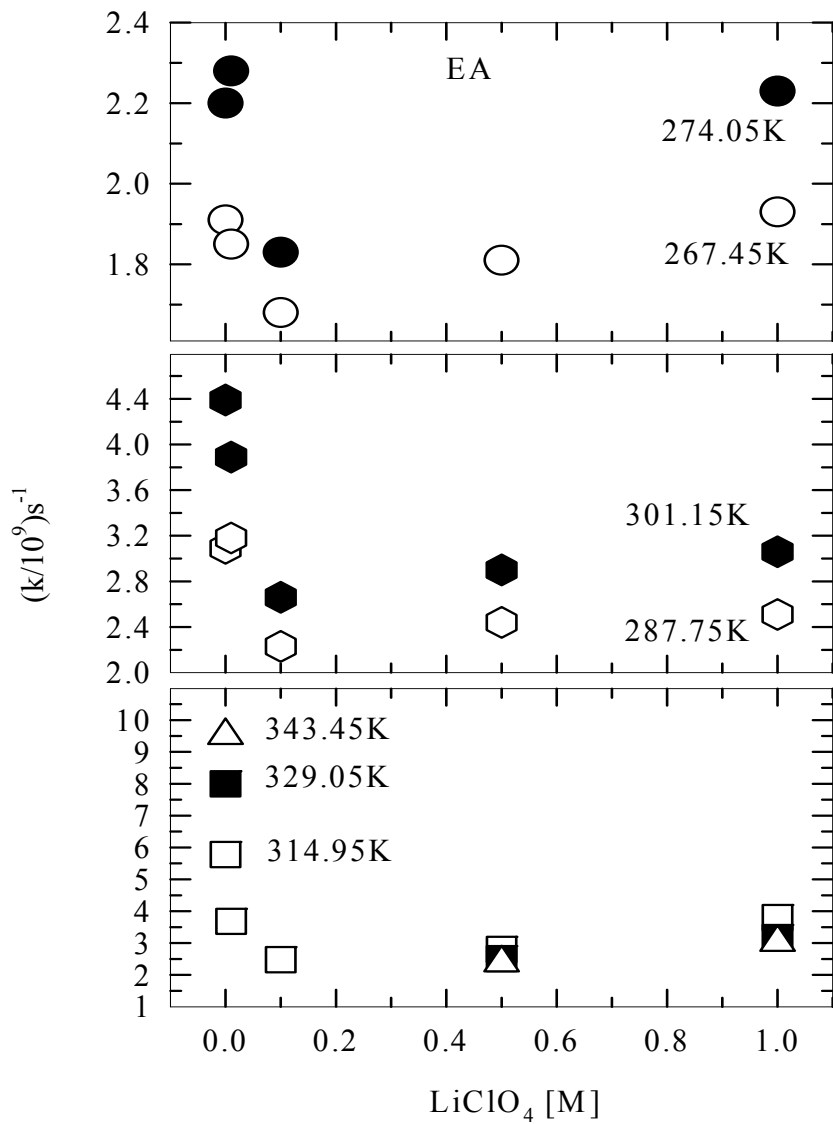


**Fig.A9.** Electrolyte concentration dependence of reaction rate of P4C in ethyl acetate at seven different temperatures is shown. The circles, filled circles, hexagons, filled hexagons, squares, filled squares and triangles represent respectively the data at temperatures (K): 267.45, 274.05, 287.75, 301.15, 314.95, 329.05, and 343.45.

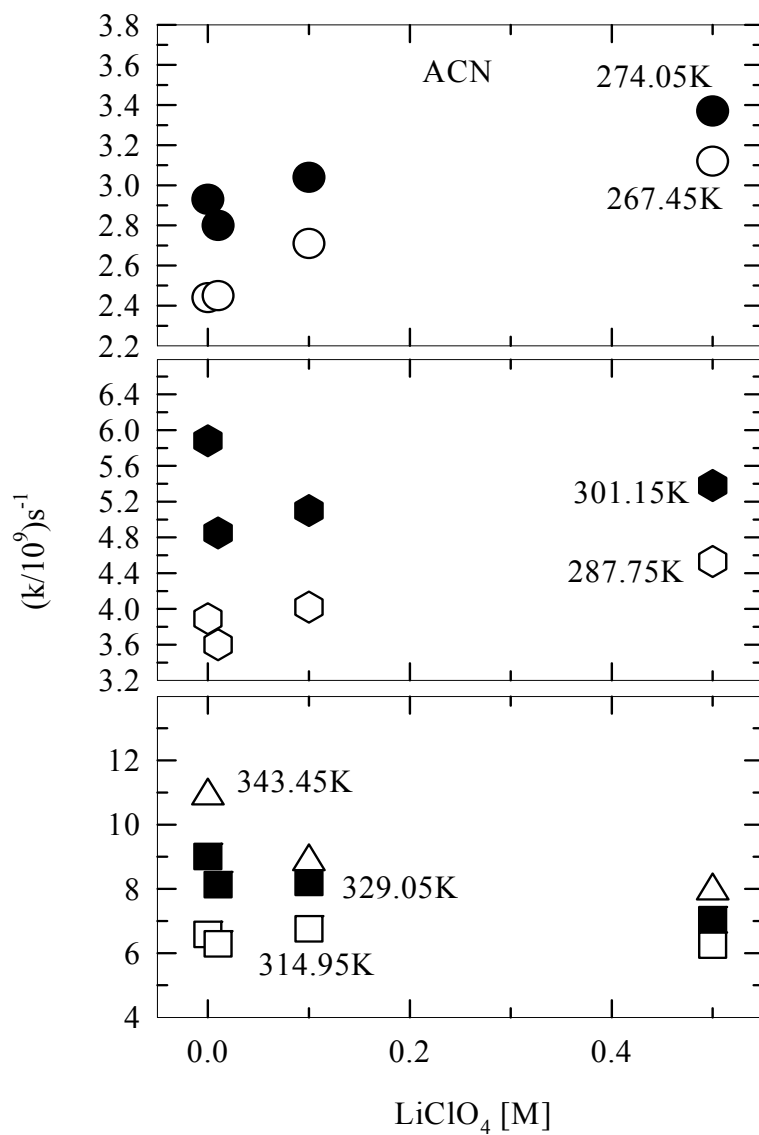


**Fig.A10.** Electrolyte concentration dependence of reaction rate of P4C in acetonitrile at seven different temperatures is shown. The circles, filled circles, hexagons, filled hexagons, squares, filled squares and triangles represent respectively the data at temperatures (K): 267.45, 274.05, 287.75, 301.15, 314.95, 329.05, and 343.45.

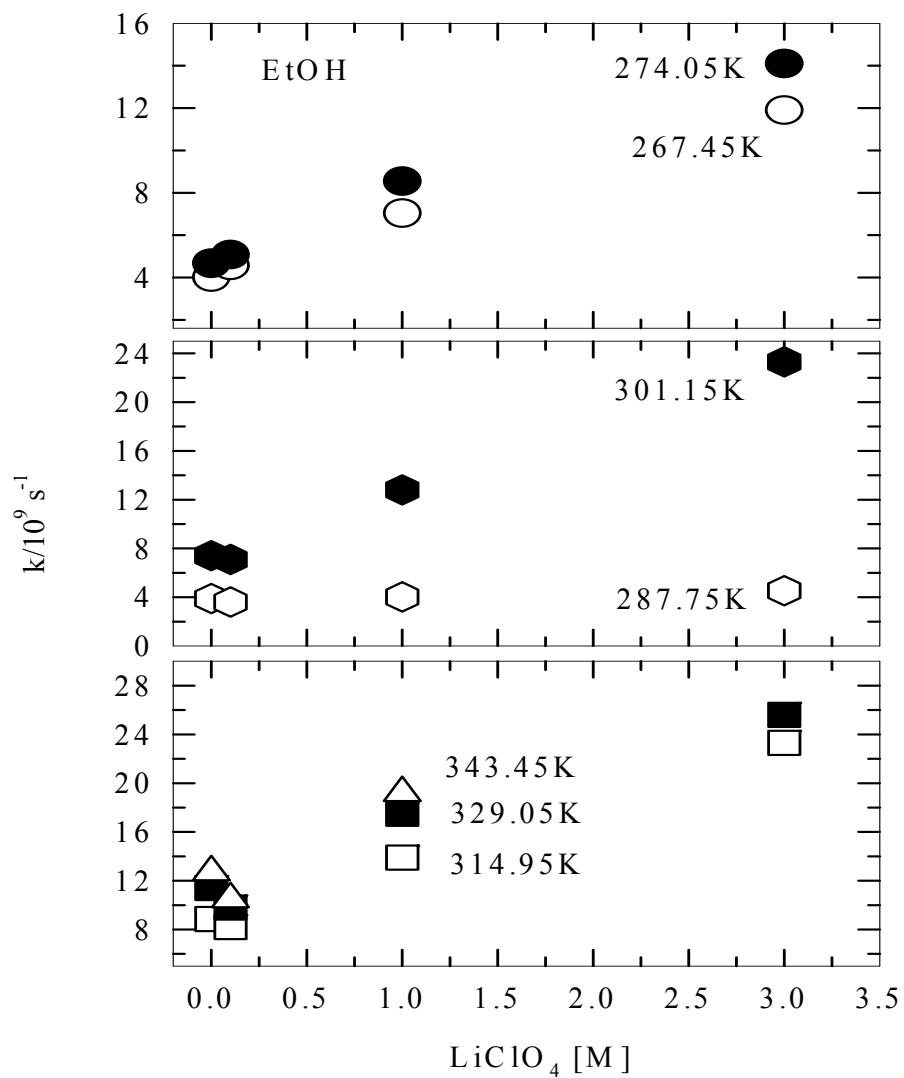


**Fig.A11.** Electrolyte concentration dependence of reaction rate of P4C in ethanol at seven different temperatures is shown. The circles, filled circles, hexagons, filled hexagons, squares, filled squares and triangles represent respectively the data at temperatures (K): 267.45, 274.05, 287.75, 301.15, 314.95, 329.05, and 343.45.

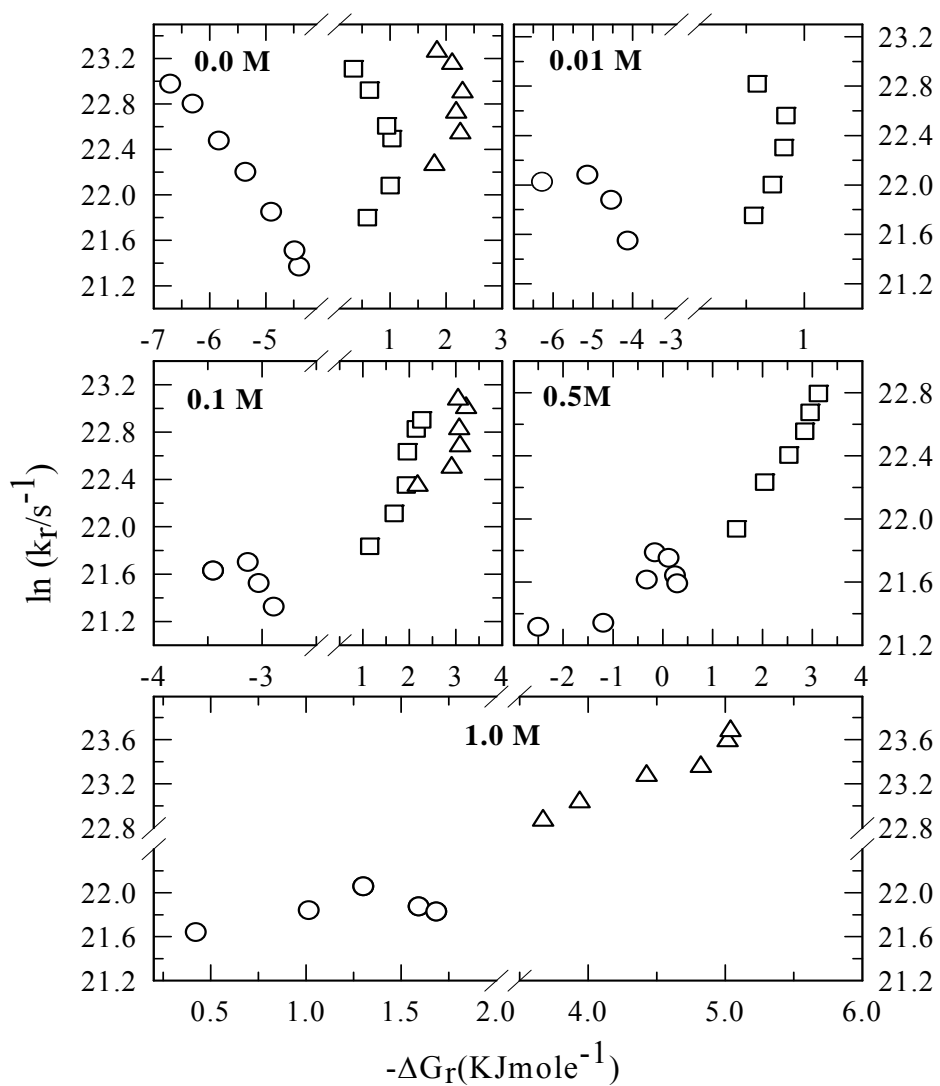


**Fig.A12.** Dependence of the reaction rate on the change in reaction free energy ( $-\Delta G_r$ ) has been shown. The circles, squares and triangles represent respectively ethyl acetate, acetonitrile and ethanol. Note that electrolyte concentrations are indicated in each of the panels.

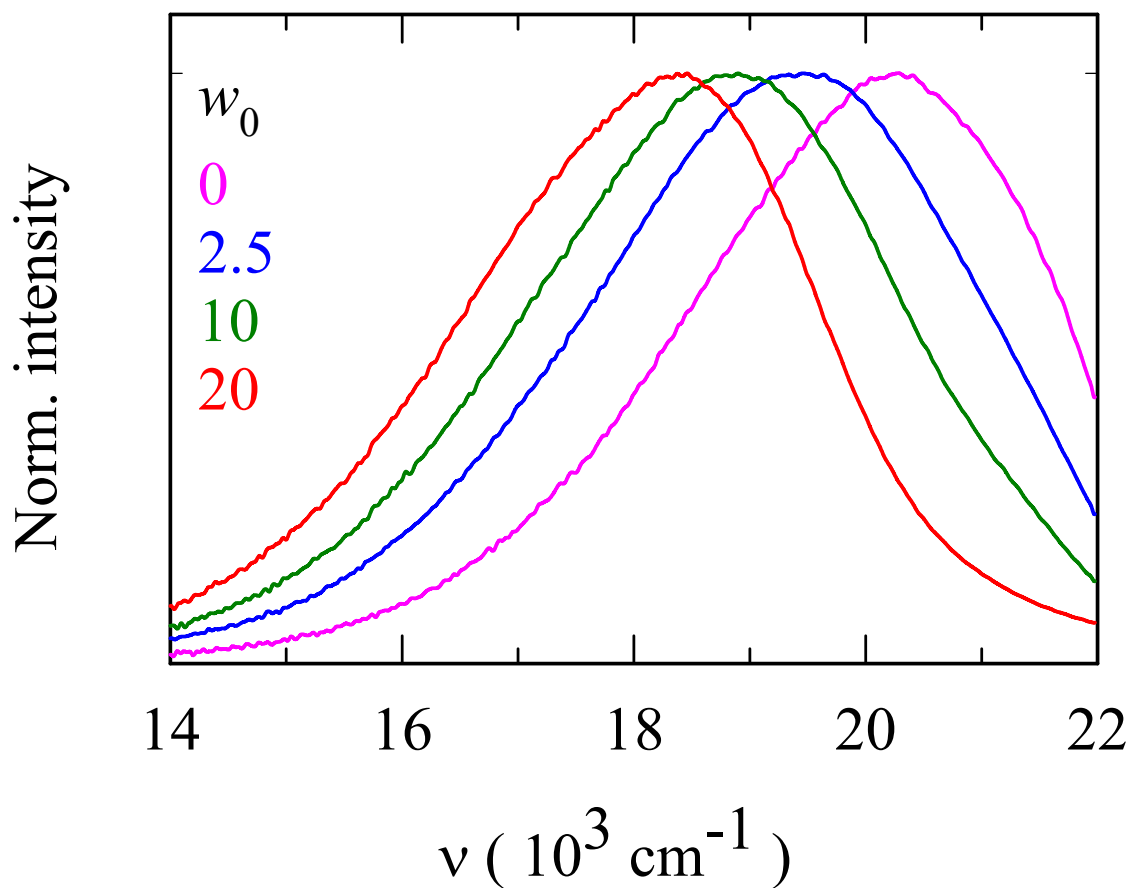
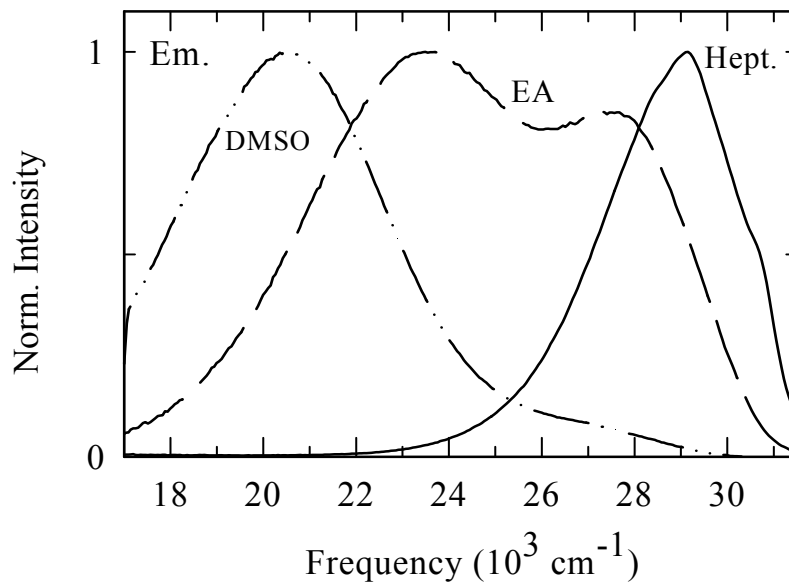


**Fig. A13:** Representative emission spectra of C153 in AOT/water/heptane reverse micelles at several pool sizes ( $w_0$ ). The peak frequencies obtained from these spectra were then used in a continuum model based expression to estimate the average static dielectric constant of the trapped pool. Note that as these systems are known to show excitation wavelength dependence, the estimated value of dielectric constant may vary for the same pool with a different excitation wavelength.



Solvent	$\epsilon_0$	$\nu_{\text{abs}}$	$\nu_{\text{LE}}$	$\nu_{\text{CT}}$	$\Gamma_{\text{abs}}$	$\Gamma_{\text{LE}}$	$\Gamma_{\text{CT}}$	$\alpha_{\text{CT}} / \alpha_{\text{LE}}$
Heptane	1.92	35.85	28.83	-	3.98	3.67	-	-
EA	6.02	35.04	27.78	23.24	4.30	1.18	5.80	1.78
PrOH	20.45	34.76	27.56	24.66	4.54	1.66	4.39	14.97
DMSO	46.45	34.09	25.846	20.53	4.38	3.36	3.61	11.15

**Fig. A14:** Emission spectra of M6C in heptane (solid line), ethyl acetate (dashed lines) and dimethyl sulfoxide (DMSO, dashed-dot-dot lines). Various steady state spectroscopic properties of M6C in these solvents are also summarized in the accompanying table. The unit for both the frequency ( $\nu$ ) and width ( $\Gamma$ ) is  $10^3 \text{ cm}^{-1}$ .